UNIVERSITY OF SOUTHAMPTON

FACULTY OF ENGINEERING AND APPLIED SCIENCE

SUB-DEPARTMENT OF ENGINEERING MATERIALS

STAINLESS STEEL CLADDING OF MILD STEEL SHAFTS USING PULSED METAL-INERT-GAS WELDING TECHNIQUES.

Author: Kostas Kalligerakis.

Supervised by: Dr. B.G. Mellor

Prof. G.A. Chadwick.

Submitted for the Degree of Doctor of Philosophy.

August 1990

to James, Anne and Jennifer.

ERRATA

at page xx, para 3, line 5 - should read family

at page 146, para 4, lines 3 & 4 - should read 12% and 13% instead of 11% and 17%

at page 146, para 4, line 5 - should read 10.6% to 27.0% instead of 7.6% to 27.8%

at page 153, para 2, line 3 - should read grain structure instead of crystal structure

at page 164, table 8.5, column 4, last value should read 15.0 instead of 24.0

at page 187, para 4, line 2 - should read included instead of inluded

TABLE OF CONTENTS.

Table of Contents i
Abstract viii
Acknowledgements ix
List of Figures x
List of Tables xii
List of Graphs xiv
List of Plates xvi
List of Symbols xviii
Preface xx

Chapter One Overlay Welding 1
1.1 Historical Note 1
1.2 Selection of Methods and Materials 2
1.2.1 Welding Processes 2
1.2.2 Materials 3
1.3 Selected Materials and Welding Techniques ... 5

Chapter Two Gas Metal Arc Welding 7
2.1 Introduction 7
2.2 The Gas Metal Welding Arc 9
2.2.1 Anode, Arc Column and Cathode 12
2.2.2 Anode 12
2.2.3 Arc Column 13
2.2.4 Vapour and Plasma Jets 14
2.2.5 Cathode 15
2.3 Gas Metal Arc Welding Process Parameters ... 16
2.4 Electrical Parameters 16
2.4.1 Welding Current 16
2.4.2 Arc Voltage and Arc Length 18
2.4.3 Polarity 18
2.4.4 Other Polarity Associated Effects . 20
2.4.5 Stickout 21
2.5 Material Parameters 21
2.5.1 Filler Wire 22
2.5.2 Base Material 22
2.6 Shielding Gas 23
2.6.1 Shielding Gases and their Properties 24

Chapter Three **Metal Detachment and Transfer in GMA Welding Process** 27
3.1 Introduction 27
3.2 Transfer Types 27
3.2.1 Free Flight Transfer 28
3.2.2 Bridging Transfer 30
3.2.3 Slag Protected 32
3.3 Droplet Evolution in Free Flight Transfer .. 32
3.3.1 Globular transfer 32
3.3.2 Streaming Spray Transfer 34
3.4 Metal Detachment Models 34
3.4.1 Static Forces model 35
3.4.2 Pinch Instability Model 36
3.5 Discussion: On Aspects of the Static Forces and Pinch Instability Model 38
3.5.1 Effects of Surface Tension on Metal Transfer 38
3.5.2 The Tapering Factor 39

Chapter Four **Pulsed MIG welding: An Introduction to the Process** 41
4.1 Pulsed Metal Inert Gas Welding 41
4.2 Operational Stability 42
4.2.1 Burnoff Balance 42
4.2.2 Arc Continuation 44
4.2.3 Metal Transfer Stability 44
4.2.3.1 Spatter 45

Chapter Five **Control of Metal Transfer in Pulsed MIG Welding** 47
5.1 Introduction 47
5.2 Natural Detachment Times 47
5.2.1 Introduction: Techniques for the Detection of Droplet Detachment .. 47
5.2.2 Experimental Arrangement 48
5.2.3 Results 52
5.2.3.1 Transfer Modes of the 316S92 Electrode Wire 52

5.2.4 Discussion:On the Natural Detachment Times 54
5.2.4.1 Scatter in the Natural Detachment Times 57
5.3 Welding with Pulsed Current 64
5.3.1 Modelling of Metal Detachment in Pulsed MIG Welding 64
5.3.2 Experiments on the Classification of Metal Transfer in P-MIG 66
5.3.2.1 Effects of Cycle Frequency on Droplet Detachment at Constant Pulse Amplitudes 66
5.3.2.2 Results 68
5.3.2.3 Effects of Pulse Amplitudes on Droplet Detachment for Constant Cycle Times 69
5.3.2.4 Results 70
5.3.3 Discussion: Metal Transfer in Pulsed MIG welding 71
5.3.3.1 The Phenomenon of Droplet Growth .. 71
5.3.3.2 Classification of Metal Transfer in Pulsed MIG Welding 73
5.3.3.3 Aspects of Metal Detachment in Relation to Pulse Current Configuration 75
5.4 Selection of Electrical Parameters 77
5.4.1 Projected Spray Transfer 77
5.4.2 Streaming Spray Transfer 78
5.4.3 Detachment by Growth 79
5.5 Discussion 81
5.5.1 Control of Metal Transfer and Droplet Detachment 81
5.5.2 Spatter 83
5.6 Conclusions 83

Chapter Six **The Burnoff Criterion and the Burnoff factor in Pulsed MIG Welding** 86
6.1 Introduction 86
6.2 Theory 86
6.3 Experimental Work: The Burnoff Factor in Pulsed MIG Welding 88
6.3.1 Observations on the Applicability of the Burnoff Factor in Pulse Current Configuration 88
6.3.2 Effect of Wire Feed Speed on the Stability of the Arc and Metal Transfer 89
6.4 Discussion 91
6.4.1 Calculation of the Burnoff Factor and Comparison with the Experimentally Obtained Value 91
6.4.2 Arc Length Fluctuation 94

Chapter Seven **Fusion Characteristics of 316S92 Stringer Beads on 070M20 plates** .. 96
7.1 Introduction 96
7.2 Weldpool and the Formation of the Reinforcement Bead 96
7.2.1 Heat Distribution 96
7.2.2 Droplet Heat Content and Momentum . 98
7.2.2.1 Droplet Velocity and Acceleration . 99
7.2.3 Weldpool Convection 99
7.2.4 Modelling and Formulation of the Arc 100
7.2.5 The Effect of Process Parameters on the Dimensions of the Weldbead . 102
7.2.6 Effects of Dimensions and Temperature of the Base Material on the Bead Profiles 103
7.2.7 Geometrical features of the bead .. 104
7.3 Experimental Work on the Fusion Characteristics of 316S92 Stringer Beads on 070M20 plates 107

7.3.1 Introduction 107
7.3.2 Experimental Arrangement 108
7.3.3 Experimental Method for the Measurement of Bead Profiles 108
7.4 Results 110
7.4.1 Effects of Dimensions and Temperature of the Base Material on the Bead Profiles 110
7.4.2 Effects of Welding Parameters on the Cross Sectional Areas of the Deposit 111
7.4.3 Effects of Welding Parameters on the Levels of Dilution 113
7.4.4 Effects of Welding Parameters on the Depth of Penetration 116
7.4.5 Effects of Welding Parameters on Contact Angles 116
7.4.6 Effects of Pulse Parameters on Bead Profiles 119
7.4.6.1 Effects of Background Detachments on Bead Profiles 121
7.4.7 Effects of Incident Electrode Angles on Bead Shape 123
7.4.8 Bead on Plate Deposition Using Low Mean Currents 126
7.5 Discussion 128
7.5.1 Deposition Ratio 128
7.5.2 Weldbead Width 129
7.5.3 Melting Rate Characteristics of the Electrode and Base Plate Material and their Effects on the Bead Profile Shape 131
7.5.4 Effects of Irregular Metal Transfer on the Bead Profiles 131
7.6 Conclusions 132

Chapter Eight Overlay Welding 139
8.1 Experimental Arrangement 139
8.1.1 Experimental Rig 139
8.1.2 Set Up 140
8.1.3 Welding Set 142
8.2 Experimental Work 143
8.2.1 Identification of Operational Parameters in Overlay Welding 143
8.2.2 Experiments and Results 145
8.2.2.1 Profile Examination 145
8.2.2.2 Presentation of Results 145
8.2.3 Discussion: Single Spiral Overlaying Technique 153
8.2.3.1 Examination of the Deposit/Substrate Interface 153
8.2.3.2 Effects of Metal Transfer on the Stability of the Process 154
8.2.3.3 Effects of Overlap on the Stability of the Process 157
8.2.3.4 Effects of Arc Length on the Process 157
8.2.4 A Proposed Overlay Welding Technique 159
8.2.4.1 Experiments 161
8.2.4.2 Results 161
8.2.5 Discussion: Comparison between the Single and the Double Spiral Overlaying Techniques 163
8.2.5.1 Machining Requirements of the Deposits 163
8.2.5.2 Calculation of Welding Parameters 164
8.3 Metallurgical Examination of the Overlayers 166
8.3.1 Introduction 166
8.3.1.1 Weldability of Substrate 167
8.3.1.2 Weldability of Filler Wire 168
8.3.2 Metallurgical Examination of the Deposits 169
8.3.2.1 Partial Dilution and Microalloying 169

8.3.2.2 Energy Dispersive Analysis with X ray Techniques (EDAX) 169
8.3.3 Discussion:Dilution and its Metallurgical Effects on the Deposit 175
8.3.3.1 Dilution in the Deposit and the Schaeffler Diagram 175
8.3.3.2 Dilution and Corrosion Properties . 177
8.4 Destructive Testing 178
8.4.1 Introduction 178
8.4.2 Experimental Arrangement 180
8.4.3 Results 180
8.4.3.1 Analysis and Discussion of the Fatigue Crack Propagation Results . 187
8.4.4 Experimental Reliability 189
8.4.5 In Service Performance 190

Chapter Nine General Discussion and Conclusions 203
9.1 Introduction 203
9.2 Pulsed MIG Welding: Control of Metal Transfer 203
9.3 Pulsed MIG Welding as an Overlaying Process 204
9.3.1 Dilution 204
9.3.2 Limitations due to Compositional Variations 205
9.3.3 Pulsed MIG Welding Compared with Other Welding Processes 206
9.4 Fatigue Crack Propagation Experiments 206

Chapter Ten Further Work 207
10.1 Introduction 207
10.2 Control of Metal Transfer 207
10.3 Overlay Welding Techniques 207
10.4 Testing of Overlayers 207

References 208
Appendix I 225

UNIVERSITY OF SOUTHAMPTON

ABSTRACT

FACULTY OF ENGINEERING AND APPLIED SCIENCE
ENGINEERING MATERIALS

Doctor of Philosophy

STAINLESS STEEL OVERLAY CLADDING OF MILD STEEL SHAFTS USING PULSED METAL-INERT-GAS WELDING TECHNIQUES

by Kostas Kalligerakis

The present work examines the overlay welding of 070M20 mild steel shafts with 316S92 filler wire electrode using pulsed current metal inert gas welding.

Firstly the literature review investigates the criteria for the selection of methods and materials in overlay welding. The largest part of the literature review focuses on the understanding of the gas metal arc welding family of processes and in particular metal inert gas welding. The review covers topics such as arc phenomena, process parameters, types and mechanisms of metal transfer and finally the electrical parameters, and criteria for their selection, in pulsed metal inert gas welding.

Prior to overlay welding, a series of preliminary experiments on the control of metal transfer, burnoff and fusion characteristics of the filler wire in pulse current configuration were carried out. It was found that control of metal detachment was limited because of scatter in the natural detachment times. A simple method to select electrical parameters for a stable and regular metal transfer is presented.

Examination of the burnoff characteristics of the filler wire shows that it may easily and accurately be derived by a trial and error method as well as be calculated. It was also found that for the specific material used, errors of the order of ±15% in the setting of the wire feed speed had no significant effects on arc stability.

Overlay welding was examined as a process for the deposition of coatings. Initially coatings were deposited using the single spiral overlapping technique and it was found that this method of deposition was adequate for sound coatings. An alternative deposition technique has been proposed which enables the deposition of low dilution coatings at welding parameters that would result in high dilution if the single spiral method were used. In this technique a non overlapping narrow gap spiral is deposited at first using very low dilution welding parameters. Then a covering spiral is deposited in the gap at higher welding currents thus ensuring good fusion characteristics.

Metallurgical examination of the deposits using Energy Dispersive Analysis X-ray techniques and with reference to the Schaeffler diagram showed that for the specific alloys used, the required duplex austenitic/ferritic structure could be obtained for dilutions below 7.5%. However, at higher dilutions, phenomena such as solidification cracking or hot cracking were not observed.

Exploratory fatigue crack propagation testing of the overlayed specimens indicated that internal residual stresses influence the propagation of fatigue cracks. However, all overlayed specimens exhibited prolonged fatigue life when compared to a stainless steel specimen.

Acknowledgements.

I would like to express my gratitude to Dr. B.G. Mellor for his guidance, supervision and patience throughout the course of this project.

I would also like to thank:

Mr. R.J. Hammond for his technical assistance.

Mr. M.J. Griffiths (B.Sc) and Mr. P.J.M. Squires (B.Eng) for their assistance during the operations (1988-1989).

Mr. G. Smith (B.Sc) of A.M.C for consultations during the initial stages of the project.

Last but not least I would like to thank:

James and Anne for without them nothing at all would have been possible and Jennifer for her inexhaustable moral support.

LIST OF FIGURES.

Figure	Title	page
2.1	MIG Welding. Schematic Arrangement	8
2.2	Schematic Representation of the Voltage Distribution across the Arc	11
2.3	GMAW Process Parameters	17
2.4	Voltage-Current Characteristics of Consumable Electrode Arc System	19
2.5	Terminology	19
3.1	Types of Metal Transfer in GMA Welding	29
3.2	Metal Transfer Modes in GMAW	31
4.1	Pulse Current Configuration	43
5.1	Metal Detachment Recording Set Up	49
5.2	Schematic Representation of Typical Oscilloscope Arc Voltage Traces	51
5.3	Droplets Prior to Detachment	55
5.4	Metal Detachment in Pulsed MIG Welding	65
5.5a	Constant Amplitude / Decreasing Cycle Frequency	67
5.5b	Constant Cycle Frequency / Increasing Amplitude Differential	67
5.6	Wavefroms a) Normally Occuring b) Showing Arc Continuation Irregularities	67
7.1	Metal Flow in MIG Weldpools during Streaming Transfer	105
7.2	Types of Bead Profiles	105
7.3	Bead Dimensions	106
7.4	Bead Areas	107
7.5	Effects of Pulse Current Configuration and Type of Metal Transfer Modes on the Shape of Bead Profiles	122
7.6	Longitudinal (α) and Lateral (β) Angles ...	125
7.7	Effects of Lateral Inclination on Bead Profiles in Projected and Globular Transfer	125
8.1	Set Up	141
8.2	Deposition and Machining Sequence	160
8.3	Overlay Welding-Selection of Parameters ...	165

8.4 Element Distribution across a Bead Profile 172
8.5 Dilution in Overlayer: EDAX Technique 173
8.6 Dilution in Overlayer: EDAX Technique 173
8.7 Schaeffler Diagram 176
8.8 Fatigue Crack Growth Specimens 179
A.1 Bead Profiles from Table 7.1 225
A.2 Bead Profiles from Table 7.2 226
A.3 Bead Profiles from Table 7.3 226
A.4 Bead Profiles from Table 7.4 226
A.5 Bead Profiles from Table 7.5 229
A.6 Bead Profiles from Table 7.6 230

LIST OF TABLES

Table	Title	page
3.1	Effects of Surface Tension on Natural Detachment Times	39
5.1	Natural Detachment Times for 316S92 1.2mm Diameter Welding Wire in Ar 1%O_2 Reverse Polarity	52
5.2	Statistical Presentation of Natural Detachment Times	58
5.3	Effects of Cycle Frequency on Metal Detachment	68
5.4	Effects of Pulse Amplitude on Metal Detachment	70
5.5	Welding Parameters for a Drop per Pulse Detachment	77
5.6	Detachment by Growth: Electrical Parameters	81
5.7	Welding Parameters for a Drop per Pulse Detachment	81
6.1	Data of Wire Feed Speed Fluctuation Experiments	89
6.2	Burnoff Factor Adjustment for Low Current Welding	91
6.3	Calculated Wire Feed Speed for Pulse Current	92
6.4	Percentage Difference between Experimentally Derived and Calculated Wire Feed Speeds ...	94
7.1	Welding Parameters	134
7.2	Welding Parameters	135
7.3	Welding Parameters	135
7.4	Welding Parameters	136
7.5	Welding Parameters	137
7.6	Welding Parameters	138
8.1	Overlay Welding Parameters. Single Spiral Technique	145
8.2	Dilution in Single Spiral Overlayers	146
8.3	Overlay Welding Parameters. Double Spiral Technique	161
8.4	Dilution in Double Spiral Overlayers	162
8.5	Deposit Thickness & Machining Requirements	164

8.6 British Standards Base Metal and Filler Wire Compositions 167
8.7 Chemical Analysis of Filler Wire and Base Metal 167
8.8 Element Distribution in Bead Profile 170
8.9 Composition Analysis (EDAX), Single Spiral Overlayer 174
8.10 Composition Analysis (EDAX), Double Spiral Overlayer 174
8.11 Effects of Dilution on the Composition of the Deposit and the Schaeffler Diagram 175
8.12 Fatigue Crack Propagation Experiments. Specimen Loading 180
8.13 Fatigue Crack Propagation Data. 316S92 Stainless Steel Specimen (S1) 197
8.14 Fatigue Crack Propagation Data. 070M20 Mild Steel Specimen (S2) 197
8.15 Fatigue Crack Propagation Data. Overlayed Specimen (S3) 198
8.16 Fatigue Crack Propagation Data Overlayed Specimen (S4) 199
8.17 Fatigue Crack Propagation Data Overlayed Specimen (S5) 200
8.18 Fatigue Crack Propagation Data Overlayed Specimen (S6) 201
8.19 Fatigue Crack Propagation Data Overlayed Specimen (S7) 202

LIST OF GRAPHS

Graph	Title	page
5.1	Effects of Welding Current on Frequency of Detachment	59
5.2	Welding Current vs Natural Detachment Times	60
5.3	Welding Current vs Natural Detachment Times	61
5.4	Logarithmic Plot of Welding Current vs Natural Detachment Times	62
5.5	Scatter in Natural Detachment Times. Welding Current vs Standard Deviation	63
6.1	Welding Current vs Wire Feed Speed	93
7.1	Effects of Welding Current on Bead Areas ..	112
7.2	Effects of Electrode Travel Speed on Bead Areas	112
7.3	Effects of Welding Travel Speed on Dilution	115
7.4	Effects of Electrode Travel Speed on Dilution	115
7.5	Effects of Welding Current on Depth of Penetration	117
7.6	Effects of Electrode Travel Speed on Depth of Penetration	117
7.7	Effects of Welding Current on Bead Contact Angles	118
7.8	Effects of Electrode Travel Speed on Bead Contact Angles	118
7.9	Effects of Types of Metal Transfer on the Bead Dimensions for a Range of Mean Currents	120
7.10	Effects of Deposition Ratio on Bead Width	130
8.1	ln da/dN vs ln DK. 316S11 Stainless Steel Specimen (S1)	182
8.2	ln da/dN vs ln DK. 070M20 Mild Steel Specimen (S2)	182
8.3	ln da/dN vs ln DK. Overlayed Specimen (S3)	183
8.4	ln da/dN vs ln DK. Overlayed Specimen (S4)	183
8.5	ln da/dN vs ln DK. Overlayed Specimen (S5)	183
8.6	ln da/dN vs ln DK. Overlayed Specimen (S6)	184
8.7	ln da/dN vs ln DK. Overlayed Specimen (S7)	184

8.8 Crack Length vs No. of Cycles. Stainless and Mild Steel Specimen 185
8.9 Crack Propagation in Relation to Notch Positioning (S3, S4, S5) 185
8.10 Crack Length vs No. of Cycles Specimen (S6) 186
8.11 Crack Length vs No. of Cycles Specimen (S7) 186

LIST OF PLATES

Plate	Title	page
I	Overlayed Specimen No.1. Profile	148
II	Overlayed Specimen No.2. Profile	148
III	Overlayed Specimen No.3. Profile	149
IV	Overlayed Specimen No.4. Profile	149
V	Overlayed Specimen No.5. Profile	150
VI	Overlayed Specimen No.6. Profile	150
VII	Overlayed Specimen No.7. Profile	151
VIII	Overlayed Specimen No.9. Profile	151
IX	Overlayed Specimen No.10. Profile	152
X	Overlayed Specimen No.8. Profile	152
XI	Surface Finish and Appearence of Overlayed Shaft	155
XII	Surface Finish and Appearence of Overlayed Shaft	155
XIII	Interface Appearence-Regular Metal Transfer	156
XIV	Interface Appearence-Irregular Metal Transfer	156
XV	Flow Patterns on Transverse Face of Overlayed Specimen after Continuous Etching	171
XVI	EDAX Sampling Points on Bead Profile	171
XVII	Fatigue Crack Growth Test. Overlayed Specimen No.8 (S3)	191
XVIII	Fatigue Crack Growth Test. Overlayed Specimen No.8 (S3)	191
XIX	Fatigue Crack Growth Test. Overlayed Specimen No.8 (S3)	192
XX	Fatigue Crack Growth Test. Overlayed Specimen No.8 (S3)	192
XXI	Fatigue Crack Growth Test. Overlayed Specimen No.8 (S3)	193
XXII	Fatigue Crack Growth Test. Overlayed Specimen No.8 (S3)	193
XXIII	Fatigue Crack Growth Test. Overlayed Specimen No.8 (S3)	194

XXIV Fatigue Crack Growth Test. Overlayed Specimen No.8 (S3) 194
XXV Fatigue Crack Growth Test. Crack Surfaces Stainless Steel (S1), Mild Steel (S2) Overlayed Specimen No.8 (S3) 195
XXVI Fatigue Crack Growth Test. Crack Surfaces Overlayed Specimen No.8 (S4), Overlayed Specimen No.8 (S5), Overlayed Specimen No.9 (S6) Overlayed Specimen No.10 (S7) 196

LIST OF SYMBOLS

A	electrode csa	(mm^2)
A_d	csa of deposit	(mm^2)
A_W	electrode csa	(mm^2)
a_1	material constant	($m^3A^{-1}s^{-1}$)
a_2	material constant	($m^4A^{-2}s^{-1}$)
b_v	volumetric burnoff rate	($m^3A^{-1}s^{-1}$)
C	constant	
Fc	forces acting on droplet, generated by the effects of surface tension	(N)
Fem	forces acting on droplet, generated by the welding current	(N)
Fg	forces acting on droplet, generated by the effects of gravitational acceleration	(N)
Fs	forces acting on droplet, generated by gas flow past the droplet	(N)
H_m	total energy required to melt unit volume of electrode wire $1.75 \cdot 10^{10}$	(J/m^3)
I	welding (arc) current	
Ib	background current	(A)
I_m	mean current	(A)
Ip	pulse current	(A)
J	current density	($A \cdot m^{-2}$)
K	stress intensity factor	($MNm^{-3/2}$)
K	detachment coefficient	
K_1	material constant (arc heating) $0.35 \cdot 10^{-3}$	(m/A/s)
K_2	material constant (resistance heating) $K_2=\sigma/A^2 \cdot H_m$ $1.139 \cdot 10^{-4}/A^2/s$	
l	stickout	(m)
m	burnoff factor	(m/s/A)
m_{DC}	burnoff factor in Direct Current	(m/s/A)
n	detachment index	
Pb	pressure acting at bulged region of a deformed liquid cylinder	(Pa)

Pp	pressure acting at pinched region of a deformed liquid cylinder		(Pa)
R	R-value		
R_e	wire radius		(m)
T	cycle time		(ms)
T_{DC}	detachment time		(ms)
Tb	background time		(ms)
Tp	pulse time		(ms)
TS	electrode travel speed		($mm \cdot s^{-1}$)
v	droplet volume		(mm^3)
v_d	droplet volume		(mm^3)

Greek Symbols.

α	longitudinal angle		(deg)
ß	lateral angle		(deg)
γ	surface tension		($N \cdot m^{-1}$)
δ	tapering factor		
θ	bead contact angle		(deg.)
σ	wire resistivity	$2.55 \cdot 10^{-6}$	(Ωm)
σ	stress		($N \cdot m^{-1}$)

Preface.

This study investigates the deposition of stainless steel overlayers on a mild steel substrate using pulsed Metal Inert Gas Welding implementing a small droplet volume high impact type of metal transfer at low heat inputs.

The study takes the following format:

The first part of the literature review examines overlay welding as a process, its requirements and the criteria for the selection of welding process and materials.

The remainder of the literature review examines the welding process used for the deposition. This involves investigation into arc phenomena, process parameters, types and mechanisms of metal transfer in the gas metal arc welding familiy of processes and then the additional parameters met in pulsed metal inert gas welding together with the criteria for their optimum selection.

The experimental part examines the control of metal transfer in pulsed Metal Inert Gas welding and the means of obtaining the desired type of metal transfer with the correct selection of electrical parameters. In addition, the melting rate characteristics of the electrode material as well as the fusion characteristics of the electrode material with the base metal are examined. This set of experiments serves as a foundation

for the following experimentation on overlay welding.

The overlay welding experiments can be divided into three sections. The first section examines the process parameters involved and their effects on the deposit. The second section investigates the metallurgical constitution of the deposits. The third section aims to assess the in service fatigue performance of the overlayed specimens by conducting a series of fatigue crack growth rate tests on them.

CHAPTER ONE

Overlay Welding.

Chapter One Overlay Welding.

1.1 Historical Note.

Overlay welding as a hardfacing treatment was proposed in a patent by J.W. Spencer in 1896 although the process was not developed until the 1920's. In its early days overlay welding was carried out by the oxyacetylene process (Riddihough 1949) the oxyacetylene torch having been devised by Fouche and Picard in 1903 (Houldcroft 1977).

By 1925 overlay welding was being carried out by the method of automatic welding (Wilson 1925). This method had been developed by the British Thomson-Houston Co., Ltd. and worked on the same principles as gas metal arc welding but without the shielding gas.

Overlay welding may be used as a method to restore worn components or to improve the corrosion or wear resistance of a component by the application of a coating with the appropriate metallurgical properties.

From an economic point of view the advantages of overlay welding are enormous because as a hardfacing or corrosion resistance method it increases the working life of a component. Also, rather than using an expensive material to make up the entire component, it is more economical to use such a material as only part of it. Furthermore, optimum mechanical and surface properties may be achieved by the right combination of substrate and overlaying materials.

1.2 Selection of Methods and Materials.

The great number of surfacing alloys and welding processes available present a problem in the selection of the most appropriate combination of method and material.

The overlay welding process is chosen from the requirements of the job: the economics involved in the process, the size of the job, the deposition rates permitted and the location ie. in situ repair or workshop production line.

1.2.1 Welding Processes.

Oxyacetylene or gas welding is a manual process used for small jobs. The dilution attainable may be as low as 1% and the maximum deposition rates below 1kg/hr.

Manual Metal Arc (MMA) welding is a process widely used for in situ repair work. The equipment is fairly mobile and may be carried as far as 100 metres from the power source. Being a manual process it may be used to overlay components with a relatively complex shape. Deposition rates vary between 1 and 7kg/hr with an overlayer thickness of 3mm and above. The resulting dilution depends on the welding technique and varies between 10% and 30%.

Gas Tungsten Arc welding is a high quality manual or mechanised process. It is a slow process with deposition rates of up to 2kg/hr and dilution of 4% to 10%. GTA welding is extensively used in the cladding of nuclear reactor components.

Plasma arc welding and its two versions plasma TIG and plasma MIG, all offer very good control of

profile characteristics due to the ability to control the arc heat distribution. This also minimises finishing requirements. Plasma TIG gives dilution of 5% and a deposition rate of 3.5 kg/hr.

A fully mechanised overlay process is submerged arc welding. The deposition rates are 10 to 30 kg/hr and above. This process uses cylindrical and strip electrodes for bulk deposition. Dilution is comparatively high due to the high rates of deposition.

Gas Metal Arc welding is a continuous process which means that there is no waste of electrode material as in MMA welding. GMA welding can be used in semi automatic or fully mechanised modes. The equipment is less transportable as it requires a gas bottle for the shielding gas and a wire feeder. Welding is restricted to around four metres from the wire feeder. It is possible however to increase the distance to fifteen metres with the aid of special intermittent wire feeders although in practice the length between the torch and the wire feeding mechanism should be kept to a minimum. Deposition rates obtainable with GMA are 1 to 8kg/hr, the deposit thickness may be from 3mm upwards and dilution varies from 10% to 30%. Pulsed GMA welding improves dilution and the use of flux cored wires which require no shielding gas increase the deposition rate up to 12kg/hr.

1.2.2 Materials.

The primary criterion in the selection of the overlaying material is the required surface properties of the component for the working environment in which it is

intended to be used.

Providing that the substrate or base material satisfies all but the surface requirements of the working environment a few considerations are in order concerning the resulting properties of the component during and after the overlaying process.

Contraction of the weld deposit during solidification may cause not only distortion of the component but also cracking. It is possible to avoid distortion by welding simultaneously and symmetrically from the neutral axis of the component. This may not be practical as it requires two welding sets and the dimensions and shape of the component may be too complex and unsuitable for this technique. To avoid distortions and cracking, it is common practice to preheat the workpiece. The preheat temperature depends on the material but for arc welding processes where the heat input is higher, the preheat temperature may be lower than that for gas welding.

The thickness of a deposit can in theory be built up as much as required. However, in practice this is limited by the hardness of the deposited material. Thick coatings have the advantage of lasting longer under wear conditions therefore delaying restoration. Weld deposits, with the exception of oxyacetylene and gas tungsten arc welding which may give a deposit thickness of 1mm, are at least 3mm thick. Hard materials are prone to cracking therefore multilayered deposits of alternating layers of hard and soft ductile weld metals may be applied in order to prevent the propagation of

cracks (Gregory 1980).

Overlay welding is a fusion process and metallurgical continuity exists between the weld deposit and the base material. During welding the fusion zone becomes a mixture of base metal and filler wire ie. dilution between the weld metals occurs. For gas welding dilution is less than 5%, for MMA, MIG, TIG and flux core wire 10-30%, while submerged arc welding gives 10-40% dilution. The amount of dilution depends on the welding parameters such as current, travel speed and welding technique. As dilution changes the composition of the weld deposit it can substantially change both the microstructure and the properties of the deposit. Dilution can be reduced with the deposition of two or more layers or by using a slow welding process where the deposition rate is low (Gregory 1980).

For some applications such as overlaying excavator blades or rock crushers, the surface finish is not important and the beads are left as welded. However, in most other applications machining is necessary which implies that the coating alloy must have adequate machinability. Some alloys can be softened by annealing then machined, then rehardened and followed by finish grinding.

1.3 Selected Materials and Welding Techniques.

This study investigates the deposition of an 18/10 austenitic stainless steel (316S92) on a mild steel shaft (070M20) using pulsed Metal Inert Gas Welding.

The base material, 070M20 drawn mild steel, is a

general use engineering material which exhibits reasonable mechanical properties, is machinable, weldable and relatively cheap. However, it is susceptible to corrosion and oxidation which limits its use. The overlaying material is 316S92 stainless steel which exhibits relatively good corrosion and oxidation resistance and is readily available in the market.

CHAPTER TWO

Gas Metal Arc Welding.

Chapter Two Gas Metal Arc Welding.

2.1 Introduction.

Gas Metal Arc welding, GMAW, is a fusion welding process where an arc is sustained between a consumable electrode and the workpiece. The electrode wire is fed to the weldpool through a specially designed welding torch by a wire feeder. The weldpool, electrode and arc are shielded and protected from atmospheric contamination by an externally supplied gas or gas mixture.

GMAW was first proposed by van Nuys and Roberts in 1919 and a variety of shielding gases were considered such as inert, active, and even combustible gases. In 1948 GMAW was developed from Gas Tungsten Arc Welding (GTAW), but instead of using a refractory tungsten electrode it employed a consumable electrode wire (Houldcroft 1977).

A schematic arrangement of the GMAW or pulsed MIG welding is shown in figure 2.1.

The GMAW process differed from other consumable electrode welding methods, notably manual metal arc welding, because new concepts of current density, electrode feeding methods, control and adjustment of the arc length, travel speed and operator skill requirements emerged. Perhaps the most important of all these differences was the manner in which the droplets from the electrode wire detached and transferred across the arc (Tuthill 1954).

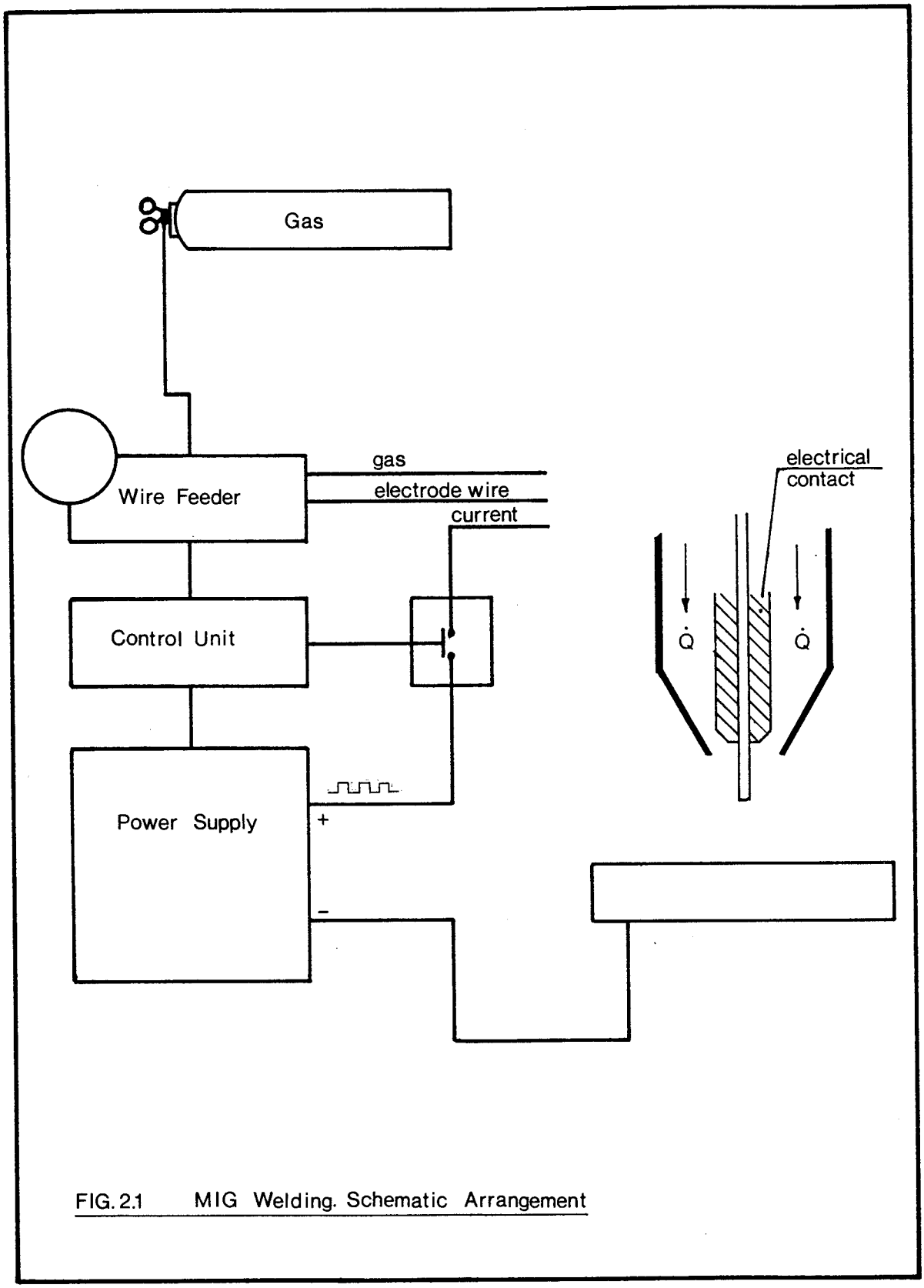

FIG. 2.1 MIG Welding. Schematic Arrangement

Although GMAW was closely associated with the welding of aluminium, most common engineering metals such as steels, copper, copper alloys (Moore & Taylor 1955) and nickel and its alloys were weldable.

The increased range of applications gave rise to a number of GMAW variations such as Metal Active Gas Welding (MAG) or CO_2 welding, Flux Cored Welding, Rapid Arc Welding (Craig 1987), Plasma MIG and pulsed MIG welding. Much of the recent development of the process can be attributed not so much to new ideas but to the progress of solid state electronics and computers. Pulsed MIG welding is an example of this, because when it was introduced (Needham 1965) (Needham & Carter 1965), pulsed current frequencies were limited to multiples and fractions of the mains frequency. However, once frequency modulation became possible, pulsed MIG welding had become after fifteen years of being a theoretical curiosity, a versatile advanced GMAW process.

At present, design and development of "intelligent" power sources is taking place where by incorporating a microcomputer in the power source the optimum electrical parameters for the material used can be automatically computed and set by the power source itself.

2.2 The Gas Metal Welding Arc.

The welding arc is a gaseous conductor which transforms electrical energy into heat; electrical discharges between the anode and the cathode are formed and sustained by the development of a gaseous conduction

medium, the arc column, which is made up of gas and/or electrode metal vapour. The current carriers in the arc column are electrons and are produced by thermal means and field emissions (AWS 1976).

The electrodes have a cooling effect and the arc column cannot exist in the region near the electrodes, thus a high voltage drop ensures continuity of conduction. The voltage drops at the electrode regions are, 1 to 12V for the anode region and of the order of the excitation potential of the electrode vapour for the cathode region. This is approximately 10V (fig 2.2).

The voltage gradient near the anode is of the order of 10^6 to 10^7 V/m (Block & Finkelnberg 1953). The voltage gradient of the arc column is as low as 10^3 V/m, as against that of the cathode region which may exceed 10^9 V/m (Guile 1979).

Near the electrode regions there are high electric fields which give rise to a higher concentration of electrons in the anode, and to positive ions and electrons in the cathode. These regions are called contractions and as they tend to restrict the current flow, they may have a temperature higher than that of the rest of the arc column. Direct measurements in the arc are very difficult to make due to the physical size of its constituents. However, indirect observations show that the anode current density is from 10^6 to 10^9 A/m^2 (Guile et al. 1975), the thermionic cathode current density is from 10^6 to 10^8 A/m^2, and the non thermionic Cathode current density is above 10^{10} A/m^2.

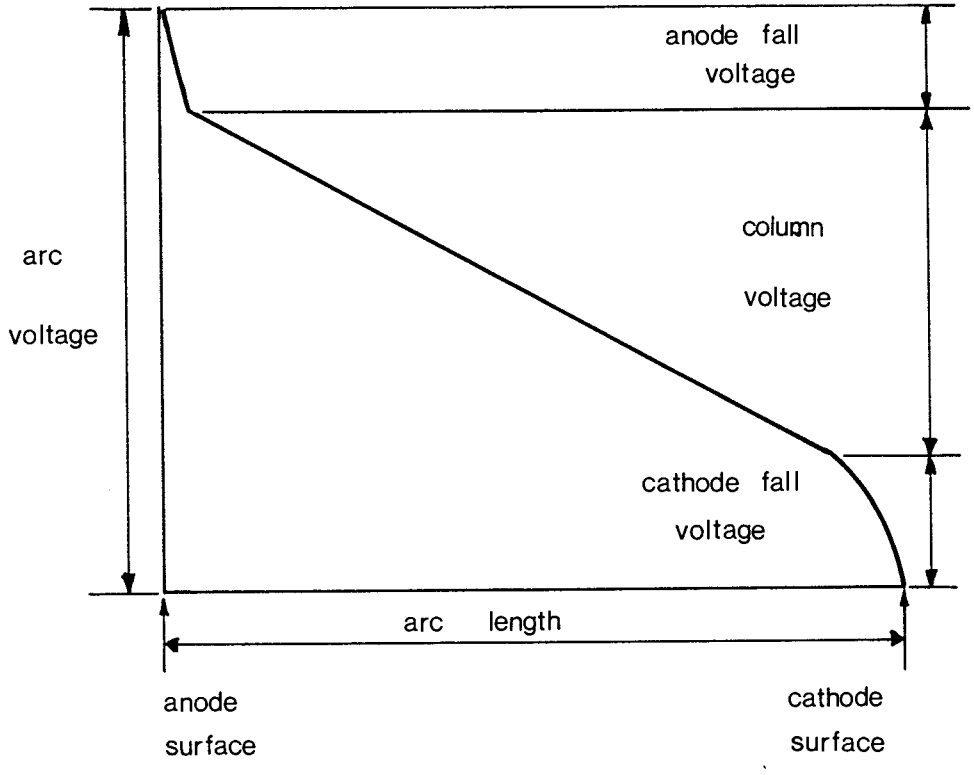

FIG. 2.2 Schematic Representation of the Voltage Distribution across the Arc.

2.2.1 Anode, Arc Column and Cathode.

The Cathode and Anode regions have many similarities. However, less research has been carried out on the nature of the anode. This is due to a tendency amongst researchers to agree that although the anode plays a vital part in preserving the current continuity by receiving an electron flow, it has less influence on the arc than the cathode. In addition most of the research has been focused on Gas Tungsten Arc welding which uses the electrode in negative configuration.

2.2.2 Anode.

The current in the anode region, under normal conditions, is carried entirely by electrons. However, positive ion emission may occur due to the existence of surface impurities at the electrode (Ludwig 1967). An area of contraction exists between the column and electrode and there is a voltage drop extending over a very small distance from the electrode as a result of the space charge. The low voltage drop near the anode implies that the positive ions must be formed very near to the anode surface. For carbon arcs this has been estimated to be of the order of 10^{-5} m (Block & Finkelnberg 1953).

The energy supplied to the anode is mainly due to the kinetic energy of the incident electrons. However, additional energy sources may be heat conduction and radiation from chemical reactions and Joule heating.

Energy losses from the anode may be caused by the vaporisation of metal atoms, by relatively large metal particles being driven from the anode, by radiation

from hot spots on the anode surface, by dissociation of molecular gases at the heated anode surface, by heat conducted away through the anode structure, and by heat conducted or convected away to the surrounding gas. In addition energy losses may result from ion emission (Lancaster 1986).

2.2.3 Arc Column.

The arc column is the part of the arc located between the cathode and the anode. It is electrically neutral and is composed of neutral particles such as atoms and molecules, both in excited and non excited state, and charged particles such as electrons and ions. In order for the arc column to conduct it has to be maintained at a temperature sufficiently high to be ionised. The gas temperature depends on and varies with the nature of the electrodes and the gas. For most arcs at atmospheric pressure this is about 6000° C (Suits et al 1939).

The high temperature causes dissociation and ionisation of the metal vapour and, to a much smaller degree, of the shielding gas. Due to the electrical neutrality of the column, or the absence of space charge an electric field is set up. The field is of the order of 10^3 V/m and causes the electrons to move towards the anode and the positive ions towards the cathode.

The mobility of the electrons makes them carriers of virtually all the current. The column temperature is maintained by the fact that the electrons passing through the electric field acquire energy which

is dissipated by direct collision with neutral atoms.

2.2.4 Vapour and Plasma Jets.

Vapour and plasma jets can greatly influence the appearance and directionality of the arc which in turn can affect the metal transfer characteristics as well as weldpool formation. The jets that originate at the electrode surface are called vapour or anode and cathode jets and they tend to be almost perpendicular to the electrode surfaces for some distance away from them.

Vapour jets may be generated by bulk ebullition of electrode material such as cadmium, zinc, copper and brass and may sometimes contain relatively large pieces of unmelted electrode material which have been ejected by the explosion of gas inside the electrode.

The vaporisation of surface layers of metal oxide and other impurities at the cathode or anode spot, due to the interaction of charged particles with the surface of the electrodes may cause the formation of vapour jets.

In addition vapour jets may be formed as a result of chemical reactions. For example the oxidation of carbon in steel may generate gases, such as carbon monoxide and carbon dioxide.

The plasma jet is an electromagnetically induced flow of gas in the arc column which is directed away from the constriction at the electrode.

2.2.5 Cathode

In the cathode, the current may be carried by positive ions as well as by electrons because electron emission also takes place. Electron emission from a surface can occur due to an applied external electric field provided it is large enough and enhanced by surface roughness, oxide films, non metallic impurity inclusions, surface layers of positive ions, elevated temperature and variations of fields with time.

There are two types of cathode in arc welding, the non thermionic and the thermionic. The temperature of a non thermionic cathode spot is too low for thermionic emission of electrons; it is thus called a cold cathode. Usually a thermionic cathode has a fixed spot whereas a non thermionic is characteristically mobile. This mobility is caused by oxides or other areas with higher emissivity. A cathode spot has many emitting sites that operate simultaneously by breaking down and regenerating when the current is redistributed to neighbouring emission sites activated by an ion bombardment. Emissivity is short lived $2\text{-}3 \cdot 10^{-6}$s for vacuum arcs on solid cathodes. For copper and steel the corresponding values are approximately 10^{-9}s (Guile and Hitchcock 1978).

Electron emission takes place when the cathodic material is sufficiently heated. The current density from thermionic emission depends critically upon the surface temperature and unless this can be increased to a sufficiently high value, it is not possible to reach the current densities encountered in welding arcs.

2.3 Gas Metal Arc Welding Process Parameters.

Gas Metal Arc welding is a complicated process consisting of a number of variables. It is therefore essential to be able to identify each parameter and assess their influence on the process. It may be advantageous to place the parameters into various groups in order to simplify the analysis. It is difficult however, to isolate a single parameter or a group of parameters from the others and determine its influence on the process, because they tend to interact with each other.

The grouping of the parameters may differ depending on the manner in which the process is being viewed. Here, three groups of parameters have been considered; the electrical parameters group which consists of the variables set by the power source; the materials parameters group which deals with the materials and shielding gas used; and finally the welding techniques group which considers the parameters that are not classified within the previous groups (fig. 2.3).

2.4 Electrical Parameters.

2.4.1 Welding Current.

The welding current is the primary variable of the process because it regulates the heat input to the electrode wire (melting rate), the heat input to the workpiece, and the type of metal transfer. It also gives rise to secondary effects such as dissociation and chemical reactions which contribute to the change in shape of the bead.

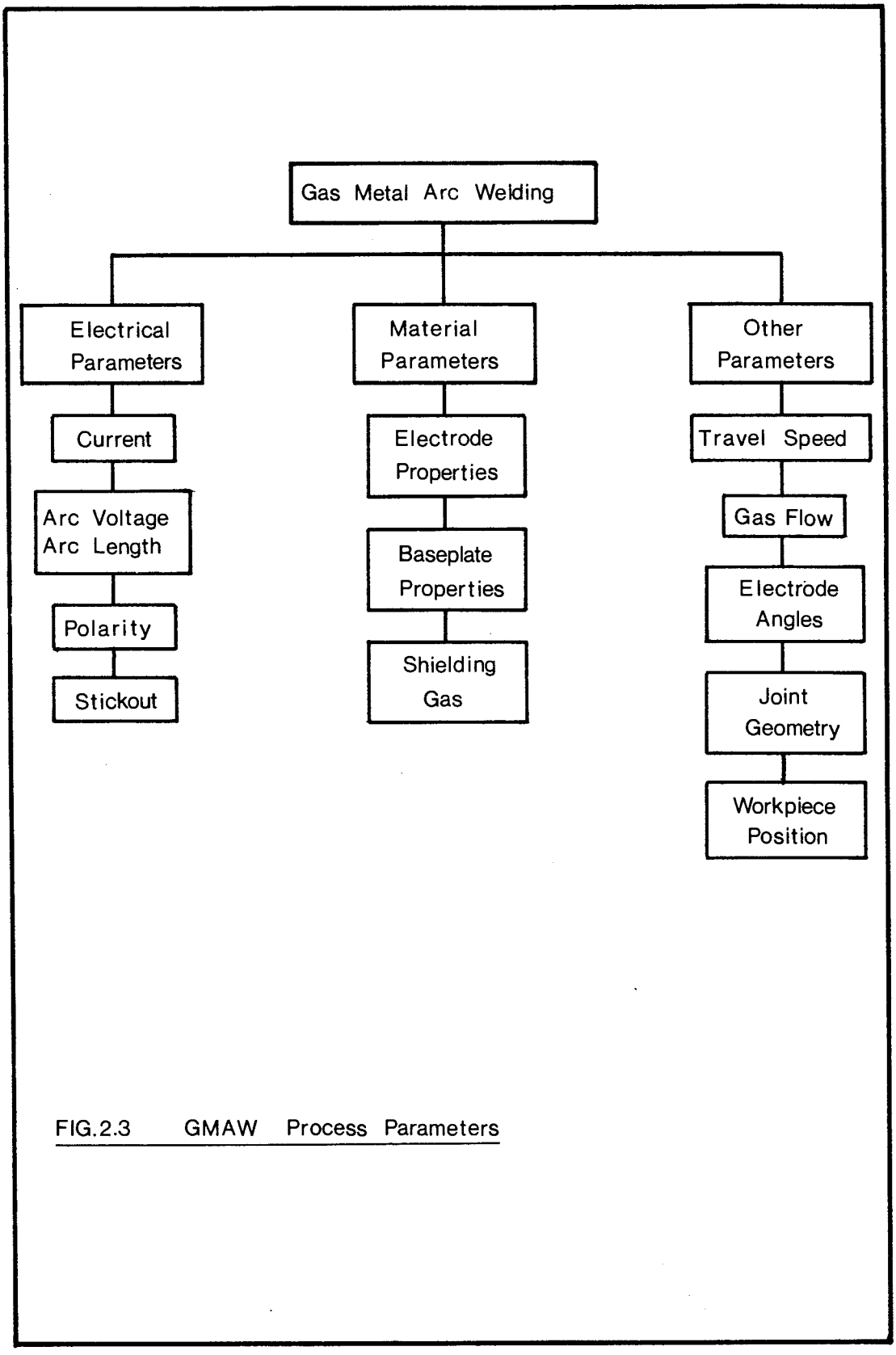

FIG.2.3 GMAW Process Parameters

2.4.2 Arc Voltage and Arc Length.

The arc voltage depends on many factors including the welding current, arc length and shielding gas. It is associated with the activation of emission sites in the cathode area and affects the arc stability, metal transfer and heat distribution to the weldment.

The arc voltage is closely related to the arc length. The total potential of the arc generally tends to increase if the arc length increases because a greater requirement on the maintenance of the charge carrier is imposed due to radial losses and decreased arc efficiency. Similarly, if the welding current is increased the arc voltage will tend to increase too. This has been attributed to the same reasons of decreased arc efficiency due to radial losses (Niles & Jackson 1975) (Ghent et al. 1979). Therefore in order to maintain the conductivity of the arc column the potential must be increased (fig. 2.4) (Jackson 1960).

High or low voltage settings cause problems with metal transfer resulting in spatter and short circuit respectively which in turn give rise to a porous and defective deposit.

2.4.3 Polarity.

Welding can be performed with the electrode as the cathode (straight polarity) or with the electrode as the anode (reverse polarity). There are significant differences in the deposition characteristics when the two different polarities are applied. The velocity of the detaching droplets is observed to be lower with straight

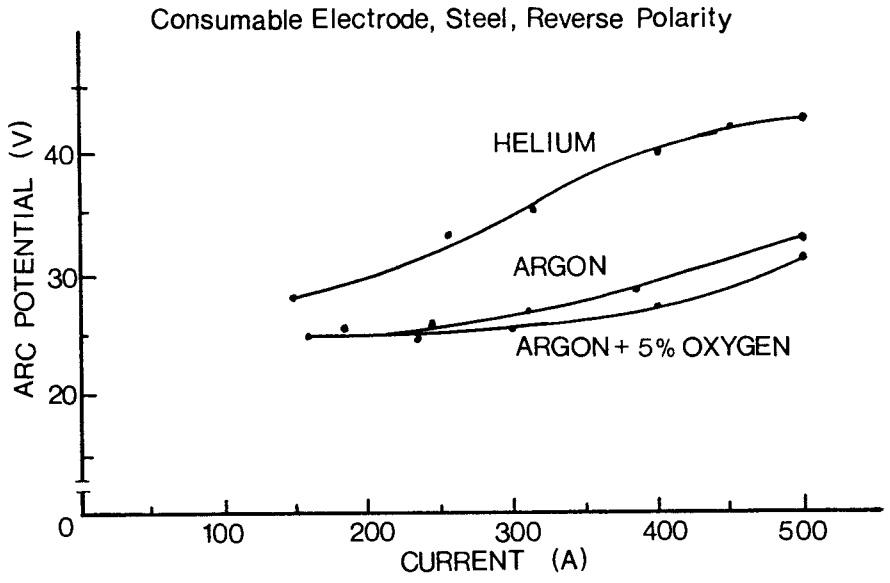

FIG.2.4 Voltage-Current Characteristics of Consumable Electrode

Arc System

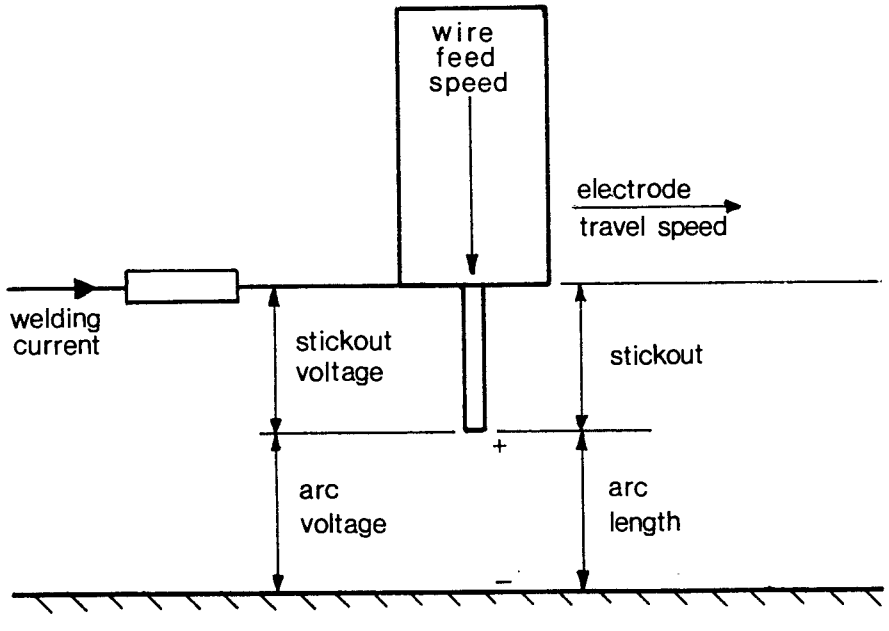

FIG.2.5 Terminology

polarity and this may be explained by the fact that the cathode tends to be displaced above the droplet thus reducing the area and subsequently the pinch force (Essers & Walter 1979) (Houldcroft 1977).

Reverse polarity in gas metal arc welding is the usual practice as it results in better metal transfer characteristics and consequently better fusion, but it increases both penetration and dilution. In addition reverse polarity lowers the transition current from projected to streaming spray transfer (Felmley 1955).

The use of alternating current has not been commercially accepted because the arc extinguishes every half cycle as the current reaches its zero value. This results in stability problems especially when the cathode is not sufficiently heated.

2.4.4 Other Polarity Associated Effects.

When welding in reverse polarity, the cathode may be displaced by higher emissivity sites which in practice are metallic oxides. The travelling arc enters new surface regions prepared for cathodic function by arc emitted radiation. Local discharges are attracted by surface oxides which have higher emissivity than the metal. Some metals form oxides that vaporise at rather low temperatures and others melt before the base metal liquefies thus shrinking out of the path of the cathode. However, if the oxides are refractory, they tend to overheat as the cathode focuses on them. Local evaporation of the metal under them causes an explosion thus removing the oxide from the weldpool (Mantel 1962).

This cleaning effect is quite advantageous as the weldpool avoids contamination, however, excessive amounts of oxides may cause spatter giving rise to defective deposits.

2.4.5 Stickout.

The stickout is the length of the electrode wire which is electrically live. The length of the stickout influences the amount of electrode resistance heating which in turn affects the actual melting rate. Increasing the stickout increases the electrode melting rate thus, for a constant welding current, the deposition may be controlled. Long stickouts in the range of 25.4-100mm have been reported to decrease penetration down to virtually nil (Wilson et al. 1956) (Lesnewich 1958) (De Long et al. 1960). In order to exploit the benefits of resistance heating but to avoid the inconvenience of long stickouts, specially designed welding torches (Stol 1989) can preheat the filler wire independently of the power source.

The terminology of the electrical parameters is schematically represented in figure 2.5.

2.5 Material Parameters.

This group of variables consists of the filler wire, the shielding gas and the base material.

2.5.1 Filler Wire.

The properties of the material as well as its physical dimensions play an important part. The diameter of the wire affects the current density; higher current densities concentrate heat transfer over a small area resulting in deeper penetration.

During welding some vaporisation of the filler wire takes place. If the vapour pressure of a metal is high, a back reaction thrust is generated and the droplets tend to be repelled from the plate. This applies irrespective of polarity. For metals with low vapour pressure a plasma jet is generated which, combined with the pinching effect causes a change in tip geometry leading to streaming spray transfer. Metals which have high thermal conductivity do not exhibit any transition from projected spray transfer to streaming spray transfer, whereas metals with low heat conductivity do (Cooksey & Milner 1962).

The arc stability, metal transfer, deposition rates and consequently penetration, size and shape of the deposited bead may be altered if dilute coatings of certain metals and oxides are applied on the electrode wires (Lesnewich 1955) (Hazlett & Parker 1956) (Hazlett 1957) (Agusa et al. 1981).

2.5.2 Base Material.

The welding of similar materials requires examination of joint geometry and choosing the right welding conditions for the thickness and dimensions of the base material. However, when dissimilar metals are to

be welded, in addition to the above considerations, comparison of the physical properties of the materials is necessary in order to establish the compatibility of the electrode material and the base material.

2.6 Shielding Gas.

The selection of the shielding gas depends on the materials welded, its function, the costs involved and the environmental effects ie. health hazard.

The basic function of the gas is to shield the arc and the weldpool from atmospheric contamination. To do this, it must be delivered in sufficient quantity and in an effective manner. Insufficient gas flow may not provide adequate shielding of the arc and weldpool and may be susceptible to external disturbances such as draughts. High gas flows may give rise to turbulence thus resulting in the contamination of the gas shield with air (Autio et al. 1980).

Shielding gases may be used to regulate the heat input to the electrode wire and the weldment. Gases with higher ionisation potential such as Helium give rise to "hotter" arcs because when ionised particles return to their ground state they liberate their ionisation energy. In addition, the conductivity of the gas affects the heat distribution, the higher the conductivity the wider the heat distribution (Lancaster 1986).

The atomicity of the gas also affects the characteristics of the arc. At high currents, diatomic gases such as nitrogen, oxygen, hydrogen, and carbon dioxide tend to dissociate near the electrode region and

associate near the weldpool releasing their dissociation energy thus increasing the heat transferred to the weldpool (Sambamurti 1983). For the common diatomic gases the energy levels of ionisation are much higher than that for dissociation, thus dissociation occurs before ionisation.

In some cases pure inert gases are not the best to use and the addition of active elements may be beneficial with respect to the stability of the arc and the appearance of the bead profiles. Active elements stabilise the arc by increasing the emission sites, and also cause changes in the surface tension of the electrode and the weldpool (Salter & Dye 1971).

The effects of the gas on arc characteristics may be decreased by the fact that the arc column is contaminated by metal vapours of very low ionisation potential (Dunn et al 1986). However, surface tension changes are likely to be less affected by such contaminations (Dunn & Eagar 1986).

A big disadvantage of some active elements and rare earths is that they are poisonous eg. chlorine in argon in aluminium welding (Patchett 1978).

2.6.1 Shielding Gases and their Properties.

The pure gases and gas mixtures most commonly used for the welding of stainless steel are presented below:

Commercially pure argon was the first gas to be used in MIG welding. As it is 1.4 times denser than air it is an excellent shield. Despite its satisfactory

shielding effect and metal transfer stability it has an adverse effect on the shape of the bead as it promotes finger penetration which is very undesirable in welding.

The argon oxygen mixtures with up to 5% oxygen are used in the welding of stainless steel, especially fully austenitic ones where control of the weld metal composition is important. The addition of an oxidising medium in the arc improves the stability of the arc and metal transfer. In addition it tends to lower the surface tension of the weldpool thus reducing porosity. The association of the oxygen at the weldpool enhances penetration giving a good quality weld (Wilson 1981).

Up to 5% oxygen gives good wetting properties as FeO is formed which is easily melted and has high fluidity. However, over 5% oxygen the FeO tends to react with carbon to give Fe+CO which may cause porosity.

The use of pure carbon dioxide for the welding of stainless steel is usually unacceptable due to carbon pick up. The use of argon and carbon dioxide reduces carbon pick up by the weldpool and combines the advantages of each gas. The mixture of 80% argon 20% carbon dioxide is regarded as the optimum for welding ferrous metals and can be used for stainless steels as long as it is metallurgically acceptable. Argon promotes good spatter free spray transfer and carbon dioxide hinders finger penetration.

The mixture of argon, carbon dioxide and oxygen is basically impure argon and it contains approximately 2% oxygen and 0.2% nitrogen with 5 to 20% carbon dioxide. This gas is used for welding ferrous metals and stainless

steel provided it is metallurgically acceptable. The addition of carbon dioxide is claimed to be superior to oxygen in the welding of ferritic steels because it reduces porosity by reducing weldpool surface tension effects (Boughton et al 1967).

CHAPTER THREE

Metal Detachment and Transfer in GMA Welding Process.

Chapter Three Metal Detachment and Transfer in the GMA Welding Process.

3.1 Introduction.

The conditions under which a droplet of molten electrode wire is formed, detached and transferred to the weldpool strongly influence the size, shape and the possible presence of weld defects in the resulting deposit. The parameters that affect and set such conditions are mainly the arc current, the pressure of the environment, the wire composition and diameter, polarity, voltage and shielding gas composition. When welding under ambient pressure conditions, the parameter which has the most profound effect is the arc current. All other parameters have a secondary effect, minor in comparison to that of the arc current. Additionally, in some cases they tend to depend on the arc current. Usually where interaction between the current and another parameter takes place, the secondary effect is enhanced by the current increase.

3.2 Transfer Types.

There are three types of metal transfer as classified by the International Institute of Welding (Lancaster 1986), Free flight Transfer, Bridging Transfer and Slag Protected Transfer. They are presented here as adapted for the Gas Metal Arc processes, Metal Inert Gas (MIG), pulsed Metal Inert Gas (p-MIG), Metal Active Gas (MAG) and Flux cored welding. The classification is based

on their physical characteristics, that is the shape and manner in which droplets detach (fig. 3.1 & fig. 3.2).

3.2.1 Free Flight Transfer.

At low welding currents globular transfer takes place with large droplets detaching from the electrode wire.

In reverse polarity the droplets are symmetrical and elongated because the anode spot is formed symmetrically around the electrode tip.

In straight polarity a mobile cathode spot is formed which upsets the symmetrical evolution of the droplet. This, combined with an upwards reaction thrust caused by the cathode repels the droplet sideways and upwards.

In CO_2 (MAG) welding the dissociation of the gas near the electrode region has a cooling effect which reduces the anode or cathode spot, depending on the polarity, to less than the drop diameter. The converging current causes an upwards force (Defize et al. 1960) which, combined with an upwards force caused by the metal vapour pressure hinders detachment and displaces the droplet upwards. This type of detachment is called repelled transfer.

In both globular drop and repelled transfer positional welding is not possible which suggests that detachment is predominantly dependent on the balance between gravitational forces and surface tension.

As the current is increased the droplets become smaller and the frequency of detachment increases. When

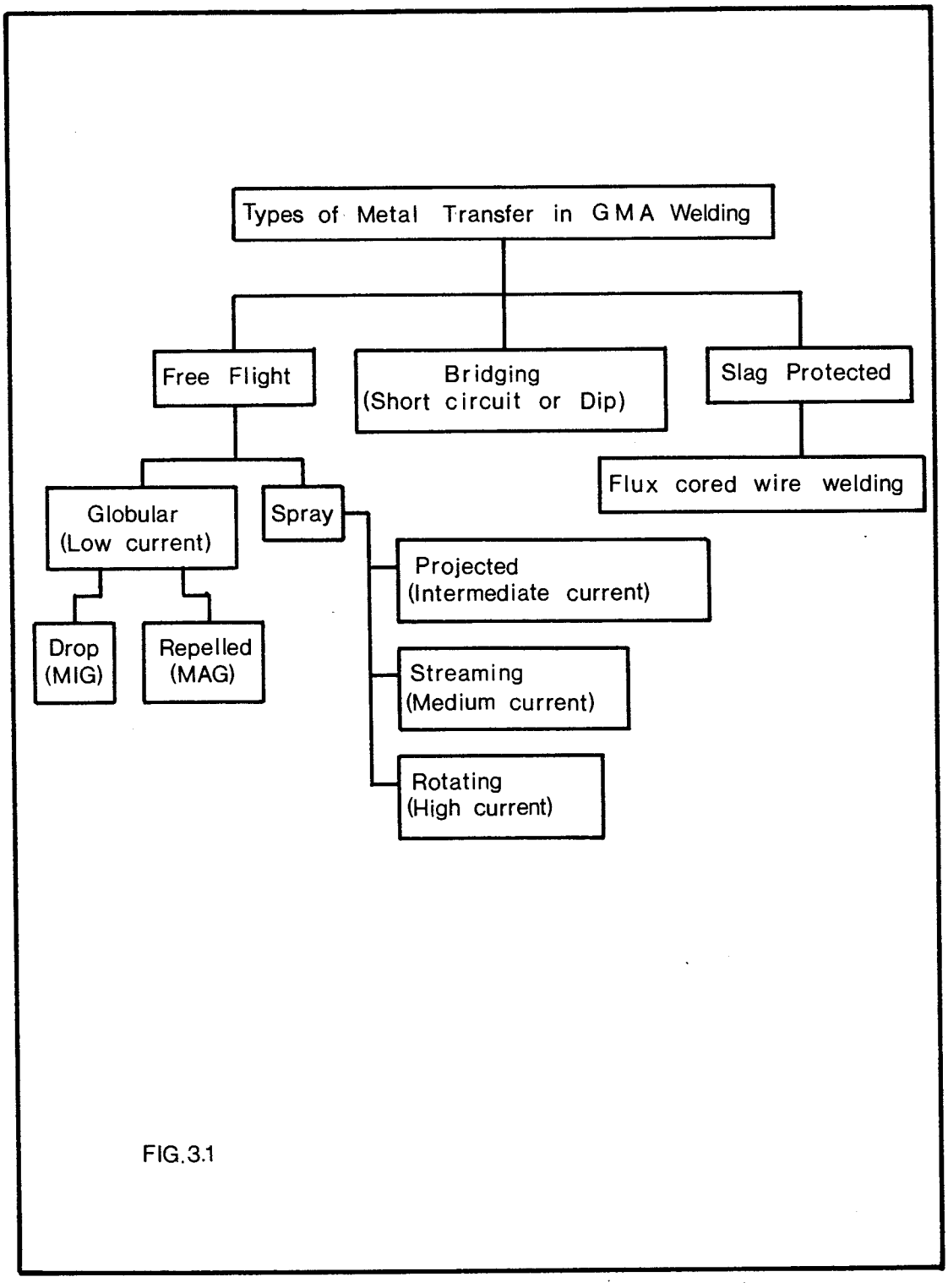
Types of Metal Transfer in G M A Welding
Free Flight
Bridging
(Short circuit or Dip)
Slag Protected
Flux cored wire welding
Globular
(Low current)
Spray
Projected
(Intermediate current)
Drop
(MIG)
Repelled
(MAG)
Streaming
(Medium current)
Rotating
(High current)

FIG.3.1

their acceleration is such that detachment is independent of gravity then this type of detachment is called projected spray. The size of the droplet diameter varies between 1.5 and 0.9 times the electrode wire diameter.

Further increase of current gives rise to another transfer mode called streaming spray transfer. This mode has a fundamental difference from both drop and projected transfer as there is a change in electrode tip geometry, the tip becoming conical in shape. This is caused because at high arc currents the anode tends to "climb up" the electrode, heating and partially melting its sides. It is possible that the increased pinch force (contraction) may mechanically deform the "paste like" solid + liquid area aiding tapering (Jilong Ma & Apps 1983a). The liquid flows towards the electrode tip and detaches in a streaming array of very small diameter droplets.

At even higher current levels a rotating electromagnetic field is set up which makes the tapered part of the wire rotate in a spiral causing the droplets to be ejected sideways. This transfer mode is called spray rotating but more commonly rotating.

3.2.2 Bridging Transfer.

Metal flow from the electrode to the weldpool is not achieved by the evolution and detachment of droplets but by the controlled "dipping" of the electrode into the weldpool.

The arc is struck and some melting occurs at the electrode tip but no detachment takes place. As the wire

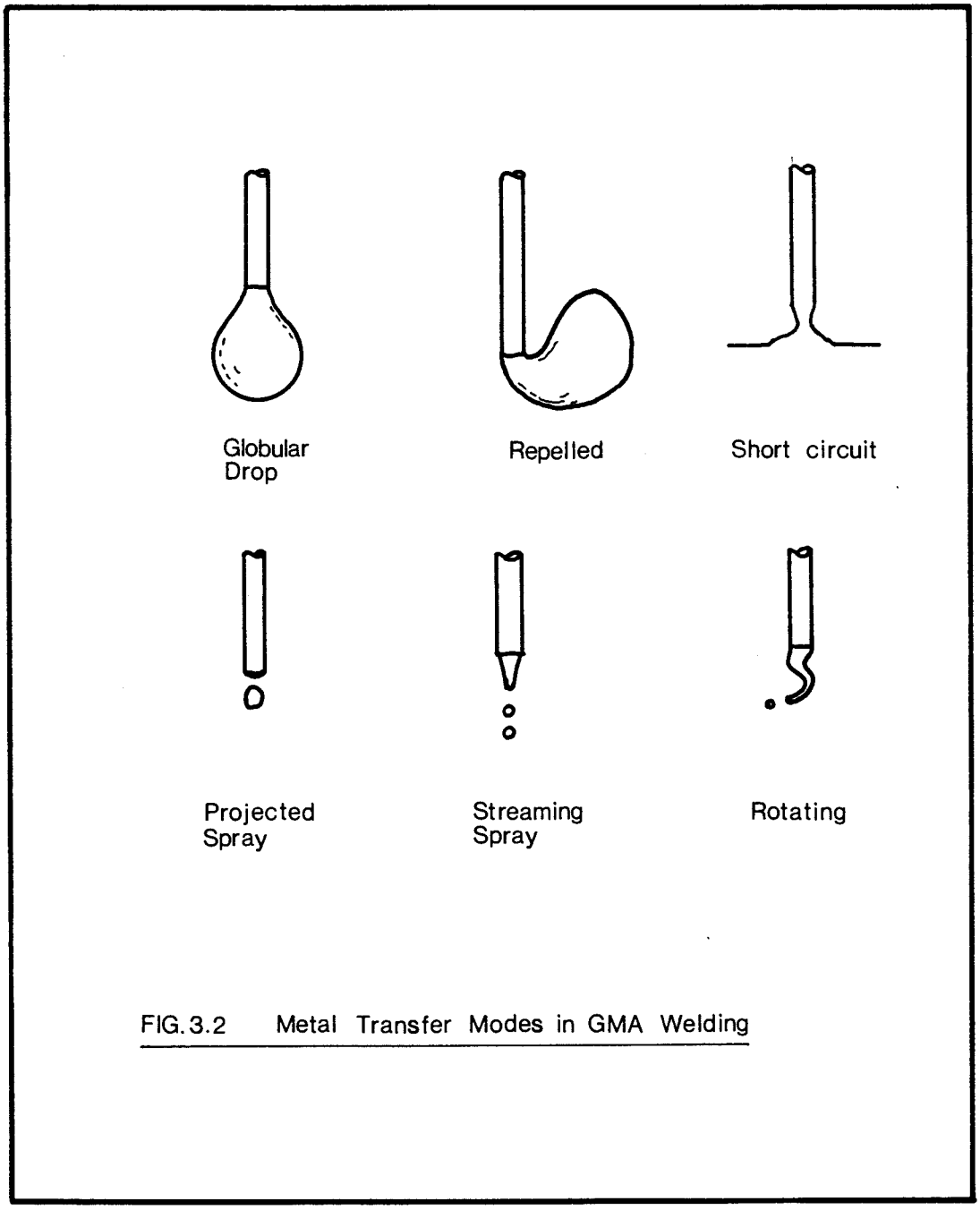

FIG. 3.2 Metal Transfer Modes in GMA Welding

feed speed is set at a higher rate than the melting rate of the electrode, the electrode comes into contact with the weldpool. Then the arc is extinguished and more melting takes place by resistance heating. Surface tension and electromagnetic pinch then ruptures the liquid portion of the electrode and the arc is ignited again. The cycle is then repeated.

3.2.3 Slag Protected.

Slag protected metal transfer takes place in flux cored welding. The detaching droplets are engulfed by the molten slag and thus are protected from oxidation. Flux cored welding may use additional gas shielding.

3.3 Droplet Evolution in Free Flight Transfer.

3.3.1 Globular transfer.

The electrode is heated up by joule heating due to its resistance and by electron absorption at the anode spot at the solid electrode tip. Local melting takes place and heat transfer occurs from the liquid anode surface to the solid metal by conduction and convection.

Convection currents within the evolving droplet can be formed by electromagnetic forces generated by the current diverging through the drop (Maecker 1955), by the liquid entering the droplet (Abonnenc 1925), by a gradient in the surface tension caused by a high temperature gradient across the droplet (Pearson 1958). Buoyancy forces may be neglected as their ratio to the dominating electromagnetic forces is of the order of 0.01 (Waszink et al 1982).

Flow patterns in droplets may hinder or aid metal transfer. If flow takes place downwards along the vertical axis then it will tend to elongate the droplet and aid detachment by inducing a secondary force at the neck of the droplet. If the generated flow is upwards then the drop will tend to become more oblate and therefore hinder droplet detachment. It has been shown that steady state flows caused by electromagnetic forces take a time of the order of 1s to develop fully (Sozou & Pickering 1976). This length of time is far in excess of the frequency of detachment that is encountered in DC and pulsed GMA welding in the projected spray transfer region. Nevertheless, metallurgical observations suggests that some flow patterns, although not fully developed, are present in the droplet (Lancaster 1987).

The formation and detachment of a droplet especially in globular transfer depends very much on the size of the anode or cathode spot. If the welding current diverges through the droplet a force is generated which aids detachment whereas if the current converges through the droplet a generated upper thrust hinders detachment (Greene 1960) (Cooksey & Milner 1962).

Direct effects of surface tension or indirect effects such as generation of flow fields during droplet detachment appear to play an important role in the globular transfer mode. However, the addition of various active elements to alter the surface tension effects and control metal detachment is most likely to enhance the stability of the arc and increase the anode spot area and aid detachment.

3.3.2 Streaming Spray Transfer.

This type of transfer is characterised by a continuous flow of liquid metal down the conical tip of the electrode. Analysis of film images shows that the velocity of the liquid below the tip is between 1.0m/s and 2.5 m/s. The thickness of the flowing film which surrounds the tip is of the order of 0.1 mm. The outer surface of the liquid acts as an anode and its temperature increases in the direction from the base to the tip of the cone (Villeminot 1967). The liquid is accelerated downwards by electromagnetic forces while the heat evolved at the surface is partly carried away by the flowing material and partly transferred to the solid cone by conduction. It has been found that the thickness of the boundary layer between the liquid and the solid is about the thickness of the whole flowing layer (Waszink et al 1982). Analysis of this model is limited due to the lack of information concerning the distribution of current density over the anode surface.

3.4 Metal Detachment Models

There are two models that have attempted to describe metal transfer from the electrode to the weldpool. These are namely the static forces model and the pinch instability model. In the static forces model detachment occurs when the forces aiding detachment are equal to the forces hindering detachment. The pinch instability model considers detachment to occur after a critical length of the droplet has been reached and an instability has been initialised. A brief outline of both

models is presented in the following sections.

3.4.1 Static Forces model.

The forces acting on the drop or the liquid tip of the electrode are gravity Fg, a drag force due to the flow of gas around the drop Fs, the electromagnetic force Fem and a surface tension Fc. Surface tension acts against detachment.

Thus detachment occurs according to the mathematical expression:

$$Fg + Fs + Fem = Fc \quad \ldots\ldots\ldots\ldots\ldots\ldots \quad [3.1]$$

When pure gravitational detachment is considered, the electromagnetic force is neglected. The liquid detaches when the drop has reached a critical mass. Then the gravitational forces will equal the surface tension forces:

$$Fg \approx Fc \quad \ldots\ldots\ldots\ldots\ldots\ldots\ldots\ldots \quad [3.2]$$

The critical mass of the droplet for detachment to occur depends on the density of the liquid and the surface tension of the droplet. Both these factors are related and vary with temperature.

Plasma jets and the shielding gas flowing past the droplet generate drag forces. Although the droplet is considered to have a spherical shape a correction is necessary to account for the area that the electrode is sheltering (Waszink & Graat 1983).

At higher currents both gravitational forces and drag forces can be neglected and detachment occurs when:

$$Fem \approx Fc \quad \ldots\ldots\ldots\ldots\ldots\ldots\ldots\ldots \quad [3.3]$$

3.4.2 Pinch Instability Model.

The model is based on the dispersion of a liquid cylinder (Lord Rayleigh 1879) which carries an axial current (Northup 1907) (Murty 1960) (Murty 1961) (Lancaster 1979).

In this model the most significant effects are associated with the influence of current flow. The main force is the electromagnetic force which is generated either by the interaction of the current passing through the electrode with an externally applied magnetic field or with its own generated magnetic field (Lancaster 1979) (Lancaster 1986). This electromagnetic force will influence the pressure distribution and mass flow within the droplet. It will generate a static pressure in the surrounding arc plasma influencing the pressure field around the droplet. It will also generate a dynamic pressure in the form of a gas flow around the drop which exerts shear forces on the drop surface. Finally, the heating effects of the current will cause either surface evaporation which hinders detachment providing that the vapour pressure is higher than the surrounding atmosphere (Cooksey & Milner 1962), or ebullition from within the droplet which will aid detachment.

Other forces that affect detachment are: surface tension, hydrostatic pressure due to the fluid column, gravity and inertial and viscous forces.

Detachment occurs when the droplet has reached a critical mass or wavelength and an instability growth has commenced due to a minute disturbance. Disturbances may be the result of arc rooting erosion although wire

deformations and vibrations of the wire feeder are the most likely cause. The magnitude of those disturbances is of the order of 1-0.1% of the wire diameter with arc rooting effects being the smallest.

The model considers a sinusoidal liquid cylinder profile caused by sinusoidal disturbances. Dispersal of the cylinder into droplets will occur when the forces acting on the pinched regions are greater than the forces acting on the bulged regions Pp>Pb. If Pp<Pb then the bulge will tend to fill up the pinched region thus restoring the original shape of the cylinder.

Based on this model (Allum 1985a), the detachment in GMAW welding can be described by the following equation: (Allum 1985b)

$$T_{DC}(a_1 \cdot J^n + a_2 \cdot l \cdot J^{2+n}) = C \cdot R_e^m \cdot \gamma^x \cdot \delta^y \quad \ldots\ldots\ldots [3.4]$$

$$J = I/\pi R_e^2$$

m=0.166 x=0.278 y=2.722 C=192.7 n=1.556

The left hand side of the equation represents the welding current and the time for detachment. It can be clearly seen that both arc and resistance heating are taken into account. For materials with high resistivity such as steel and in particularly stainless steel, the term $(a_2 l J^{2+n})$ becomes significant. Contrary to that in alumunium welding this term is negligible.

The right hand side of the equation shows the effects of electrode wire diameter, tapering factor and surface tension.

Surface tension (γ) appears to play a less significant role than in the static forces model. In addition, the effects of surface tension on detachment

are simplified because of their complexity; hence it is assumed that surface tension is uniform over the surface of the droplet.

The tapering factor accounts for the various modes of metal transfer and can take values of $\delta>1$ for globular transfer, $\delta=1$ & $\delta<1$ for projected spray transfer and $\delta<<1$ for streaming spray transfer.

3.5 Discussion: Aspects of the Static Forces and Pinch Instability Model.

The static forces model is only valid up to the transitional region of projected to streaming spray transfer (Pintard 1966) (Waszink & Graat 1979) (Waszink & Graat 1983). The pinch instability model appears to have overcome the limitations of the static forces model and is applicable for the whole range of welding current.

3.5.1 Effects of Surface Tension on Metal Transfer.

The pinch instability equation, [3.4] may be used to calculate metal transfer characteristics of a welding electrode wire ie. the natural detachment times for any current or range of currents. However, in order to do so the material constants a_1 and a_2, surface tension of the liquid electrode, and the tapering factor must be known.

Table 3.1 shows the effects of surface tension on the natural detachment time of a type 316 stainless steel electrode for a given welding current. The surface tension data extend from 1.6N/m to 2.0N/m at the melting temperature of approximatelly 1470°C but the range

narrows as the temperature increases (Keene et al 1985).

table 3.1 Effects of Surface Tension on Natural Detachment Times

Surface Tension N/m	%(a)	T_{DC} ms	%(b)
1.6	0.0	1.07	0.0
1.7	6.8	1.09	1.8
1.8	11.1	1.11	3.6
1.9	15.2	1.13	5.3
2.0	20.0	1.14	6.1
Re=0.6•10-3 m, δ=0.8, I=180A, n=2			
%(a) percentage increase of surface tension %(b) percentage increase of natural detachment times			

It can be seen that a 20% change in surface tension results in a 6% difference in the natural detachment time. The scatter in the natural detachment time (T_{DC}) caused by the surface tension change when compared with the scatter in detachment times of 50% or more encountered in Chapter Five, is negligible. Indeed if the surface tension of the material is taken as 1.6N/m, in order to achieve a 30% change in the natural detachment times from purely surface tension effects, the value of the surface tension must be increased four times.

3.5.2 The Tapering Factor (δ).

The empirical nature of the pinch instability model is shown by the introduction of terms such as the tapering factor. Although (δ) as a term provides a solution to the problem of electrode tip geometry changes in different metal transfer modes, its value depends on qualitative information based on experimental

observations. In order to set a value for (δ), knowledge of the electrode material transfer characteristics is needed especially of the current levels at which metal transfer transitions exist.

CHAPTER FOUR

Pulsed MIG Welding: An Introduction to the Process.

Chapter Four Pulsed MIG welding: An Introduction to the Process.

4.1 Pulsed Metal Inert Gas Welding.

The major disadvantage of DC GMAW is that heat input and metal transfer are dependent on each other. For example the overhead welding of a thin plate is impossible if free flight transfer is to be implemented. Some control of metal transfer can be achieved by altering the voltage, or by using different mixtures of gases or even by attempting to alter the surface tension of the electrode in order to promote detachment. However, none of these solutions is really satisfactory. Pulsed MIG has been developed in order to overcome this significant disadvantage of the ordinary MIG process. Independence of heat input and metal transfer can be achieved if a pulse current configuration is implemented which results in high current type metal transfer at relatively low heat inputs. However, the pulse current configuration introduces extra electrical parameters that may complicate the process. In addition it is absolutely necessary to select the correct electrical parameters otherwise incorrect selection will inevitably give rise to a spattery unstable process which in turn will result in defective deposits.

The welding parameters in pulsed MIG are the same as in DC MIG with the exception of the welding current. There is a Pulse current (Ip), a Pulse duration (Tp), a Background current (Ib), a Background duration

(Tb) and a Mean current (Im) which corresponds to the DC configuration welding current. The pulse current configuration is shown in figure 4.1. The mathematical expression that correlates the pulse and background parameters is:

$$Im=[Ip \cdot Tp+Ib \cdot Tb] \div T \quad \ldots\ldots\ldots\ldots\ldots\ldots\ldots \quad [4.1]$$

4.2 Operational Stability.

There are three conditions that have to be met in order to assure a stable process. These are the burnoff balance, arc continuation and a regular metal transfer.

4.2.1 Burnoff Balance.

In GMA welding, as in any other welding process where metal transfer from an electrode to the weldpool takes place, the electrode melting rate and the electrode feed rate must be balanced. This is partly due to the requirement of a constant and uniform supply of filler wire to the weldpool and partly due to the requirement of a constant arc length. In manual operations such as manual metal arc, gas tungsten arc and oxyacetylene welding and brazing, the balance between the electrode and the melting and feeding is controlled directly by the skills of the operator. In GMA welding and in pulsed MIG welding this balancing is controlled electronically and mechanically by the wire feeder.

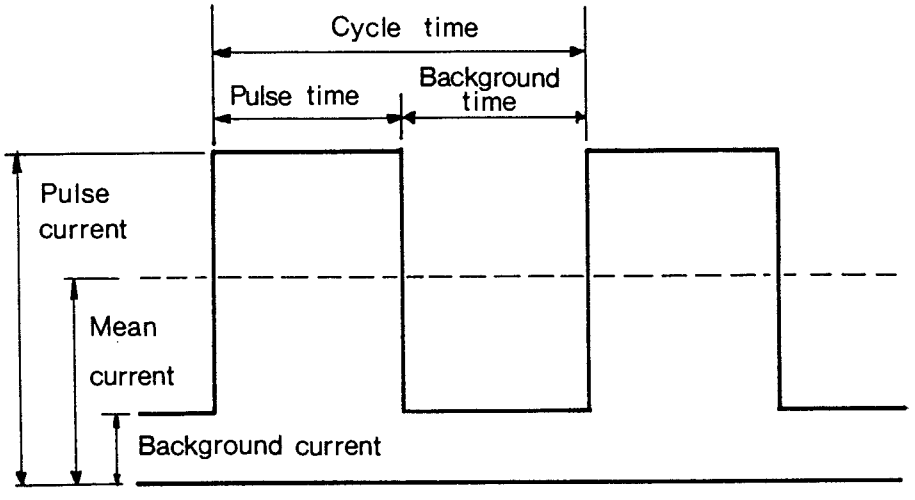

FIG.4.1 Pulse Current Configuration

4.2.2 Arc Continuation.

This relates to the lower limit of background current capable of keeping the arc ignited and stable. Typical values of the lower current limit for a range of electrode wire materials of 1.0-1.6mm diameters are 7.5-10A (Amin 1983). In pulsed MIG welding the background current is usually in the range of 50-100A, and therefore problems of arc continuation are not encountered.

4.2.3 Metal Transfer Stability.

The passage of droplets through the arc column causes a disturbance in the steady state of the arc. A regular metal transfer will cause less arc column disturbance than a series of irregular detachments with varying droplet volumes. Therefore, one of the requirements for a stable welding process is regular metal transfer. The same criterion for stability applies for pulsed GMA welding as well, and it is generally agreed that the smoothest metal transfer occurs when one droplet is detached at the end of every pulse. To achieve a detachment per every pulse, the correct pulse current and background current amplitudes and durations in relation to the melting characteristics of the electrode wire must be set. The fundamental goal is to have a low heat input where globular transfer would naturally occur and by the introduction of a high current pulse, produce a projected or streaming spray transfer. In DC MIG welding the relationship between the arc current and the droplet natural detachment time is given by the equation:

$$I^{n} \cdot T_{DC} = K \quad \ldots\ldots\ldots\ldots\ldots\ldots\ldots\ldots \quad [4.2]$$

The value of n depends on the material and has been found to be between 1.556 to 2.5 (Matsuda et al 1983) (Amin 1983) (Allum & Trindade 1984) (Allum 1985b) (Smati 1986). Equation [4.2] does not apply directly for pulsed MIG welding because the metal transfer mode is relatively independent of the welding current.

4.2.3.1 Spatter.

Spatter is an undesirable condition which causes electrode material losses, fusion defects, work surface damage and reduces weld quality. It is therefore important to eliminate the causes of spatter where possible.

A common cause of spatter is when the electrode comes into contact with the weldpool such as in short circuit transfer. Short circuit between the electrode and the weldpool has been observed during globular transfer with short arc lengths. It has also been reported, and supported by photographic evidence, that sometimes long pulse times tend to elongate the neck between the electrode and the droplet to such an extent that short circuit occurs (Ueguri et al 1985).

Spatter is present during repelled transfer because the droplets are detached as the neck is ruptured by an explosion. In addition the forces generated by the explosion give rise to a non symmetrical detachment (Defize & van der Willigen 1960) which may cause the droplets to scatter into and around the weldpool rather than to focus on one spot as in axisymmetrical detachment. Repelled transfer occurs during straight

polarity and CO_2 welding.

Spatter in globular transfer is caused by the overheating, ebullition and explosion of the droplets as they remain for a relatively long time in the arc column. Similarly in streaming spray transfer ebullition may arise at the tip of the taper causing the droplet to explode and disperse into spatter (Jilong Ma & Apps 1983).

Spatter may not be a result of irregular metal transfer or short circuit, but may originate purely from the weldpool. Local evaporation of the metal under refractory oxides during reverse polarity welding has the beneficial effect of cleaning the weldpool from such contaminants. However, if large concentrations of oxides are involved the severity of the cleaning effect may result in heavy spatter and defective deposits.

Spatter originating from the edge of the weldpool in fine droplet form has been observed when welding with a gas mixture of 75% Helium, 23% Argon, 2% CO_2 (Allum & Quintino 1984a).

EXPERIMENTAL PART.

CHAPTER FIVE

Metal Transfer in Pulsed MIG Welding.

Chapter Five Control of Metal Transfer in Pulsed MIG Welding.

5.1 Introduction.

This chapter examines the metal transfer characteristics in DC MIG and p-MIG welding of a 1.2mm diameter 316S92 stainless steel electrode wire in an Argon 1% Oxygen shielding gas atmosphere at positive polarity.

5.2 Natural Detachment Times.

The natural detachment times in MIG welding show the general transfer characteristics of any electrode wire for a given polarity and shielding atmosphere. The knowledge of the metal transfer characteristics in direct current MIG is essential in the selection of pulse parameters in pulsed MIG welding.

5.2.1 Introduction: Techniques for the Detection of Droplet Detachment.

The most commonly used technique to detect and record metal detachment during welding is by high speed cinematography combined with arc voltage measurements (Allum & Trindade 1984) (Jilong Ma & Apps 1983a) (Amin 1983) (Ueguri et al 1985). This method uses a high speed camera filming at a rate of approximately 3000 frames per second and a cathode ray oscilloscope measuring and displaying the arc voltage on the monitor. The cine

camera requires a double lens in order to film the arc as well as the monitor of the oscilloscope. Thus each stage of the droplet evolution, detachment and transfer can be correlated with the voltage wave form. The advantage of this process is that it provides direct viewing of the arc and the resulting electrical waveforms. However, the equipment and materials used are expensive and the set up for the right exposure of the film when a double lens is in use is not easy.

Another method involves the audio fingerprinting of the arc but the results are susceptible to acoustic interference which makes the interpretation of the results difficult (Arata et al 1979).

5.2.2 Experimental Arrangement.

The method employed during the present work was the measurement and recording of the arc voltage and the experimental arrangement used for this purpose is shown in figure 5.1.

The arc voltage was measured between a live point in the welding torch as close as possible to the nozzle tip and a point on the weldplate as far as possible from the earth (Street 1987).

The signal passed through a fuse box and an attenuator and was displayed on a cathode ray oscilloscope and recorded on tape by a variable speed audio recorder.

The fuse box was connected with both torch lead and return lead in order to provide total cut out in case adverse conditions arose. The attenuator gave a 10:1

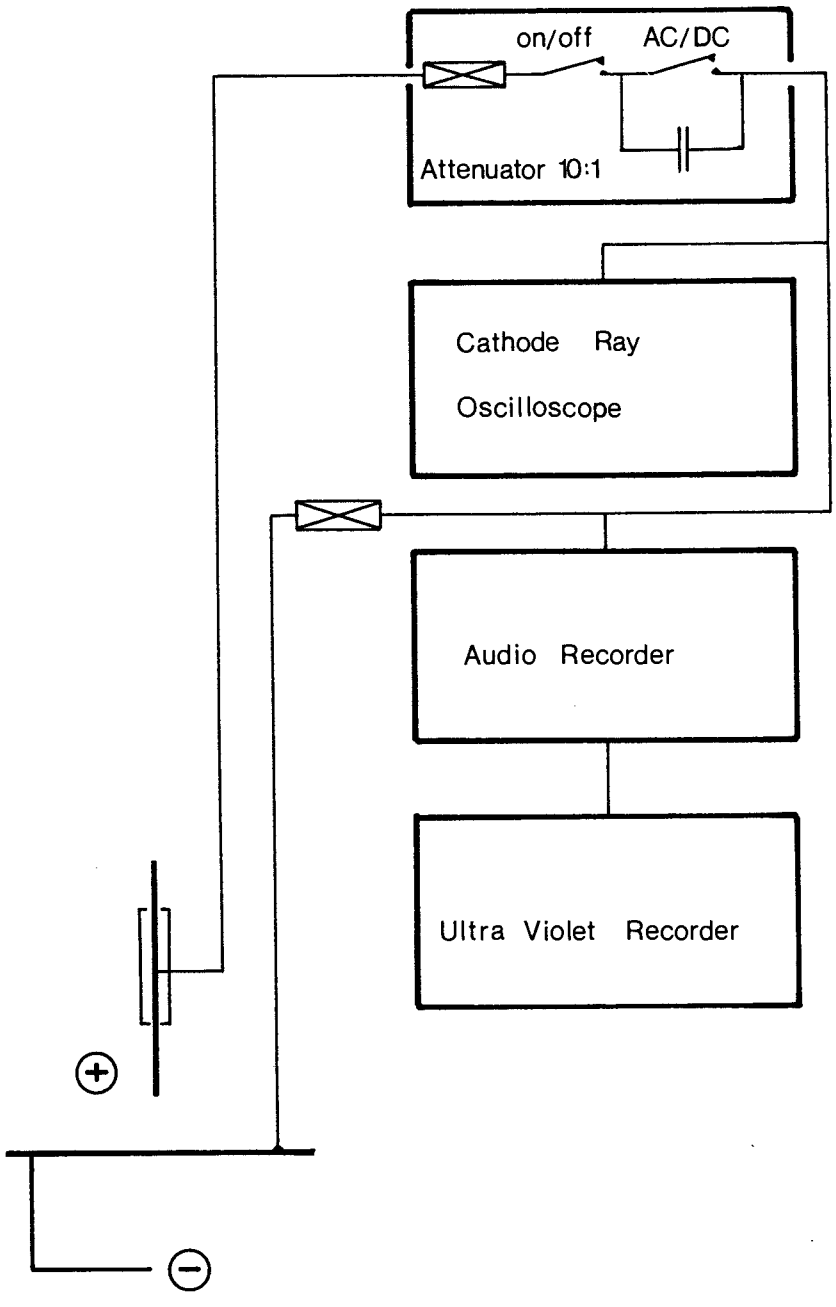

FIG. 5.1 Metal Detachment Recording Set up

ratio of input to output signal and had a dual purpose; it would prevent any signal distortions and in a severe case magnetic saturation of the tape. In addition data provided a choice of an AC or DC mode. The AC mode employed a capacitor which blocked all DC signals but allowed through only the sudden voltage changes, such as detachment spikes. The signal could be observed on the screen of an oscilloscope and it was recorded at a tape speed of 15 inches per second.

Tape recording has the advantage of instant playback for preliminary assessment. In addition, it can be stored and retrieved for printing on paper by means of an ultraviolet recorder or fed into a computer for further processing. Typical waveforms obtained for Direct Current during the present work are shown in figure 5.2.

Droplet detachment registers as a spike and the interval between successive detachment spikes is the detachment time. At low welding currents where globular transfer takes place the detachment times are easy to assess because the spikes are quite distinctive. At high welding currents where the droplet volumes are very small slight arc instabilities can lead to some difficulties in precisely defining droplet detachment on the oscilloscope trace. This exemplifies the need for the combined use of high speed photography with arc voltage readings. However, in order to avoid misinterpretations arising from any such conditions, records of traces found in literature (Jilong Ma & Apps 1982) (Jilong Ma & Apps 1983a) (Allum & Trindade 1984) were carefully examined and compared with those obtained in this study.

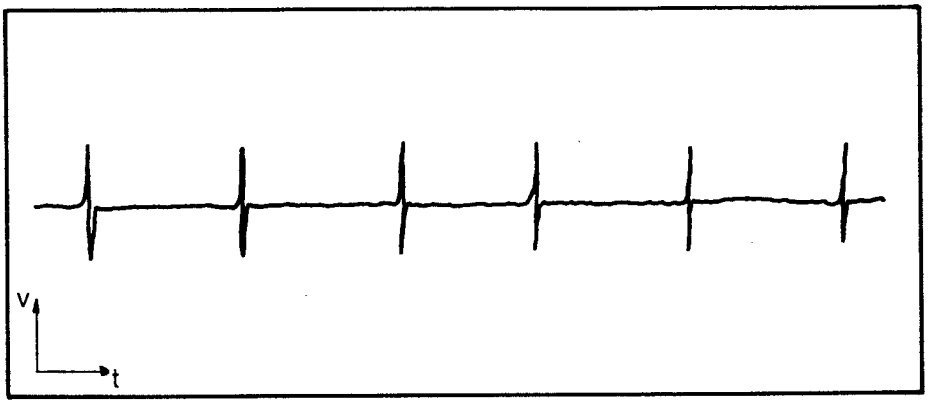

Globular Transfer

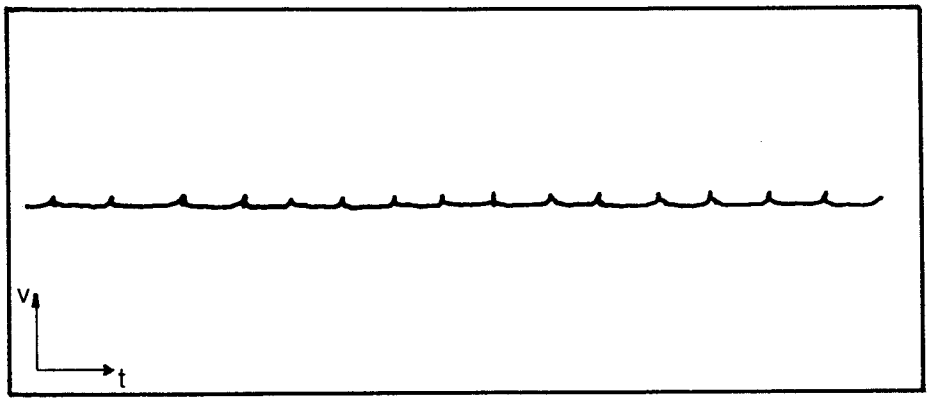

Projected Transfer

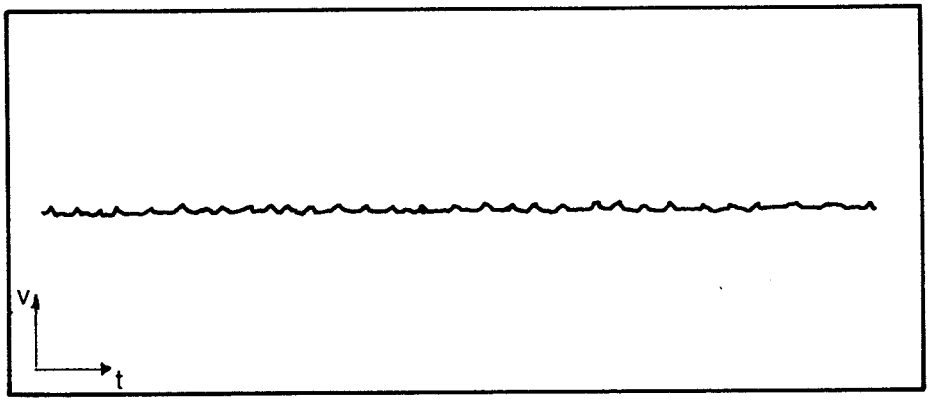

Streaming Transfer

FIG.5.2 Schematic Representation of Typical Oscilloscope Arc Voltage Traces.

5.2.3 Results.

The natural detachment times for the current range of 80A to 300A were examined. The method used to detect the droplet detachments was quite satisfactory up to currents of 200A. Above this value and up to 250A there was some difficulty in reading the traces but from 260A up to the end of the range considerable problems arose due to the low resolution of the equipment. Thus the results for this range of currents may not be accurate. Table 5.1 shows the natural detachment times for welding currents from 140A up to 300A.

table 5.1 Natural Detachment Times for 316S92, 1.2mm diameter welding wire in Ar.1%O_2 reverse polarity.

I (A)	TDC (ms)	Freq. (Hz)	I (A)	TDC (ms)	Freq. (Hz)	I (A)	TDC (ms)	Freq. (Hz)
140	160.00	6.3	200	2.96	338	260	1.90	526
150	83.00	12	210	2.69	372	270	1.85	540
160	33.00	29.9	220	2.40	417	280	1.80	556
170	15.40	65	230	2.20	455	290	1.78	562
180	4.30	233	240	2.14	467	300	1.75	571
190	3.45	290	250	2.00	500			

5.2.3.1 Transfer Modes of the 316S92 Electrode Wire.

Graph 5.1 shows the effects of welding current on the frequency of detachment whereas, graphs 5.2 and 5.3 show the plot between natural detachment times and welding current. Graph 5.4 is the logarithmic plot of equation [4.1]: $\mathbf{I^n \cdot T = a\ constant\ K}$

These plots combined with experimental observations have been used to identify each metal transfer mode for the electrode wire used.

Observations of the arc during experimentation revealed that the electrode material exhibited three

modes of metal transfer; globular, projected spray and streaming spray transfer. Rotating spray transfer was not evident partly due to lack of any means of detecting such an occurrence and partly due to relatively low welding currents examined.

Globular transfer took place up to a current of 140A and the droplets could be observed clearly forming and detaching from the electrode tip. Around 150A the transition to projected spray transfer occured. Droplet formation and detachment could no longer be observed visually. In addition, this was confirmed by the directionality of the detaching droplets and the preliminary qualitative examination of the penetration shape of the various deposits at this current range. Around 220A to 230A the transition from projected spray transfer to streaming spray transfer occurred. This was accompanied by a high pitch "hissing" sound, which is characteristic of this transfer mode.

Graph 5.4 shows the logarithmic plot of welding current against natural detachment times. On the same graph the various metal transfer modes have been identified.

According to experimental observations and based on the definitions of the International Institute of Welding for the various metal transfer modes of GMAW, globular transfer occurs up to a current of 140A and streaming spray transfer above 220A. Thus in the region of 150A to 220A projected spray transfer takes place. Graph 5.4 clearly shows, with a change in slope, that between 220A and 230A the metal transfer changes

from projected to streaming spray.

In the projected spray transfer region there is a distinctive transition which appears to take place between 170A and 180A. The current level at which this transition takes place corresponds to the stage in projected spray transfer where droplet growth and detachment take place from a liquid conical tip. This is supported by (Lancaster 1979) (Lancaster 1986) where, for a 1.2mm diameter mild steel electrode, this transition takes place around 190A. Figure 5.3, taken from (Lancaster 1979), shows the droplets prior and after detachment for a range of welding currents between 60A and 220A. Thus the logarithmic plot of welding current against natural detachment times identifies the occurring transfer modes according to electrode tip geometry, but it does not identify the transition between globular and projected spray transfer. In order to find this transition, examination of the penetration characteristics of the deposit, plus observation of the arc is required.

5.2.4 Discussion: Natural Detachment Times.

Three metal transfer modes, globular, projected spray and streaming spray were identified for the electrode material used.

The results for the whole range of currents examined are in very good agreement with the general trends of metal transfer in GMA welding especially for

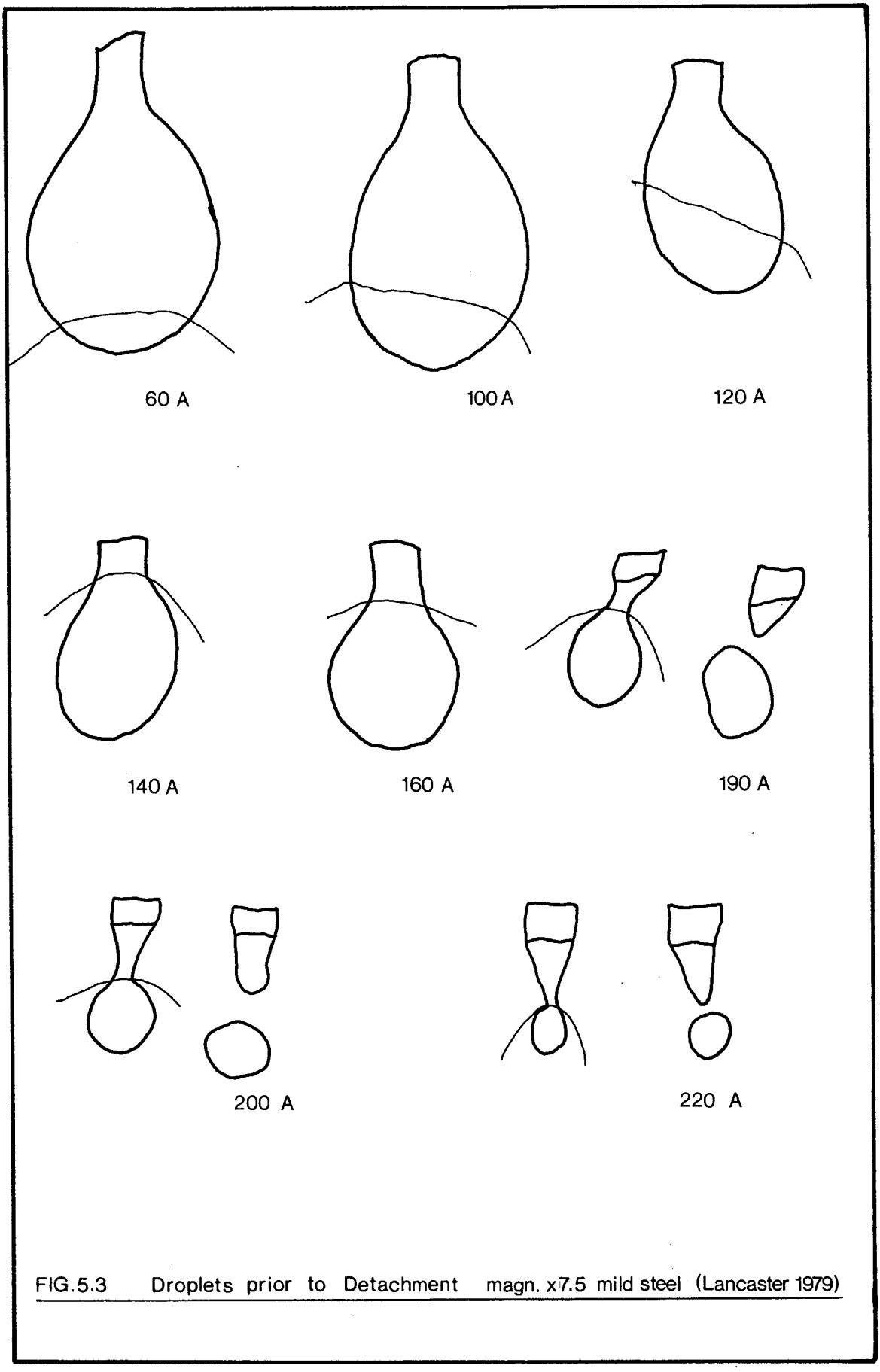

FIG.5.3 Droplets prior to Detachment magn. x7.5 mild steel (Lancaster 1979)

ferrous metals (Lesnewich 1958) (Amin 1983) (Lancaster 1986). However, it appears that all the transitions encountered in stainless steel occur around 15A below the values for mild steel electrodes. This may be attributed to the slightly different physical properties of the stainless steel.

The power factor (n) can be extracted from the logarithmic form of equation [4.1]:

$$n \cdot \log_n I + \log_n T = \log_n K \quad \ldots\ldots\ldots\ldots\ldots\ldots \quad 5.1$$

For streaming spray transfer n=1.92 which agrees with reported results (Allum 1985b) (Lancaster 1986) that suggest the value of (n) may range from 1.55 to 2.55. In projected spray transfer from a conical tip n=2.67 which is just outside this range. This may be attributed to experimental error. For globular transfer and projected spray transfer n=14.2. As globular transfer offers no interest as an employable type of metal transfer no data have been found to verify or contradict the value of the power factor obtained in the current experiments.

Fume generation and spatter were minimal during projected spray transfer. The worst spatter occurred during globular transfer mainly due to short circuit between the droplets and the weldpool. Although spatter was absent during streaming spray transfer fume generation appeared to be at higher levels than that of projected spray transfer. This observation is in agreement with literature (Jilong Ma & Apps 1983b) and it suggests that the increased melting efficiency during this transfer mode results in a reduced material vaporisation (Jilong Ma & Apps 1983b).

5.2.4.1 Scatter in the Natural Detachment Times.

The natural detachment times exhibit scatter therefore the values presented in graphs 5.1, 5.2, 5.3 and 5.4 are the mean values for each current setting.

Graph 5.5 shows the standard deviation of the scatter in the natural detachment times for each current setting used. Table 5.2 shows the data used in the statistical analysis. From the plot it can be seen that scatter may be directly correlated to the transfer mode and specifically to the droplet volume.

From observations during experiments the stability of the arc and transfer is greatly influenced by the size of the droplet. Large droplets tend to cause severe disturbances to the stabilty of the arc in the form of large arc length fluctuations and in extreme cases short circuit. At higher currents where the droplets are very small the arc column is not severely disturbed thus scatter is significantly reduced.

table 5.2 Statistical Presentation of Natural Detachment Times

140 A		150 A		160 A		170 A	
D.Time	freq.	D.Time	freq.	D.Time	freq.	D.Time	freq.
110-120	2	45-50	1	10-15	9	10-11	1
130-140	11	55-60	3	20-25	34	12-13	29
150-160	26	65-70	15	30-35	43	14-15	42
170-180	10	75-80	34	40-45	20	16-17	30
190-200	6	85-90	26	50-55	12	18-19	8
210-220	2	95-100	14	60-65	7	20-21	3
		105-110	9			22-23	7
Mean=159.5 ms		Mean=83.1 ms		Mean=33.5 ms		Mean=15.4 ms	
σ=21.85		σ=12.80		σ=12.64		σ=2.65	

180 A		190 A		200 A		210 A	
D.Time	freq.	D.Time	freq.	D.Time	freq.	D.Time	freq.
2.5-3.0	13	1.5-2.0	9	1.0-1.5	3	2.2-2.2	5
3.5-4.0	26	2.5-3.0	38	2.0-2.5	48	2.4-2.5	25
4.5-5.0	28	3.5-4.0	46	3.0-3.5	49	2.6-2.7	17
5.5-6.0	13	4.5-5.0	14	4.0-4.5	12	2.8-2.9	28
6.5-7.0	2	5.5-6.0	3	5.0-5.5	3	3.0-3.1	12
		6.5-7.0	1	6.0-6.5	1	3.2-3.3	2
Mean=4.3 ms		Mean=3.45 ms		Mean=2.96 ms		Mean=2.69 ms	
σ=1.01		σ=0.94		σ=0.84		σ=0.24	

220 A		230 A		240 A		250 A	
D.Time	freq.	D.Time	freq.	D.Time	freq.	D.Time	freq
1.8-1.9	13	1.5-1.6	6	1.7-1.8	2	1.5-1.6	2
2.0-2.1	30	1.7-1.8	7	1.9-2.0	24	1.7-1.8	23
2.2-2.3	23	1.9-2.0	19	2.1-2.2	40	1.9-2.0	45
2.4-2.5	9	2.1-2.2	31	2.3-2.4	17	2.1-2.2	27
2.6-2.7	27	2.3-2.4	28	2.5-2.6	4	2.3-2.4	14
2.8-2.9	15	2.5-2.6	17			2.5-2.6	2
3.0-3.1	10	2.7-2.8	8				
Mean=2.40 ms		Mean=2.20 ms		Mean=2.14 ms		Mean=2.00 ms	
σ=0.36		σ=0.29		σ=0.17		σ=0.2	

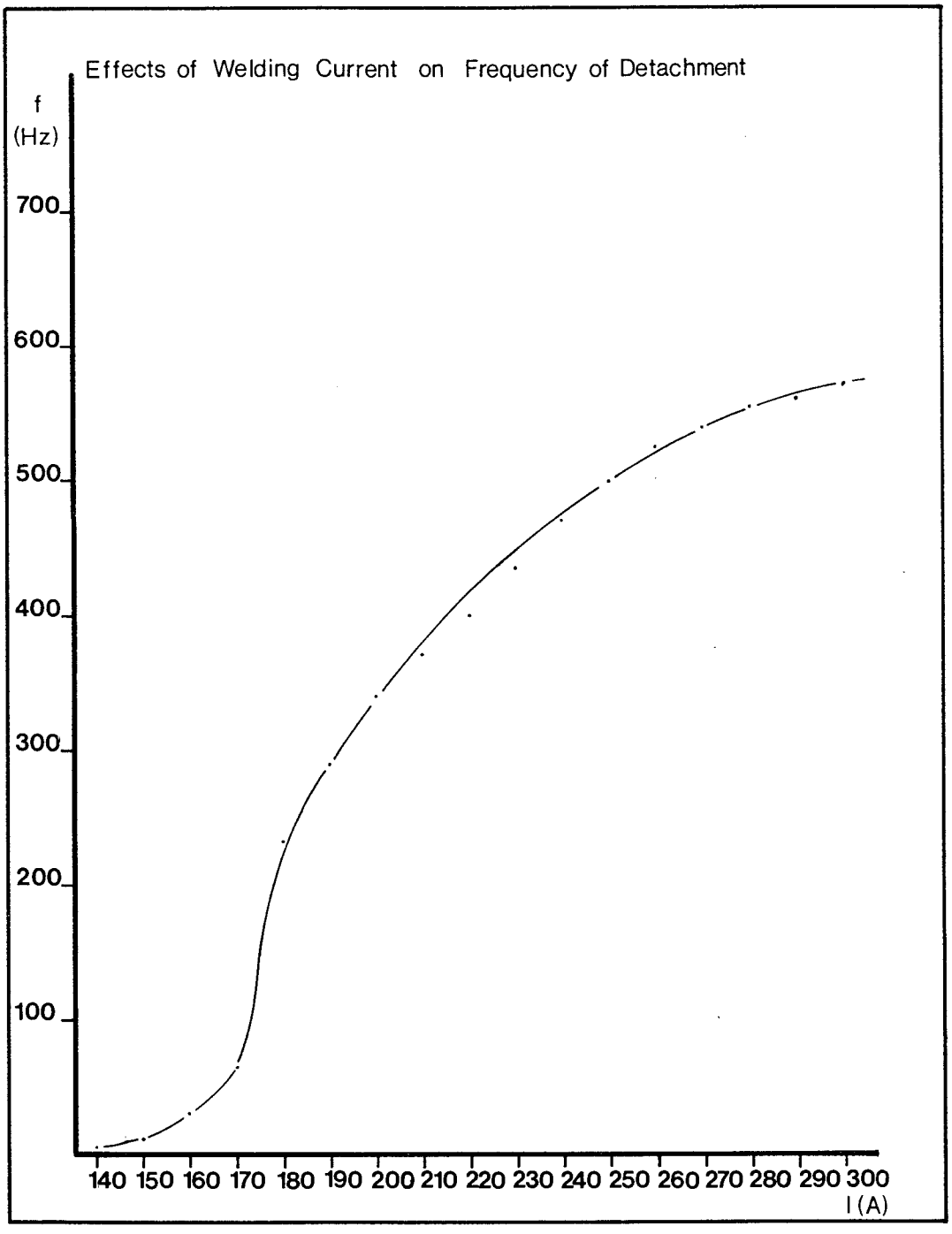
Effects of Welding Current on Frequency of Detachment
f
(Hz)
700
600
500
400
300
200
100
140 150 160 170 180 190 200 210 220 230 240 250 260 270 280 290 300
I (A)

Graph 5.1

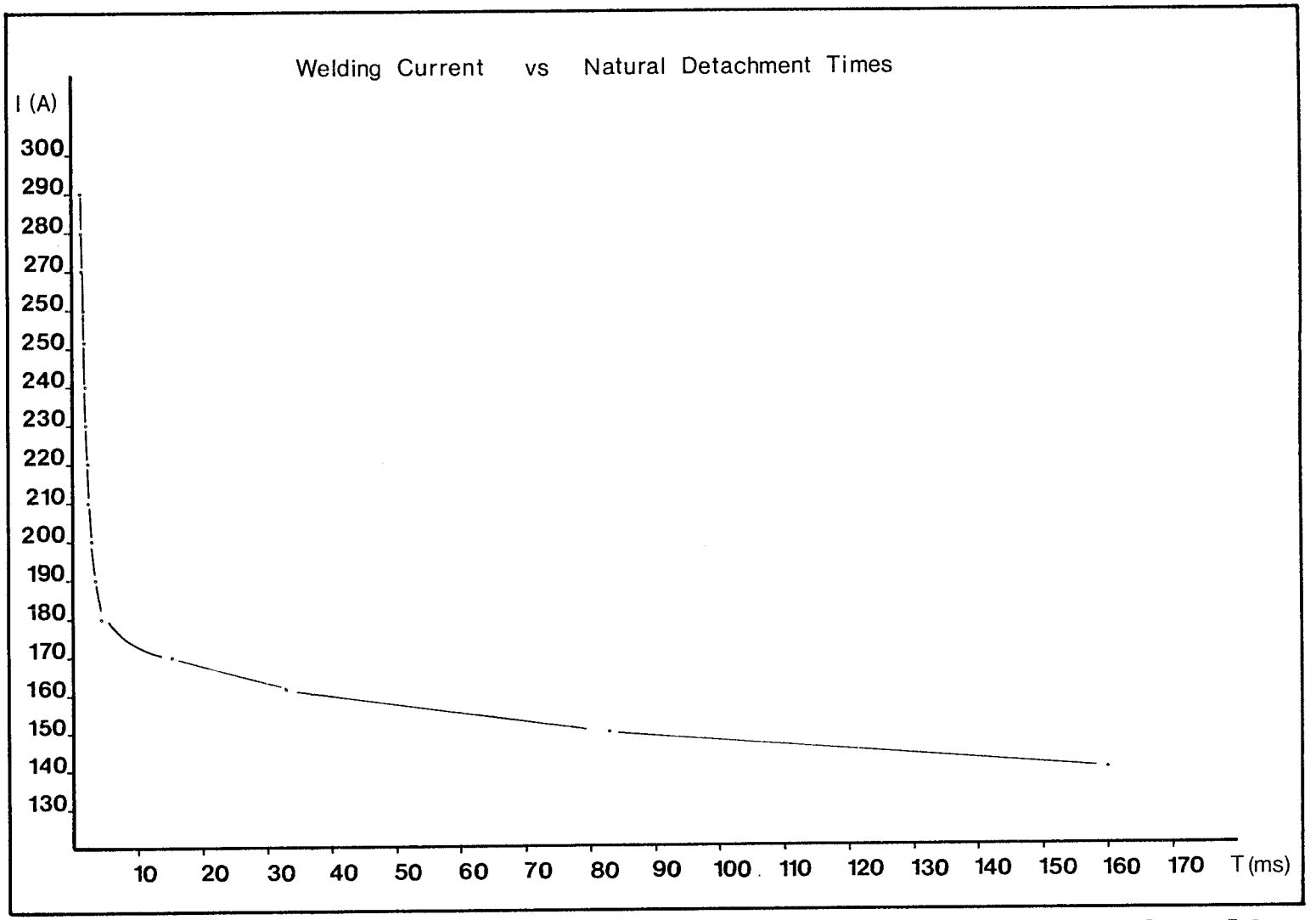
Welding Current vs Natural Detachment Times
I (A)
300
290
280
270
250
250
240
230
220
210
200
190
180
170
160
150
140
130
10
20
30
40
50
60
70
80
90
100
110
120
130
140
150
160
170
T (ms)

Graph 5.2

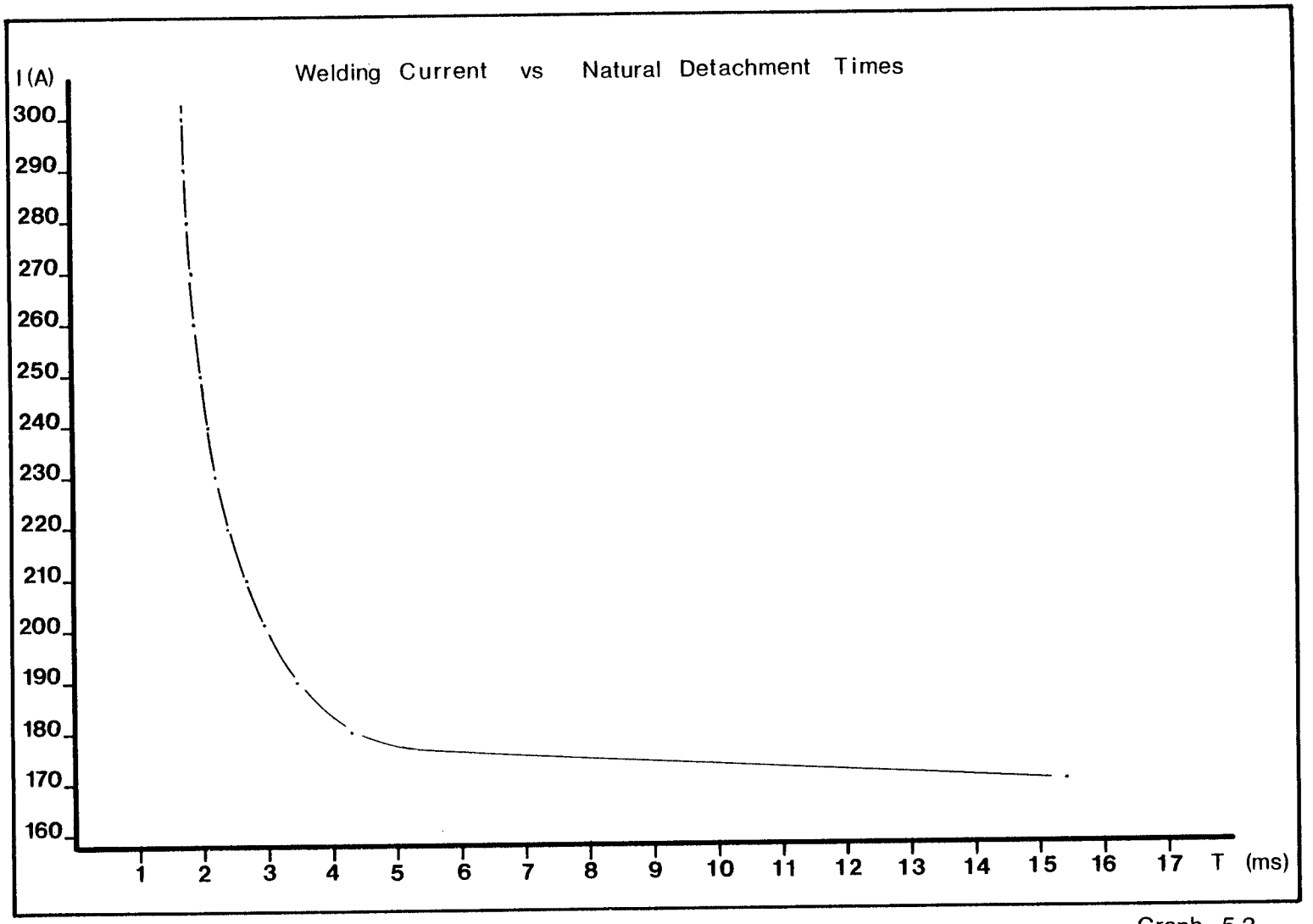
Welding Current vs Natural Detachment Times
I (A)
300
290
280
270
260
250
240
230
220
210
200
190
180
170
160
1
2
3
4
5
6
7
8
9
10
11
12
13
14
15
16
17
T (ms)

Graph 5.3

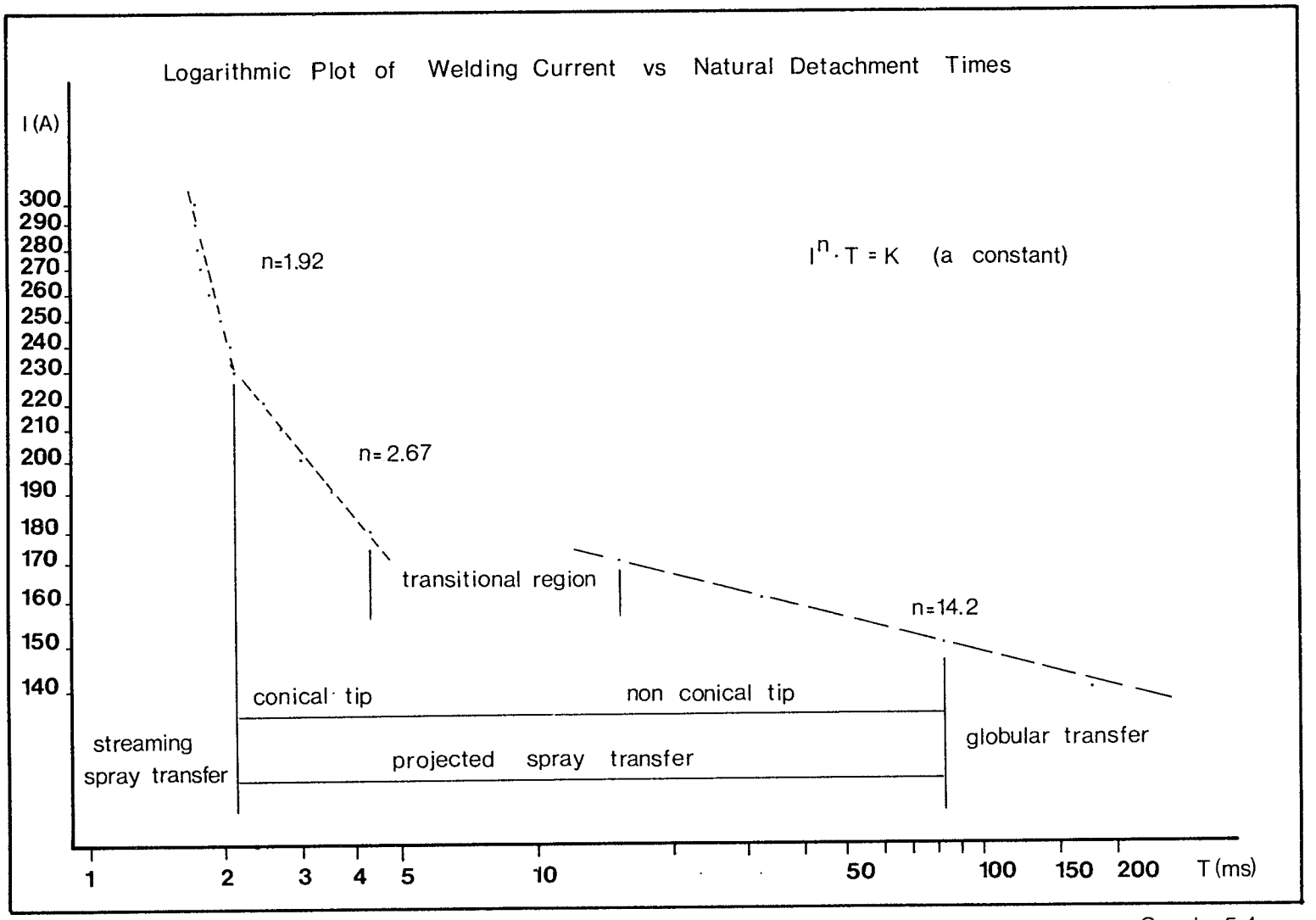
Logarithmic Plot of Welding Current vs Natural Detachment Times
I (A)
300
290
280
270
260
250
240
230
220
210
200
190
180
170
160
150
140
n=1.92
n= 2.67
$I^n \cdot T = K$ (a constant)
transitional region
n=14.2
conical tip
non conical tip
streaming
spray transfer
projected spray transfer
globular transfer
1
2
3
4
5
10
50
100
150
200
T (ms)

Graph 5.4

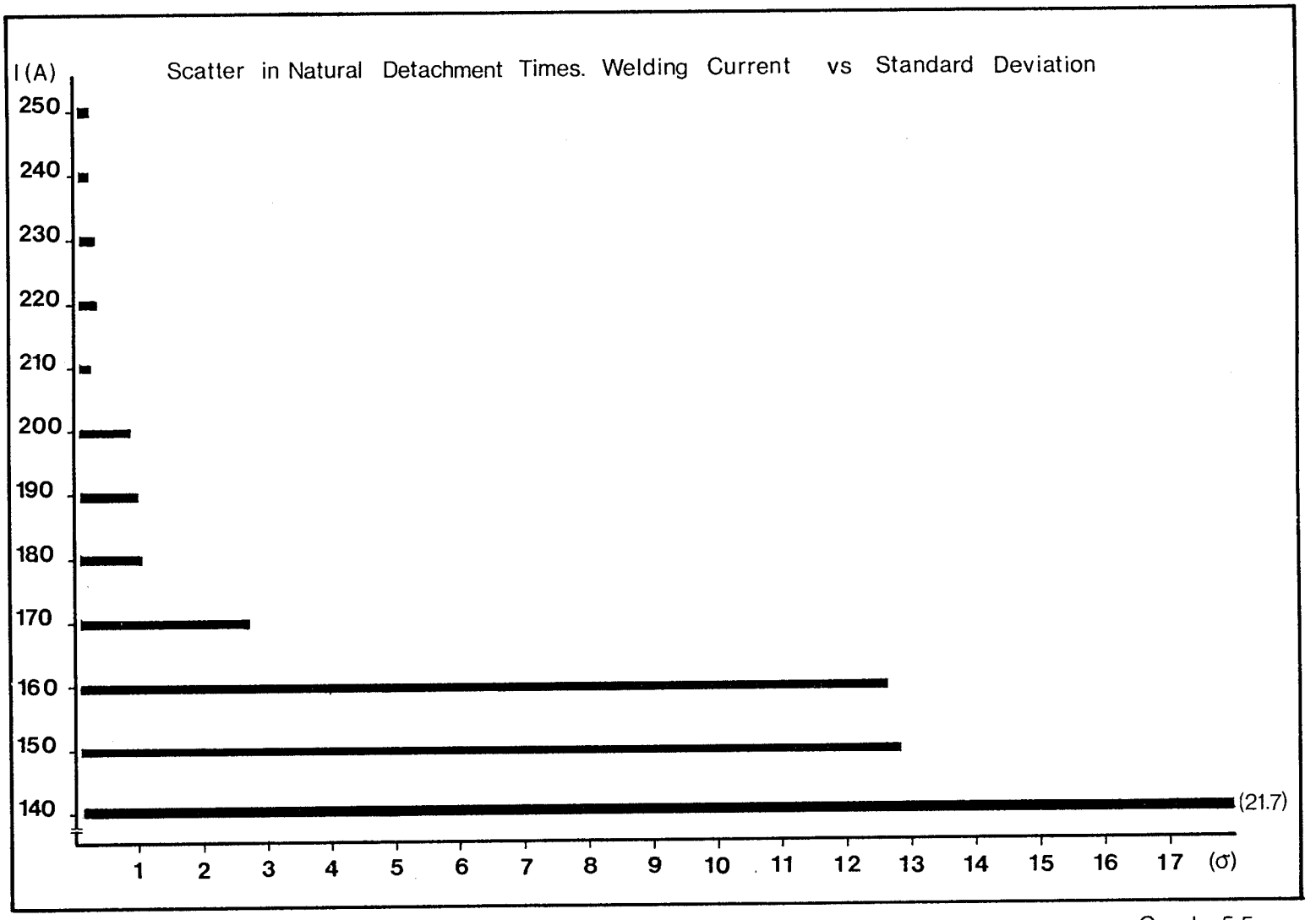
Scatter in Natural Detachment Times. Welding Current vs Standard Deviation
I (A)
250
240
230
220
210
200
190
180
170
160
150
140
(21.7)
1 2 3 4 5 6 7 8 9 10 11 12 13 14 15 16 17 (σ)

Graph 5.5

5.3 Welding with Pulsed Current.

This section of the present chapter examines the prerequisites that a pulse current configuration must satisfy in order to create the conditions for droplet detachment.

5.3.1 Modelling of Metal Detachment in pulsed MIG Welding.

When the arc is struck and welding commences there is a short transient until a steady state is reached. Consider that the process has reached a steady state and droplet evolution and detachment is constantly monitored. Let us also make a purely theoretical assumption that the welding current can be interrupted at will and changed to a different value without disturbing the balance of the arc length.

Figure 5.4a shows conditions of an uninterrupted welding current. In this case the droplet will form and evolve as a result of arc and resistance heating of the electrode. When the droplet reaches its critical size necking will commence and detachment will occur. This will take place at a predetermined time depending on the current and other welding parameters. Necking is an irreversible process and once it has commenced detachment will certainly take place (Jilong Ma & Apps 1983a).

Figure 5.4b shows that detachment is not possible if the droplet has formed but necking has not started when the current is reduced to a lower value (background). However, if necking has commenced detachment will occur irrespective of the current

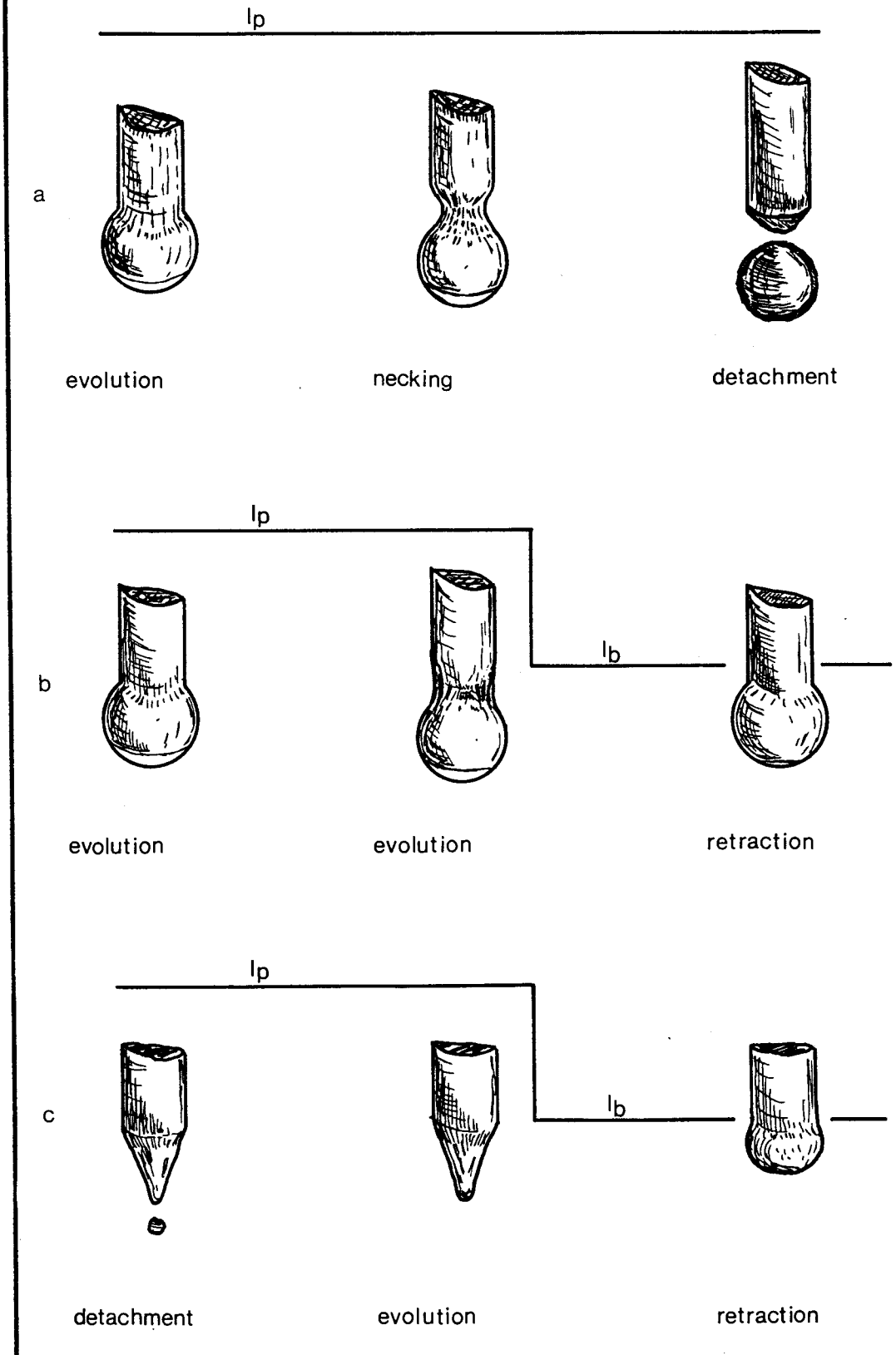

FIG.5.4 Metal Detachment in Pulsed MIG Welding

configuration.

Figure 5.4c shows streaming spray transfer taking place and between two detachments the current is interrupted by the background phase. Based on the postulate that the anode spot size and the pinch force will decrease (Amson 1965), at a certain stage of the background conditions the pinch force will not be sufficient to maintain the tapered geometry, thus the conical tip will collapse and retract upwards forming a droplet.

5.3.2 Experiments on the Classification of Metal Transfer in P-MIG.

Two experiments were carried out to determine the effect of pulsed current on metal transfer.

5.3.2.1 Effects of Cycle Frequency on Droplet Detachment at Constant Pulse Amplitudes.

In the first series of experiments the current was set such that:

$$Ip-Im=Im-Ib$$

and remained constant; and the pulse and background times were equal:

$$Tp=Tb$$

but were increased from Tp=Tb=0.5ms up to 99ms. Figure 5.5a shows a schematic representation of the current configuration used.

The pulse current (Ip=175A) was chosen to be in the projected spray transfer region and both the mean (Im=110A) and background (Ib=50A) currents in the

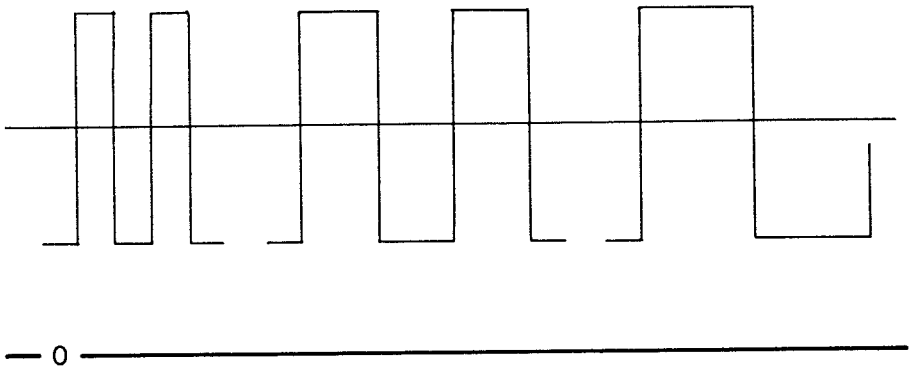

FIG.5.5a Constant Amplitude / Decreasing Cycle Frequency

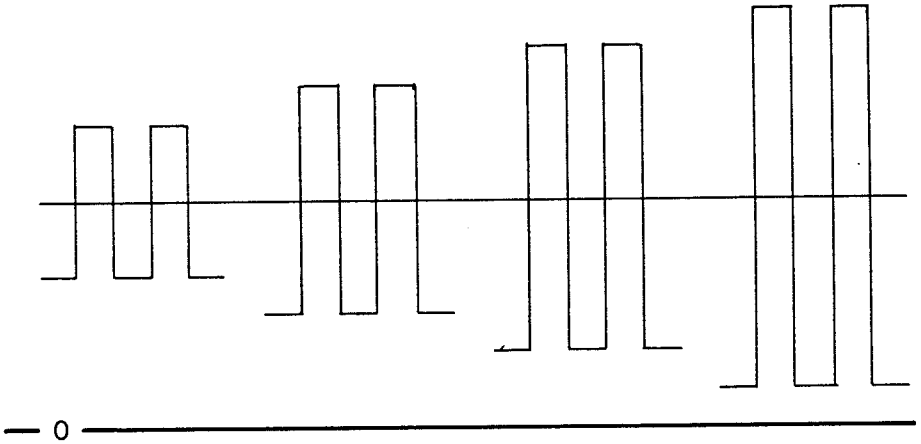

FIG. 5.5b Constant Cycle Frequency / Increasing Amplitude Differential

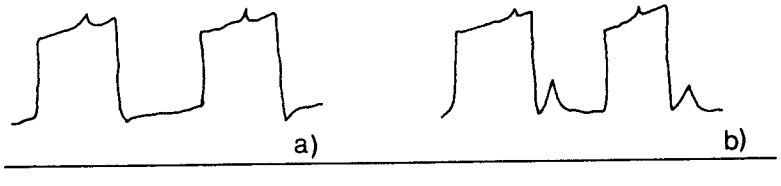

FIG. 5.6 Waveforms a) Normally Occurring.
b) Showing Arc Continuation Irregularities.

globular transfer region. The electrical parameters are given in table 5.3

table 5.3
Effects of Cycle Frequency on Metal Detachment

Im (A)	W (m/min)	Ip (A)	Ib (A)	Tp=Tb (ms)	Metal Transfer Type
110	3.45	175	50	0.5	Globular Transfer
110	3.45	175	50	1.0	" "
110	3.45	175	50	2.0	" "
110	3.45	175	50	5.0	Globular/Projected
110	3.45	175	50	8.0	Projected Transfer
110	3.45	175	50	10.0	" "
110	3.45	175	50	15.0	Multiple Detachments
110	3.45	175	50	20.0	" "
110	3.45	175	50	30.0	" "
110	3.45	175	50	50.0	" "
110	3.45	175	50	99.9	" "

5.3.2.2 Results.

At Tp=Tb=0.5ms, large globular transfer took place with a detachment time varying between 180 to 190ms which proved that when high frequency cycles are applied pulsed welding metal transfer has the characteristics of DC GMAW. However, the same type of detachment persisted up to Tp=Tb=2.0ms and the droplets were clearly visible.

AT Tp=Tb=5.0ms, a mixture of projected and globular transfer took place. The detachments were irregular, occurring mostly during peaks but with some in the background. In addition a large globule detached every one to two seconds.

At Tp=8.0ms and 10ms pure projected spray transfer was observed with regular detachments in every pulse. This type of metal detachment was expected as the pulse time was approximately equal to the natural detachment time for the pulse current used. However, the detachments did not occur at a precise point of the cycle

but fluctuated around the middle of the peak.

At Tp=15.0ms, the transfer remained projected but there were one to two detachments per pulse. As the time was just too short to provide regular multiple detachment background detachments occurred. These background detachments were rare and very irregular.

At Tp=20.0ms, two detachments occurred per pulse but no detachment was observed in the background. The arc was very stable, there was no spatter and the fume levels were very low.

The same phenomena were observed at Tp=30.0ms only there were three detachments per pulse. It was observed that in multiple detachment the spikes recorded on the CRO screen were different in amplitude. The first spike was more intense than the succeeding ones which suggests that the first droplet is larger than the following ones due to the background melting. A similar observation has been made by (Allum 1985c).

When Tp=Tb were set at 50.0 and 99.9ms respectively multiple detachments were observed in the peak, with the first detachment being of the globular transfer type due to background melting.

5.3.2.3 Effects of Pulse Amplitude on Droplet Detachment for Constant Cycle Times.

In the second experiment, the pulse and background times were kept constant and equal. The mean current was kept constant and the background current was decreased by the same amount the pulse current was

increased, ie. the expression Ip-Im=Im-Ib was always satisfied. The electrical parameters are presented in table 5.4 and the current configuration in figure 5.5b.

table 5.4
Effects of Pulse Amplitude on Metal Detachment

Im (A)	W (m/min)	Ip (A)	Ib (A)	Tp=Tb (ms)	Metal Transfer Type
110	3.45	120	100	5.0	Globular Transfer
110	3.45	140	80	5.0	Globular Transfer
110	3.45	160	60	5.0	Globular/Projected
110	3.45	180	40	5.0	Projected/Globular
110	3.45	200	20	5.0	Projected Transfer
110	3.45	220	0	5.0	Unstable Arc

5.3.2.4 Results.

The settings of Ip=120A and Ib=100A resulted in globular transfer with a tendency to short circuit. Detachment occurred approximately every 190 ms. Large globular transfer was expected as the pulse, background and mean currents give rise to this type of transfer.

The same type of detachment and for the same reasons as above, was present when the settings were Ip=140A and Ib=80A.

With Ip=160A and Ib=60A irregular projected transfer occurred with a large droplet detaching approximately every one second.

Transfer was less irregular and predominantly projected with Ip=180A and Ib=40A. Detachment of large droplets was not evident.

Purely projected transfer took place with Ip=200 and Ib=10A as expected, however, the waveform recorded showed a characteristic spike of 1-1.3ms duration at the beginning of the background phase. As a result of low

background currents the conductivity of the arc was reduced and thus the arc voltage was increased to maintain conduction. Hence the appearance of the spike on the waveform (figure 5.6).

The last setting had Ip=220A and Ib=0A. The use of zero backround current did not satisfy the arc continuation criterion and resulted in an unacceptable, unstable arc which was constantly extinguished during the background phase and ingnited during the pulse phase.

5.3.3 Discussion: Metal Transfer in Pulsed MIG Welding.

5.3.3.1 The Phenomenon of Droplet Growth.

It was found that high frequency cycles in p-MIG with $T_p<T_{DC}$ promote metal transfer at detachment times corresponding to the natural detachment time of the mean current. The metal transfer modes observed during the experiments on the effects of cycle frequency on droplet detachment at constant pulse amplitudes exhibit a sudden transition, as the pulse time approaches the natural detachment time for that pulse current. This transition, from globular transfer to the type of metal transfer expected for the given pulse current, goes through a highly unstable zone of a mixture of metal transfers. The fact that there was not any gradual reduction in the droplet volumes and smooth transition, means that the idea of forcing detachment by introducing a high amplitude pulse appears not to be straightforward. The question that arises from this observation is that why does the droplet not detach when it reaches its critical

size for detachment, but continues to grow until it detaches in the manner described previously.

The phenomenon of droplet growth, unstable metal detachments and the inability to produce the desired metal transfer in pulse MIG welding can be associated either with the inability of the pulse phase to provide the right conditions for detachment or the conditions set by the background phase.

In p-MIG welding the low currents and long durations of the background phase upset the arc conditions set by the pulse phase and promote globular metal transfer. The low current background conditions not only reduce the anode spot size and pinch force, but may cause excessive build up of molten metal at the end of the tip. At some stage in the evolution of the droplet it appears that the pulse phase not only is incapable of detaching the droplet but contributes to its growth until mean current type detachment occurs. This observation partly contradicts the pinch instability model which assumes that multiple detachment would take place if the droplet mass were bigger than the critical mass. Multiple detachment seems to be true only if the pulse time is sufficiently long to be a multiple of the natural detachment time for the pulse current used.

The phenomenon of droplet growth may be attributed to the relation of the anode spot size to the droplet volume during the process. It is suspected that during the background current the anode spot will be very small and confined to the electrode tip. However, at the beginning of the pulse phase a surge of current will pass

through the existing anode spot and initially oppose detachment by setting up an upper thrust reaction as the current will tend to diverge through the droplet. Although subsequently the current will tend to increase the area of emission and the pinch force if the pulse phase does not detach the droplet, additional melting during the following background phase will minimise any chance of detachment and globular transfer will occur.

5.3.3.2 Classification of Metal Transfer in pulsed MIG welding.

The standard classification of metal transfer has been set down by the IIW and has been examined in the chapter on metal transfer in GMAW. In order to avoid any confusion with the IIW classification of metal transfer, the metal transfer types encountered in p-MIG will be called detachment types.

The detachment types encountered in p-MIG are the following:

1) Standard metal detachment (SMD).
2) Mean Current Type metal detachment (MCT).
3) Mixed Detachment (MD).
4) Multiple Detachment Type (MDT).

The natural detachment times are considered to be the standard metal transfer characteristics, therefore this will be referred to as standard metal detachment (SMD).

In some cases in p-MIG the detachment times correspond to the natural detachment times of the mean current used. This is called mean current metal

detachment (MCT) and occurs when the cycle frequency is relatively high and/or droplet growth is promoted due to background current melting.

Mixed detachment (MD) is an unstable condition which should be avoided in order to minimise any weld defects. Mixed detachment can be homogeneous, which involves droplets of the same type of metal transfer or non-homogeneous, which involves droplets of two different types of transfer. The most noticeable non-homogeneous mixed detachment is when projected and globular transfer take place. Homogeneous mixed detachment may not affect the stability of the arc but it has been found to cause irregular penetration depths.

Multiple detachment type (MDT) metal detachment occurs when the pulse time used is a multiple of the natural detachment time for that current. The first droplet is usually larger than the succeeding ones as it has gained volume from the melting during the background stage. In p-MIG welding multiple detachments do not seem to offer any real advantages over DC-MIG welding because in order to keep down the heat input (mean current) long background times are required thus in effect giving rise to mixed detachments. In addition, if the background times are short enough not to contribute to any additional melting, the resulting mean currents values will be relatively high approaching the value of the pulse current thus defeating the point of having metal transfer independent of heat input.

5.3.3.3 Aspects of Metal Detachment in Relation to Pulse Current Configuration.

The selection of electrical parameters that will result in a controlled metal transfer of one droplet detachment per pulse may be achieved by using the natural detachment characteristics of the electrode wire. Subsequently, the natural detachment characteristics are used directly to set the pulse conditions. Thus the pulse current is given a value and the pulse time takes the corresponding natural detachment time value for the pulse current used.

Using the natural detachment characteristics and providing that no melting takes place during the background phase and that there is no scatter in the natural detachment times, droplet detachment is expected to occur at the end of each pulse time.

The introduction of melting during the background phase will cause the droplet to reach its critical size before the end of the pulse. Subsequent cycles will cause detachment to be displaced towards the beginning of the pulse thus giving rise to a cyclic pattern of detachment.

As with direct welding current, there is scatter in the detachment times in the pulse welding current configuration. This was observed in the form of detachment time fluctuation during one droplet per pulse transfer. Therefore the scatter in natural detachment times necessitates the setting of the pulse time according to the probability of detachment. The experiments described in section 5.3.2.1 have shown that

the most satisfactory welding conditions are obtained when the pulse times ensure a 0.8 probability of detachment. Shorter pulse times make the stability of metal transfer increasingly more sensitive to the background conditions.

It is possible to obtain projected spray transfer, when using the natural detachment characteristics, for mean currents ranging from 70A up to 230A. The pulse parameters form and detach the droplet as in DC-MIG, whereas the background conditions regulate the mean current. Low mean currents require relatively long background times which cause droplet growth, resulting in unstable mixed detachments of globular and projected spray transfer modes. Thus any limitations this method has are caused by the settings of the background.

Experimental trials showed that in order to avoid any limitations caused by the background conditions the relationship between the pulse parameters and the background parameters had to be $Ib \cdot Tb \leq 0.4 \cdot Ip \cdot Tp$. In this way the possibility of droplet growth during the background phase is reduced considerably.

In addition it has been found that waveforms with background times shorter than the pulse times tend to promote unstable metal transfer. It is therefore good practice to set the background time equal to or longer than the pulse time. As discussed earlier, if the background times are very short then the mean current tends to approach the value of the pulse current, thus making the use of pulsed current pointless.

5.4 Selection of Electrical Parameters.

5.4.1. Projected spray transfer.

A set of electrical parameters is presented below where all have been set in compliance with the rules and limitations met previously. The parameters are mean current Im=100A, pulse current Ip=180A, pulse time Tp=6ms, background current Ib=50A, background time Tb=9ms (table 5.5).

table 5.5
Welding Parameters for a Drop per Pulse Detachment

Mean Current	100	A
Pulse Current	180	A
Pulse Time	6	ms
Background Current	50	A
Background Time	9	ms
Wire feed speed	3.18	m/min

Q=20lt/min, l=8mm, standoff=17mm, position vertical.

The resulting metal transfer was stable with spatter and fumes absent. In addition a droplet detachment per pulse had been achieved.

Direct observation of the oscilloscope screen without AC modulation showed that regular transfer was taking place with the vast majority of detachments occurring during the pulse time. However, the occurrence of detachment was focused between the middle and the end of the pulse. Examination of recorded waveform traces revealed that out of a sample of 137 cycles, 85% of all detachments occurred during the pulse time. This figure agrees with the pulse time which was set as to ensure 0.8 probability of detachment. From the total number of pulse detachments 98% occurred between 3ms and 6ms as expected from the natural detachment times. Background detachment

accounted for 11% of the total transfers and it usually occurred at the beginning of the background time, which indicates that necking between the droplet and the electrode had commenced when the pulse current was interrupted. The remaining 4% of all detachments accounted for some instabilities and one mean current type metal detachment. The growth of this droplet lasted for approximately 12 cycles and resulted in a volume of $9.899mm^3$ which is characteristic of the droplet volumes encountered in DC-MIG at 100A. The sample used had a duration of approximately two seconds. However, despite its relatively short duration and an uncharacteristic instability it provides quite an accurate picture of metal transfer under the welding conditions used.

Droplet growth is highly unlikely because the duration of the pulse ensures detachment; in addition at all times the droplet remains engulfed by the anode spot and the current converges within the droplet which aids detachment.

5.4.2 Streaming Spray Transfer.

By definition droplet detachment in streaming spray transfer takes place from the tapered electrode tip. Therefore, in order to obtain streaming spray transfer in pulsed MIG the tapered electrode tip geometry must be present, the taper being formed and maintained by the welding parameters. It has been found that in order to form and constantly maintain the tapered electrode tip, the mean current has to be above 230A. If the taper is constantly maintained, then the pulse parameters may

be set in accordance with the natural detachment characteristics.

Lower mean currents that do not sustain the tapered tip must have pulse times long enough to form the taper and detach a droplet. Unfortunately low mean currents require long background times, thus background melting may give rise to projected spray transfer and in extreme cases globular transfer. If multiple detachments during the pulse time are acceptable then the pulse time must be long enough to detach the liquid accumulated during the background phase and then create the conditions for a streaming spray transfer detachment.

5.4.3 Detachment by Growth.

This is an alternative method where a droplet is formed during the background phase and a pulse is used to detach the droplet and cause some additional melting.

In order to obtain the above conditions the pulse phase must be set in the streaming spray transfer region and the background phase must be set so as to:

1) cancel the tendency for streaming spray transfer of the pulse current,

2) regulate the additional melting,

3) contribute to the regulation of the mean current.

It is essential that the volume of molten electrode material formed during the cycle is adequate to form a droplet but also it must be ensured that no excessive growth takes place.

A series of experiments were conducted to verify

the validity of this method especially in projected spray transfer using mean currents between 100A and 170A.

The results which are shown on table 5.6 were satisfactory and stable metal transfer was present in all cases. An example of one of the settings is presented in table 5.7

A mean current and a type of metal transfer must be selected eg. 100A and projected spray transfer. The pulse current is then set well in the region where projected spray transfer occurs, eg. 300A. The selection of the background current conditions as well as the pulse duration depends on the droplet volume required.

With the electrical parameters selected, the volume produced during the pulse time is:

$$\pi \cdot 1.44 \cdot 4 \cdot 9.54/240 = 0.719 \text{ mm}^3$$

of molten electrode material, whereas during the background,

$$\pi \cdot 1.44 \cdot 16 \cdot 1.59/240 = 0.479 \text{ mm}^3.$$

The term 240 in the calculations above is used to make the units consistent.

At the end of the cycle the total volume will be approximately 1.2 mm^3 and it is most likely that detachment will occur in every cycle. This is supported by UV traces that show detachment taking place regularly during the pulse phase.

table 5.6
Detachment by Growth: Electrical Parameters.

No.	Im (A)	W (m/min)	Ip (A)	Tp (ms)	Ib (A)	Tb (ms)	V_T mm^3
1	100	3.18	300	4	50	16.0	1.199
2	100	3.18	300	4	60	20.0	1.438
3	100	3.18	300	4	70	26.7	1.838
4	120	3.81	300	4	50	10.3	1.030
5	120	3.81	300	4	60	12.0	1.237
6	120	3.81	300	4	70	14.4	1.323
7	140	4.45	300	4	50	7.1	0.932
8	140	4.45	300	4	60	8.0	1.007
9	140	4.45	300	4	70	9.1	1.101
10	160	5.10	300	4	50	5.1	0.872
11	160	5.10	300	4	60	5.6	0.920
12	160	5.10	300	4	70	6.2	0.979
13	170	5.40	300	4	70	5.2	0.937

Torch Positioning: Vertical. Shielding
Gas Flow: 15lt/min. Travel Speed 5.75 mm/s.

table 5.7
Welding Parameters for a Drop per Pulse Detachment

Mean Current	100	A
Pulse Current	300	A
Pulse Time	4	ms
Background Current	50	A
Background Time	16	ms
Wire feed speed	3.18	m/min

Q=20lt/min, l=8mm, standoff=17mm, position vertical.

5.5 Discussion.

5.5.1 Control of Metal Transfer and Droplet Detachment.

Controlled metal transfer in p-MIG welding is possible. However, there are some limitations as metal transfer is not totally independent of heat input. Experiments have shown, for the material used, that purely projected spray transfer can be obtained with mean currents ranging from 50A to 230A whereas for streaming

spray transfer mean currents over 230A are required.

Controlling metal detachment so as to detach a droplet at any point during the pulse or background phase is also possible. Pulse detachments are easier to obtain as the primary function of the pulse is to cause detachment.

Regular detachments in the background current are possible if the pulse current is interrupted just as necking has started to take place. However, this implies that in every cycle at the precise moment of interrupting the pulse the droplet will have evolved to its critical length and necking will have commenced. However, this does not take into account that detachment times exhibit some scatter.

In order to simulate conditions that would give rise to regular background detachments, the pulse duration was reduced fractionally, thus interrupting the pulse current as necking would occur. It was found that despite the tendency to have some background detachments, unstable mixed detachments predominated.

The inability to obtain total control of detachment may be attributed to a large extent to the scatter in detachment times. The cause of such an irregularity is the combination of electrical and mechanical characteristics of the apparatus.

The electronic control of the waveforms must be accurate and the time delays between background and pulse conditions must be kept to a minimum. An external disturbance will have different effects on the arc depending on the current-voltage characteristic of the

apparatus. Scatter in the detachment times may be augmented during manual operations as the process is subjected to the hand movements of the operator.

Mechanical disturbances may be caused by the wire feeder and the contact tube in the welding torch which may result in arc length fluctuations consequently affecting the regularity of droplet detachment.

5.5.2 Spatter.

During the present work two types of spatter were encountered, the most common being the result of large droplets coming into contact with the weldpool.

The other type of spatter occurred exclusively during the implementation of the detachment by growth model. In some cases very fine spray was ejected from the arc column, however there was no spatter noise or fume generation. Based on this evidence, droplet explosion due to contact with the weldpool seemed not to be the cause. The cause of this type of spatter is most likely to be the ebullition and subsequent dissintegration of some droplets having been overheated by the pulse current while in flight after detachment.

5.6 Conclusions

It has been shown that metal transfer and detachment control is possible in pulsed MIG welding despite the large number of parameters and combinations to be considered.

The method used to select the electrical parameters uses an empirical approach, where the droplet

formation and detachment is assessed according to the ability of the welding cycle to reproduce the conditions for detachment found in the natural detachment characteristics of the material.

This method has given satisfactory results such as controlled metal transfer and droplet detachment and minimal spatter and fume generation.

Approach to the selection of pulse parameters.

A guidance to the selection of electrical parameters is presented below:

Step 1. Select the heat input required - Mean Current.

Step 2. Consider Metal Transfer Mode required.

Step 3. Consider Metal Detachment Type.

Step 4. Set pulse time and pulse current according to the characteristics of the natural detachment times. It is essential to take into account the probability of detachment.

Step 5. Set the background phase in accordance with the choice of mean current and the limits of droplet growth.

Step 6. If the selected combination of parameters is not feasible:

a) Consider altering the electrical parameters or

b) Consider using the detachment by growth model if the previous selection has been for projected spray transfer.

Detachment by Growth Model.

Step 7. Select the droplet volume required which is to be detached in every cycle. The droplet volumes for any welding current can be calculated by $V=W \cdot A \cdot T_{DC}$.

Step 8. Set the pulse phase at a high current in the

streaming spray transfer region and the pulse time around 4 to 6 ms.

Step 9. Calculate the volume melted during the pulse phase and set the background phase in accordance with the droplet volume and mean current required.

CHAPTER SIX

The Burnoff Criterion and the Burnoff Factor in Pulsed MIG Welding.

Chapter Six The Burnoff Criterion and the Burnoff Factor in Pulsed MIG Welding.

6.1 Introduction

In this chapter the burnoff factor is examined in terms of how to derive or calculate it and its role and interaction with the other electrical parameters in pulsed MIG welding. In particular its sensitivity to various process changes such as type of metal transfer and wire feed speed is investigated.

6.2 Theory.

In direct current MIG welding the balancing between the wire feed speed and the melting rate is expressed by:

$$W=m_{DC}\cdot I_{DC} \quad \ldots\ldots\ldots\ldots\ldots\ldots\ldots\ldots \quad [6.1]$$

The term designated by the symbol m_{DC} is called the burnoff factor and is the balancing term between the wire feed speed and the melting rate. Its value depends on the physical properties of the electrode material, the diameter of the electrode wire, the arc length, the shielding gas and the welding current.

There are two components that contribute to the wire heating and melting, arc heating and resistance heating. This can be expressed as (Smati 1986) (Halmoy 1979):

$$W = K_1 \cdot I + K_2 \cdot l \cdot I^2 \quad \ldots\ldots\ldots\ldots\ldots\ldots [6.2]$$

$$W = (K_1 + K_2 \cdot l \cdot I) \cdot I \quad \ldots\ldots\ldots\ldots\ldots\ldots [6.3]$$

therefore from [6.1] and for direct current:

$$m_{DC} = K_1 + K_2 \cdot l \cdot I \quad \ldots\ldots\ldots\ldots\ldots\ldots [6.4]$$

The first part of equation [6.2], represents the effects of arc heating ($K_1 \cdot I$) and the second part, ($K_2 \cdot l \cdot I^2$) represents the effects of resistance heating which is significant for stainless steel electrodes. For pulse current the wire feed speed is given by:

$$W = (Wp \cdot Tp + Wb \cdot Tb)/T \quad \ldots\ldots\ldots\ldots\ldots\ldots [6.5]$$

and therefore substituting [6.2] into [6.5] gives:

$$W = [(K_1 \cdot Ip + K_2 \cdot l \cdot Ip^2)Tp + (K_1 \cdot Ib + K_2 \cdot l \cdot Ib^2)Tb]/T$$

$$W = K_1(Ip \cdot Tp + Ib \cdot Tb)/T + K_2 \cdot l \cdot (Ip^2 \cdot Tp + Ib^2 \cdot Tb)/T \quad [6.6]$$

In this equation the arc heating is generated by the mean current. However, as shown in equation [6.7] the resistance heating term is not the mean current to the power of two.

$$[(Ip \cdot Tp + Ib \cdot Tb)/T]^2 < [(Ip^2 Tp + Ib^2 Tb)/T] \quad .. [6.7]$$

Therefore, in pulsed welding the resistance heating term is higher than in direct current welding. Also the resistance heating term depends on the magnitude of the pulse current. This is supported by (Matsuda 1983) (Allum & Quintino 1984a) (Smati 1986) (Halmoy 1986).

Simple mathematical manipulation of equation [6.6] gives:

$$W = [(Ip \cdot Tp + Ib \cdot Tb)/T] \cdot [K_1 + K_2 \cdot l \cdot (Ip^2 \cdot Tp + Ib^2)/(Ip \cdot Tp + Ib \cdot Tb)]$$

but as $Im = (Ip \cdot Tp + Ib \cdot Tb)/T$, then the equation above becomes: $W = Im \cdot [K_1 + K_2 \cdot l \cdot (Ip^2 \cdot Tp + Ib^2)/(Im \cdot T)]$,

where: $$m = [K_1 + K_2 \cdot l \cdot (Ip^2 \cdot Tp + Ib^2)/(Im \cdot T)] \quad \ldots\ldots\ldots [6.8]$$

6.3 Experimental Work: The Burnoff Factor in Pulsed MIG Welding.

Values for the burnoff factor of the filler wire employed can be obtained from literature (Amin 1983) (Allum & Quintino 1984a) (Lancaster 1986) (Smati 1986), calculation, or by experiment. The burnoff factor for the material used was found to be $0.53 \cdot 10^{-3}$ $m \cdot s^{-1} \cdot A^{-1}$ having been derived from existing data and slightly adjusted by trial and error using a range of direct currents from 100A to 200A.

6.3.1 Observations on the Applicability of the Burnoff Factor in Pulse Current Configuration.

The burnoff factor was obtained under direct current conditions therefore experiments had to be carried out to ascertain whether the obtained value of (m) could be used in pulse current configuration.

Satisfactory balance between the wire feed speed and the melting rate was achieved for a range of direct currents from 100A to 250A and a range of mean currents from 50A to 260A. A slight departure from linearity was observed in the lower current range between 50A and 90A where short circuit transfer occurred. This may be attributed to the characteristics of the power source as these currents are at the lower end of its operating range. Above 260A and up to 300A, the highest direct current used, some increase in the burnoff factor was observed. However, most of the welding in the present work was carried out in the region between the range of 100A to 220A. Therefore, the mathematical expression:

$$W=m\cdot Im \quad \ldots\ldots\ldots\ldots\ldots\ldots\ldots\ldots\ldots\ldots \quad [6.9]$$

is valid for pulse currents as well as direct currents up to 260A.

6.3.2 Effect of Wire Feed Speed on the Stability of the Arc and Metal Transfer.

In order to assess the sensitivity of the burnoff factor a sudden imbalance between the wire feed speed and the mean current was induced. To simulate the conditions of such an imbalance, a mean current was chosen (150 A), then the calculated wire feed speed for this current was first increased by 10% and by 20% above the calculated value, and then decreased by the same amounts below the original value. The electrical parameters chosen are presented in table 6.1.

table 6.1
Data of Wire Feed Speed Fluctuation Experiments

Im (A)	W (m/min)	% (change)	Im (equiv.)	Rate of Imbalance (mm/s)
150	5.72	+20	180	+15.5
	5.28	+10	165	+8.7
	4.77	0	150	0.0
	4.29	-10	135	-8.7
	3.81	-20	119	-15.5

Ip=300A,Tp=1.36,Ib=50, Tb=2.04, TS=4.49mm/s, Q=15lt/min

The quantity designated as Im(equiv.) is the mean current which corresponds to the particular wire feed speed set during the experiment. Table 6.1 also shows that the imbalance between the original wire feed speed and the 10% increased wire feed speed is 8.5mm/s and the imbalance between the original wire feed speed and the wire feed speed increased by 20% is 15.8mm/s. These

results show that welding would be impossible because for an arc length of 10mm, short circuit would occur in around one second. Similarly with the 10% and 20% decrease in wire feed, burnback would occur in a matter of a couple of seconds as the stickout normally used is around 10mm to 12mm.

When the wire feed speed was increased by 10%, the arc length decreased fractionally, but it was apparent that the stability of the arc was not affected at all. Spatter or fumes were absent, and the bead appearance remained satisfactory. When the wire feed speed was decreased by 10%, there was a tendency for longer arc lengths but the appearence and the stability of the arc remained unchanged. The 20% increase in wire feed speed resulted in some tendency for very short arc lengths with some random occurrence of short circuiting. The 20% decrease in wire feed speed gave rise to long arc lengths with some effects on the stability of the arc. Although metal transfer had remained stable, the arc wandered, resulting in a randomly varying bead width unacceptable for welding.

The results were contrary to the predictions made on the sensitivity of the arc length, as a result of an increased or decreased wire feed speed. This may be attributed to the current voltage characteristics of the power source.

When welding at a low mean current (50 A) under short circuit transfer conditions spatter and fume generation were present. The reduction or elimination of the fume and spatter was achieved when the wire feed

speed was reduced thus preventing short circuit metal transfer from taking place (table 6.2).

table 6.2 Burnoff Factor Adjustment for Low Current Welding

Im (A)	W (m/min)	% (change)	Ip (A)	Tp (ms)	Ib (A)	Tb (ms)	TS (mm/s)	Q (t/min)	Transfer type
50	1.59	0	300	3	40	65.2	1.89	15	(S)*
	1.40	11.9							(S)/(G)*
	1.30	18.2							(G)*
	1.20	24.5							(G)

(S) Short circuit, (G) Globular, * spatter.

6.4 Discussion.

The burnoff factor employed throughout this work gave a very satisfactory balance for the welding range used and it proved that the equation $W=m \cdot Im$ is valid at least for that welding range.

For the stainless steel electrode used, when the wire feed speed was set at higher or lower values than the calculated one, the process remained satisfactory as long as the change was between +10% to +15% and -10% to -15%. The duration of each run was long enough to ensure that burnback or short circuit would have taken place. It can be concluded therefore that (m) for this particular material is not sensitive to this type of disturbance.

6.4.1 Calculation of the Burnoff Factor and Comparison with the Experimentally Obtained Value.

The calculation of the burnoff factor (m) is possible and relatively accurate providing all the required data are known. On this aspect the data for material properties may not be available thus they may

either have to be approximated, which will reduce the accuracy of the calculation, or derived experimentally. The data used for the calculations and results presented in this section have been obtained either from the literature or have been approximated.

Graph 6.1 shows the relationship between the welding current (mean current) and the wire feed speed for three different sets of burnoff factor. The first plot used the experimentally derived burnoff factor whereas the other two plots used the calculated burnoff factor for direct current and pulsed current configuration respectively. Table 6.3 shows the electrical parameters used for this calculation and their selection was purely theoretical without taking into account metal transfer stability.

table 6.3 Calculated Wire Feed Speed for Pulse Current

No.	Im (A)	Ip (A)	Tp (ms)	Ib (A)	Tb (ms)	W (m/min)
1	100	300	4	50	12.75	3.31
2	120	300	4	50	10.25	4.23
3	140	300	4	50	7.15	5.12
4	160	300	4	50	5.10	6.03
5	180	300	4	50	3.70	6.93
6	200	300	4	50	2.65	7.85
7	200	300	4	100	4.00	7.30

The pulse current, pulse time and background current have been kept constant and the background time has been adjusted suitably to provide the desired mean current range.

The wire feed speeds calculated using the experimental burnoff factor and the ones calculated using equation [6.2] for direct current and equation [6.6] for pulsed current configuration are presented in table 6.4.

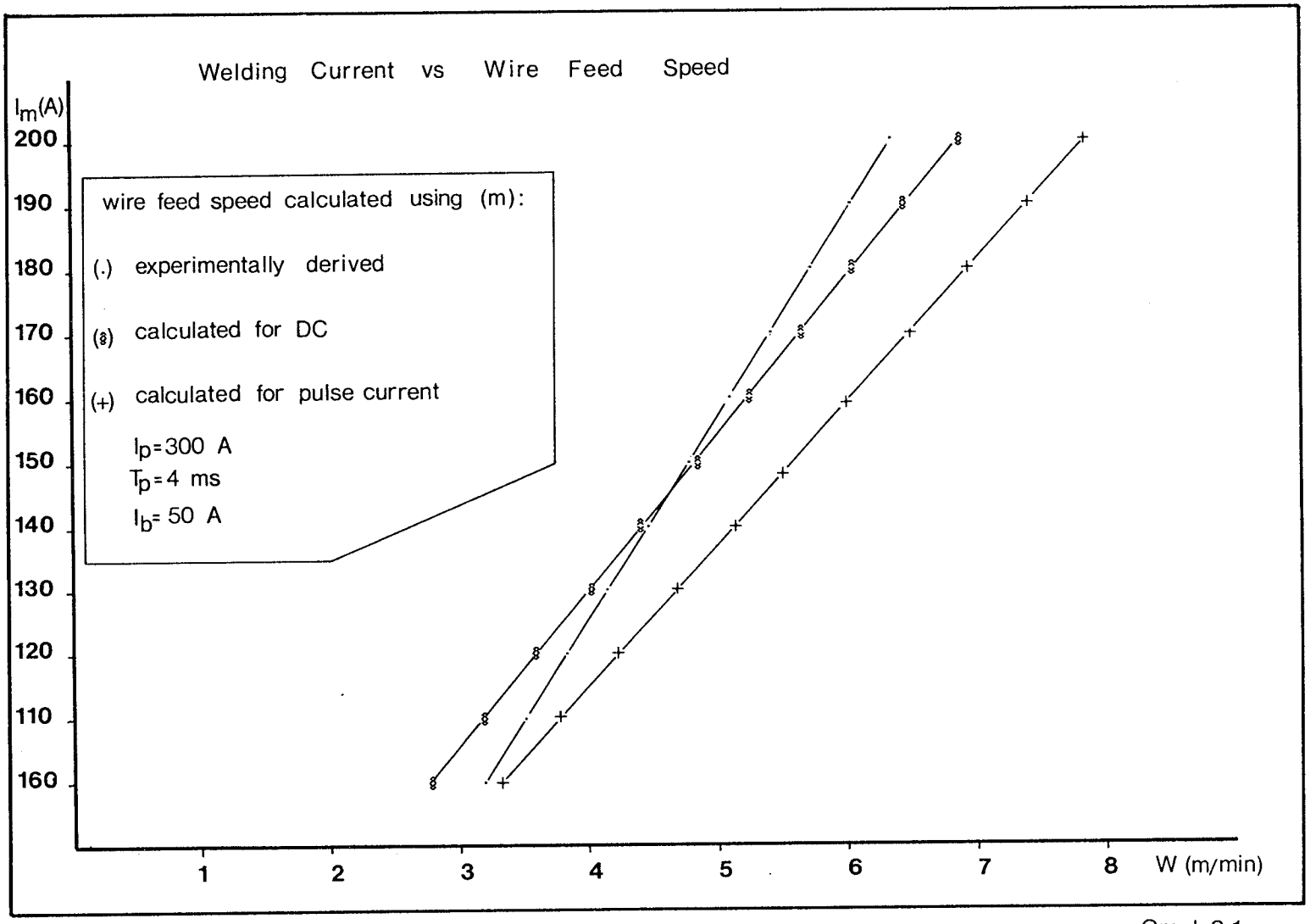
Welding Current vs Wire Feed Speed
I_m(A)
200
190
180
170
160
150
140
130
120
110
160
wire feed speed calculated using (m):
(.) experimentally derived
(8) calculated for DC
(+) calculated for pulse current
I_p=300 A
T_p=4 ms
I_b= 50 A
1
2
3
4
5
6
7
8
W (m/min)

Graph 6.1

table 6.4 Percentage Difference between Experimentally Derived and Calculated Wire Feed Speeds

I (A)	W (m/min)	W_{DC} (m/min)	%(a)	W pulse (m/min)	%(b)
100	3.18	2.77	-12.8	3.31	+3.9
120	3.80	3.48	-8.4	4.23	+10.1
140	4.45	4.25	-4.5	5.12	+13.0
160	5.08	5.08	0.0	6.03	+15.7
180	5.72	5.95	+3.8	6.93	+17.4
200	6.36	6.88	+7.5	7.85	+19.0
200				7.30	+12.8

%(a) shows the % difference between experimental and calculated wire feed speed for direct current
%(b) Shows the % difference between experimental and calculated wire feed speed for pulse current

The results show that the difference between the calculated burnoff factor wire feed speeds and the experimentally derived one lie within the 15% band of tolerance as discussed in 6.3.2.

It may be concluded therefore, that both the experimental method and the calculation to obtain the burnoff factor and the wire feed speed give satisfactory results. However, the experimental method has the advantage that it is simple to perform and avoids the inaccuracies involved with approximations if data are not available.

6.4.2 Arc Length Fluctuation.

Fluctuation of the arc length during experimentation was observed even under stable metal transfer conditions.

Arc fluctuation is expected to occur when irregular metal transfer takes place due to variations in the droplet volume. This may occur at current levels

where metal transfer modes change. For the electrode material used, the maximum disturbances due to inconsistent droplet volumes is expected to occur up to mean currents of 160A where the droplet volumes for Mean Current Type of detachment (see chapter 5) are large. At higher mean currents any droplet volume variations are expected to be very small, thus arc fluctuation caused by irregular transfer should not occur.

Arc fluctuation due to the pulse current configuration is not possible especially when the duration of the pulse and background phases is too short to cause any imbalance in the dynamic stability of the arc. This statement is supported by (Halmoy 1979) (Halmoy 1986).

Other causes of arc fluctuation may be attributed to the adhesion of the electrode wire on the electrical contact in the welding torch (Yamada & Tanaka 1987), probable resonance as a result of the electronic controls of the welding machine, slip of the wire feeder rollers or a combination of these.

During the current work most of the incidents of low frequency arc fluctuation coincided with some irregularity of metal transfer.

CHAPTER SEVEN

Fusion Characteristics of 316S92 Stringer Beads on 070M20 Plates.

Chapter Seven Fusion Characteristics of 316S92 Stringer Beads on 070M20 plates.

7.1 Introduction.

This chapter describes the mechanisms of the formation of the weldpool and the reinforcement bead. It also examines the effect of the welding parameters and their various combinations on the fusion characteristics of 316S92 stainless steel deposits on 070M20 mild steel plates using predominantly projected spray transfer at low heat inputs.

7.2 Weldpool and the Formation of the Reinforcement Bead.

The shape of the weldpool and the resulting bead profile in GMA welding depends on two mechanisms; the heat distribution over the weldplate and the droplet heat content and momentum.

7.2.1 Heat Distribution.

For a constant total energy input per unit time the manner in which the heat is distributed on the surface of the weldment will influence the width to depth ratio of the weldpool.

The heat generated by the arc is transferred to the weldpool by means of electron kinetic energy, the work function at the weldplate surface, radiation, thermal conduction and thermal convection (Glickstein & Yeniscavich 1977). Of the total heat transferred to the

weldplate from the arc approximately 80% is contributed by the electron (and ion) kinetic energy and the surface work function (Quigley et al 1973), and approximately 20% by plasma convection and radiation (Lancaster 1954). The amount of kinetic energy supplied to the electrons and ions in the space charge zone depends on the voltage drop in this area which in turn depends on the degree of vaporisation and ionisation in the space charge zone.

The heat distribution is virtually the same as the welding current density distribution and depends on the conductivity of the arc which in turn is temperature dependent. The arc column temperature depends on the ionisation potential of the shielding gas and the ionisation potential of the baseplate material (Glickstein 1979).

As the ionisation potential of metals is much lower than of the shielding gases it appears that the metal vapours in the arc column will tend to decrease the temperature of the arc column to approximately 6000°C when ferrous electrodes are used (Lancaster 1986).

The heat distribution input to the weldment has a significant effect on weld penetration. For a given total energy input per unit time an increase in the width of the energy distribution reduces the depth of the weldpool ie. the penetration.

7.2.2 Droplet Heat Content and Momentum.

A detaching droplet has kinetic energy and contains heat. In GMA welding of the total heat received by the base metal, approximately 70% is delivered by the arc column and approximately 25%-30% by the heat content in the droplets (Essers & Walter 1979). Measurements of the temperature of the detaching droplets suggest that they are superheated. The temperatures for 1.2mm diameter mild steel electrode wire range from 2000°C to 2700°C (Lancaster 1986). However, the droplet temperatures depend on the transfer mode. Measurements have shown that projected spray transfer exhibits the lowest droplet temperature relative to the other transfer modes (Jilong Ma & Apps 1983).

High speed filming of the arc and the weldpool has revealed, particularly at high welding currents, that every impact forms a marked indentation on the surface of the pool. At relatively lower currents the indentation tends to fill up with liquid metal but when the frequency of detachment is high the indentation is not filled up. This phenomenon is connected with the occurrence of finger penetration. It can therefore be concluded that kinetic energy although negligible in comparison to the heat content (Essers & Walter 1979), contributes appreciably to the shape of the weldpool. Droplets are detached, accelerated and driven into the weldpool dissipating their heat content while penetrating further into the base metal. In addition at higher currents the projected droplets tend to be focused at one point thus promoting finger penetration.

7.2.2.1 Droplet Velocity and Acceleration.

After detachment a droplet is accelerated towards the weldpool at a constant acceleration (Jilong Ma & Apps 1983) by plasma jets. Typical values for plasma jet velocities when metal transfer is absent are in the range of 100 to 1000m/s (Weinecke 1955). However, droplet evolution restricts the plasma jets and does not allow them to develop their full velocity. The larger the droplet the bigger the restriction. For mild steel the droplet velocity ranges from 0.35 to 1.33m/s (Waszink & Piena 1986). With projected and streaming spray transfer the arc forces, combined with the small size of the droplets, have more profound effects on weldpool geometry and in particular on the depth of penetration.

7.2.3 Weldpool Convection.

Research has shown that certain characteristics of the weldpool shape and size are linked with the phenomenon of weldpool convection (Woods & Milner 1971) (Mills 1979). Therefore if a flow field has a known magnitude and direction the bead profile, penetration, dilution and porosity may be predicted (Kou & Wang 1986). Models for the prediction of the weldpool geometrical features, involving magnetohydrodynamic flow have been developed (Sozou & Pickering 1978) (Andrews & Crane 1978) but many simplifications have been made.

The flow fields are set up by electromagnetic fields due to the current flow; electrode inclination (Woods & Milner 1971), temperature gradients (Oreper et al 1983) (Lancaster 1986) and arc pressure (Lin & Eagar

1985) may change these flow fields dramatically. On surface tension flows (Velarde & Norman 1980), research has concentrated on the effect of minor elements on the flow fields and consequent penetration characteristics (Glickstein & Yeniscavich 1977) (Heiple & Roper 1982) (Heiple et al. 1983) (Walsh & Savage 1985). This type of flow field is characteristic of GTAW and takes approximately one second (1 s) to develop fully (Sozou & Pickering 1976). In gas metal arc welding metal transfer occurs every 1-10ms, 0.1s during globular transfer. It is highly unlikely that the same flow patterns are present as in GTAW, but flow will be dominated by metal transfer forces especially in streaming spray transfer (Tsao & Wu 1988). A simplified model (Ishizaki 1962) (Bradstreet 1968) is shown in figure 7.1 and has been derived by metallography and high speed photography.

7.2.4 Modelling and Formulation of the Arc.

The difficulty of modelling the arc is that all the welding parameters must be translated into mathematical terms to be used in the heat conduction equations. Furthermore, the final form of the equations must be able to account for all the combinations of materials and welding parameters. The heat flow to the weldment from the arc is complicated by non constant thermal properties of the material, the heat of phase transformation, the thickness of the plate, convection in the weldpool, depression of the molten metal surface (Lin & Eagar 1985) (Lin & Eagar 1986) and the physical and thermal properties of the base material (Eagar & Tsai

1983).

Analytical solutions (Rosenthal 1946) (Mahla et al 1941) (Wells 1952) (Christensen et al 1965) (Meyers et al 1967) (Malmuth et al. 1974) (Paley & Hibbert 1975) (Tsai 1982) (Eagar & Tsai 1983) (Szekely et al 1987) were not used in the present work because their complexity did not match their accuracy. In addition the authors examined GTAW which does not include metal transfer or manual metal arc welding which exhibits a different mechanism of metal transfer than that of p-MIG welding.

Computer simulations have been implemented for both GTAW (Kou 1981) (Ecer 1981) (Szekely 1986) and GMAW (Tsao & Wu 1988). However, the GMAW model is limited to streaming spray transfer.

The relationship between the bead height, width and angle of contact can be used to predict bead shapes and dimensions (Nishiguchi et al. 1977), but knowledge of one or two of the geometrical features is required which makes this method semi-theoretical / experimental. In addition there are some unknown quantities, especially the surface tension of the weldpool material. This is complicated further when two different materials are fused together as the amount of dilution may affect the surface tension values.

Empirical models using statistical techniques (McGlone 1980) (McGlone 1982) (Harris & Smith 1983) (Raveendra & Parmar 1987) can be effective but require a substantial amount of data.

7.2.5 The Effect of Process Parameters on the Dimensions of the Weldbead.

The dimensions of the bead depend mainly on the welding current and the travel speed. However, voltage, arc length, polarity and shielding gas contribute sometimes significantly to variations in the dimensions.

The welding current and the electrode travel speed determine the amount of heat and metal supplied to the weldpool. If the welding current is increased, the heat input to the weldment will also increase despite a drop of efficiency due to radial losses (Niles & Jackson 1975) (Ghent et al 1979). Additionally, the intensity and frequency at which droplets impact the weldpool will increase.

The relation of the arc length and arc voltage is nearly linear, the longer the arc gap the greater the voltage drop (Milner et al 1960). It has been found that at low heat inputs the width of the weldbead decreases as the arc length increases. At high heat inputs the width of the bead tends to increase as the arc length increases (Glickstein 1975). The heat input where this transition takes place for stainless steel is around 190A (Tsai 1982).

Polarity affects metal transfer. In particular reverse polarity increases penetration because it promotes regular accelerated metal transfer (Felmley 1955) and because increases the heat transfered to the base material (Smith 1984).

The shielding gas contributes to a certain extent depending on its ionisation potential and its

atomicity. The atomicity of the gas determines whether dissociation of the gas near the filler wire and association near the surface of the weldpool takes place. Association of the gas near the weldpool releases extra energy which in effect causes an increase in the dimensions of penetration. Certainly the difference in ionisation potential changes the thermal and electrical properties of the arc. The higher the ionisation potential, the higher the voltage required across the arc to conduct equally for the same arc length (Tsai 1982).

7.2.6 Effects of Dimensions and Temperature of the Base Material on the Bead Profiles.

The dimensions of the base material determine the manner in which the heat supplied by the arc is dissipated. For example, if a stringer bead is deposited in the centre of a plate the heat will dissipate in a different manner than when welding close to the edge of the plate. In terms of the set up used and type of deposition, the thickness of the plate is the critical dimension because it determines the type of heat flow that takes place; ie. thin plate analogy which considers bi-thermal heat flow or thick plate analogy which considers tri-thermal heat flow. In the bi-thermal model, the bottom surface of the plate has a temperature close to that on the top surface and the heat flows sideways in two directions. In the tri-thermal model the bottom surface is significantly lower in temperature than the top surface and the heat flows sideways as well as towards the bottom surface. The type of model appropriate

for each case is determined mainly by the combination of welding parameters and plate thickness (Adams 1958) (Blodgett 1984).

7.2.7 Geometrical features of the bead.

The shapes and geometrical features of the bead are shown in figure 7.2, figure 7.3 and figure 7.4. The bead shapes have been classified for the purpose of this study as regular, irregular and obtuse. A regular bead shape has relatively low angles of contact and is symmetrical, whereas an irregular bead shape has a non symmetrical profile. Profiles that have angles of contact $\Theta > 90^{\circ}$ are classified as obtuse. The geometrical features of the beads are the depth of penetration, the height, the width, the angles of contact, the deposited area, the penetration area, the total area and the dilution. Dilution is the percentage of base metal in the total fused metal and is given by the expression:

Dilution= [penetration area]/[total area]

$\delta = Ap/Ap+Ad$ ..... [7.1]

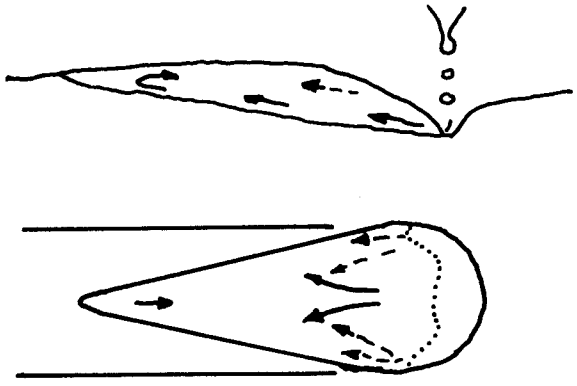

FIG.7.1 Metal Flow in MIG Weldpools during Streaming Transfer

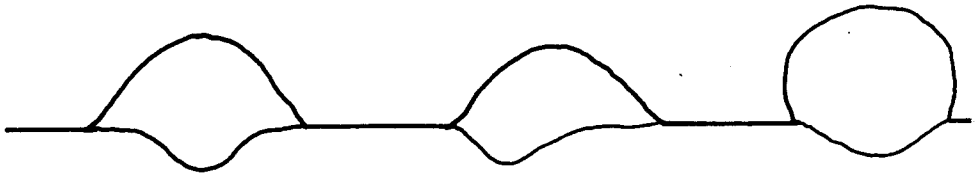

Regular Irregular Obtuse

FIG.7.2 Types of Bead Profiles

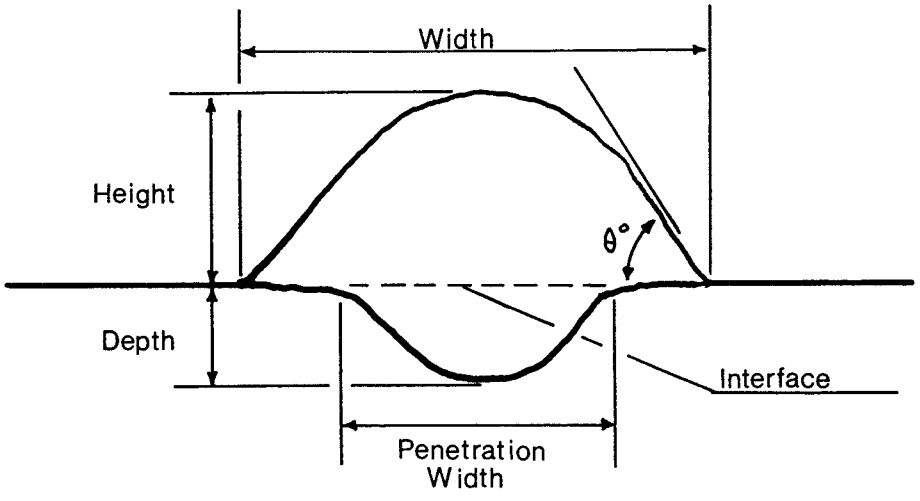

FIG.7.3 Bead Dimensions

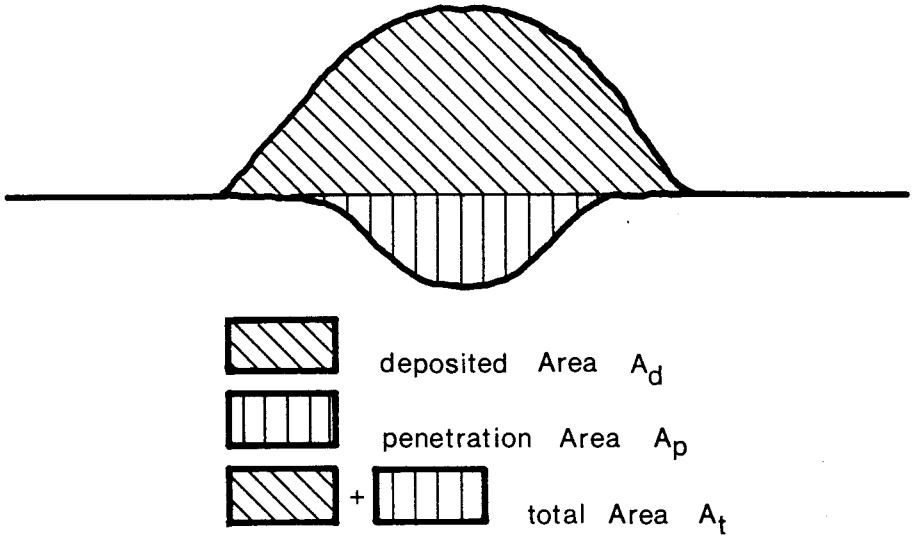

FIG.7.4 Bead Areas

7.3 Experimental Work on the Fusion Characteristics of 316S92 Stringer Beads on 070M20 plates.

7.3.1 Introduction.

There are two types of process parameters, the ones that are set before each run to some desired value and the ones that, under certain circumstances, may change during the operation. The parameters, for this particular experimental arrangement, that are set and remain constant are: the shielding gas pressure, welding current pulse configuration, electrode polarity, standoff, torch incident angles as well as electrode travel speed. However, there are parameters, such as the arc length, arc voltage and metal detachment that are sensitive to small instabilities during the process and are prone to small changes. In addition they interact with each other causing larger scale effects, such as unstable metal transfer.

Two physical limits are considered in the analysis of the fusion characteristics of the materials employed. One is the point at which burn through of the plate occurs and the other is when the deposit comes into contact with the electrode due to excessive build up.

Burn through is an extreme case. Therefore the present work considers as a limit the point where heat dissipation in the base plate ceases to be tri-thermal and becomes bi-thermal. The arc length is the other limiting factor in the analysis and ranges between 5-10mm.

All experiments were conducted in reverse polarity, the arc length was kept between 5-8mm although

variations were observed during instabilities. In addition, other constant settings were the standoff 18mm, the shielding gas flow rate at 20lt/min, the gas composition Ar 1%O_2 and ambient pressure and temperature.

The mean currents used, varied from 50A up to 200A although 100A was mainly used. The electrode material used was 1.2mm diameter stainless steel wire and it was deposited on 300x150x12.25mm mild steel plates. The thickness of the plate was sufficient to maintain a three dimensional heat flow analogy for the heat inputs employed. In addition, it was thin enough to be easily cut in order to provide specimens for analysis.

7.3.2 Experimental Arrangement.

For the experiments discussed in this section the following experimental arrangement was used:

The plates to be welded were placed on a lathe bed where they were secured and earthed. The torch was positioned above the plate and supported by a torch holder which was attached on the lathe saddle. Then by using the lathe longitudinal carriage speeds the welding speed was set and controlled ranging from 0.054mm/s to 17.3mm/s.

7.3.3 Experimental Method for the Measurement of Bead Profiles.

Observation and measurement of bead profiles, involved the preparation of specimens by cutting transverse thin sections from the deposit. These sections were then mounted in bakelite, ground, polished and

etched.

The specimen profile was then observed and drawn on tracing paper using a low magnification macroscope. Direct measurements could then be made for the height, width and depth of penetration. The bead areas were measured by cutting out the bead shape and weighing it on a high precision balance. The weight of the cut-out was then compared with the weight of the whole sheet of paper. Thus knowing the weight and area of the whole sheet, the area of the cut out could be calculated. The method used, despite being crude, was simple, fast and reasonably accurate.

The major disadvantage of bead profile measurements is the time consuming process of cutting and preparing specimens. Ideally, from one stringer bead five to ten specimens would give a more accurate measurement of the bead profile. However, considering the time involved to prepare specimens this is impractical.

It has been found that even during stable transfer the values of the geometrical features within a bead exhibit some scatter. Measurement of the amounts of scatter has not been carried out or examined in detail. A high degree of scatter in the values of the bead dimensions is encountered only during mixed and unstable metal transfer, but such conditions are unacceptble for welding and are therefore not considered in the present work. Thus, in this case the use of only one section as a representative of one deposit can provide an accurate and satisfactory picture of the fusion characteristics of a stringer bead.

7.4 Results.

In this section the results from the experiments on the fusion characteristics of the alloys employed are presented. In all cases unless stated the metal transfer is projected spray. All the data used are in tables 7.1 to 7.6.

7.4.1 Effects of Dimensions and Temperature of the Base Material on the Bead Profiles.

In the present work, the low heat input resulting from the welding parameters used, combined with the plate dimensions corresponded to a tri-thermal heat flow analogy. One experiment involving stringer bead deposition at three different preheat temperatures, 250°, 170°, 130° was performed and compared with results from cold start welding. The parameters used and the results obtained are shown in table 7.3. Comparisons were made using specimens 14, 15, 19 from table 7.1 and table 7.2.

The results obtained from this experiment show that the effects of preheat on the geometrical features of the bead are not very significant at least for the preheat temperatures employed.

The only noticeable difference was the slightly improved arc stability perhaps due to the presence of a blue oxide film.

7.4.2 Effects of Welding Parameters on the Cross Sectional Areas of the Deposit.

Graph 7.1 shows the effects of welding (mean) current on the cross sectional areas of the deposit made at a constant speed of 7.45mm/s. The graph for the total area follows a linear relationship whereas the graphs for the deposited area and the penetration area are near linear for up to 160A. At 170A the deposited area decreases slightly whereas the penetration area increases.

Allum & Quintino (1985b), have proposed the equation:

$$A_d=(W/TS)A_W \quad \ldots\ldots\ldots\ldots\ldots\ldots\ldots \quad [7.2]$$

to derive approximately the area of the deposited bead as a function of wire feed speed, electrode travel speed and electrode wire diameter. This relationship is also plotted in graph 7.1 and as can be seen there is good agreement with the experimental results.

Graph 7.2 shows the areas of stringer bead profiles deposited at a constant mean welding current of 100A and constant pulse parameters configuration. The electrode travelling speed employed, varied between 2.49mm/s and 7.45mm/s. Welding above the highest speed was not possible due to irregular formation of the bead.

The shape of the graph is not linear which is contrary to the prediction of equation [7.2]. This shows that [7.2] can only be used as a first approximation. A near linear region of the graph may be identified between the travel speeds of 7.5mm/s and 3.8mm/s, but at lower welding speeds a noticeable change in the slope of the

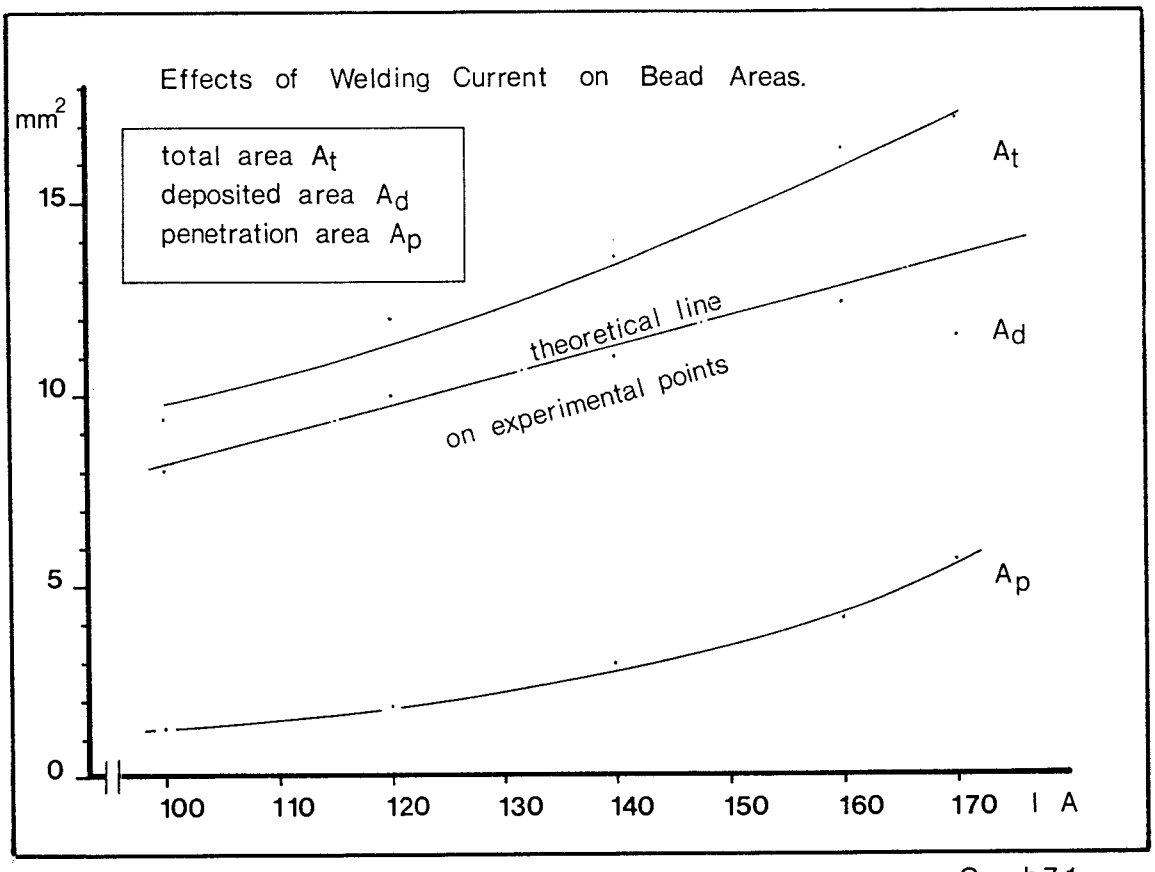

Graph 7.1

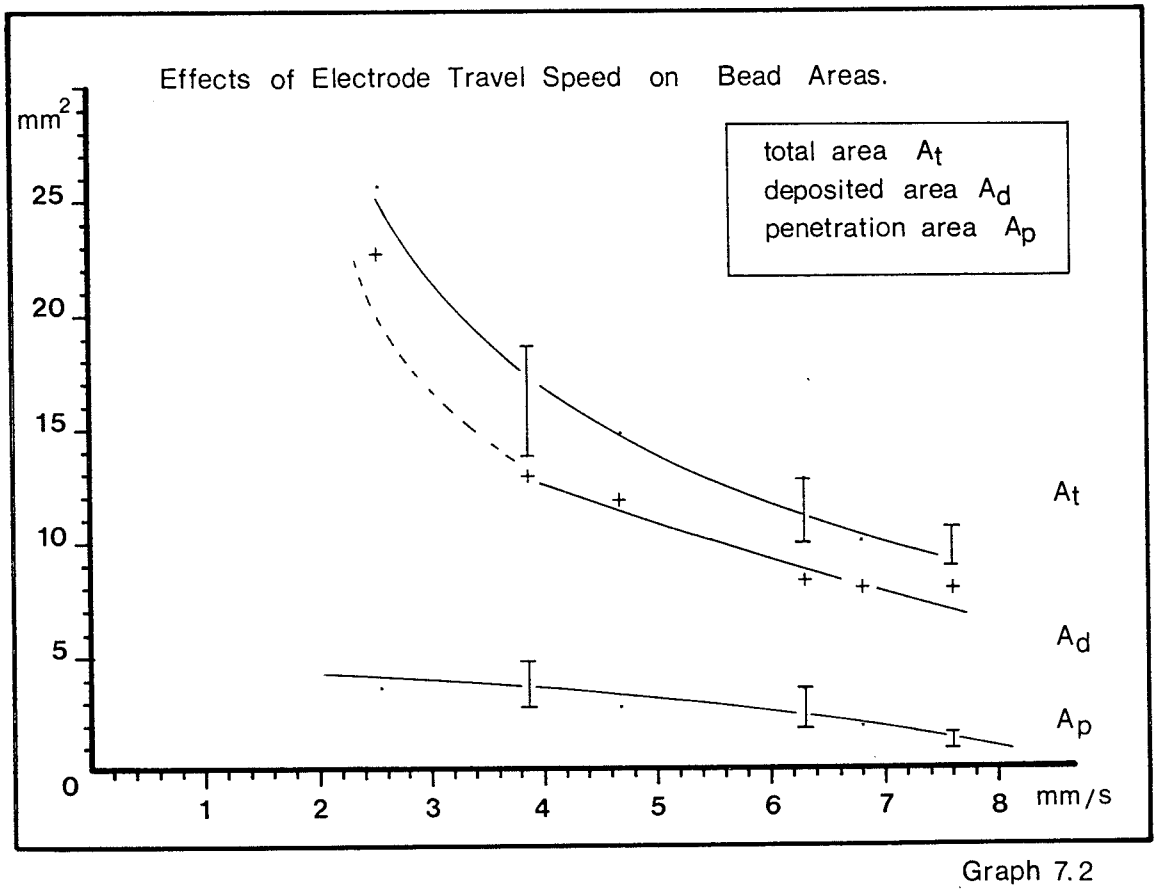

Graph 7.2

graph takes place.

It can be seen from the graph that the penetration area increases as travel speed decreases but at a speed around 3mm/s, it reaches a maximum value and then remains approximately constant. This is because after a certain point the deposit acts as a buffer to the detached droplets thus hindering any further penetration. However, this characteristic depends on the welding current and the thickness of the plate. For example if higher currents were to be employed the shape of the graph would show a steady increase of penetration as in graph 7.2 up to the point where heat dissipation would change into a bi-thermal analogy. It is anticipated that when the heat dissipation changes into a bi-thermal analogy, the penetration area will continue to increase until burn through of the plate occurs.

7.4.3 Effects of Welding Parameters on the Levels of Dilution.

Dilution is the ratio between the penetration area and the total area of the bead. Therefore, its value depends on how the penetration area and the deposited area are affected by the welding conditions as has been seen in equation [7.1].

In the case of an infinitely thick plate, and for any welding current used, low travel speeds will tend to promote the deposition of obtuse profiles which usually have very low dilution. For a constant welding current, using graph 7.2 as reference, increasing the electrode travel speed will result in higher dilution

levels because despite a minute decrease in the penetration area, the deposition area decreases in comparison at a higher rate.

Graph 7.2 also shows that at higher travel speeds the area of penetration decreases, whereas the deposition area remains almost unaffected. Therefore, at higher electrode travel speeds dilution decreases.

This sequence of events is clearly illustrated in graph 7.4 which shows that dilution is very low at slow travel speeds due to the buffer effect the deposit has on penetration. Dilution increases as the increasing travel speed reduces the deposited amount of filler metal and reaches a maximum after which it rapidly decreases as penetration is affected by the increased travel speed.

Graph 7.3 shows the effects of welding current on dilution. For an electrode travel speed of 7.45mm/s dilution increases as the welding current is increased. If the same graph was plotted at significantly lower speed, the increasing welding current would tend to promote obtuse profiles thus either not affecting dilution at all or actually causing it to decrease.

The dilution levels measured during the present work, for the alloys used, varies between 8.5% and 33% which is typical of the MIG and pulsed MIG welding process and agrees with previous research (Allum & Quintino 1985a).

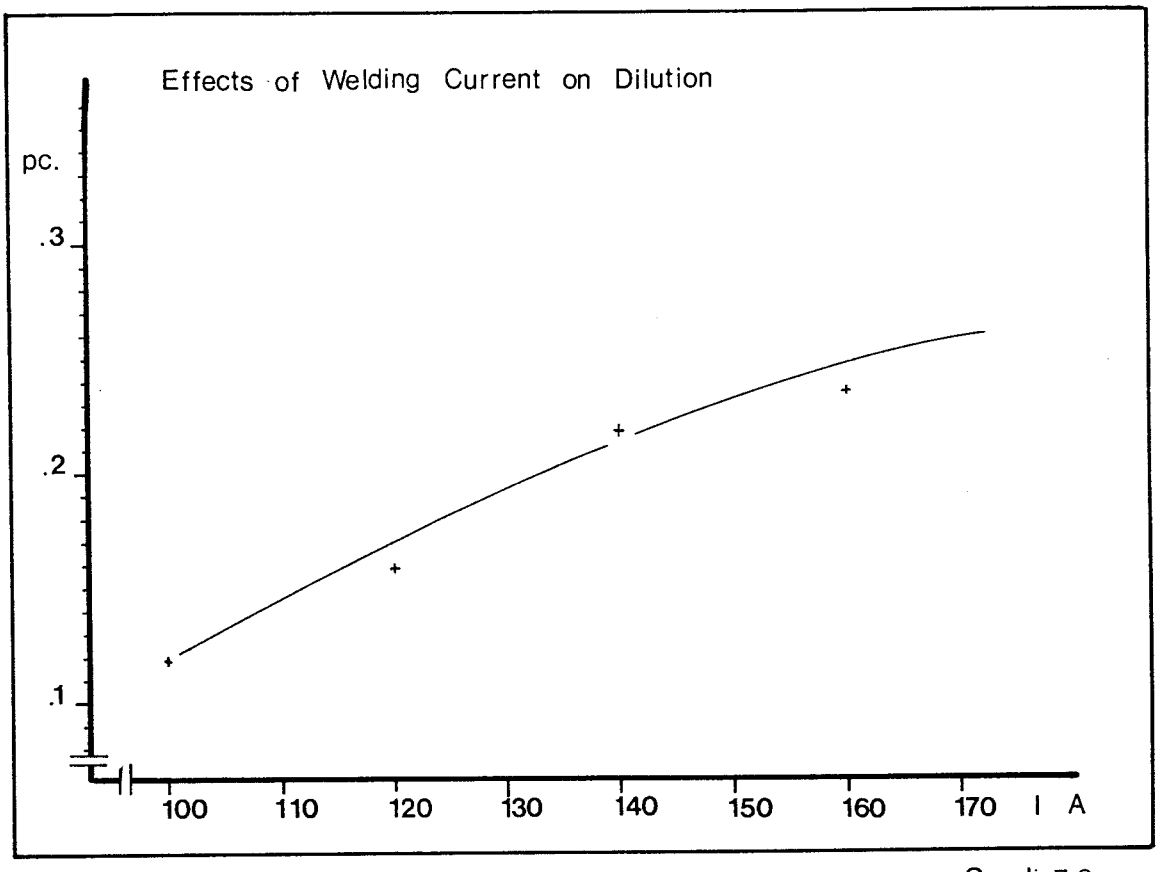

Graph 7.3

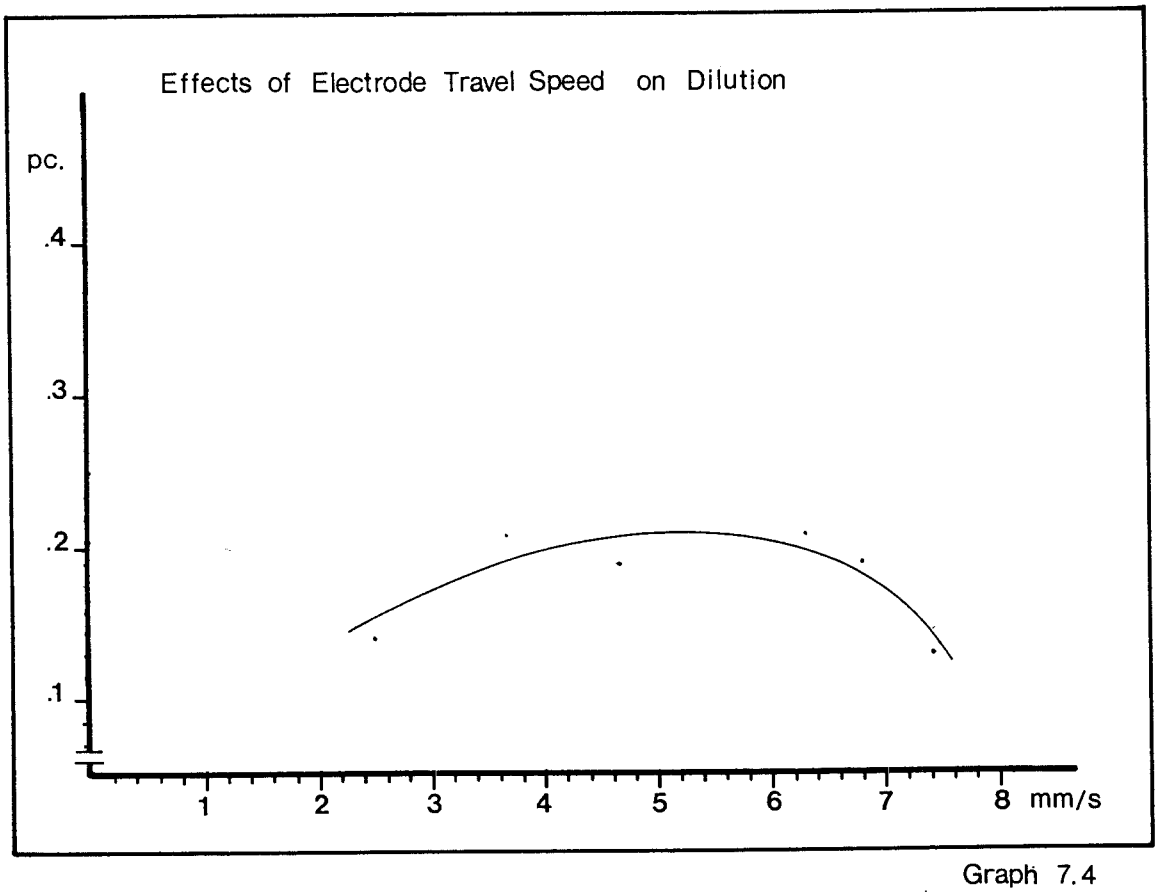

Graph 7.4

7.4.4 Effects of Welding Parameters on the Depth of Penetration.

The effects of welding current on the depth of penetration are shown on graph 7.5. Penetration becomes deeper as the welding current increases. This may be attributed to the increased heat input from the arc to the weldplate.

Graph 7.6 shows the effects of travel speed on the depth of penetration for a mean current of 100A. The depth of penetration increases as the travel speed decreases. However, the rate at which the depth of penetration increases is limited by the deposit which acts as a buffer.

7.4.5 Effects of Welding Parameters on Contact Angles.

Graphs 7.7 and 7.8 show the effects of welding current and travel speed on the contact angle θ between the bead and the base metal.

Graph 7.8 shows that at low travel speeds the deposit exhibits an angle of $\theta \geq 90^{\circ}$ (obtuse shape) but as the welding speed is increased, the contact angles decrease to a minimum of around $\theta \approx 60^{\circ}$ and then at higher speeds the angles of contact start to increase again.

The occurrence of obtuse and in general relatively large angles of contact shows that excessive electrode material has been supplied in the weldpool.

Large angles of contact occur at low travel speeds because the amount of electrode material supplied to the weldpool causes the deposit to roll over. As the travel speed increases less material is transferred to

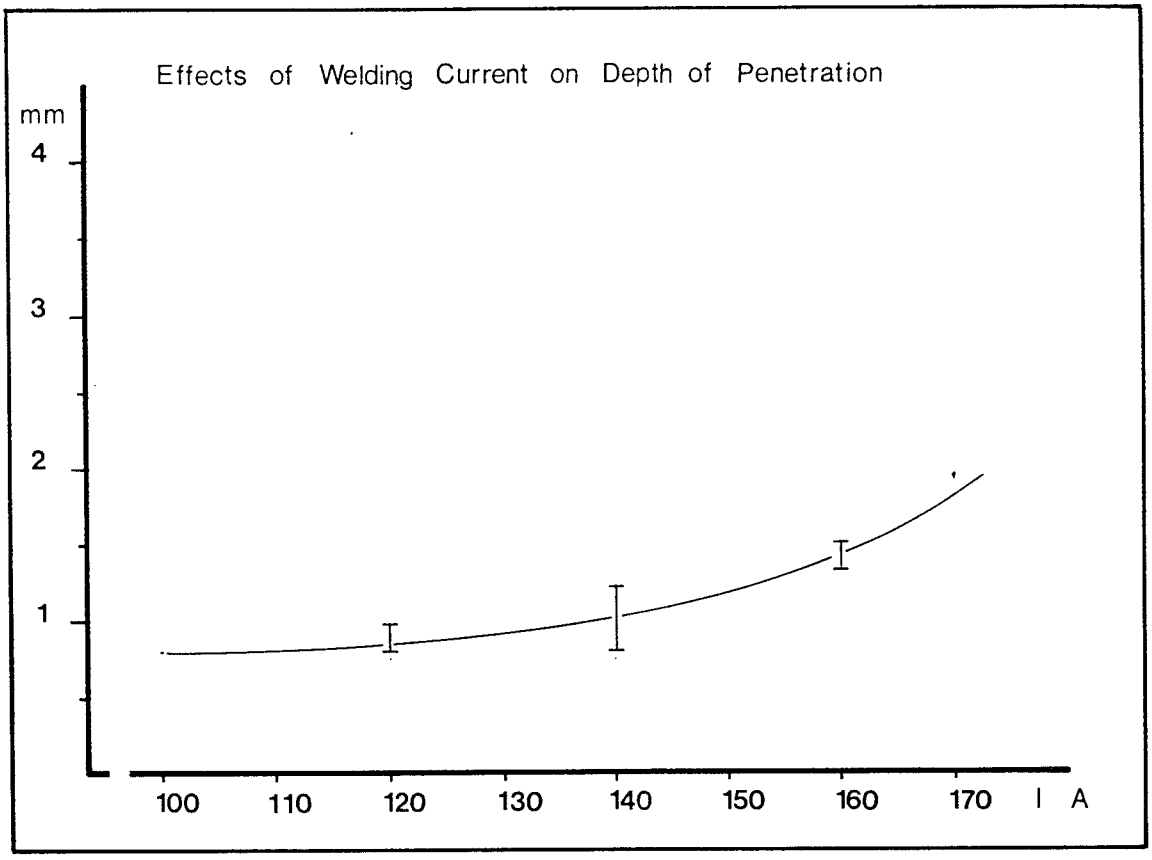

Graph 7.5

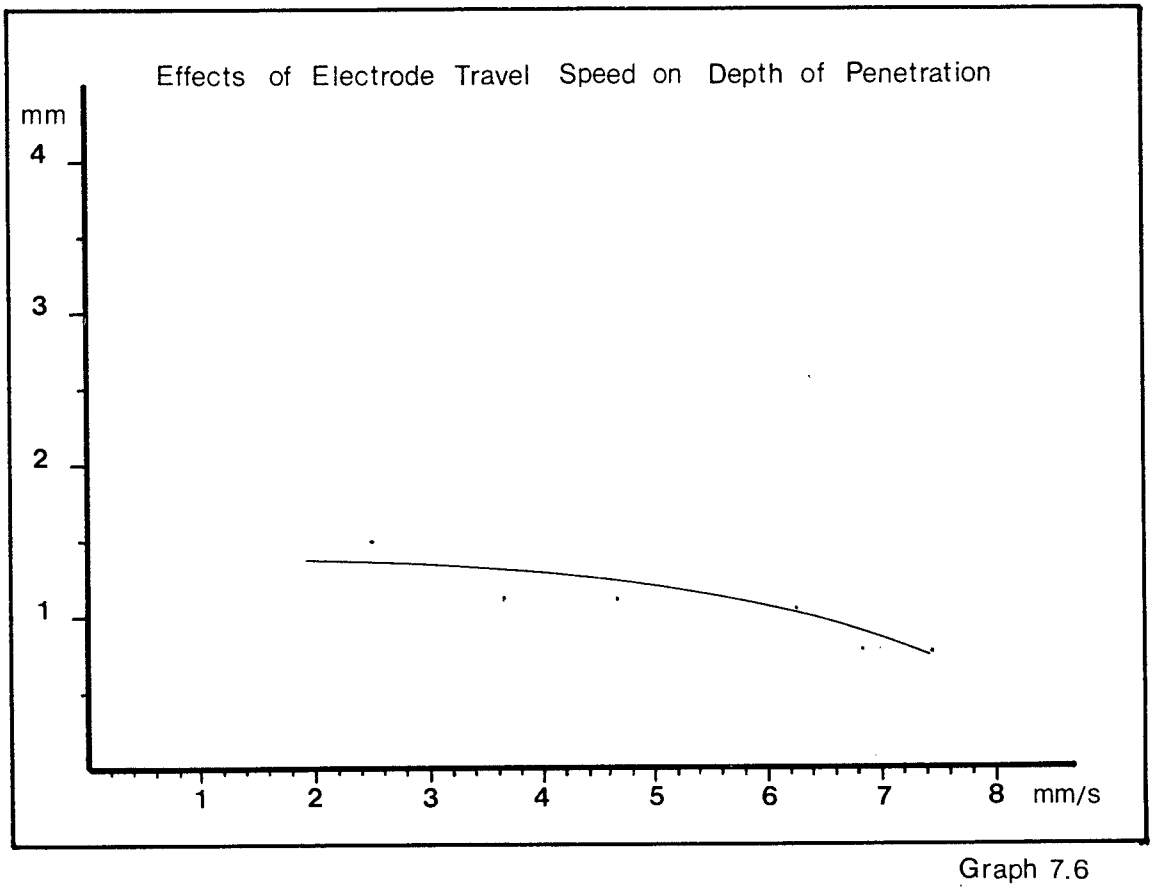

Graph 7.6

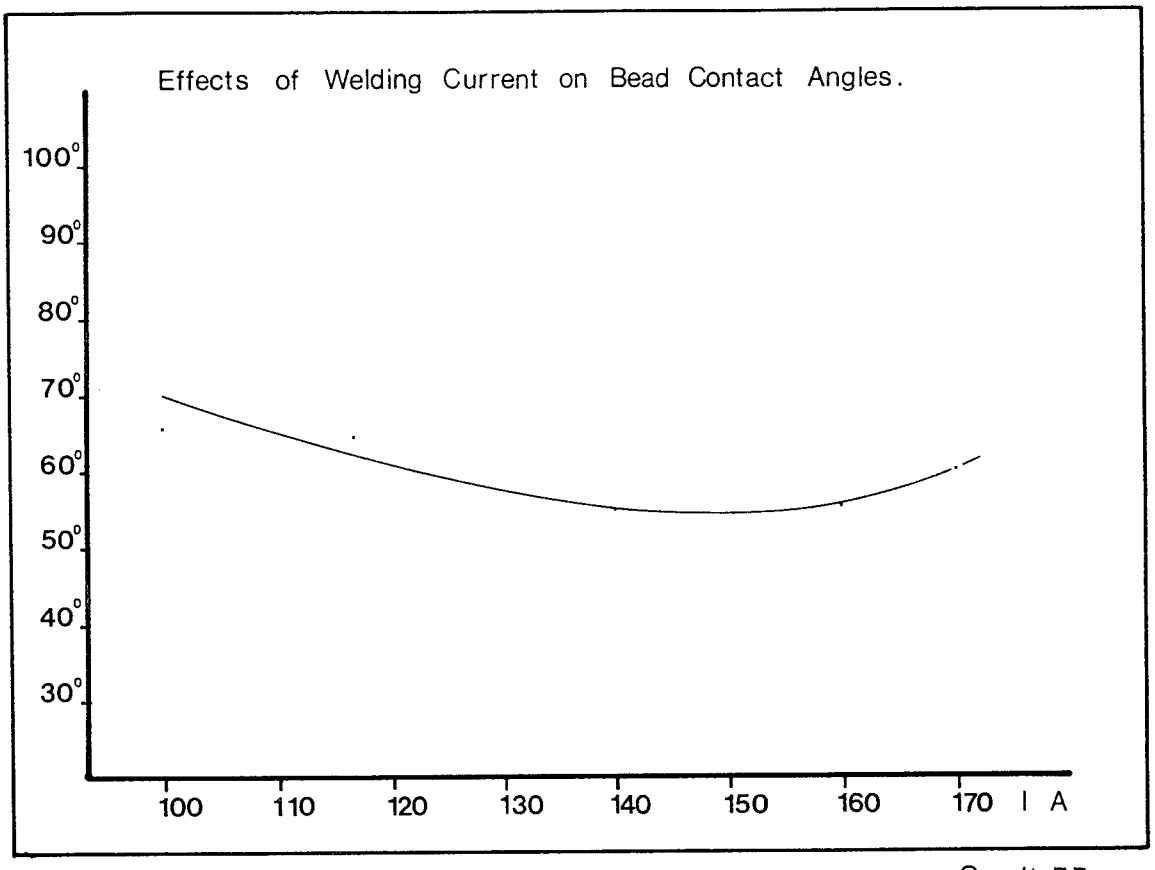

Graph 7.7

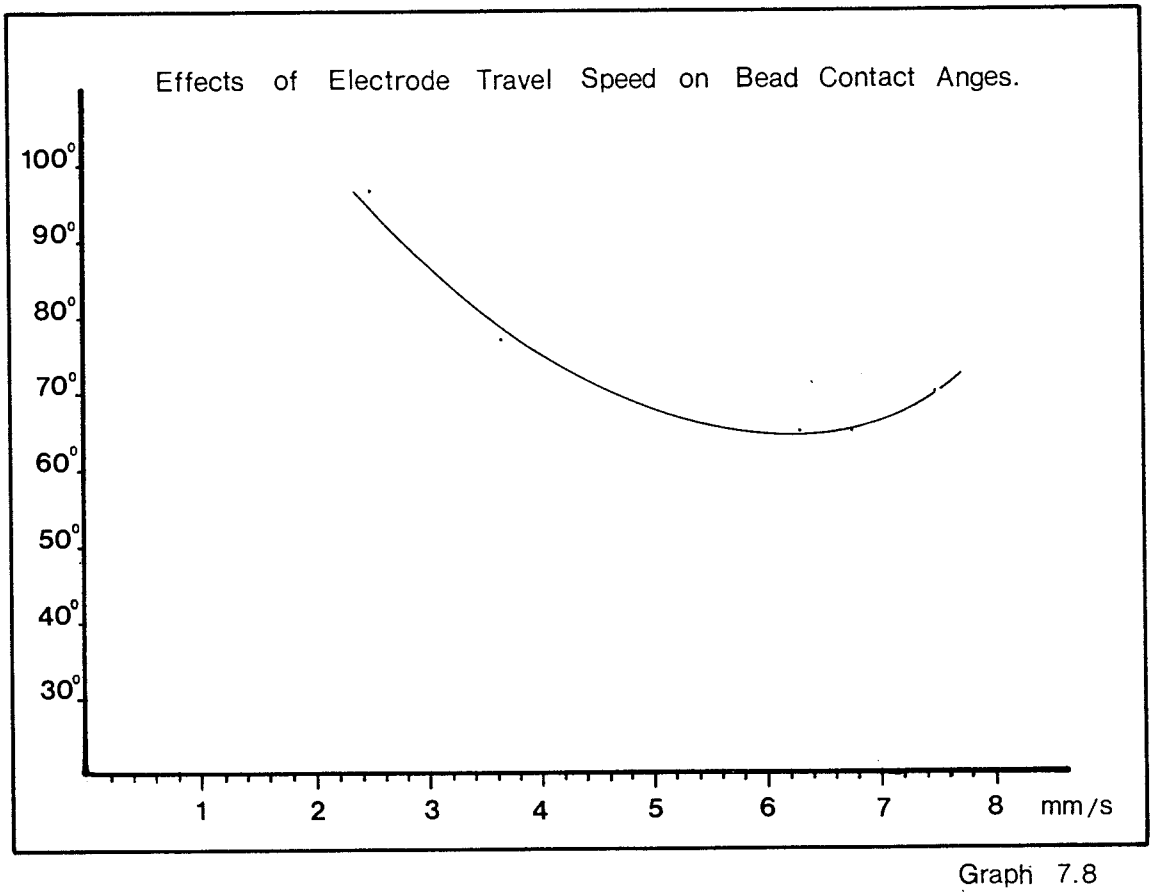

Graph 7.8

the weldpool thus the angles of contact decrease. However, as the travel speed increases further, the rate at which the weldpool decreases in size is higher than the rate at which the electrode material is supplied to the weldpool, thus the net effect is to promote obtuse bead shapes.

Graph 7.7 shows the effects of welding current on the contact angles for a constant electrode travel speed. The graph exhibits the same trend as graph 7.8 but the effects are not as marked due to the limited range of currents used.

7.4.6 Effects of Pulse Parameters on Bead Brofiles.

Pulse parameters affect the bead geometry as a result of the metal transfer mode they promote. It would be more accurate to say that the effect of pulse parameters on the bead profile is indirect. The droplet volume and its acceleration is the main influence.

It was found that the smaller the droplet volume, the deeper the penetration. Graph 7.9 shows the effects that projected and globular transfer have on the bead width, bead height and depth of penetration, for a range of mean currents and a constant travel speed.

The depth of penetration is shown in graph 7.9 where projected spray transfer exhibits a higher degree of penetration than globular transfer due to the increased droplet momentum.

Globular transfer gives rise to slightly wider beads whereas projected spray transfer to narrower beads. However, as the mean current is increased the bead width

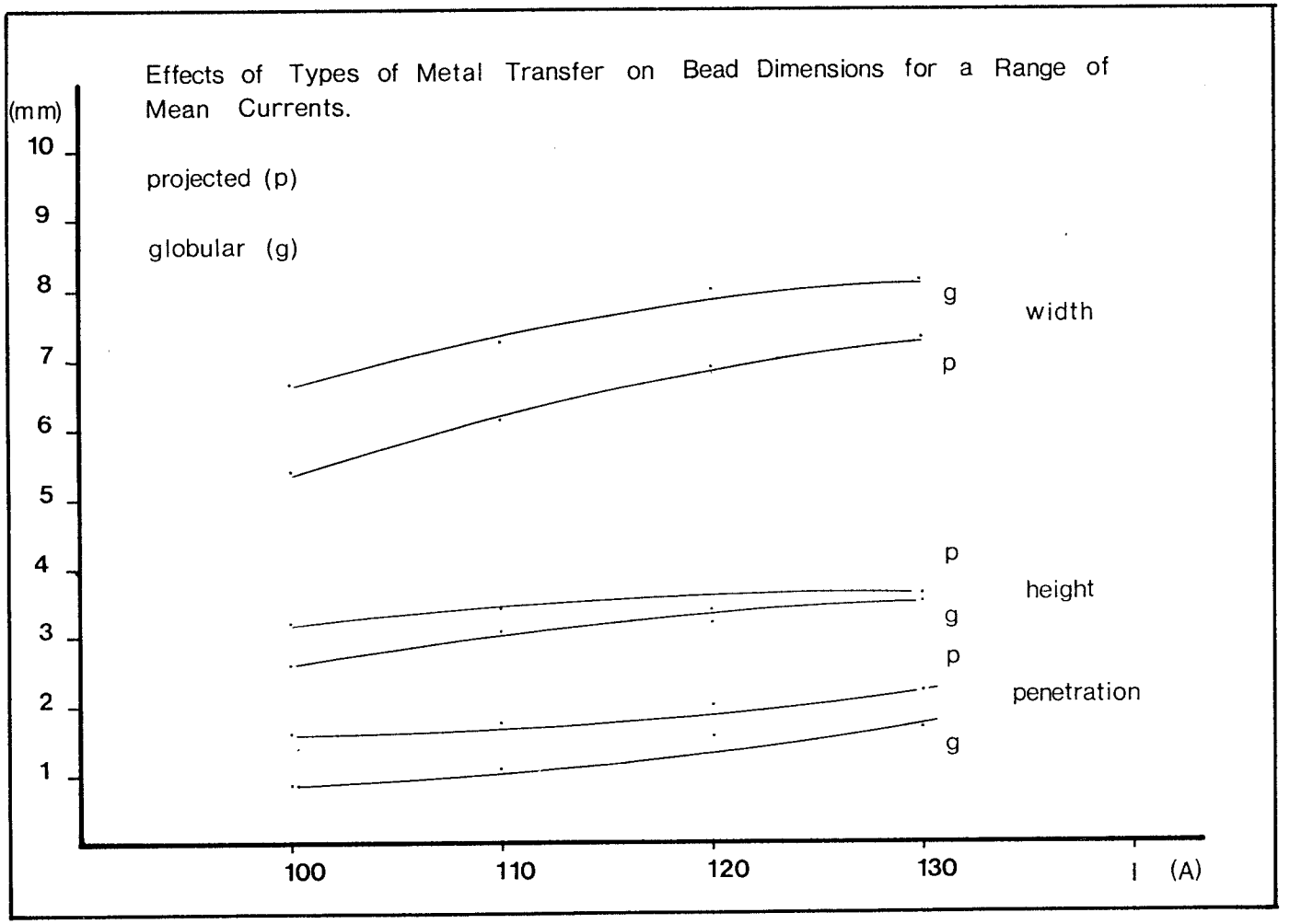
Effects of Types of Metal Transfer on Bead Dimensions for a Range of Mean Currents.
(mm)
10
9
8
7
6
5
4
3
2
1
projected (p)
globular (g)
g
width
p
p
height
g
p
penetration
g
100
110
120
130
I (A)

Graph 7.9

difference between the transfer modes tends to decrease. Globular transfer gives rise to wider profiles partly due to the size of the droplets and partly due to the pulse configuration. For this experiment long pulse times were used (table 7.4) thus increasing the weldpool size and consequently its width during the pulse phase.

Penetration during globular transfer was shallower than that measured for projected spray transfer because in globular transfer detachment and acceleration of the droplets takes place mainly due to gravity. Figure 7.5 shows the profiles used for graph 7.9.

Based on observations from the results presented in table 7.1, it can be seen that in most cases penetration tends to increase as the droplet volumes decrease while the pulse current is kept constant.

7.4.6.1 Effects of Background Detachments on Bead Profiles.

It is expected that regular background detachments will result in a shallower penetration due to the decreased acceleration of the detached droplets in the arc column. Examination of profiles, where some background detachments occurred, showed that penetration had been reduced. However, since regular and stable background detachments could not be obtained it was not possible to fully assess their effect on the shape of the bead profiles. Under conditions of non regular background detachments the resulting bead profiles have irregular shapes and non uniform penetration, which is not acceptable.

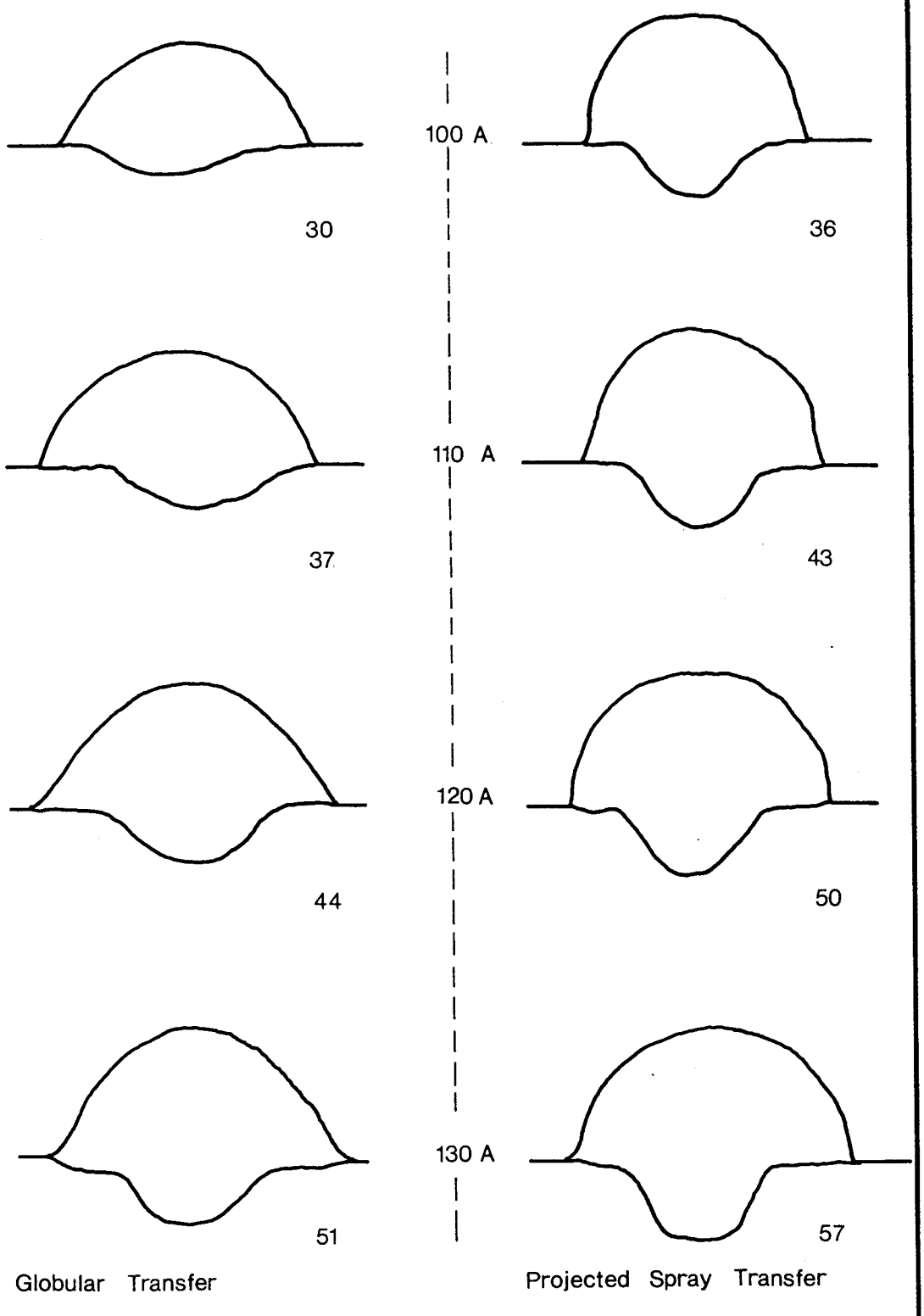

FIG. 7.5 Effects of Pulse Current Configuration and Type of Metal Transfer Mode on the Shape of Bead Profiles.

7.4.7 Effects of Incident Electrode Angles on Bead Shape.

There are two incident electrode angles, one that points the electrode forward or backwards in relation to the travel direction (longitudinal angle α), and one on a plane at right angles to the direction of travel (lateral angle β) (figure 7.6).

Preliminary experiments on the effects of incident angles on the bead shape showed that whereas the longitudinal angle α had no noticeable effects, lateral torch inclination promoted irregular profiles.

Forward and backward torch inclinations are used in welding in order to alter the heat input to the weldplate. A forward angle α is anticipated to result in shallower penetration than vertical torch positioning, because the droplets are directed towards the cooler part of the weldpool and by being projected at an angle, the momentum upon impact will have a reduced effect.

Positioning the welding torch at a lateral inclination at angles $\beta \leq 70^{\circ}$ and when welding takes place at relatively high travel speeds no significant effects are observed on the shape of the bead profile. However, at low travel speeds lateral inclination promoted irregular profiles.

Observations showed that during welding with lateral torch inclination the axis of the core of the arc column was the continuation of the axis of the electrode whereas the rest of the arc column was slightly deflected towards the plate. Microscopic and macroscopic examination of the heat affected zone showed that the weldpool is formed directly under the arc and the

detached droplets are directed towards the far end of the weldpool thus forming irregular profiles.

Figure 7.7 shows schematically the effects of lateral inclination on the shape of the bead profile. The first stage of the sequence shows the weldpool in relation to the arc, then a droplet is detached and directed towards the far side of the weldpool where penetration is increased after impact. The last sequence shows the cross section of the resulted profile and although the deposit is smooth, the profile is irregular.

The results from these experiments are presented on table 7.6.

It was found that the size of the deposited areas were not affected by the electrode inclination. For welding conditions that give rise to obtuse profiles lateral angles can give a smoother appearance to the deposited bead. However, for stringer bead deposition any longitudinal or lateral inclination of the torch has not proved beneficial to the bead profile appearance.

The low travel speeds used during this experiment appear to have cancelled the effects of the longitudinal angle α anticipated and enhanced the effects of the lateral angle ß.

In globular transfer, torch inclination does not affect the profile at all. Figure 7.7 also shows globular transfer during welding with lateral torch inclination. Since droplet detachment in globular transfer takes place under the influence of gravity as the droplet evolves on the electrode tip it will always tend to swing to a

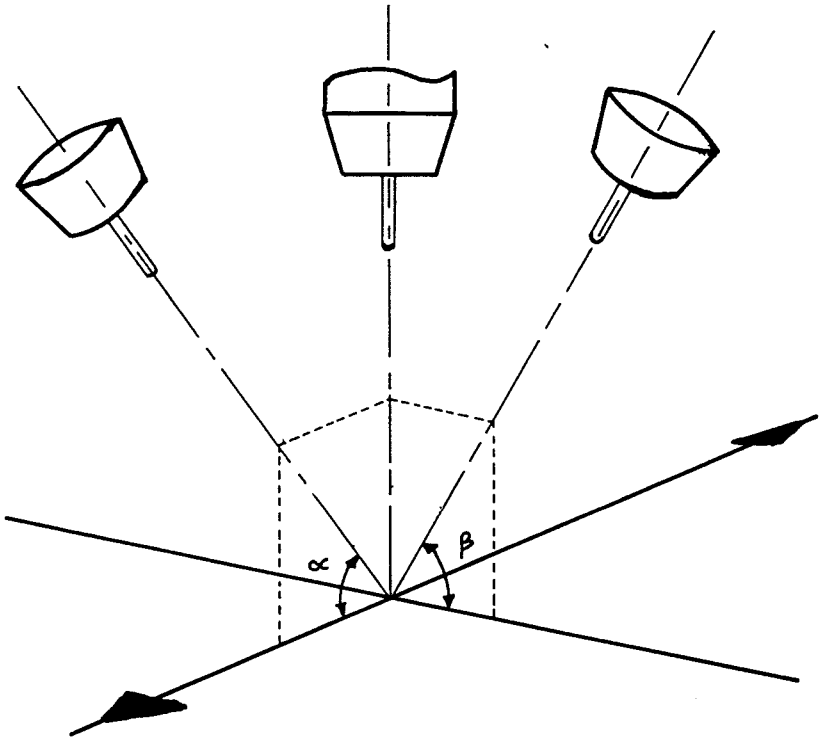

FIG. 7.6 Longitudinal (α) and Lateral (β) Angles.

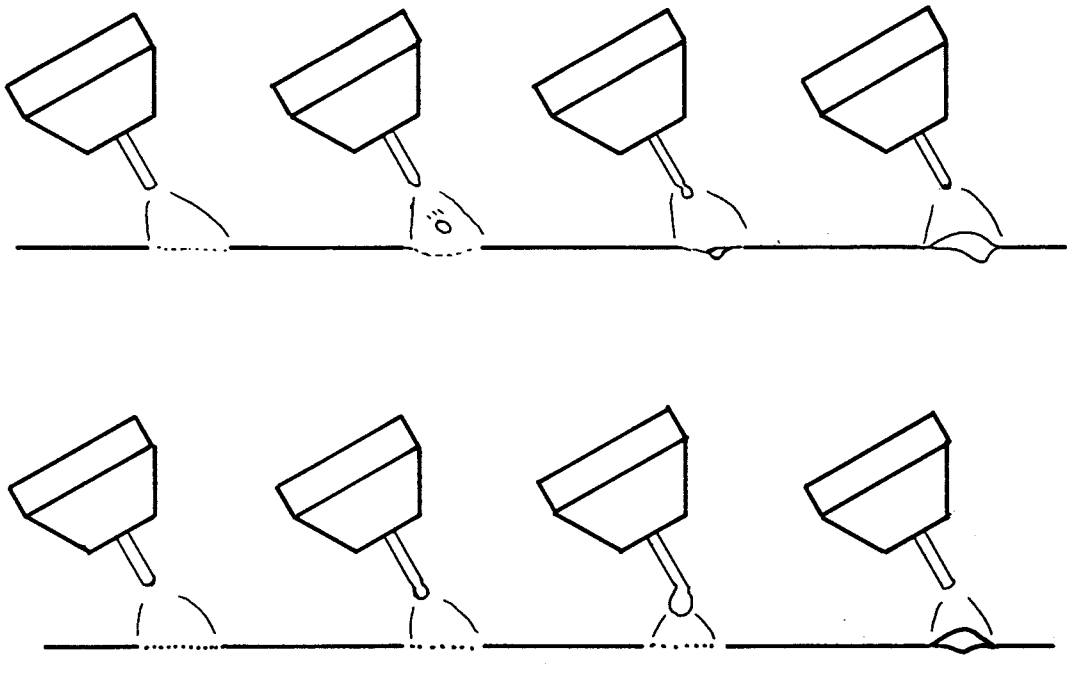

FIG. 7.7 Effects of Lateral Inclination on Bead Profiles in Projected and Globular Transfer.

position perpendicular to the plate. So when detachment takes place the droplet will have a trajectory at right angles to the plate.

7.4.8 Bead on Plate Deposition Using Low Mean Currents.

An investigation was carried out on the possibility of bead deposition using very low mean currents. The welding parameters and results are presented on table 7.5 and the bead profiles are shown in figure A.5 (Appendix I).

The results may be summarised as follows:

At 50A mean current penetration was kept very shallow between 0.01mm and 0.35mm, and dilution ranged from 2.9% to 11% with an average value of 5.5%. The profiles however, were unsatisfactory as they exhibited obtuse shapes. The shallow penetration and obtuse bead profiles in this case reveal the arc's inability to melt the baseplate and form a weldpool. Therefore, it is anticipated that if the weldplate was to be contaminated with spatter globules, the arc would not be capable of melting these thus giving rise to defective deposits.

At 60A mean current the bead profiles had more regular shapes than those welded at 50A. However, the angles of contact were quite high. Penetration ranged from 0.44mm to 0.77mm, and dilution from 3.8% to 11.3% with a mean value of 6.7%. As with the 50A deposits the main problem with such low current deposition is the high probability of defects.

Whereas at 50A and 60A projected spray transfer could not be obtained and short circuit and globular

transfer were dominant, at 70A projected spray transfer was obtained and therefore the transfer stability improved significantly. The resulting beads were regular in shape with smaller angles of contact. However, penetration and dilution were increased, with dilution ranging from 9.9% to 12.9% giving a mean value of 11.5%.

The deposition of beads on plate using low mean currents under the specific experimental arrangement ie. shielding gas, electrode wire diameter and plate thickness, does not give satisfactory results. The main problem is the inability of the arc to form a weldpool, and fusion between the deposit and the weldplate is achieved mainly by the heat transferred from the impacting droplets. Therefore, if for example, the path of the arc is contaminated with spatter, fusion defects are certain to occur.

This problem may be eliminated if the heat input to the plate is increased. In order to avoid increasing the welding current, the heat input may be increased by either changing the shielding gas, decreasing the electrode diameter or preheating the base material. Using a gas with a higher ionisation potential will increase the heat input to the weldplate and may also reduce the current at which transition from globular to projected place transfer takes place. A thinner electrode increases the current density in the arc column which means that heating will be localised and therefore more intense. In addition, the use of a thinner electrode will result in projected spray transfer at lower currents thus

increasing the droplet momentum. The use of preheat may provide an alternative solution by slowing down the cooling rate and thus allowing the formation of a weldpool.

7.5 Discussion.

7.5.1 Deposition Ratio.

Equation [7.2] suggests that if the ratio between the melting rate and the electrode travel speed is kept constant then the resulting deposited area will remain constant as well.

An experiment was carried out to verify this assumption where five welding currents (100-200A) were used with appropriate electrode travel speeds to give a constant Deposition Ratio (table 7.2 specimens 19-23). As expected the bead profiles were similar in all dimensions and it appears that this is a useful shortcut in the prediction of the bead shape and size.

However, caution is in order as the range of parameters where this simplification is valid may be limited. There is one specific reason that may limit this simplification. It was found that the bead profile deposited at 200A had a fractionally larger width than the rest of the deposits. In GTAW if the vertex (electrode tip) angle is decreased from 120° to 30°, the weld bead width increases by nearly a factor of 2 (Savage et al 1965), because the sharper the electrode tip the bigger the arc voltage and thus the wider the heat distribution. At around 200A the metal transfer changes from projected to streaming, accompanied by tapering of

the electrode tip. It is possible therefore, and supported by observations that the bead profiles generated in streaming spray transfer may deviate from any prediction made at projected spray transfer when the deposition ratio is employed.

7.5.2 Weldbead Width.

The bead width is perhaps the most important parameter when overlay welding is concerned. Measurements of the bead width showed a considerable amount of scatter. In the process of the experimental work it was found that the most significant factors that affected the scatter in the results of the bead width were irregular metal transfer and the phenomenon of arc deflection.

Graph 7.10 shows the relationship between the bead width and the deposition ratio. This graph has been plotted using all the available data of table 7.1 to table 7.6.

The bead width increases when the deposition ratio is increased. At deposition ratios DR>10 the bead width appears to increase at a lower rate and at deposition ratios DR>14 obtuse profiles occur.

Arc deflection was encountered when a stringer bead was deposited close to another bead with a distance between them of the order of up to 20mm. Although the bright core of the arc appeared to be the continuation of the axis of the electrode wire, the rest of the arc was slightly displaced towards the neighbouring bead. The resulting bead profile had an increased bead width, smaller angles of contact but a slightly irregular

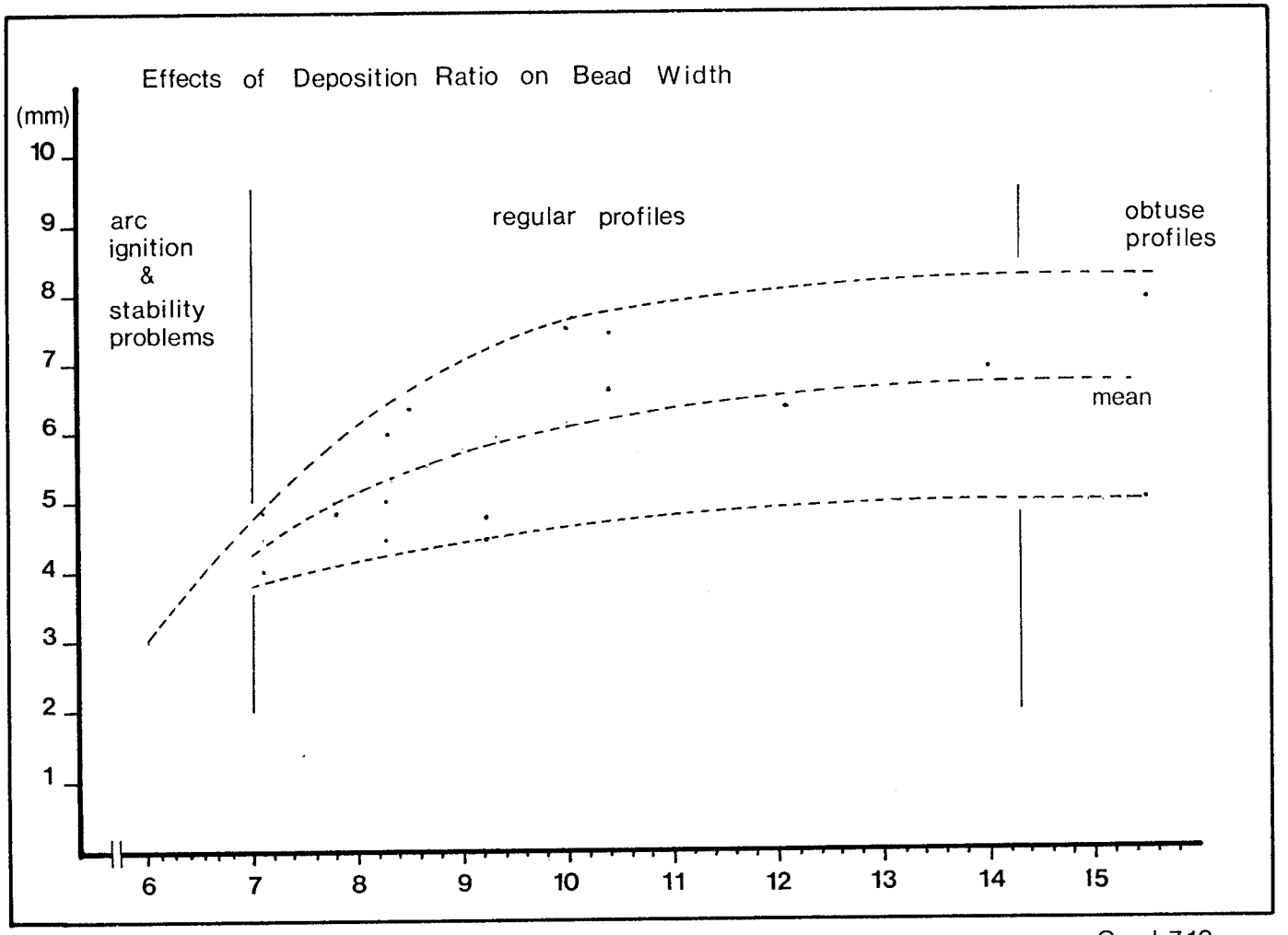
Effects of Deposition Ratio on Bead Width
(mm)
10
9
8
7
6
5
4
3
2
1
arc ignition & stability problems
regular profiles
obtuse profiles
mean
6
7
8
9
10
11
12
13
14
15

Graph 7.10

profile. The phenomenon of arc deflection was also observed when a bead was deposited in between two other beads; it resulted in an increase in bead width and in some cases there was a change in profile shape from obtuse to regular.

7.5.3 Melting Rate Characteristics of the Electrode and Base Plate Material and their Effects on the Bead Profile Shape.

The bead profiles of 316S92 stainless steel deposited on mild steel plates are characterised by relatively large angles of contact.

Stainless steel has an increased melting rate compared to that of a mild steel electrode. According to data from (Amin 1983) the burnoff factor for 316 stainless steel is approximately 25% bigger than that of mild steel. Therefore, where the same mean current is employed, 25% more 316S92 electrode wire will be melted and deposited than if a mild steel electrode was used.

Although the higher deposition rates of the stainless steel electrode wire result in larger angles of contact, they also result in lower dilution which is rather beneficial, especially when dissimilar metals are fused together.

7.5.4 Effects of Irregular Metal Transfer on the Bead Profiles.

At relatively low mean current levels, if a mixture of globular and projected spray transfer occurs, it is most likely that irregularities on the bead profile

will arise. This phenomenon is more important at low deposition ratios ie. at relatively high welding speeds, and results in unacceptable deposits. This clearly illustrates the necessity in selecting parameters that will result in a stable metal transfer with regular metal detachments.

7.6 Conclusions.

The fusion characteristics of 316S92 stringer beads deposited on mild steel plates of 24.5mm thickness under conditions of projected spray transfer and three dimensional heat flow have been examined and presented.

The bead profiles are influenced by the stability of metal transfer, arc deflection and the burnoff characteristics of the electrode material used.

The introduction of the deposition ratio may be used to predict the bead shape and dimensions during projected spray transfer.

The bead width increases with increasing current but decreases with increasing travel speed.

Penetration depends on the type of metal transfer. Globular transfer gives the shallowest penetration with a tendency for a bowl-shaped weldpool. Projected spray transfer gives rise to increased penetration with a tendency for finger penetration especially when near the transitional region to streaming spray transfer.

In projected spray transfer, for constant droplet volumes, penetration increases with increasing mean current.

Background detachments reduce the depth of penetration but unless they occur regularly they tend to promote unacceptably irregular bead profiles.

Penetration is at its lowest at high travel speeds, and increases with decreasing travel speed until it reaches a maximum or burn through occurs.

Dilution is very low when obtuse profiles are deposited, it increases with increasing travel speed until it reaches a maximum and then rapidly decreases to low levels again.

Longitudinal torch inclination does not appear to have any significant effects on the profiles. Lateral inclination tends to promote irregular profiles.

Key to Tables 7.1 to 7.6
Q=Shielding Gas Flow (lt/min) S=Standoff TT=Transfer Type (G=Globular, P=Projected, S=Streaming, *=spatter ST=Stability of Metal Transfer A=Excellent B=Good C=Acceptable D=Poor E=Unacceptable. Shape (R=Regular, -R=Less Regular, I=Irregular, O=Obtuse DR=Deposition Ratio At=Total Area, Amean=Mean Area, Acalc=Calculated Area, Ap=Penetration Area δ=Dilution pc=percent

TABLE 7.1 Welding Parameters

	Electrical Parameters							Set Up Parameters				RESULTS											
												Transfer	Deposit										
													Shape DR		Areas					Linear Measurements			
No	Im (A)	W (m/min)	Ip (A)	Tp (ms)	Ib (A)	Tb (ms)	TS (mm/s)	Angle α	ß	Q	S mm	TT	ST		At (mm2)	Amean (mm2)	Acalc (mm2)	Ap (mm2)	δ pc	Width (mm)	Height (mm)	Depth (mm)	Drop.Vol. (mm3)
1	100	3.18	300	4	50	16.0	7.45	90	90	20	13	P	B	R 7.1	9.07	9.40	8.05	0.95	0.10	4.05	2.64	0.79	1.199
2	100	3.18	300	4	60	20.0	7.45	90	90	20	13	P	B	-R	9.07			1.42	0.15	4.84	2.55	0.79	1.438
3	100	3.18	300	4	70	26.7	7.45	90	90	20	13	P	B	R	10.07			1.42	0.14	4.84	2.55	0.79	1.838
4	120	3.81	300	4	50	10.3	7.45	90	90	20	13	P	B	I 8.5	12.95	12.00	9.64	1.89	0.14	5.19	2.64	0.97	1.030
5	120	3.81	300	4	60	12.0	7.45	90	90	20	13	P	B	I	10.94			1.89	0.17	5.37	2.46	0.79	1.237
6	120	3.81	300	4	70	14.4	7.45	90	90	20	13	P	B	I	12.09			1.89	0.15	6.34	2.38	0.79	1.323
7	140	4.45	300	4	50	7.1	7.45	90	90	20	13	P	B	-R 9.95	13.92	13.92	11.26	2.83	0.20	7.30	2.46	1.23	0.932
8	140	4.45	300	4	60	8.0	7.45	90	90	20	13	P	B	I	13.92			2.83	0.20	7.22	2.46	1.14	1.007
9	140	4.45	300	4	70	9.1	7.45	90	90	20	13	P	B	I	13.92			3.30	0.24	7.48	2.29	0.79	1.101
10	160	5.10	300	4	50	5.1	7.45	90	90	20	13	P	B	-R 11.41	14.91	16.40	12.90	4.24	0.25	7.39	2.73	1.32	0.872
11	160	5.10	300	4	60	5.6	7.45	90	90	20	13	P	B	-R	17.13			3.77	0.22	6.60	2.55	1.32	0.920
12	160	5.10	300	4	70	6.2	7.45	90	90	20	13	P	B	-R	17.13			4.24	0.25	7.04	2.55	1.50	0.979
13	170	5.40	300	4	70	5.2	7.45	90	90	20	13	P	B	R 12.10	17.13		13.70	5.67	0.33	6.34	2.64	1.94	0.937
14	100	3.18	180	6	50	9.6	6.35	90	90	20	13	P	C	R 8.35	12.75	11.10	9.44	3.77	0.27	5.63	2.55	1.58	0.935
15	100	3.18	180	4	72	11.6	6.35	90	90	20	13	P	C	R	11.93			2.83	0.24	5.46	2.29	1.14	0.936
16	100	3.18	300	4	35	12.3	6.35	90	90	20	13	P	D	I	9.92			1.89	0.19	5.10	2.20	0.79	0.977
17	100	3.18	300	3	55	13.3	6.35	90	90	20	13	P	D	R	10.89			1.89	0.17	5.46	2.29	1.06	0.977
18	100	3.18	350	2.6	50	13.0	6.35	90	90	20	13	P	D	I	9.92			1.89	0.19	4.93	2.11	0.97	0.935

TABLE 7.2 Welding Parameters												RESULTS									
	Electrical Parameters							Set Up Parameters				Transfer	Deposit								
													Shape DR		Areas				Linear Measurements		
No	Im (A)	W (m/min)	Ip (A)	Tp (ms)	Ib (A)	Tb (ms)	TS (mm/s)	Angle α	ß	Q	S mm	TT ST			At (mm2)	Acalc (mm2)	Ap (mm2)	δ pc	Width (mm)	Height (mm)	Depth (mm)
19	100	3.18	180	6.0	50	9.0	6.35	90	90	20	13	P A	R	8.35	10.65	9.44	2.36	0.20	4.40	2.64	1.23
20	130	4.13	300	4.0	50	8.5	7.40	90	90	20	13	P A	R	9.30	9.68	10.52	2.83	0.26	4.84	2.55	1.06
21	150	4.77	300	4.0	50	6.0	8.58	90	90	20	13	P A	R	9.27	10.65	10.48	2.83	0.24	4.40	2.73	1.32
22	170	5.40	300	4.0	70	5.1	10.51	90	90	20	13	P A	R	8.56	10.65	9.68	2.83	0.24	4.58	2.55	1.23
23	200	6.36	350	4.0	70	4.6	11.67	90	90	20	13	P A	R	9.10	12.08	10.27	2.83	0.24	4.84	2.46	1.32
24	100	3.18	300	4.0	50	16.0	2.49	90	90	20	13	P A	O	21.30	25.83	24.10	3.77	0.14	6.42	4.49	1.50
25	100	3.18	300	4.0	50	16.0	4.73	90	90	20	13	P A	R	11.20	14.61	12.66	2.83	0.19	5.54	3.26	0.97
26	100	3.18	300	4.0	50	16.0	6.81	90	90	20	13	P A	R	7.80	9.74	8.82	1.89	0.19	4.84	2.73	0.79

TABLE 7.3 Welding Parameters												RESULTS													
	Electrical Parameters							Set Up Parameters				Transfer	Deposit												
													Shape DR			Areas				Linear Measurements			Heat Affected Zone		
No	Im (A)	W (m/min)	Ip (A)	Tp (ms)	Ib (A)	Tb (ms)	TS (mm/s)	Angle α	ß	Q	S mm	TT ST			Preheat	At (mm2)	Acalc (mm2)	Ap (mm2)	δ pc	Width (mm)	Height (mm)	Depth (mm)	Area (mm2)	Width (mm)	Depth (mm)
27	100	3.18	180	6.0	50	9.0	6.35	90	90	20	13	P D	R	8.35	230°	11.93	9.44	3.77	0.31	5.98	2.38	1.14	13.87	8.36	2.64
28	100	3.18	180	6.0	50	9.0	6.35	90	90	20	13	P D	R		170°	11.93		3.77	0.31	5.98	2.46	0.88	8.95	7.92	2.02
29	100	3.18	180	6.0	50	9.0	6.35	90	90	20	13	P D	R		130°	11.93		2.83	0.23	5.72	2.38	0.88	8.95	7.48	2.02

TABLE 7.4 Welding Parameters

	Electrical Parameters											Set Up Parameters		Transfer		RESULTS										
																Deposit										
																Shape	DR	Areas					Linear Measurements		
No	Im (A)	W (m/min)	Ip (A)	Tp (ms)	Ib (A)	Tb (ms)	TS (mm/s)	Angle α	Angle ß	Q	S mm	TT	ST	Shape	DR	At (mm2)	Amean (mm2)	Acalc (mm2)	Ap (mm2)	δ pc	Width (mm)	Heig. (mm)	Depth (mm)			
30	100	3.18	150	99.0	50	99.9	3.77	90	90	15	15	G	C	R	14.05	13.81	16.70	15.90	2.83	0.20	6.64	2.63	0.84			
31	100	3.18	155	71.5	50	72.0	3.77	90	90	15	15	G	C	R		16.57			2.83	0.17	6.91	3.04	0.87			
32	100	3.18	160	50.0	50	55.0	3.77	90	90	15	15	G	C	R		16.57			2.83	0.17	6.95	3.08	0.92			
33	100	3.18	165	31.0	50	37.5	3.77	90	90	15	15	GP	C	I		17.49			3.77	0.21	4.91	3.34	1.36			
34	100	3.18	170	18.0	50	23.0	3.77	90	90	15	15	P	A	R		16.57			3.77	0.23	5.98	3.17	1.50			
35	100	3.18	175	9.5	50	13.4	3.77	90	90	15	15	P	A	R		18.41			4.71	0.25	5.10	3.43	1.54			
36	100	3.18	180	6.0	50	9.0	3.77	90	90	15	15	P	A	R		17.49			4.71	0.26	5.37	3.19	1.58			
37	110	3.50	150	99.0	50	60.0	3.77	90	90	15	15	G	C	R	15.5	19.33	20.00	17.50	2.83	0.14	7.26	3.08	1.10			
38	110	3.50	155	71.5	50	50.4	3.77	90	90	15	15	G	C	R		17.49			3.77	0.21	5.81	3.17	1.45			
39	110	3.50	160	50.0	50	39.0	3.77	90	90	15	15	GP	C	R		21.18			3.77	0.18	7.92	3.18	1.54			
40	110	3.50	165	31.0	50	26.7	3.77	90	90	15	15	P	A	R		19.33			4.71	0.24	6.86	3.21	1.67			
41	110	3.50	170	18.0	50	16.8	3.77	90	90	15	15	P	A	R		21.18			4.71	0.22	6.86	3.26	1.76			
42	110	3.50	175	9.5	50	9.7	3.77	90	90	15	15	P	A	R		20.25			3.77	0.19	5.37	3.34	1.85			
43	110	3.50	180	6.0	50	6.6	3.77	90	90	15	15	P	A	R		21.18			4.71	0.22	6.16	3.43	1.76			
44	120	3.82	150	99.0	50	34.9	3.77	90	90	15	15	G	C	R	16.9	20.25	22.00	19.10	3.77	0.18	8.01	3.21	1.54			
45	120	3.82	155	71.5	50	33.1	3.77	90	90	15	15	G	C	R		21.18			3.77	0.17	8.01	3.26	1.76			
46	120	3.82	160	50.0	50	26.1	3.77	90	90	15	15	G	C	R		23.01			4.71	0.20	7.57	3.43	1.94			
47	120	3.82	165	31.0	50	18.6	3.77	90	90	15	15	P	A	R		20.09			4.71	0.21	6.42	3.52	2.07			
48	120	3.82	170	18.0	50	12.0	3.77	90	90	15	15	P	A	R		23.01			4.71	0.20	6.86	3.70	2.07			
49	120	3.82	175	9.5	50	7.0	3.77	90	90	15	15	P	A	R		23.01			3.77	0.16	6.25	3.61	1.85			
50	120	3.82	180	6.0	50	4.8	3.77	90	90	15	15	P	A	R		23.01			5.67	0.25	6.78	3.39	2.02			
51	130	4.13	150	99.0	50	21.3	3.77	90	90	15	15	G	C	R	18.3	22.09	23.30	20.60	4.71	0.21	8.10	3.56	1.63			
52	130	4.13	155	71.5	50	20.0	3.77	90	90	15	15	G	C	R		22.08			4.71	0.21	6.95	3.43	1.85			
53	130	4.13	160	50.0	50	17.0	3.77	90	90	15	15	G	C	I		23.93			4.71	0.19	8.54	3.52	1.80			
54	130	4.13	165	31.0	50	12.4	3.77	90	90	15	15	G	C	R		22.09			4.71	0.21	7.48	3.52	2.11			
55	130	4.13	170	18.0	50	8.2	3.77	90	90	15	15	P	A	R		21.18			5.67	0.26	5.98	3.43	2.16			
56	130	4.13	175	9.5	50	5.0	3.77	90	90	15	15	P	A	R		26.69			5.67	0.21	8.27	3.39	2.02			
57	130	4.13	180	6.0	50	3.5	3.77	90	90	15	15	P	A	R		24.85			5.67	0.23	7.30	3.52	2.20			

TABLE 7.5 Welding Parameters												RESULTS								
	Electrical Parameters							Set Up Parameters				Transfer	Deposit							
													Shape	DR	Areas				Linear Measurements		
No	Im (A)	W (m/min)	Ip (A)	Tp (ms)	Ib (A)	Tb (ms)	TS (mm/s)	Angle α	Angle ß	Q	S mm	TT ST	Shape	DR	At (mm2)	Ad (mm2)	Ap (mm2)	δ pc	Width (mm)	Heig. (mm)	Depth (mm)
58	50	1.40	300	3.0	40	65.2	1.89	90	90	15	13	S* E	R	12.3	11.85	10.5	1.35	0.11	6.42	2.64	0.35
59	50	1.30	300	3.0	40	65.2	1.89	90	90	15	13	SG D	R	11.5	12.87	12.41	0.46	0.035	5.54	2.73	0.18
60	50	1.20	300	3.0	40	65.2	1.89	90	90	15	13	G D	O	10.6	10.60	9.78	0.82	0.077	3.52	2.90	0.18
61	50	1.20	350	3.0	40	79.2	1.89	90	90	15	13	GP B	O	10.6	11.26	10.93	0.33	0.029	3.52	2.90	0.18
62	50	1.20	400	3.0	40	91.0	1.89	90	90	15	13	GP B	O	10.6	10.14	9.75	0.39	0.038	3.52	3.08	0.01
63	50	1.30	400	3.0	40	91.0	1.89	90	90	15	13	GS E	O	11.5	11.82	11.16	0.66	0.055	4.05	3.08	0.09
64	50	1.25	450	3.0	40	99.9	1.89	90	90	15	13	SG E	O	11.0	12.31	11.82	0.49	0.040	4.31	3.08	0.01
65	60	1.91	300	3.0	40	33.2	1.89	90	90	15	13	S E	R	16.8	20.15	19.36	0.79	0.038	5.90	3.78	0.44
66	60	1.80	300	3.0	40	33.2	1.89	90	90	15	13	S E	R	15.9	18.64	17.36	1.28	0.068	6.16	3.70	0.70
67	60	1.70	300	6.0	40	66.4	1.89	90	90	15	13	SG* E	R	15.0	17.59	16.84	0.75	0.043	5.90	3.26	0.44
68	60	1.70	300	9.0	40	99.6	1.89	90	90	15	13	G* E	R	15.0	17.59	16.57	1.02	0.057	6.69	2.99	0.44
69	60	1.65	300	9.0	40	99.6	1.89	90	90	15	13	G* E	R	14.6	16.38	15.13	1.25	0.076	7.04	2.82	0.53
70	60	1.60	300	9.0	40	99.6	1.89	90	90	15	13	G* E	R	14.1	14.44	13.36	1.08	0.075	6.16	2.82	0.26
71	60	1.70	350	3.0	40	40.0	1.89	90	90	15	13	GP D	R	15.0	16.51	15.56	0.95	0.057	6.16	2.73	0.53
72	60	1.70	350	6.0	40	80.0	1.89	90	90	15	13	G C	O	15.0	19.66	18.28	1.38	0.070	5.02	3.70	0.53
73	60	1.70	400	3.0	40	47.0	1.89	90	90	15	13	P B	R	15.0	16.41	15.23	1.18	0.072	5.72	3.52	0.44
74	60	1.70	400	6.0	40	94.4	1.89	90	90	15	13	G* E	R	15.0	18.25	16.18	2.07	0.113	6.42	2.99	0.70
75	60	1.70	450	3.0	40	54.0	1.89	90	90	15	13	G D	R	15.0	16.41	15.16	1.25	0.075	5.46	3.17	0.53
76	70	2.23	300	3.0	40	21.7	1.89	90	90	15	13	S* E	R	19.7	27.01	23.92	3.09	0.099	7.04	4.14	1.23
77	70	2.10	300	3.0	40	21.7	1.89	90	90	15	13	S* E	R	18.5	21.43	19.30	2.13	0.114	6.60	3.61	1.14
78	70	2.00	300	3.0	40	21.7	1.89	90	90	15	13	P B	R	17.6	23.86	21.07	2.79	0.117	5.72	3.96	1.23
79	70	2.00	350	3.0	40	26.5	1.89	90	90	15	13	P B	R	17.6	21.89	19.33	2.56	0.116	6.86	3.87	1.06
80	70	2.00	400	3.0	40	31.2	1.89	90	90	15	13	P B	R	17.6	22.22	19.33	2.89	0.129	6.16	4.05	1.14

TABLE 7.6 Welding Parameters												RESULTS								
	Electrical Parameters							Set Up Parameters				Transfer	Deposit							
													Shape	Areas				Linear Measurements		
No	Im (A)	W (m/min)	Ip (A)	Tp (ms)	Ib (A)	Tb (ms)	TS (mm/s)	Angle α	Angle ß	Q	S mm	TT ST	Shape	At (mm2)	Ad (mm2)	Ap (mm2)	δ pc	Width (mm)	Heig. (mm)	Depth (mm)
81	200	6.36	230	1.3	50	0.26	6.35	90	90	14	25	PS A	O	22.98	16.15	6.83	0.29	4.84	4.49	2.07
82	200	6.36	230	1.3	50	0.26	5.33	90	90	14	25	PS A	O	26.42	19.36	7.06	0.26	5.10	4.75	2.02
83	200	6.36	230	1.3	50	0.26	4.57	90	90	14	25	PS A	O	29.15	18.81	10.34	0.35	6.25	4.84	2.38
84	200	6.36	230	1.3	50	0.26	4.26	90	90	14	21	PS A	O	22.26	14.55	7.71	0.35	5.28	4.31	2.20
85	200	6.36	230	1.3	50	0.26	3.56	90	90	14	21	PS A	O	25.93	16.08	9.85	0.38	5.54	4.66	2.46
86	200	6.36	230	1.3	50	0.26	3.00	90	90	14	21	PS A	O	33.25	22.35	10.90	0.33	6.25	4.93	2.46
87	200	6.36	230	1.3	50	0.26	4.26	90	90	14	17	PS A	O	20.06	12.58	7.48	0.37	5.46	3.96	1.94
88	200	6.36	230	1.3	50	0.26	3.56	90	90	14	17	PS A	O	26.00	15.33	10.67	0.41	7.04	4.05	2.29
89	200	6.36	230	1.3	50	0.26	3.00	90	90	14	17	PS A	O	30.36	18.61	11.75	0.39	6.25	4.84	3.17
90	200	6.36	230	1.3	50	0.26	6.35	30	90	14	15	PS A	O	23.11	11.72	11.39	0.49	5.81	4.14	2.82
91	200	6.36	230	1.3	50	0.26	6.35	45	90	14	15	PS A	O	20.84	14.70	6.14	0.29	4.66	4.22	2.11
92	200	6.36	230	1.3	50	0.26	6.35	60	90	14	15	PS A	O	20.98	13.82	7.16	0.34	5.54	4.31	2.20
93	200	6.36	230	1.3	50	0.26	6.35	75	90	14	15	PS A	O	21.89	13.68	8.21	0.37	4.66	4.40	2.64
94	200	6.36	230	1.3	50	0.26	6.35	60	90	14	15	PS A	O	20.19	11.69	8.50	0.42	5.28	4.05	2.46
95	200	6.36	230	1.3	50	0.26	6.35	60	90	14	15	PS A	O	22.98	14.02	8.96	0.39	5.28	4.49	2.55
96	200	6.36	230	1.3	50	0.26	6.35	60	90	14	15	PS A	O	25.54	13.99	11.55	0.45	5.72	4.84	2.99
97	200	6.36	230	1.3	50	0.26	4.26	60	90	14	15	PS A	O	21.89	14.41	7.48	0.34	5.28	4.14	2.20
98	200	6.36	230	1.3	50	0.26	4.57	90	51	14	15	PS A	I	35.68	24.68	11.00	0.30	8.45	4.75	2.29
99	200	6.36	230	1.3	50	0.26	4.57	90	60	14	15	PS A	I	30.95	17.13	13.82	0.44	7.57	4.40	3.08
100	200	6.36	230	1.3	50	0.26	3.00	90	60	20	15	PS A	I	28.13	18.64	9.49	0.34	12.76	3.26	1.67
101	200	6.36	230	1.3	50	0.26	3.81	90	90	14	15	PS A	O	39.95	23.44	16.51	0.41	9.24	4.66	2.55
102	200	6.36	230	1.3	50	0.26	3.81	90	51	14	15	PS A	I	34.70	26.85	7.85	0.22	11.53	3.61	1.58
103	200	6.36	230	1.3	50	0.26	3.81	90	60	14	15	PS A	I	33.19	21.27	11.92	0.36	10.56	3.87	2.29
104	200	6.36	230	1.3	50	0.26	2.54	90	60	20	15	PS A	I	42.61	29.71	12.90	0.30	17.60	3.17	1.85
105	200	6.36	230	1.3	50	0.26	3.30	90	90	14	15	PS A	O	45.27	29.55	15.72	0.35	10.56	5.28	2.73
106	200	6.36	230	1.3	50	0.26	3.30	90	51	14	15	PS A	I	38.00	22.19	15.95	0.42	13.55	4.49	2.73
107	200	6.36	230	1.3	50	0.26	2.20	90	60	14	15	PS A	I	32.99	20.68	12.31	0.37	7.30	4.84	2.82

CHAPTER EIGHT

Overlay Welding.

Chapter Eight Overlay Welding.

8.1 Experimental Arrangement.

8.1.1 Experimental Rig.

Overlay welding of cylindrical components requires the continuous deposition of a spiral bead. To achieve this type of deposition the workpiece has to rotate at a certain rate while the welding torch travels at right angles to the direction of rotation at a certain speed. Both the rotational and transverse speeds must be such as to generate a spiral of a specified overlap as required.

Specially designed machines for this process are available on the market and may vary in complexity. However the use of a lathe is an attractive solution because not only does it provide both the rotational and longitudinal motions but it can also be used to machine the overlayed component without having to remove it or recentre it.

The lathe used had the slowest rotational speed at 40 rpm which was unsuitable for the component diameter. Therefore it had to be modified accordingly. The extent of the modification depends very much on the technical requirements and economic feasibility. The set up used for this project was designed on the basis of five requirements; safety, precision, simplicity, flexibility and availability of materials. The prime objective was to ensure that potential hazards were

eliminated or reduced to a minimum, the main hazards involved during the process being: electric currents, high temperatures, molten metal being ejected as spatter, toxic and carcinogenic fumes, ultraviolet and X-rays (Moreton 1984) (Willingham & Hilton 1986) and the rotating parts of the lathe.

8.1.2 Set Up.

The set up is diagrammatically presented in figure 8.1. This set up is not by far the ideal to be used on a production line. There are better and more versatile set ups where the workpiece can be surface treated, overlayed and machined without having to remove it from its position. However, the set up used was intended to provide laboratory conditions and yet not to be too different from an industrial installation.

The specimen shafts used were rotated independently of the lathe. The shaft was supported between two rotating centres one in the tailstock and the other inside the driving mandrel in the chuck and rotated by a belt drive. The specimen shaft was fitted with an attachment which incorporated a pulley. The attachment was designed to provide insulation between the shaft and the pulley as well as the lathe. In the tailstock side a brass bush was fitted as a rotating earth together with a reinforced insulating housing.

Originally, a travelling earth arrangement had been designed and fitted. This took the form of an insulating housing fitted in a T slot on the lathe saddle situated under the workpiece. A spring loaded brass

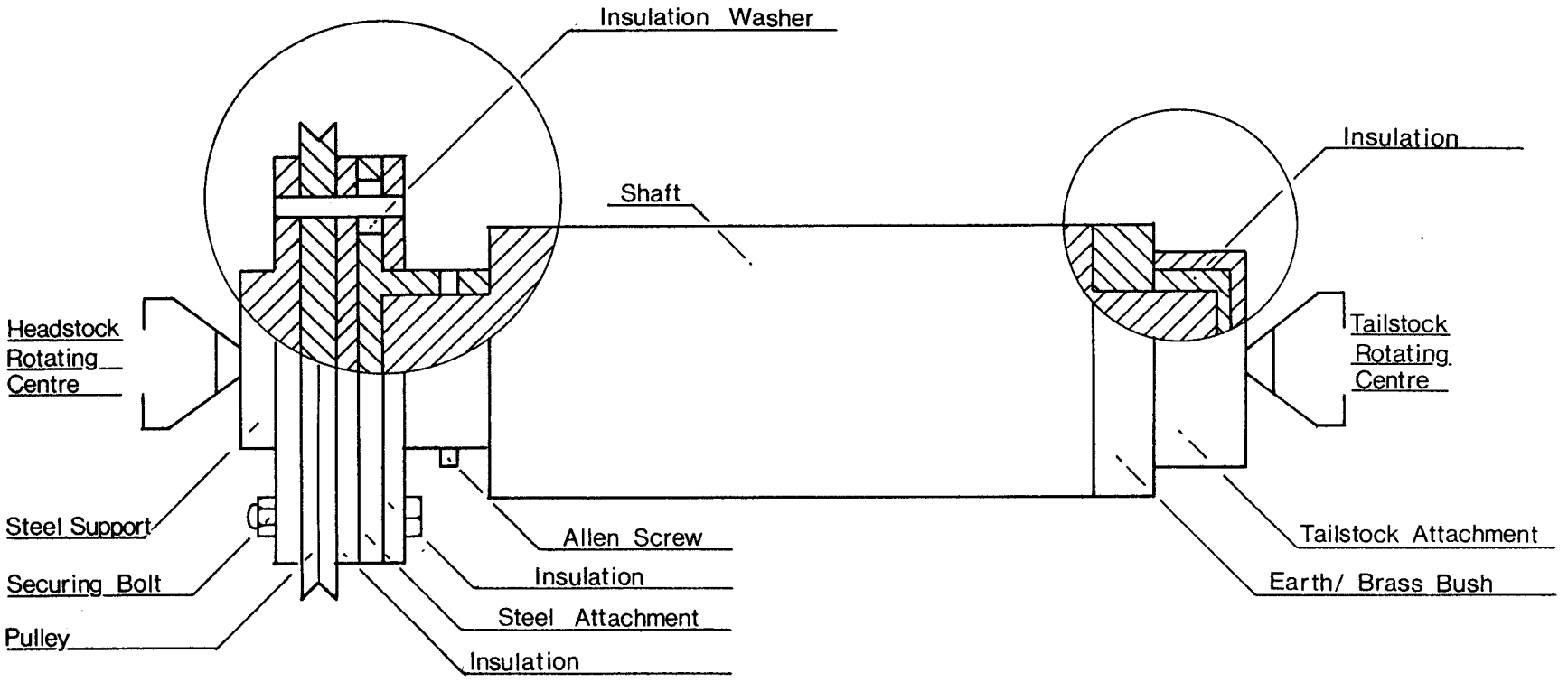
Insulation Washer
Shaft
Insulation
Headstock
Rotating
Centre
Tailstock
Rotating
Centre
Steel Support
Securing Bolt
Pulley
Allen Screw
Insulation
Steel Attachment
Insulation
Tailstock Attachment
Earth/ Brass Bush

FIG. 8.1 Set up

brush located on this housing, was pressing on the workpiece surface thus providing good electrical contact.

The concept of the earth being situated constantly at the same position in relation to the arc was part of the effort to control the possibility of arc blow suggested in the literature (Halmoy 1982) (Norman 1984a & 1984b). However, this arrangement had to be modified due to problems caused by spatter on the surface of the component.

A torch holder was designed such as to provide any possible positioning relative to the surface of the workpiece and was fitted on the lathe saddle.

The set up had rotational speeds from stationary up to a maximum of 12.0mm/s and transverse speeds from stationary up to 17.0mm/s.

8.1.3 Welding Set.

The welding set used was a GEC Advanced Welding Products M450PS. All the parameters except the voltage could be changed. The operating ranges are shown below:

Pulse current	0 - 450 A in 1 A steps.
Back. current	0 - 450 A in 1 A steps.
Pulse time	0 - 0.0999 s in 0.0001 s steps.
Back. time	0 - 0.0999 s in 0.0001 s steps.
Wire feed speed	0 - 19.9 m/min in 0.1 m/min steps.

The wire feeder was a Millermatic S54D and the torch, a swan neck water cooled Binzel MB501D.

8.2 Experimental Work.

8.2.1 Identification of Operational Parameters in Overlay Welding.

The main operational parameters, for a continuous spiral deposit, are: the metal transfer, torch positioning, overlap, rotational speed and transverse speed.

The stability and type of metal transfer determine the shape and fusion characteristics of the deposit. A stable metal transfer is essential to ensure a continuous, smooth and uniform deposit, which would be less susceptible to any fusion defects. The type of metal transfer determines the shape of the fusion interface between the overlayer and the substrate. Ideally, the deposit must exhibit a regular smooth profile with as little penetration and dilution as possible, but without the introduction of any fusion defects. In addition, it is preferable that the surface finish obtained requires the least machining, thus minimising wastage of filler wire.

Compared to short circuit and globular transfer, projected spray transfer provides excellent metal transfer characteristics with minimum spatter. Although the penetration and dilution levels of projected spray transfer are higher than those of short circuit and globular transfer modes, the higher levels of spatter these two modes exhibit increase the possibility of flaws and fusion defects between the overlayer and the substrate. In addition, the welding arc in projected spray transfer is more directional than the arc during

globular metal transfer, which means that better control during deposition may be obtained.

Although streaming spray transfer tends to result in wider and flatter beads due to an increased radial heat distribution, the penetration and dilution levels obtained are unacceptable.

In contrast with the deposition of stringer beads on flat plates where the torch may be inclined at a longitudinal and/or lateral angle, when overlaying a cylindrical component the torch may be positioned in space in such a way that the relationship between the weldpool and gravitational effects may change. For example, the torch may be positioned in such a way that overhead welding may be considered to take place.

In spiral overlay welding the overlap employed not only controls the dimensions and dilution of the deposit (Allen & Earl 1984), but also affects the duration of the process and the amount of filler metal used.

The overlap is measured in terms of a percentage and denotes how much of the previous bead the advancing arc will melt and cover. The percentage of overlap possible is determined by the melting capability of the arc and to a certain extent by the directionality of the metal transfer.

The rotational speed corresponds to the travel speed in bead on plate deposition. The width of the bead depends on the ratio between the wire feed speed and the rotational speed and for a required overlap the transverse speed may be set accordingly.

8.2.2 Experiments and Results.

Eight single layer deposits, in four groups, were overlayed on 76.2mm (3") diameter mild steel shafts by continuous spiral overlapping deposition. The welding parameters used are shown in table 8.1 and are presented in a chronological sequence.

table 8.1 Overlay Welding Parameters. Single Spiral Technique

	Im	W	Ip	Tp	Ib	Tb	Q	Rot.S	Tr.S	Angles α	Angles ß	Overlap
1	200	6.36	230	2.3	50	0.2	20	9.91	0.180	90	60	50%
2	100	3.18	350	1.6	50	8.0	20	2.85	0.047	90	60	50%
3	140	4.45	350	1.6	50	3.7	20	4.69	0.073	90	60	50%
4	160	5.08	350	1.6	50	2.8	20	5.98	0.094	90	60	50%
5	70	2.00	350	3.0	40	26.5	15	1.89	0.047	90	80	50%
6	100	3.18	165	31.0	50	37.5	15	3.77	0.047	90	80	50%
7	110	3.50	175	9.5	50	9.7	15	3.77	0.047	90	80	50%
8	200	6.36	300	5.0	100	5.0	20	8.90	0.129	90	80	50%
	"	7.45	"	"	"	"	"	10.00	"	"	"	70%

8.2.2.1 Profile Examination.

Transverse and longitudinal sections from the overlayed shafts were cut and made into specimens.

The examination of the profiles involved three aspects: firstly, microscopic examination for the detection of flaws, porosity and cracking; secondly, measurement of the dilution levels; thirdly, assessment of the surface finish after welding and hence measurement of the deposit wasted during machining.

8.2.2.2 Presentation of Results.

The first group of deposits consisted of one preliminary run and was used to assess the nature of the process and any problems associated with it. The

parameters used, in particular the mean current, were chosen so as to provide good fusion irrespective of the resulting penetration and dilution levels.

Plate I shows a transverse section of the resulting profile. Measurements of the dilution are presented in table 8.2.

table 8.2 Dilution in Single Spiral Overlayers

Specimen No.	1	2	3	4	5	6	7	8
Dilution	23.0	12.0	13.0	12.0	10.7	14.8	20.5	33.7

The second group of deposits consisted of three overlayers deposited at three different mean currents with projected spray transfer. The deposition ratios varied from 14-18.6 with a lateral torch inclination of $\beta=50^{\circ}$. It was intended to obtain relatively wide and thick deposits with low levels of dilution.

Plate II to Plate IV show the transverse profiles of these overlayers. All three deposits had relatively low dilution levels ranging between 11% and 17%. The percentage of the deposit to be machined, ranged from 7.6% to 27.8%.

The third group consisted of three overlayers as well, deposited at low heat inputs, with the aim of obtaining relatively low penetration and dilution deposits. One overlayer was deposited at 70A mean current employing projected spray transfer, one at 100A mean current employing globular transfer, and the other at 110A employing projected spray transfer.

The dilution levels ranged from 10.7% to 20.5%. Overlayer No.5 had the least dilution because of the low

welding currents and high deposition ratio employed. Overlayer No.6 had a 14.8% dilution partly due to the deposition ratio and partly due to globular transfer, whereas overlayer No.6 exhibited a dilution of 20.5% which was a result of projected spray transfer.

Plate V to Plate VII show these profiles after having been machined. The amounts of the deposit machined for each profile were 7.6%, 5% and 8% respectively.

The fourth group consisted of one overlayer deposited at 200A mean current with projected spray transfer. The object of this deposit was to investigate the effects of short arc lengths on the elimination of arc deflection and the deposit characteristics.

The parameters used are presented in table 8.1. In order to decrease the arc length, the wire feed speed was increased. The increased deposition was balanced by increasing the rotational speed but as it was not possible to increase the transverse speed of the torch, the overlap increased.

The changes in welding parameters, and in particular the increase in overlap caused an excess of deposited material which deteriorated the surface finish. Despite this, there were no defects in the coating.

Plate X shows the profile after the deposit was machined. The amount that had to be machined was 15% of the whole deposit. Dilution was relatively high at 33.7% and the interface profile was coarse. However, the deposit and the interface were free of interface defects.

PLATE I. 1mm O.1

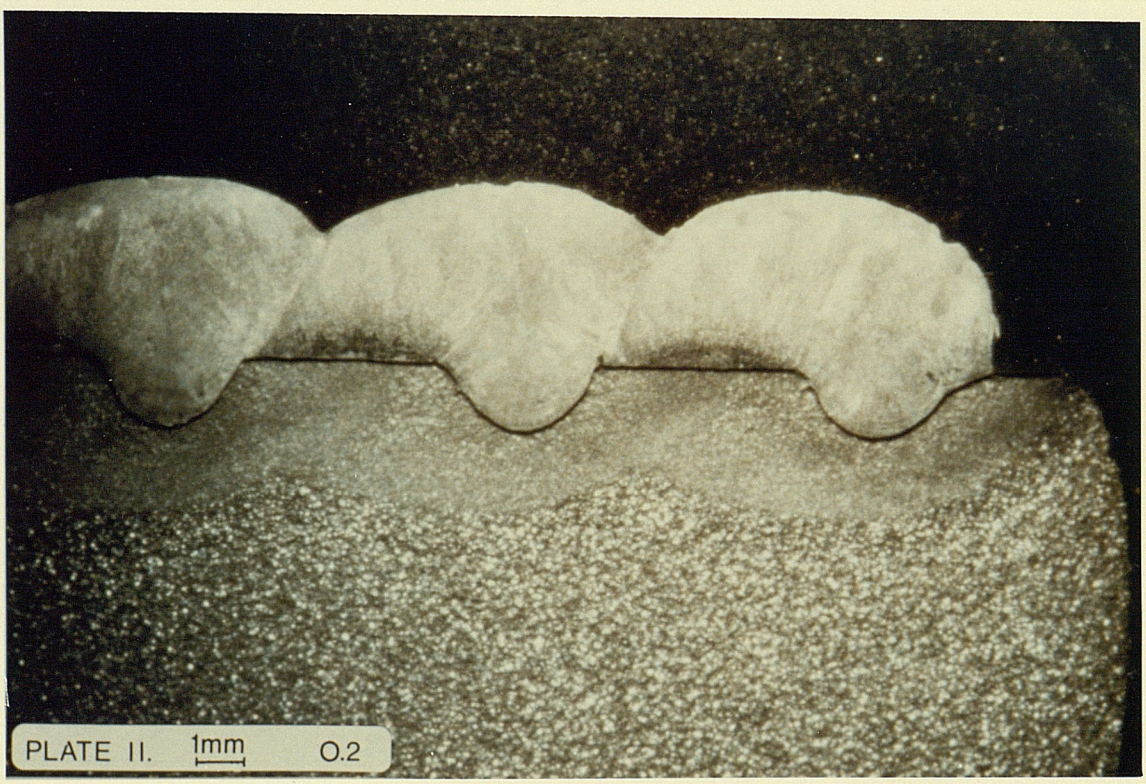

PLATE II. 1mm O.2

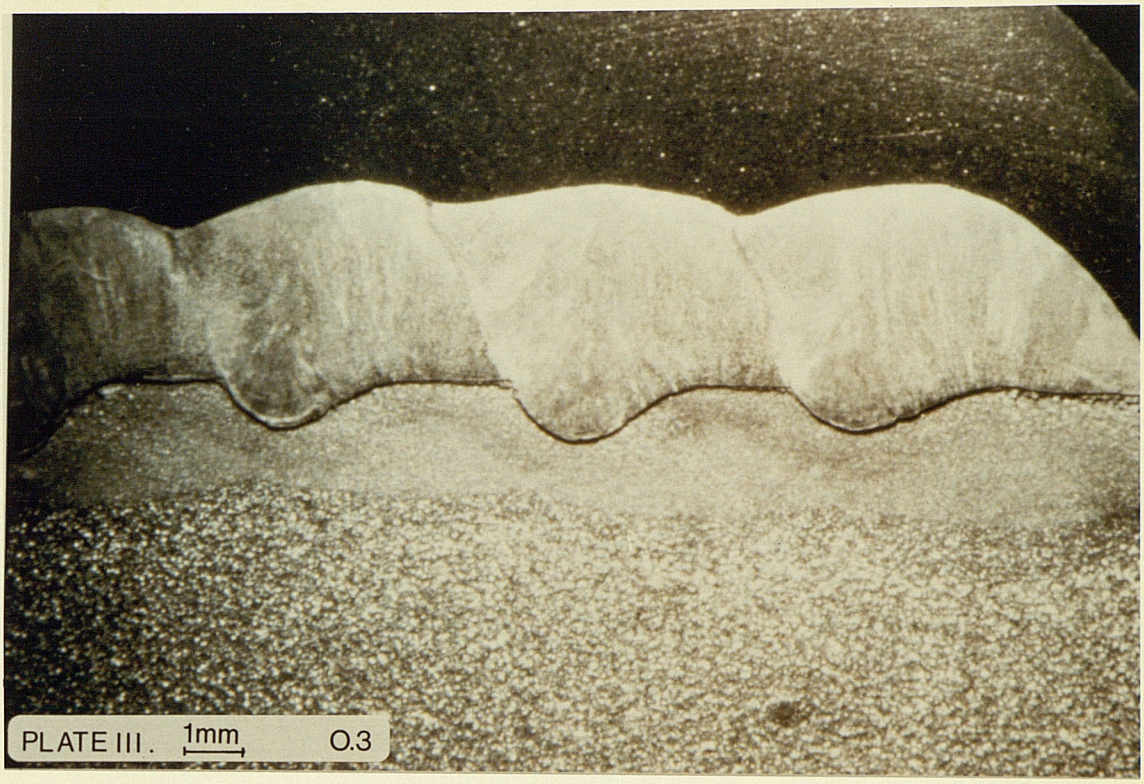
PLATE III. 1mm O.3

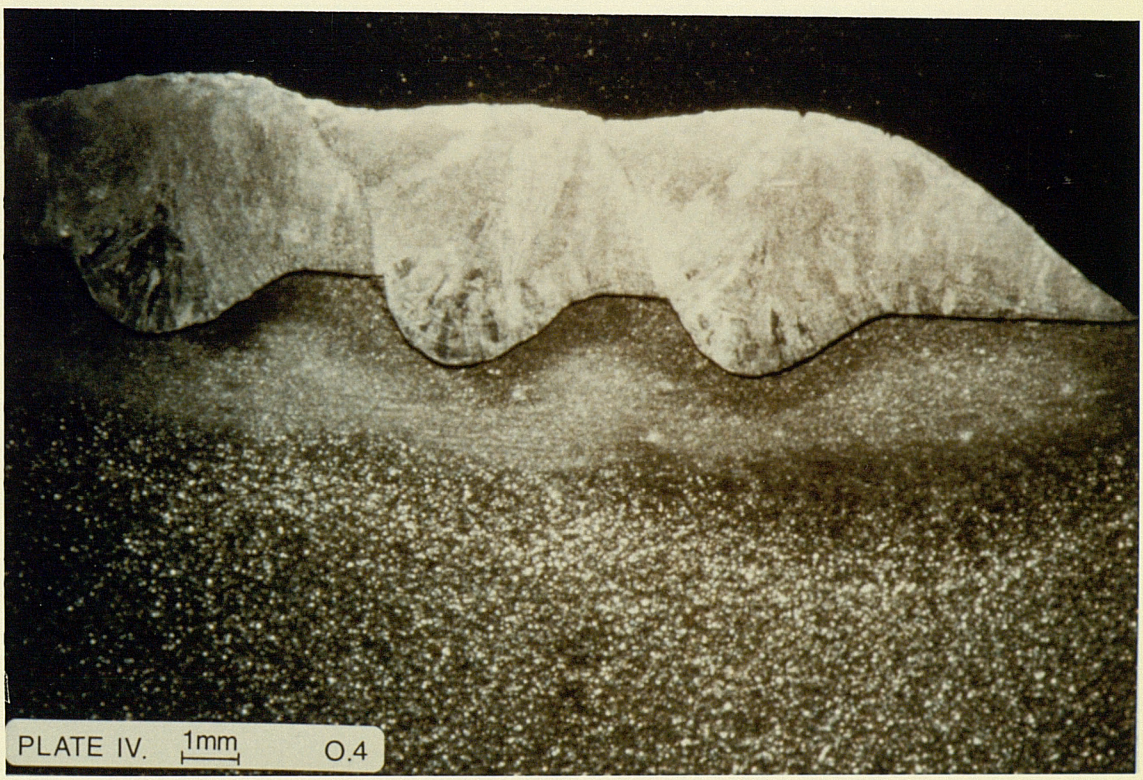
PLATE IV. 1mm O.4

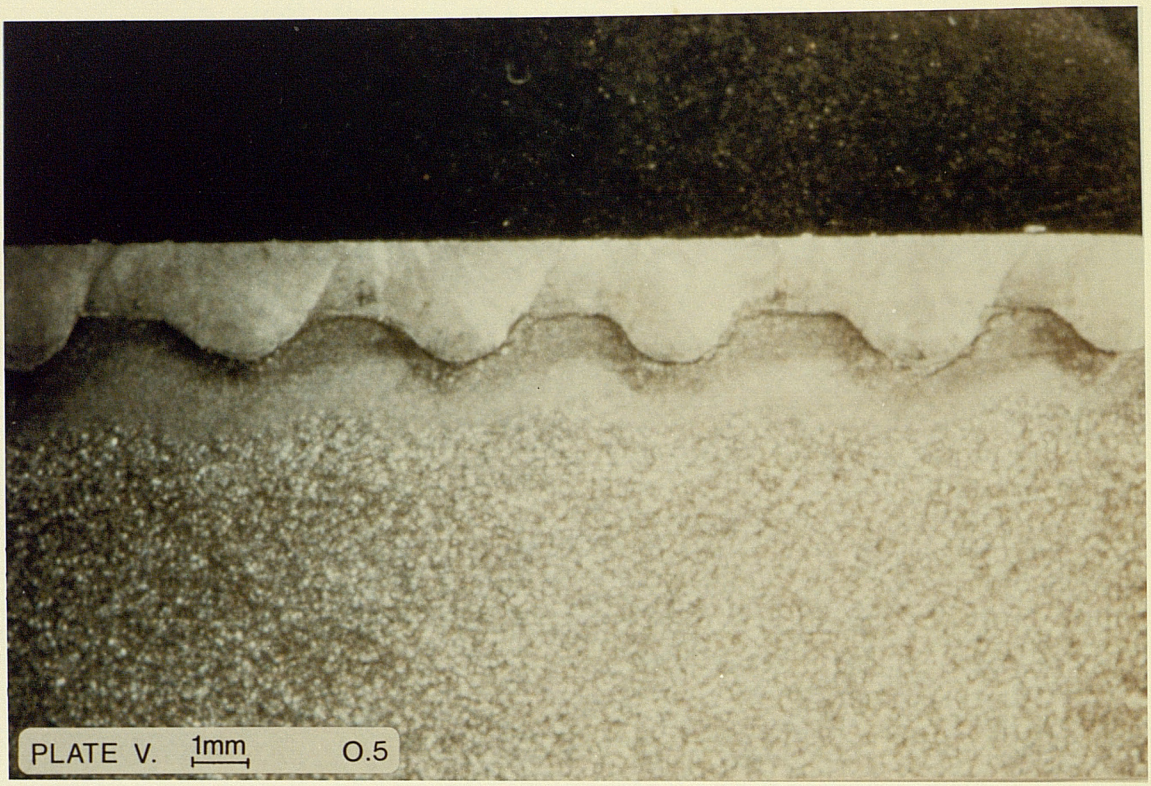
PLATE V. 1mm O.5

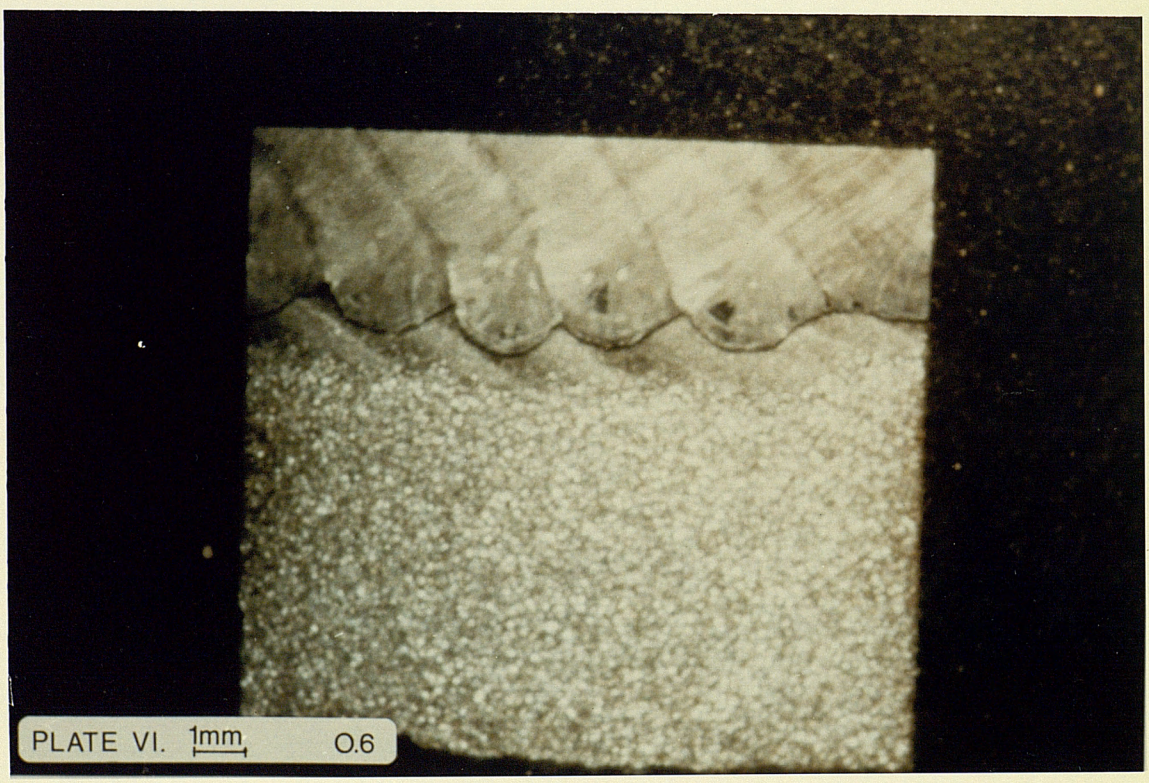
PLATE VI. 1mm O.6

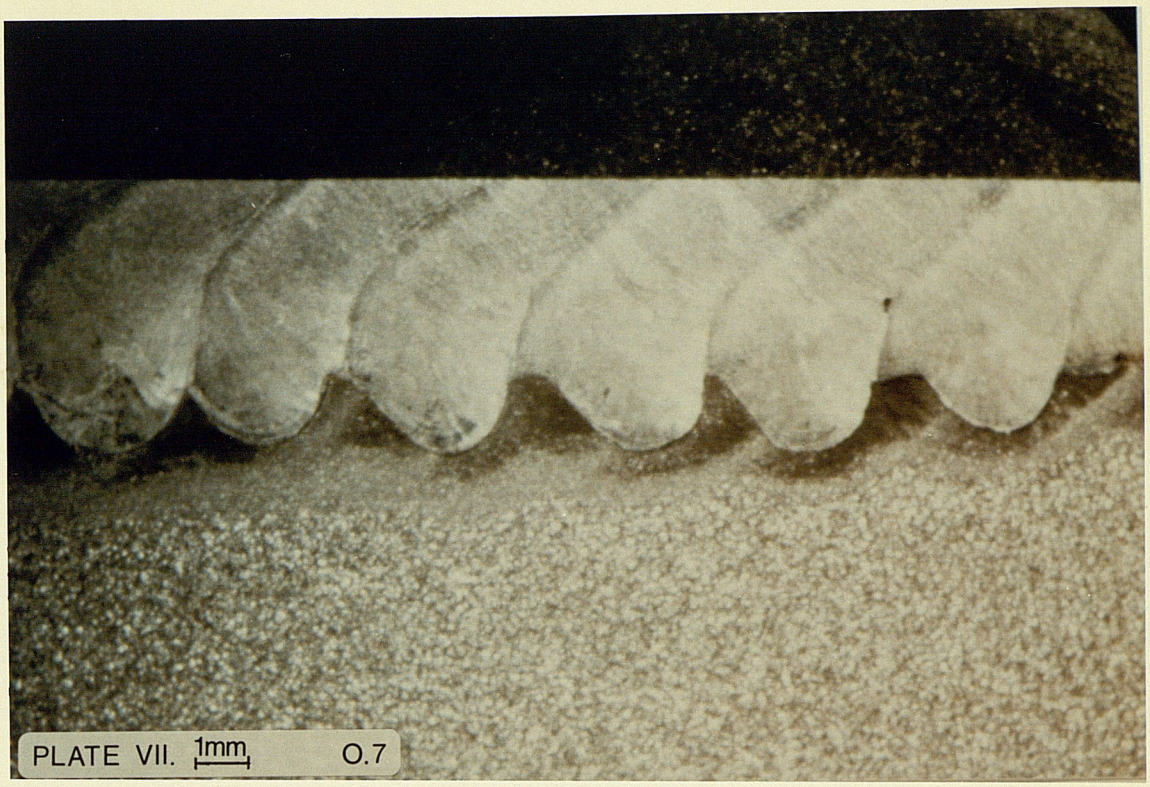

PLATE VII. 1mm O.7

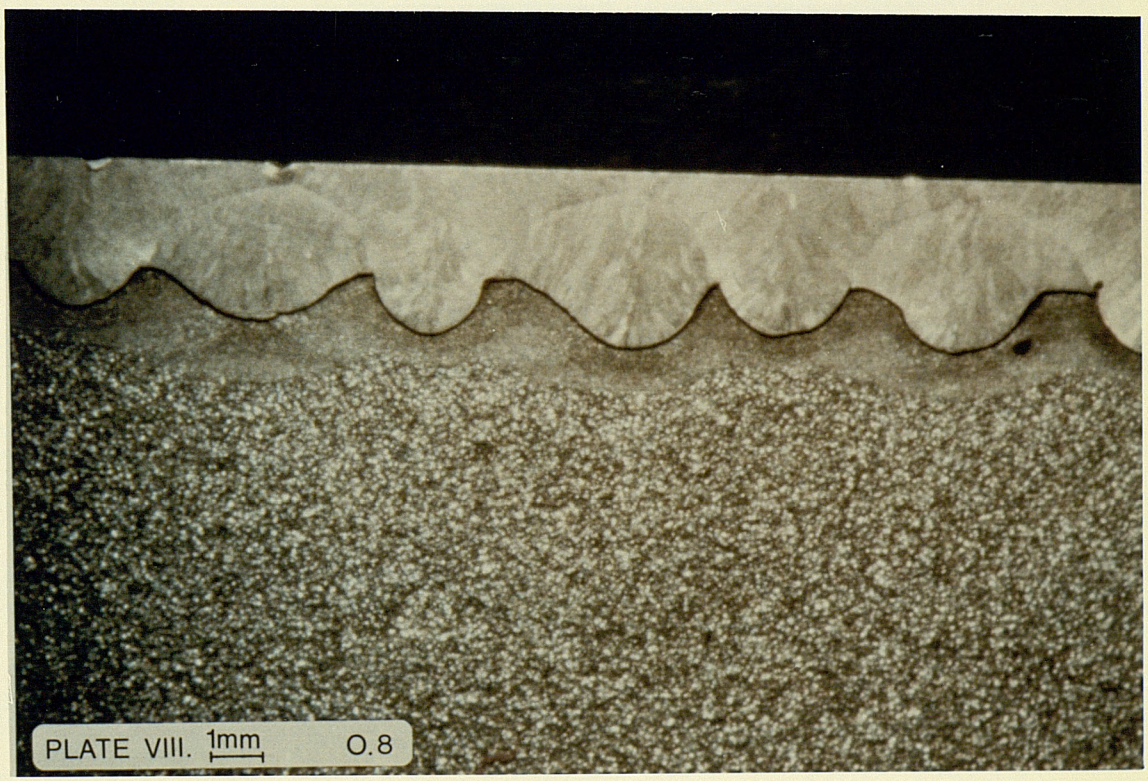

PLATE VIII. 1mm O.8

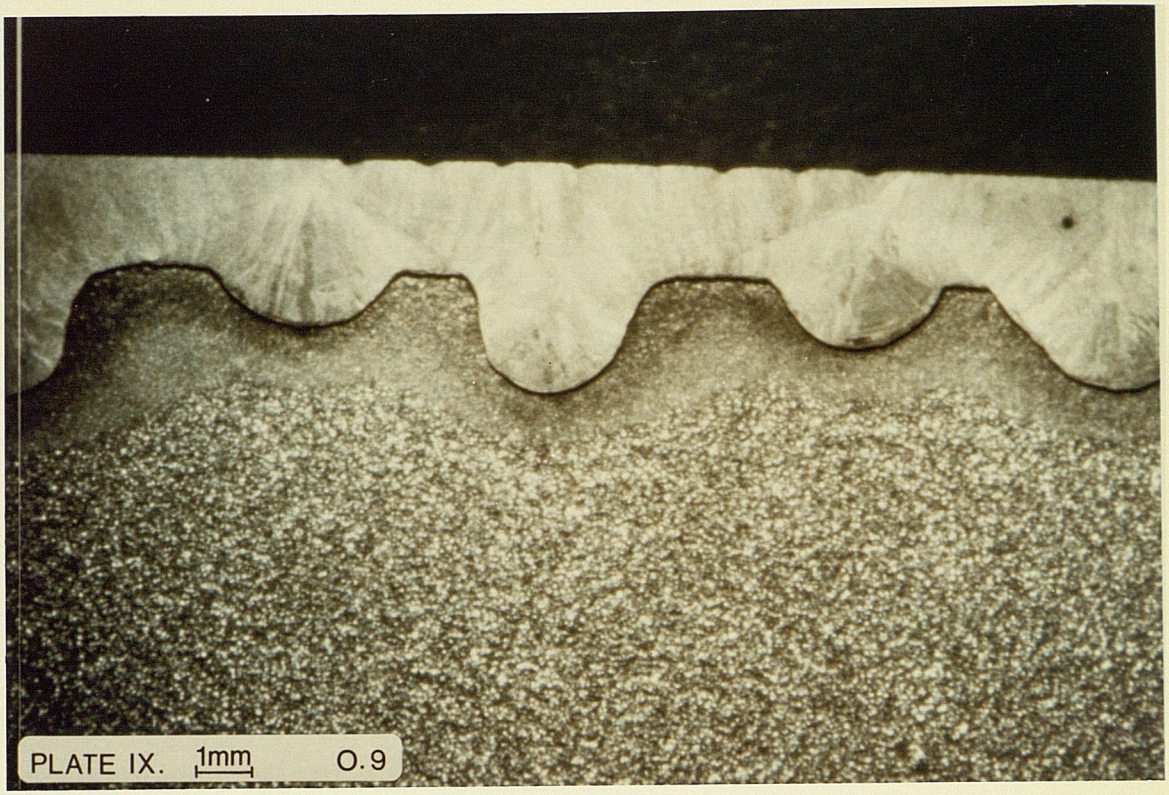

PLATE IX. 1mm O.9

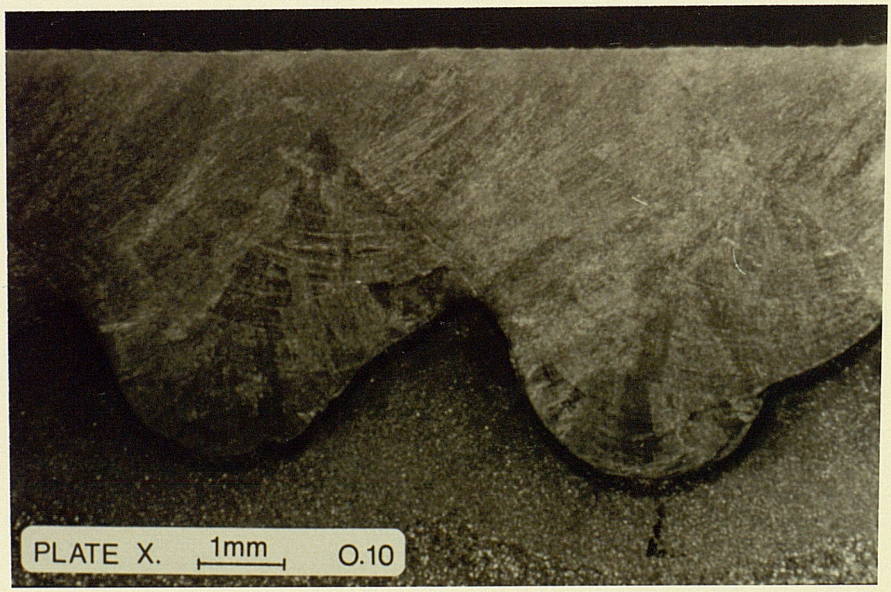

PLATE X. 1mm O.10

8.2.3 Discussion: Single Spiral Overlaying Technique.

8.2.3.1 Examination of the Deposit/Substrate Interface.

The preparation of specimens from transverse and longitudinal sections of overlayed shafts gives an indication of the nature of the interface between the deposit and the substrate at the sectioning planes. In order to have a better appreciation of the interface a very simple technique, to enable visual examination of the interface itself was employed. Cut specimens were immmersed in 10% aqueous solution of Nitric acid for approximately 100 hours and the substrate was chemically dissolved. The length of time the specimens were immersed in the acid solution depended on the amount of substrate that had to be dissolved. Segments from all the overlayed shafts were immersed in the acid solution and the substrate was dissolved away thus revealing the interface.

This technique not only exposed the interface for visual examination, but also etched the overlayer just enough to reveal the crystal structure of the deposit.

The fact that the overlayer was not attacked by the acid solution, showed that the deposit had retained its original corrosion resistance properties despite the dilution with the substrate. In addition, it indicated that the composition of the deposit was uniform at some degree as no preferential corrosion near the interface had taken place.

8.2.3.2 Effects of Metal Transfer on the Stability of the Process.

Unstable metal transfer is totally unacceptable in overlay welding. In particular mixed transfer gives rise to very irregular bead deposits with surface defects such as discontinuities and holes.

Although the effects of unstable metal transfer are immediately apparent, when irregular metal transfer takes place such as homogeneous mixed transfer, its effects may remain undetectable.

Plate XI and Plate XII show the surface finish and the appearance of an overlayed shaft. The tranverse profile of the same deposit is shown in plate I. It is clear that although the surface finish of the overlayer is quite smooth, the penetration is not very regular. A segment of this shaft was cut and immersed in 10% Nitric acid in water for a period of approximately 100 hours until the substrate was dissolved away. Plate XIV shows the interface of this specimen and it can be seen that the depth of penetration is not uniform throughout the the deposit. For example, at the lefthand side of plate XIV, four distinctive protrusions are the clear indication of irregular metal transfer.

Plate XIII shows a typical example of how the interface looks when regular transfer has been established. It can be seen that all five penetration "channels" are smooth and continuous.

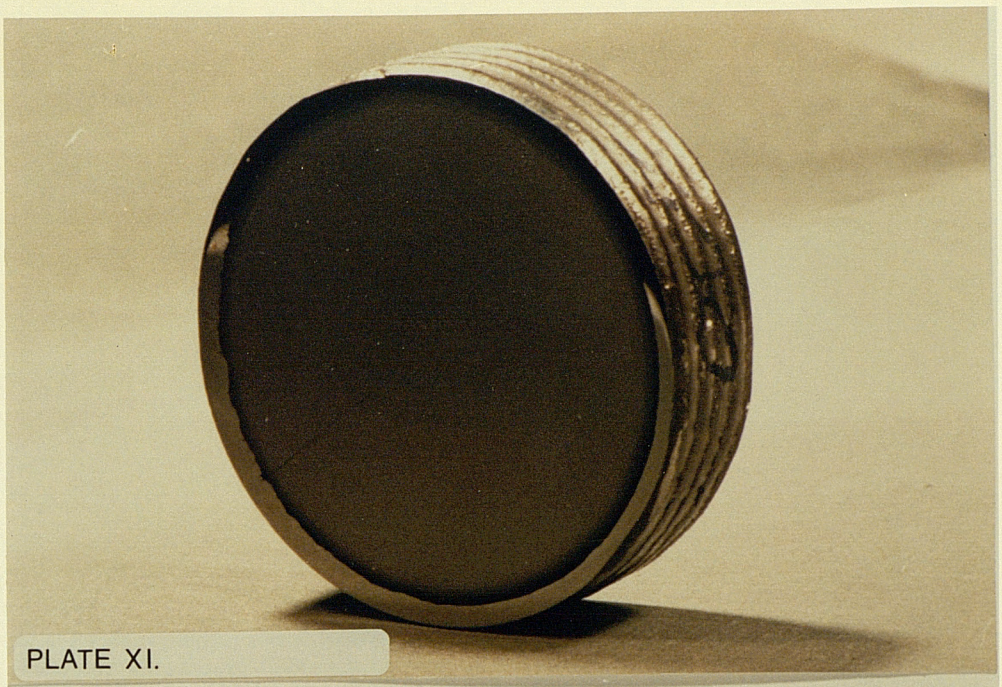

PLATE XI.

PLATE XII.

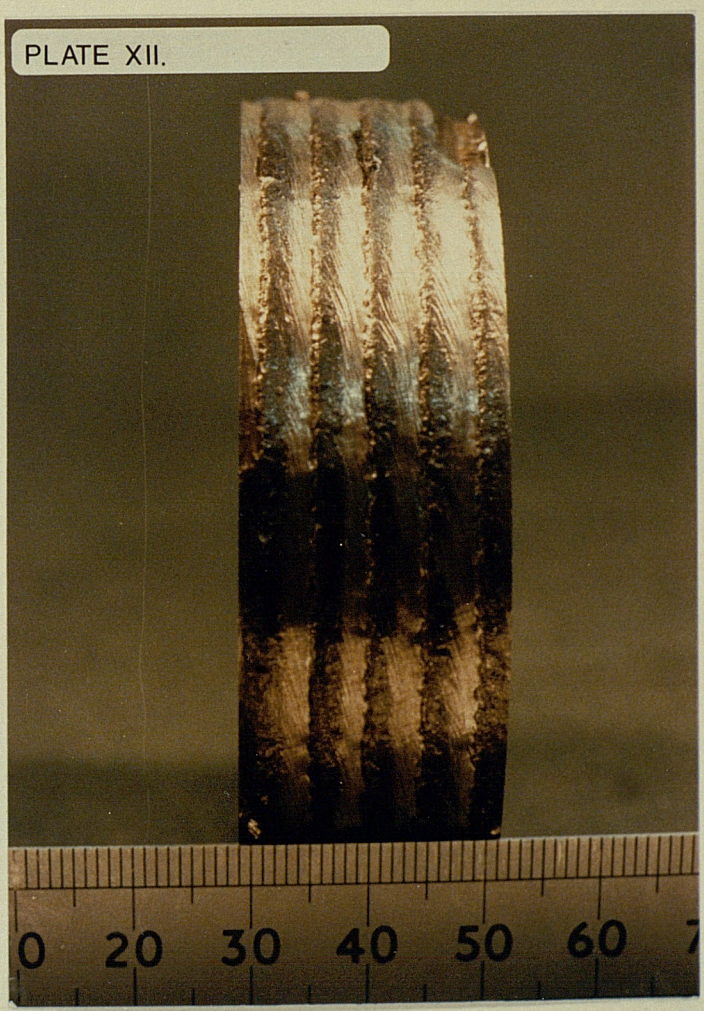

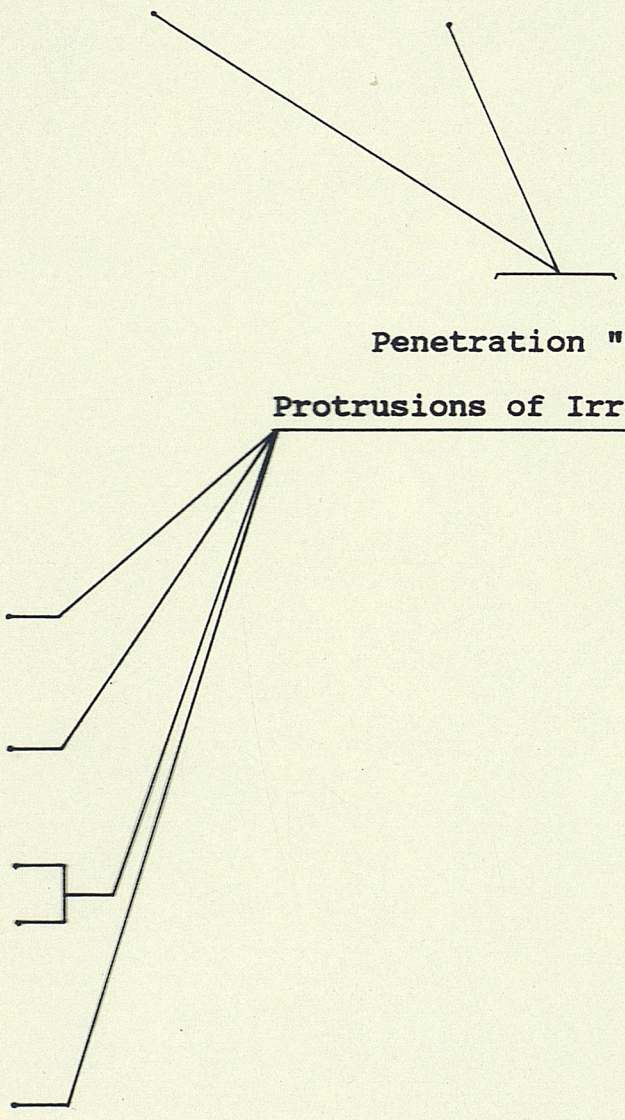
Penetration "Channels"
Protrusions of Irregular Transfer

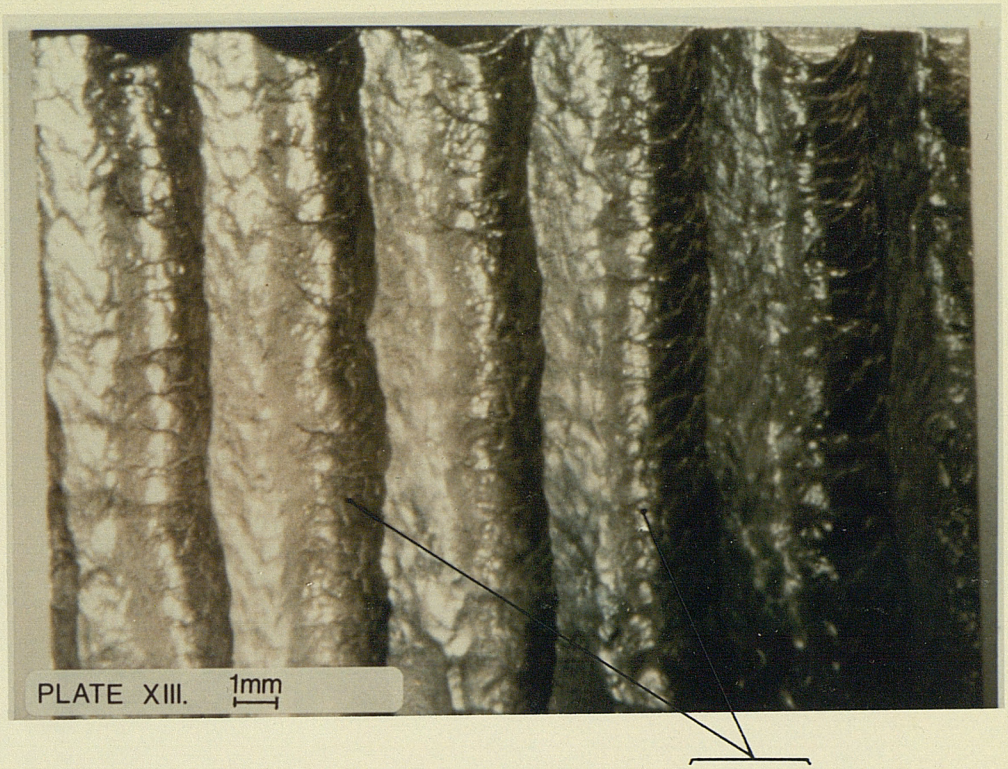

Penetration "Channels"

Protrusions of Irregular Transfer

8.2.3.3 Effects of Overlap on the Stability of the Process.

The amount of overlap employed can control the resulting amount of dilution in the deposit. The less the amount of overlap the higher the dilution, the highest level being when overlap is zero. Subsequently, the higher the overlap employed the lower the dilution. However, there is a limit to the maximum permissible overlap and this is dictated by the welding parameters used and specifically the welding current.

It has been found that the maximum overlap which will result in a satisfactory deposit for any welding conditions, is 50%. Higher overlaps with low currents are prone to result in defective deposits. Experiments showed that when overlapping was over 50%, defects were present at the toes of the beads which suggests incomplete fusion.

8.2.3.4 Effects of Arc Length on the Process.

In stringer bead deposition the profiles appeared to be relatively insensitive to arc lengths of 5-10mm in projected spray transfer. However, in the simple spiral overlaying technique the arc length appears to be a very important parameter.

Preliminary experiments in overlay welding which employed low mean currents and the single spiral overlapping technique showed that the stability of the process and consequently the soundness of the deposit was affected by the arc length used. It was observed that during the deposition of an overlayer a long arc would at

some stage of the process begin to deflect from side to side, oscillating between the previous spiral and the base metal. Deflection of the arc occurs because the distance between the electrode tip and the previous bead is shorter than the distance between the electrode tip and the base material.

When the arc is deflected towards the previous spiral, the overlap increases which results in a thicker deposit. This deposit will be closer to the electrode tip and will continue both to deflect the arc and to increase the overlap. However, as the torch moves away from the previous bead, the distance between the electrode tip and the weldpool will at some point become too long. The arc in order to maintain itself, deflects in the direction of the shortest distance which is that between the electrode tip and the base material. Such a deflection has a catastrophic effect on the continuity of the deposit and if this occurs, the process has to be stopped and the deposit must be machined off where it is irregular.

This periodic arc deflection between the previous spiral and the base metal, becomes more severe when long arcs are used. Therefore, it follows that relatively short arcs of the range of 5mm to 7mm have increased directionality and are less sensitive to deflection.

The arc length may be controlled by means of altering the arc voltage. However, where this is not possible, as with the welding set used, this may be achieved by altering the wire feed speed and by reducing the standoff.

8.2.4 A Proposed Overlay Welding Technique.

The most important requirements in overlay welding are low dilution and defect free coatings. Low dilution can be achieved when low welding currents are used. In addition, dilution can be controlled by the implementation of welding techniques. One such technique is the amount of overlap employed during deposition. However, as discussed in section 8.2.3.3 the amount of overlap that can be employed is limited.

Overlay welding using the technique of a single overlapping spiral has its limitations especially when low current depositions are considered. Additionally, high welding currents tend to give rise to coarse rather than smooth profiles because of finger penetration.

An alternative technique may be used in which the best profile and fusion characteristics of low and high current depositions can be combined. In the proposed technique a very low current spiral bead, called the primary spiral, is deposited either having zero overlap or leaving a width of exposed base metal between the weld beads. Then a second spiral bead, the covering spiral, is deposited in the gap. The electrical parameters used to close the gap must supply the necessary heat input to melt the sides of the beads and the base metal. In addition, projected spray transfer is required so that the momentum of the droplets displaces any contaminants in the gap. The covering spiral will melt the exposed base metal as well as the sides of the previous spiral, thus completing the overlayer. Figure 8.2 shows the sequence of the deposition of the primary and secondary

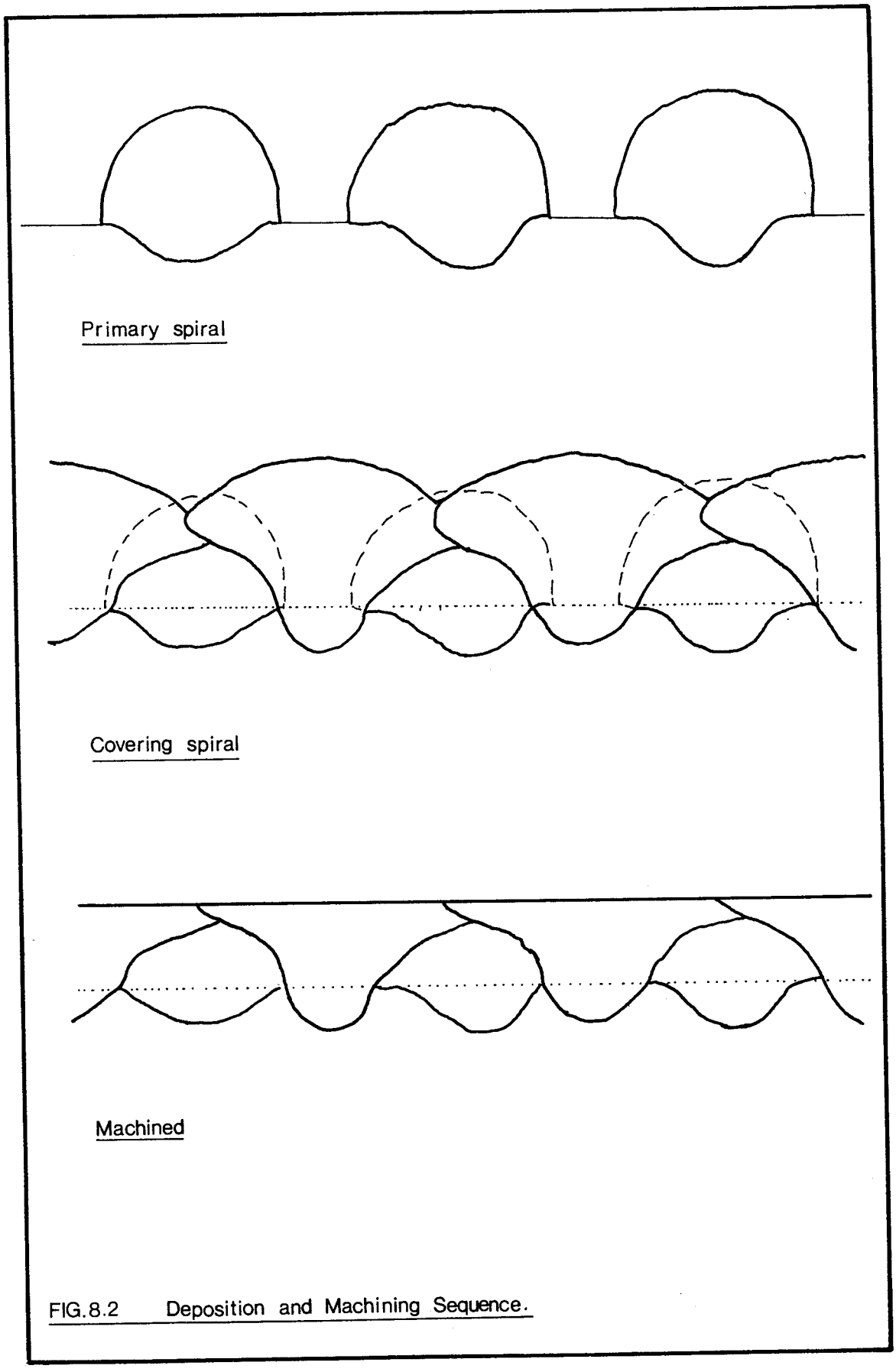

FIG.8.2 Deposition and Machining Sequence.

spirals as well as the machining after welding.

8.2.4.1 Experiments.

In order to try this technique two overlayers were deposited. The welding parameters used are given in table 8.3.

table 8.3 Overlay Welding Parameters. Double Spiral Technique

	Im	W	Ip	Tp	Ib	Tb	Q	Rot.S	Tr.S	Angles α	Angles ß	Gap(mm)
9	100	3.18	300	4.0	50	16.0	20	4.42	0.06	90	90	2.5
	180	5.72	300	4.5	60	4.5	20	10.40	0.29	90	90	
10	100	3.18	180	6.0	50	9.0	20	6.00	0.26	90	90	4.0
	180	5.72	300	4.5	60	4.5	20	5.83	0.47	90	90	

In both cases a low heat input set of parameters was used for the primary spiral. The primary spiral of the first overlayer left a gap of 2.5mm whereas the second overlayer had a gap of 4.0mm. The welding parameters used to deposit the covering spiral were set so as to provide the amount of filler wire required to cover the gap, to cause sufficient melting and deliver the filler metal in such a way that no fusion defects can result.

8.2.4.2 Results.

The deposition of the primary and covering spirals was carried out without any problems. The resulting surface finish was relatively smooth with the covering spiral not only having covered the gap of the primary spiral but the primary spiral as well.

Plate VIII and Plate IX show the profiles of the

two overlayers and table 8.4 presents the results of the analysis of the profile.

table 8.4 Dilution in Double Spiral Overlayers		
Specimen No. 9		
	primary spiral	20.0%
	covering spiral	12.9%
	overall dilution	14.0%
Specimen No. 10		
	primary spiral	16.7%
	covering spiral	24.0%
	overall dilution	16.0%

Measurements of the overlayed specimen No.9 showed that the dilution of the primary spiral is 20%. The dilution of the covering spiral with the base metal is only 12.9%. Whereas the overall dilution of the overlayer in terms of deposit areas and penetration areas is 20%, the real dilution which is that of the covering spiral is 14%.

Specimen No.10 exhibited 16.7% dilution of the primary spiral, 24% dilution for the covering spiral with the base metal and 16% overall dilution in terms of measured areas. The dilution of the covering bead with the base metal and the primary bead increased due to the wider gap of the primary bead.

The amount of machining for both overlayers were 19% and 24% respectively.

8.2.5 Discussion: Comparison between the Single and the Double Spiral Overlaying Techniques.

The double spiral deposition, as an overlay welding technique, has the following advantages over the single spiral overlapping technique:

It can employ low welding currents, but with a smaller risk of fusion defects, defects that arise from overlapping are eliminated, dilution may be kept at minimum levels even with projected spray transfer.

The major disadvantage of this technique is that it is more complex as two sets of welding parameters are employed.

Dilution may be improved if the gap of the primary pass is kept as small as possible. It must be stressed that three conditions must be met in order to ensure a sound deposit. The arc length must be kept as short as possible, metal transfer must be stable and regular and the bead profiles must not be obtuse.

8.2.5.1 Machining Requirements of the Deposits.

From the results obtained from the deposits, it appears that the single spiral technique requires less machining after welding than the double spiral technique. However, the data available are very limited in number to compare conclusively the two processes. Further experimentation is required on this topic which, although very important for the economic and efficient use of materials, is secondary to the dilution requirement. Table 8.5 shows the minimum amount of deposit machined or to be machined for all the overlayed specimens.

table 8.5 Deposit Thickness and Machining Requirements			
Specimen No.	Overlayer Thickness Tmax (mm)	Tmin (mm)	% of Deposit Machined
1	3.15	2.36	16.6
2	4.00	2.67	27.0
3	3.20	2.53	16.6
4	3.33	2.80	10.6
5	2.63	1.51	7.6
6	3.58	2.43	5.0
7	3.81	3.38	8.5
8	3.66	2.99	15.0
9	4.04	2.16	19.0
10	3.00	2.00	24.0

8.2.5.2 Calculation of Welding Parameters.

Figure 8.3 shows a schematic approach to the selection of welding parameters for the Single spiral overlay method and the Double spiral overlay method.

Single Spiral Overlap: in order to calculate the various welding parameters the width of the bead must be known. This is a function of the deposition ratio, and a specific combination of wire feed speed and travel speed can give this width. Therefore the deposition ratio will set the rotational speed of the component. Having chosen the amount of overlap and knowing the bead width and the rotational speed, the transverse speed can be set.

The torch is best set at an angle ß of 85° to 80° maximum inclination, to avoid any profile irregularities.

Having calculated all the above parameters then the duration of the operation and the material consumption may be calculated as well.

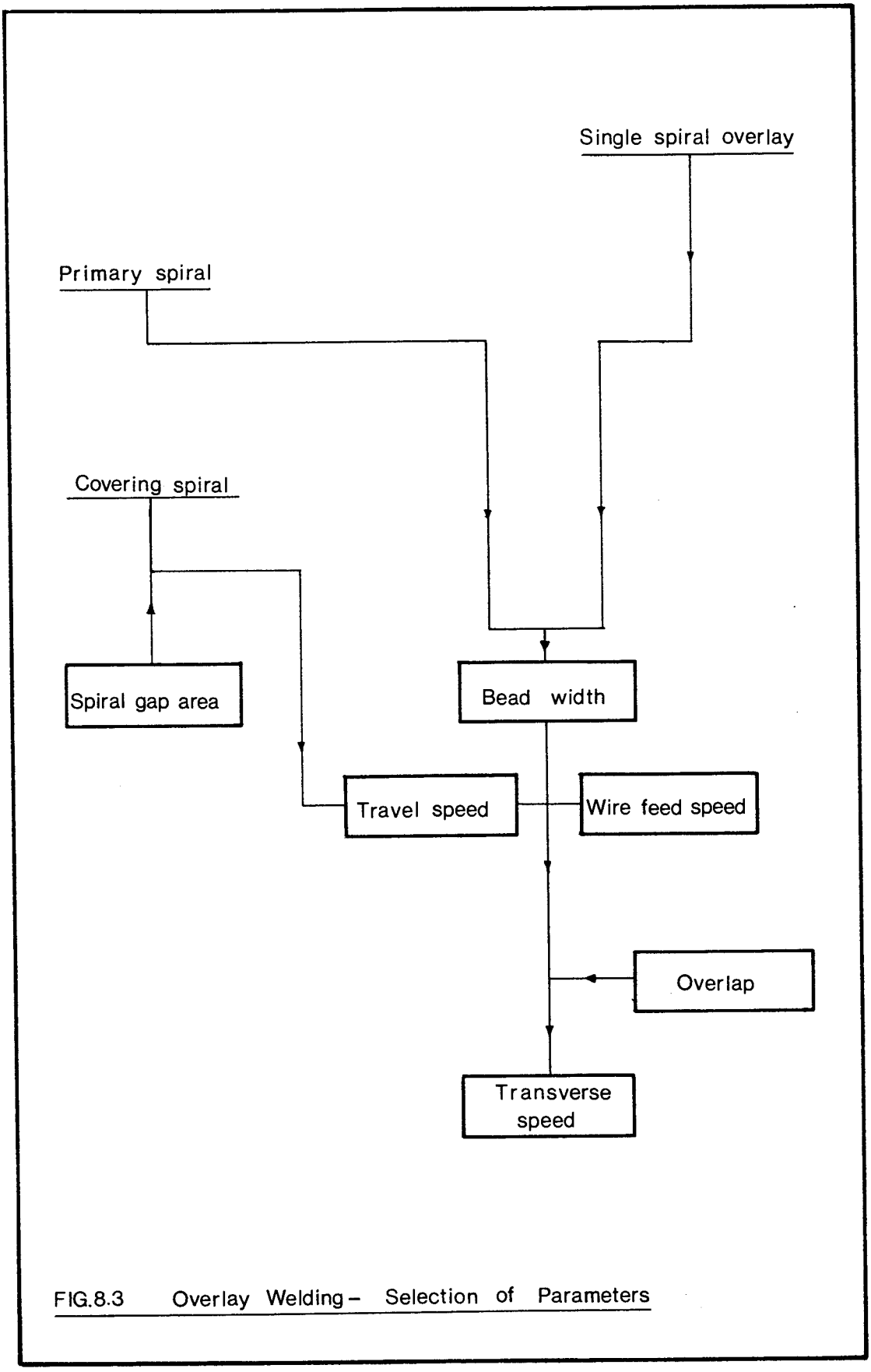

FIG.8.3 Overlay Welding – Selection of Parameters

Double Spiral Model: The same approach is applied for this technique as well, except that the overlap is zero or negative. The transverse area of the gap can be used to calculate the wire feed speed and travel speed required. The transverse feed of the torch is calculated so that the covering bead will have the same pitch as the primary bead.

8.3 Metallurgical Examination of the Overlayers.

8.3.1 Introduction.

The chemical composition of the filler wire is given in table 8.6 as specified by the British Steel Corporation and its manufacturer (ESAB). Also shown in table 8.6 is the chemical composition of the base metal as specified by the British Steel Corporation. Table 8.7 presents the chemical compositions of the two alloys as determined by chemical analysis.

However, the desired properties of both materials must be retained after the overlaying process. It is therefore essential to assess the weldability of each material separately but more importantly to be able to predict the properties of the resulting overlayed material after dilution has taken place.

table 8.6 BS Base Metal & Filler Wire Compositions.		
Base Material Composition BS 970:Part1:1983 070M20 Composition (Fe bal.)	Filler Wire Composition as given by BS 2901 316S92	as given by manufacturer
C = 0.16-0.24 Mn= 0.5-0.9 Si= 0.1-0.4 P & S 0.05 max	C = 0.03 Cr= 18.0-20.0 Ni= 11.0-14.0 Mo= 2.0-3.0 Mn= 1.0-2.5 Si= 0.25-0.65 Cu= 0.5 P = 0.03 S = 0.03	0.03 19.0 12.0 2.8

table 8.7 Chemical Analysis of Filler Wire and Base Metal

Filler Wire 316S92 (Fe bal.)			
C = 0.03	Mn= 1.66	Al= 0.00	Sn= 0.009
Cr=18.2	Si= 0.43	Ti= 0.00	Nb= 0.02
Ni=11.2	P = 0.027	Cu= 0.17	V = 0.07
Mo= 2.00	S = 0.005	Co= 0.02	W = 0.04

Base Metal 070M20 (Fe bal.)				
C = 0.17	Al= 0.02	Co= 0.01	Nb= 0.00	Sn= 0.018
Si= 0.20	As= 0.019	Cr= 0.10	Ni= 0.13	Ti= 0.00
Mn= 0.74	B = 0.0006	Cu= 0.18	P = 0.016	V = 0.00
	Ca= 0.00	Mo= 0.02	S = 0.028	W = 0.02

8.3.1.1 Weldability of Substrate.

The Dearden & O' Neil formula may be used to calculate the preheat requirement. This equation is applicable to plain carbon and carbon manganese but not to micro alloyed HSLA steels or low alloy Cr-Mo types.

$$CE=C+Mn/6+(Cu+Ni)/15+(Cr+Mo+V)/5$$

The carbon equivalent represents the hardness of the heat affected zone ie a measure of the tensile strength of the steel and gives an indication of the degree of embrittlement. Most carbon steels used in general engineering have a relatively low carbon equivalent and are not crack sensitive especially when CE<0.45. For the

base metal used its composition results in a carbon equivalent of 0.338 which is below the critical value and therefore preheating is not required.

8.3.1.2 Weldability of Filler Wire.

Fully austenitic stainless steels are susceptible to solidification cracking which depends on the solidification mode as well as the content of sulphur, phosphorus, manganese and rare earth elements. If the metal solidifies in a ferritic mode (δ-ferrite), the solubility for elements such as phosphorus and sulphur is higher. Thus these elements or a large portion of them are trapped in the ferrite before it transforms to austenite.

Austenitic grain boundaries are susceptible to wetting by P and S films. It is therefore beneficial to ensure the presence of some interdendritic ferrite. Also the addition of elements such as Ta, Nb, Zr, Mo and Mn may combine preferentially with P and S to increase their solidification temperatures. The minimum amount of ferrite required to give a relatively trouble free deposit is 3 to 10% (Colombier & Hochmann 1977) (Smithels 1978) (Fenn 1987) (Lancaster 1987).

Some indication of the microstructure after solidification can be obtained with the aid of the Schaeffler diagram and equations.

$$Ni_{eq} = 12 \cdot Ni + 30 \cdot C + 0.5 \cdot Mn$$

$$Cr_{eq} = Cr + Mo + 1.5 \cdot Si + 0.5 \cdot Nb$$

Using the Schaeffler equations for the filler wire the composition will give rise to approximately 5-6%

ferrite which is in the range required for a trouble free weldment.

8.3.2 Metallurgical Examination of the Deposits.

8.3.2.1 Partial Dilution and Microalloying.

The first metallurgical examination investigated the uniformity of the deposits' composition. (Baeslack et al 1979) suggested that unmixed regions within the bead had occurred in the welding of 310/304L and 312/304L stainless steels. In addition, the transverse face of an overlayed specimen after continuous etching in aqueous 10% Nitric acid for over 150 hours in stagnant conditions showed that preferential attack had taken place revealing flow patterns (plate XV). Although the components would not have been used in such a corrosive environment, the possible existence of layers of non uniformly diluted alloy would expose metallurgically unacceptable compositions especially after machining the deposit.

8.3.2.2 Energy Dispersive Analysis with X ray Techniques (EDAX).

A series of EDAX examinations were carried out to investigate the question of uniform deposits as well as the dilution levels in two overlayers, one deposited with the single spiral overlaying technique and the other with the double spiral technique.

Plate XVI shows the stringer bead profile examined. The microhardness indents running along the axis of symmetry indicate where measurements took place.

The results of the analysis of the specimen are presented in table 8.8, and figure 8.4 shows graphically the presence of chromium, nickel, molybdenum and silicon within the deposit and the base metal. The EDAX measurements revealed that the stringer bead had a uniform composition up to the well defined interface. Very near the interface the readings suggest a gradual transition in the composition from that of the deposit to that of the base metal. However, it is believed that this is a reading error where the EDAX spot "picked up" some base material. The dilution measured by the EDAX agrees well with the dilution obtained by area measurements, and it was found to be approximately 24%.

table 8.8 Element Distribution in Bead Profile

No.	Dist. (mm)	Elements (%) Fe	Cr	Ni	Mo	Si
1	0.22	76.23	13.44	8.36	1.61	0.36
2	0.72	75.86	13.72	8.48	1.61	0.32
3	1.16	75.65	13.89	8.64	1.51	0.30
4	1.65	75.76	13.86	8.43	1.62	0.32
5	2.13	75.60	13.92	8.58	1.55	0.34
6	2.57	75.56	13.88	8.64	1.58	0.34
7	3.05	75.17	14.22	8.60	1.65	0.37
8	3.31	76.13	13.63	8.27	1.61	0.37
9	3.62	75.37	13.98	8.69	1.63	0.32
10	3.74	75.10	14.13	8.76	1.65	0.36
11	3.80	85.35	8.18	5.02	1.13	0.33
12	3.84	98.92	0.63	0.00	0.24	0.20
13	3.88	99.03	0.31	0.00	0.28	0.24

No.=Reference point Dist.=distance from top of bead

Figure 8.5 and figure 8.6 show the profiles of the two overlayed specimens and the microhardness indentations used for reference points for the EDAX examination. The levels of dilution measured in the single spiral overlayer (specimen No.8) are 32%, a value

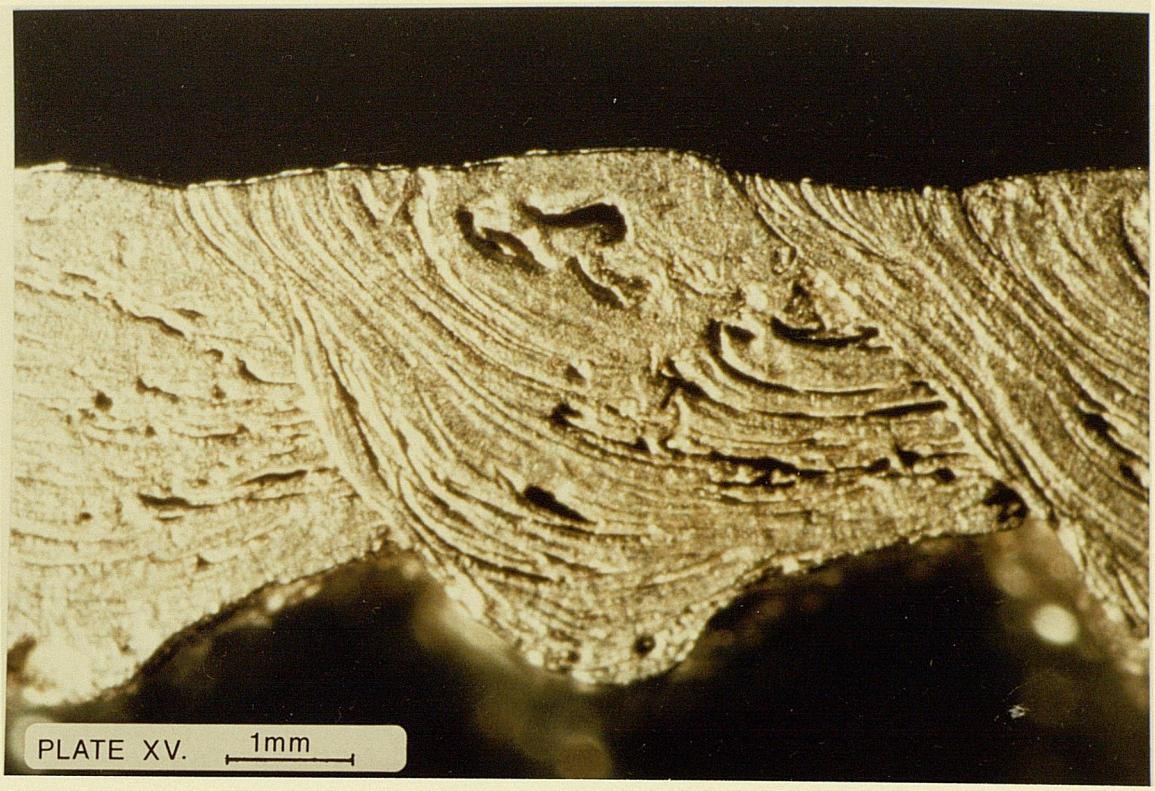
PLATE XV.
1mm

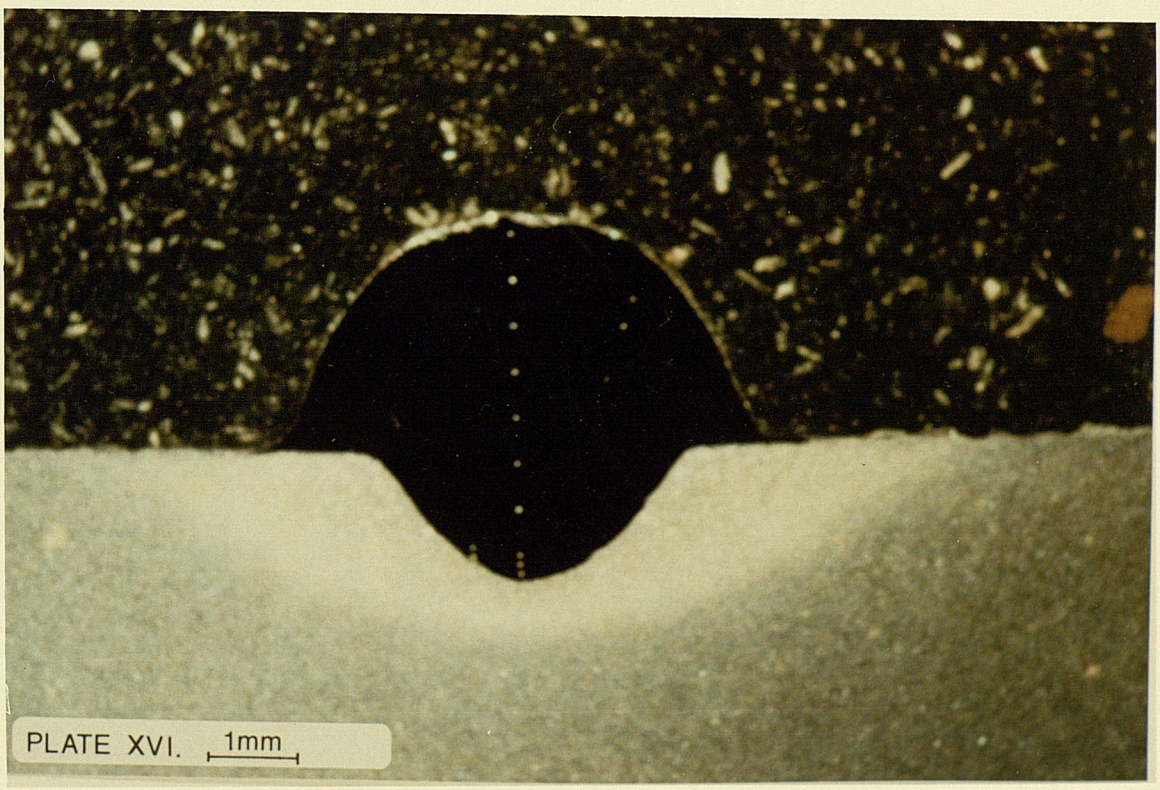
PLATE XVI.
1mm

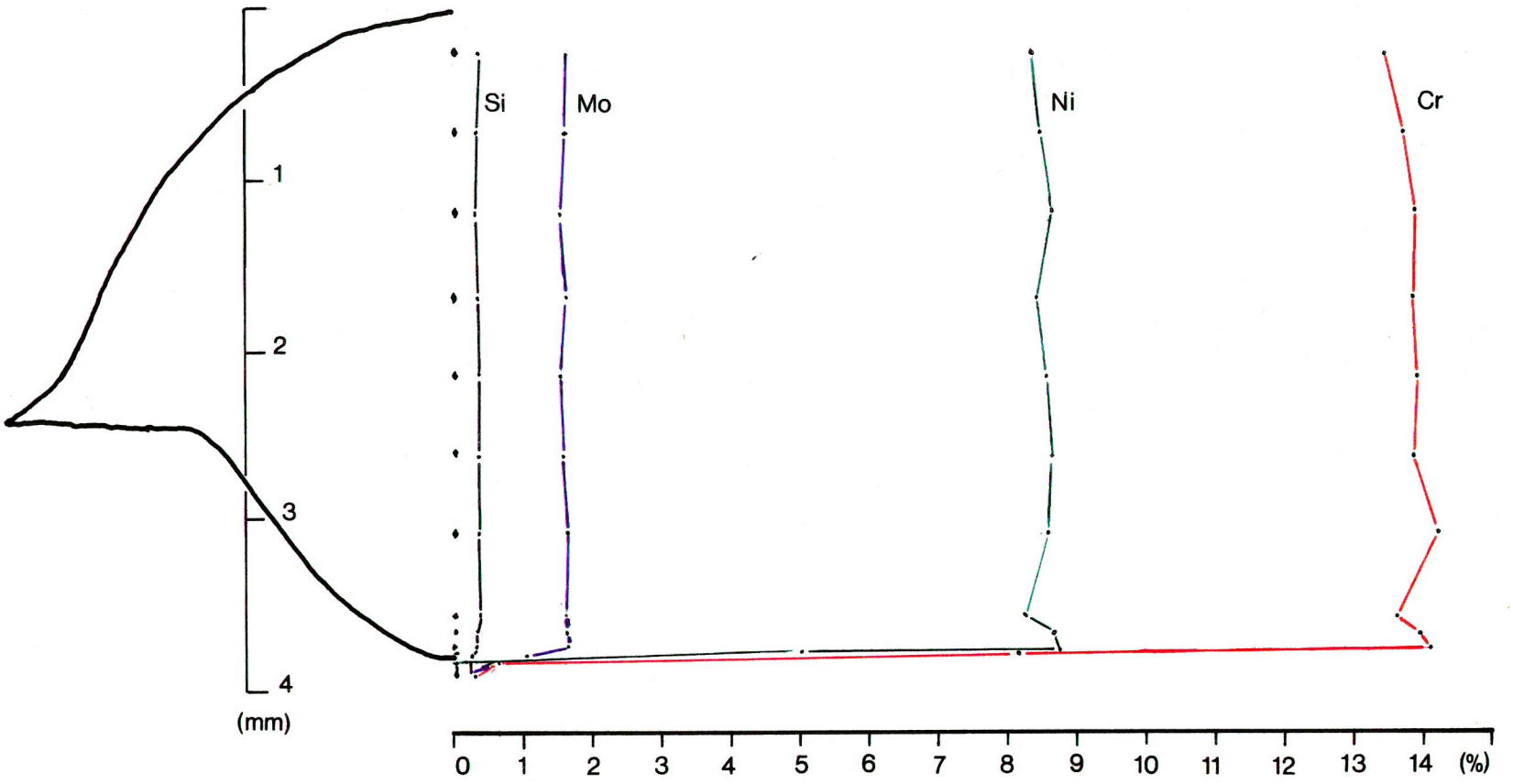

FIG.8.4 Element Distribution across a Bead Profile (24% Dilution)

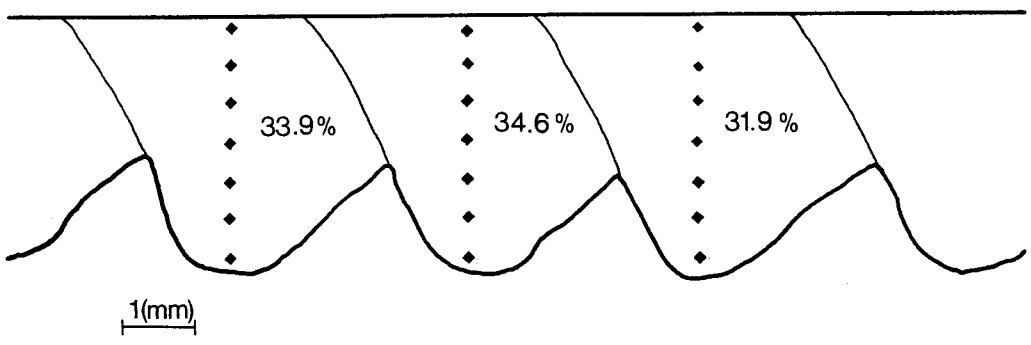

Overlay No.8

FIG. 8.5 Dilution in Overlayer: EDAX Technique.

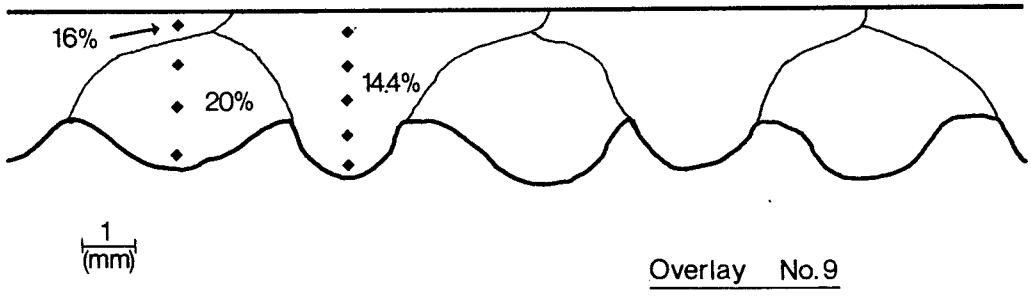

Overlay No.9

FIG. 8.6 Dilution in Overlayer: EDAX Technique.

which agrees with the dilution measured by the profile analysis. Table 8.9 shows the mean values of chromium, nickel, molybdenum and silicon present in each of the three beads examined. Mean values are presented because the composition in each turn of the spiral is uniform.

table 8.9 Composition Analysis (EDAX)
Single Spiral Overlayer.

No.	Elements (%)				
	Fe	Cr	Ni	Mo	Si
1	78.57	12.10	7.47	1.49	0.37
2	79.10	11.99	7.24	1.35	0.33
3	78.80	12.44	7.01	1.52	0.35

table 8.10 Composition Analysis (EDAX)
Double Spiral Overlayer.

No.	Elements (%)				
Primary Spiral.					
	Fe	Cr	Ni	Mo	Si
1	74.09	14.87	8.95	1.58	0.50
2	74.55	14.46	8.19	1.69	0.40
3	75.46	14.50	8.50	1.56	0.38
Dilution: 20%					
Covering Spiral (above Primary).					
	Fe	Cr	Ni	Mo	Si
4	73.48	15.28	9.26	1.63	0.34
Dilution: 15%					
Covering Spiral.					
	Fe	Cr	Ni	Mo	Si
5	72.47	15.45	9.37	1.69	1.01
6	72.71	15.70	9.52	1.71	0.36
7	73.52	15.28	9.16	1.71	0.34
8	71.01	16.76	9.93	1.80	0.50
9	74.27	14.70	9.11	1.59	0.33
Dilution: 14%					

No.=Reference point

Table 8.10 presents the results of the EDAX analysis of the double spiral overlayer (specimen No.9). The values of dilution measured with the EDAX technique for the primary and covering beads agree very well with the dilution values obtained from area measurements. The

dilution of the primary spiral is 20%, whereas the dilution of the covering spiral is 14%.

8.3.3 Discussion: Dilution and its Metallurgical Effects on the Deposit.

8.3.3.1 Dilution in the Deposit and the Schaeffler Diagram.

The Chromium and Nickel equivalents for dilution levels from 0% up to 100% for the filler wire and the base metal have been plotted on the Schaeffler diagram (figure 8.7). Table 8.11 presents the Chromium and Nickel equivalents as well as the percentage of carbon, chromium, nickel, molybdenum, manganese and silicon present in the deposit for a range of dilution levels from 0% to 40%. The resulting microstructure from the combination of the filler wire and the base metal for dilutions from 0% to 100%, and also taking into account all their possible compositional variations, is enclosed within the area given by ab, bc, cd, de, ea, on the same diagram.

table 8.11 Effects of Dilution on the Composition of the Deposit and the Schaeffler Diagram.

Dil.%	C	Cr	Ni	Mo	Mn	Si	Nb	Ni_{eq}	Cr_{eq}
0	0.03	18.2	11.2	2.0	1.65	0.43	0.0	12.93	20.84
5	0.037	17.3	10.6	1.9	1.61	0.41	0.0	12.56	19.81
10	0.044	16.4	10.1	1.8	1.57	0.38	0.0	12.20	18.77
15	0.051	15.5	9.5	1.7	1.52	0.36	0.0	11.83	17.73
20	0.058	14.6	9.0	1.6	1.48	0.34	0.0	11.46	16.70
25	0.065	13.7	8.4	1.5	1.43	0.32	0.0	11.09	15.66
30	0.072	12.8	7.9	1.4	1.38	0.30	0.0	10.73	14.63
35	0.079	11.9	7.3	1.3	1.34	0.28	0.0	10.36	13.60
40	0.086	11.0	6.8	1.2	1.29	0.26	0.0	10.00	12.55

According to the Schaeffler diagram and the dilution line, 0% dilution will result in approximately

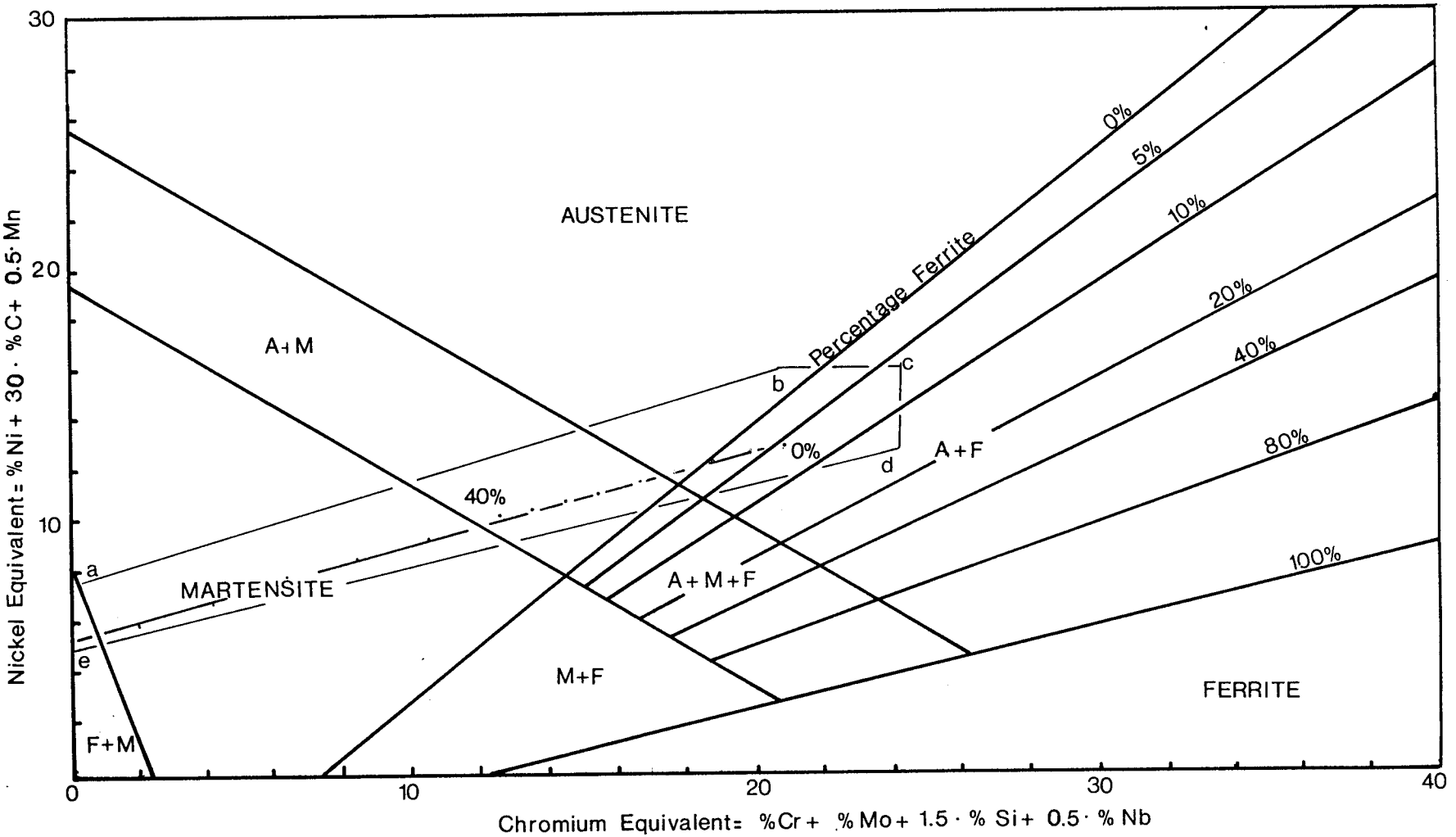

FIG.8.7 Shaeffler diagram

6% ferrite in the weldment whereas 7.5% dilution will result in 3% ferrite in the weldment. Higher dilution levels will result in an austenitic structure susceptible to hot cracking, whereas a further increase in dilution will result in a duplex austenitic/martensitic structure susceptible to hot cracking and/or solidification cracking.

The dilution of the overlayers ranged from 10.7% to 33.7%. Despite this, microscopical examination of the deposits revealed neither solidification nor hot cracking. Microstructual requirements demand very low dilution levels of the range of 0% to 7.5%. For the specific composition of the materials used, multilayered deposition is most likely to be the appropriate solution as single layered deposits have not achieved lower than 10% dilution.

Although the filler wire complies with the BS:2901 316S92 specification, it has a relatively low chromium content, lower than the manufacturer's specification. If the chromium content was higher, 19% for example, higher levels of dilution could be tolerated thus enabling a single layer deposition.

8.3.3.2 Dilution and Corrosion Properties.

In order for the deposit to maintain its corrosion resistance properties, chromium levels must be kept to 12% minimum which allows 35% dilution for the materials used. Equally, carbon levels are kept below 0.08% for dilutions of up to 35%.

8.4 Destructive Testing.

8.4.1 Introduction.

It would be futile if a component were to be replaced with another of shorter life span. It is necessary therefore, that if an overlayed component is to be useful, it must have equal or better fatigue resistance than the one it substitutes.

A series of "exploratory" fatigue crack propagation tests were carried out on three overlayed shafts. The advantage of this type of testing is that it enables direct observation of the crack initiation and behaviour during propagation. In addition, whereas S-N curves only provide the overall number of cycles for failure to occur under a particular stress, fatigue crack propagation tests can show quantitatively the manner in which the fatigue crack propagates.

Longitudinal sections from three overlayed shafts were cut and machined into specimens as shown in figure 8.8; the specimen dimensions being 150x24.5x2.7mm. A 2mm notch was machined on the top surface of each specimen in order to assist crack initiation. It was intended to produce specimens which would contain flaws either in the deposit or at the interface in order to investgate their influence on the fatigue life of the component. However, this was not possible as the overlayers did not contain any flaws. Two additional specimens were produced in order to provide some standards for comparison. One was made out of the base material and the other out of the same alloy as the filler wire, 316S11 stainless steel.

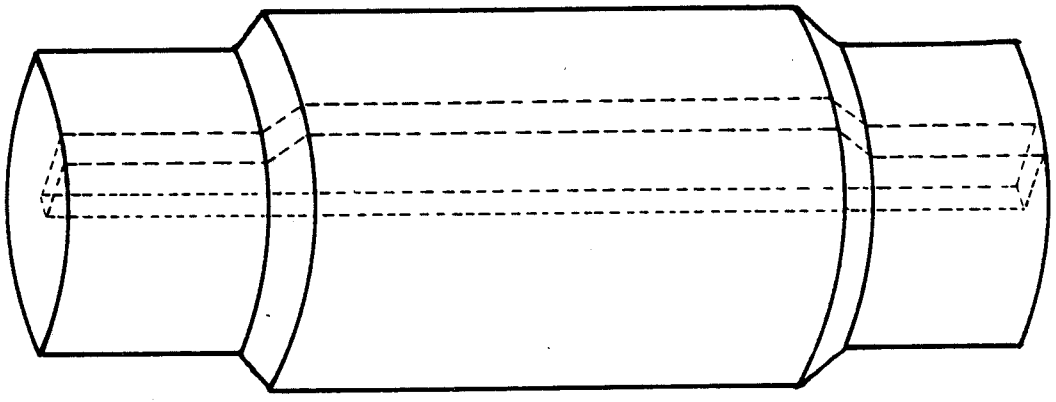

Specimens tested on a Pearson Cantilever Bend Fatigue Testing Apparatus.

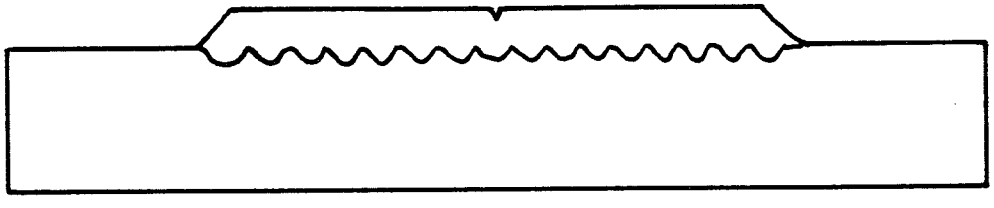

FIG. 8.8 Fatigue Crack Growth Specimens.

8.4.2 Experimental Arrangement.

Table 8.12 shows the loading of each specimen tested. Seven specimens were tested and for each specimen a table with crack propagation data is presented (tables 8.13 to 8.19). These tables contain, the number of cycles, the crack length, the difference between the maximum and minimum bending moments, the stress intensity factor range and the rate of crack propagation.

table 8.12 Fatigue Crack Propagation Experiments Specimen Loading

Specimen	No.	M max Nm	M min Nm	R	Thickness (mm)	Notch (mm)
316S11	S1	33139	12840	0.38	2.7	2
070M20	S2	33368	12189	0.37	2.7	2
Overlay	S3	37642	13790	0.36	2.7	2
Overlay	S4	33139	12840	0.34	2.7	2
Overlay	S5	33139	12840	0.34	2.7	2
Overlay	S6	33403	12963	0.34	2.7	2
Overlay	S7	33649	12330	0.33	2.7	1

8.4.3 Results.

Table 8.13 shows the fatigue crack propagation data for the stainless steel specimen (S1), and graph 8.1 shows the logarithmic plot of the rate of crack propagation against the stress intensity factor range. Similarly, table 8.14 shows the fracture data for the mild steel specimen and graph 8.2 the logarithmic plot of the rate of crack propagation against the stress intensity factor range. Graph 8.8 shows the plot of crack length against the number of cycles for the two materials.

Specimens S3, S4, and S5 were from the same

overlayed shaft (table 8.1 No.8) but for each specimen the notch was machined in a different position in relation to the interface. Plates XVII and XVIII show specimen S4 and plates XIX and XX show specimen S5 after having been tested. Their crack propagation data are presented in tables 8.15, 8.16 and 8.17 respectively whilst graphs 8.3, 8.4 and 8.5 show the logarithmic plot of the rate of crack propagation against the stress intensity factor range. Graph 8.9 shows the plot of crack length against the number of cycles. It is evident that the fatigue life varied depending on which part of the surface the crack was initiated.

Specimen S6 was produced from the overlayed shaft No.9 (table 8.3) and it is shown on plates XXI and XXII. Its crack propagation data are presented in table 8.18 and graph 8.6 shows the logarthmic plot of the rate of crack propagation against the stress intensity factor range. Graph 8.10 shows the plot of crack length against the number of cycles.

Specimen S7 was produced from the overlayed shaft No.10 (table 8.3) and it is shown on plates XXIII and XXIV. The notch was machined to 1mm rather than 2mm because of the thickness of the overlayer. Table 8.19 contains its fracture data, graph 8.7 shows the logarithmic plot of the rate of crack propagation against the stress intensity factor range and graph 8.10 shows the plot of crack length against the number of cycles.

Plate XXV and plate XXVI show the crack surfaces for all the specimens tested.

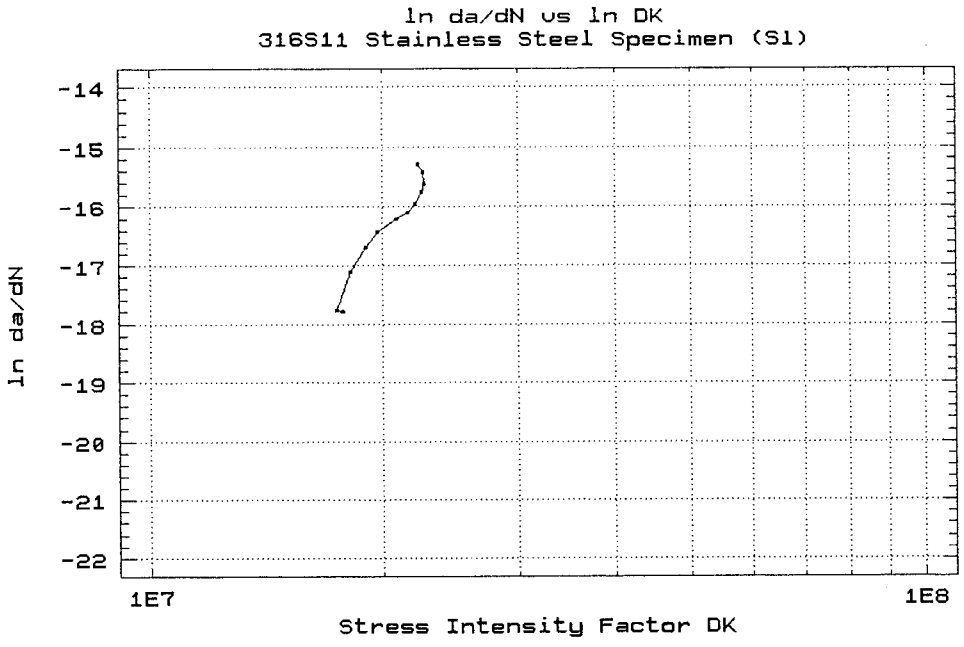

Graph 8.1

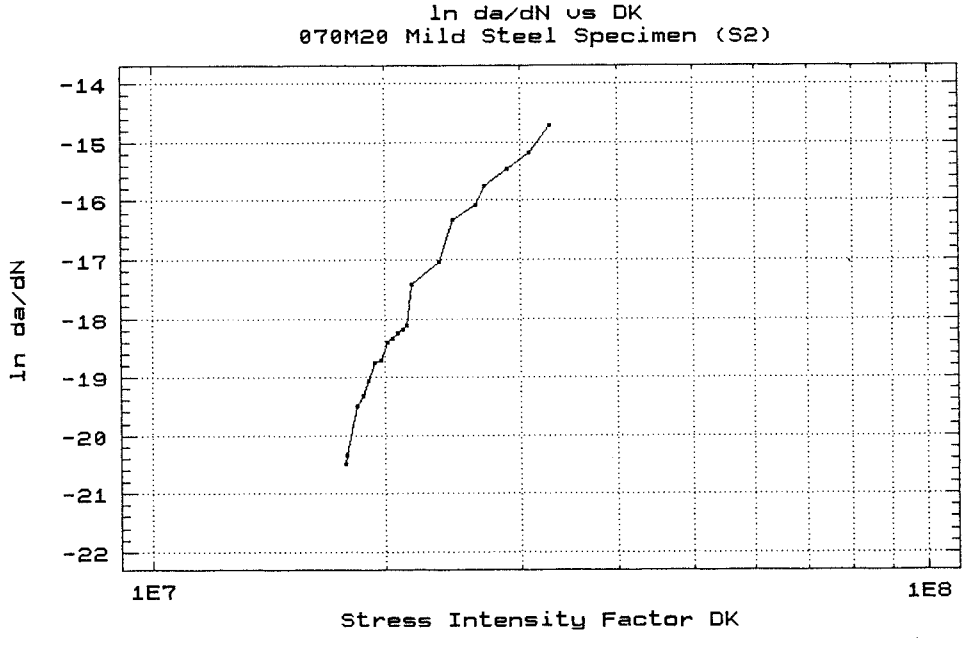

Graph 8.2

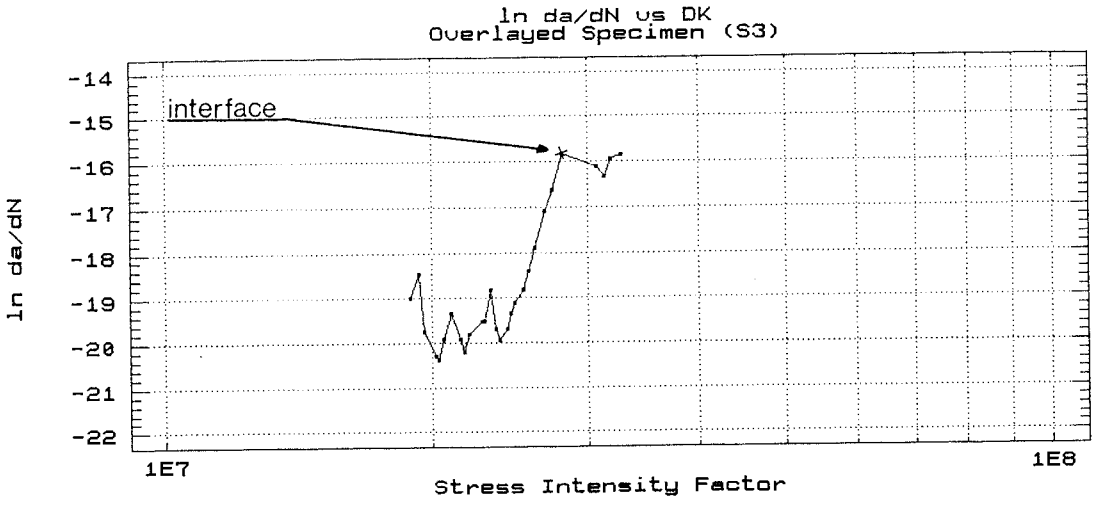

Graph 8.3

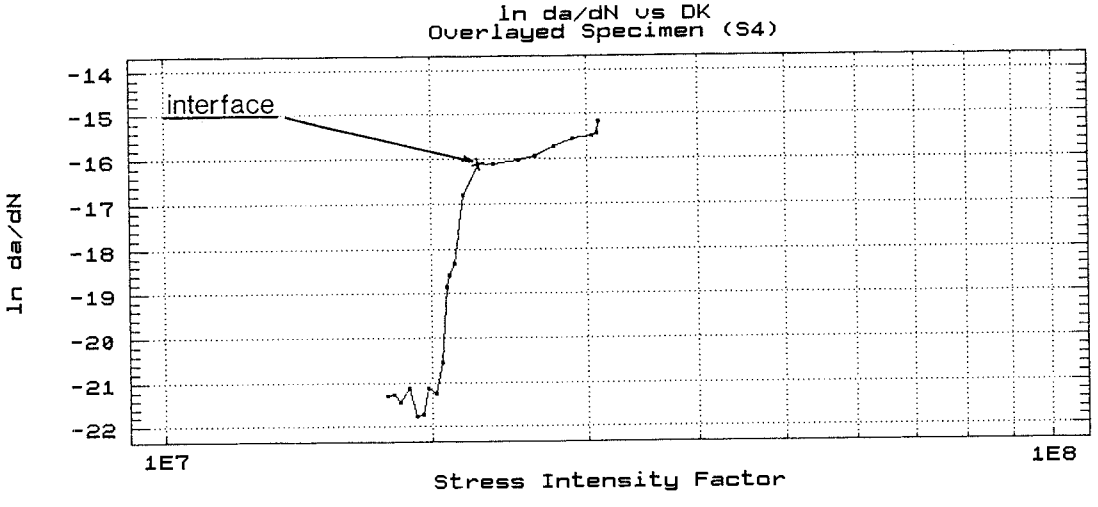

Graph 8.4

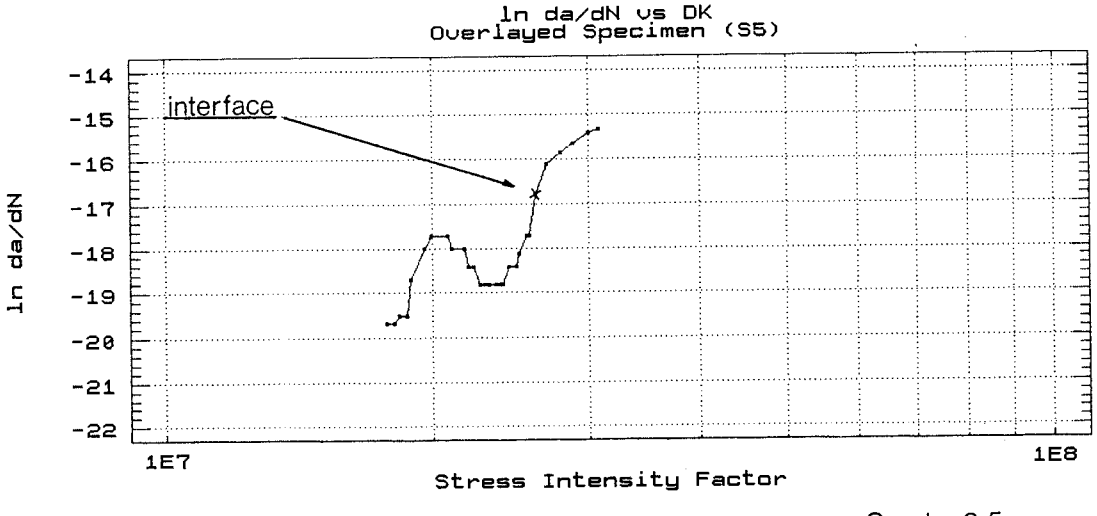

Graph 8.5

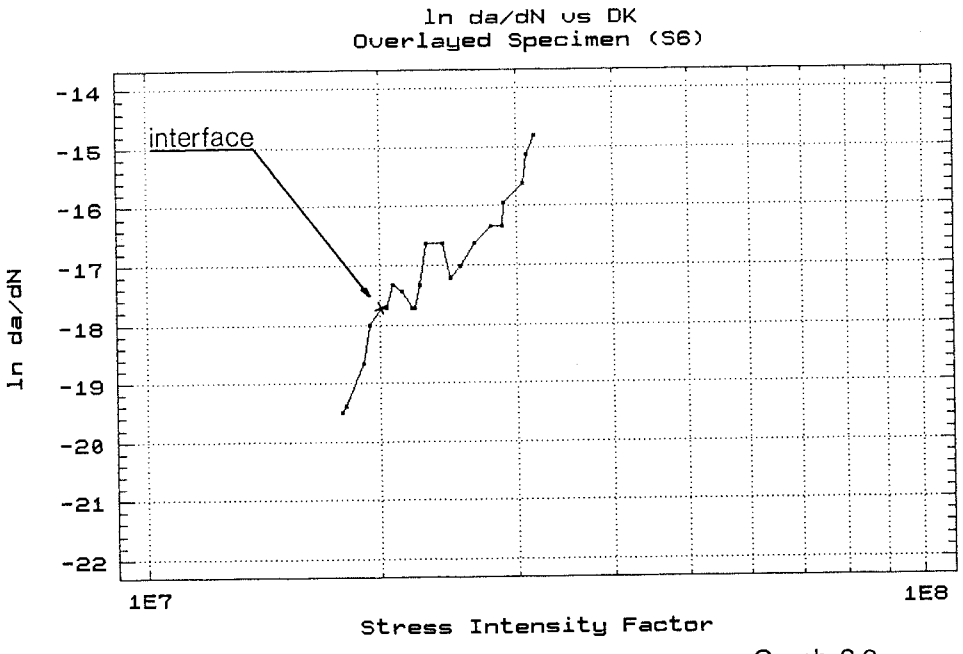

Graph 8.6

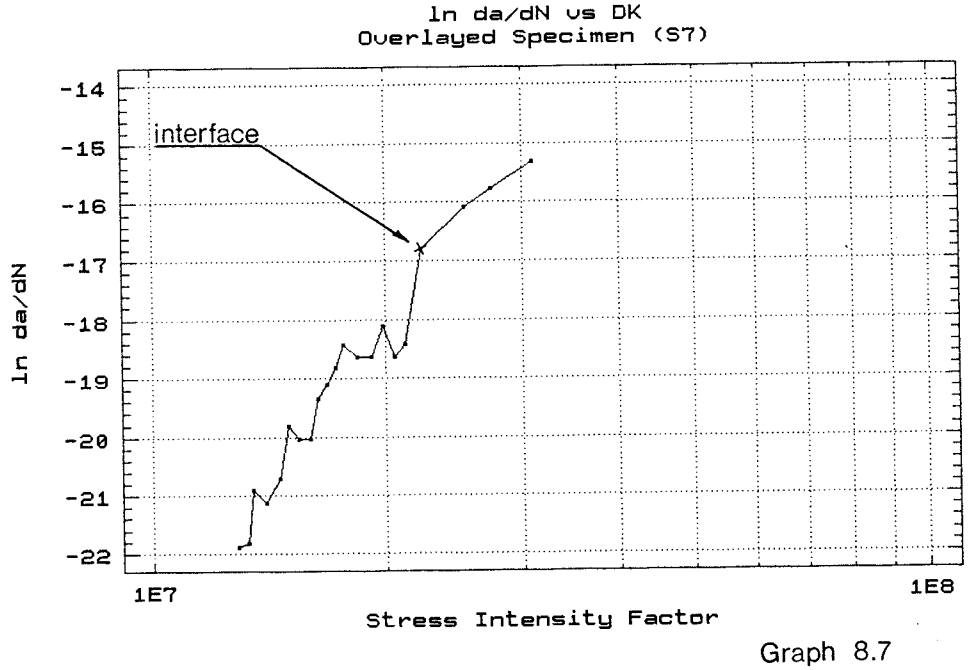

Graph 8.7

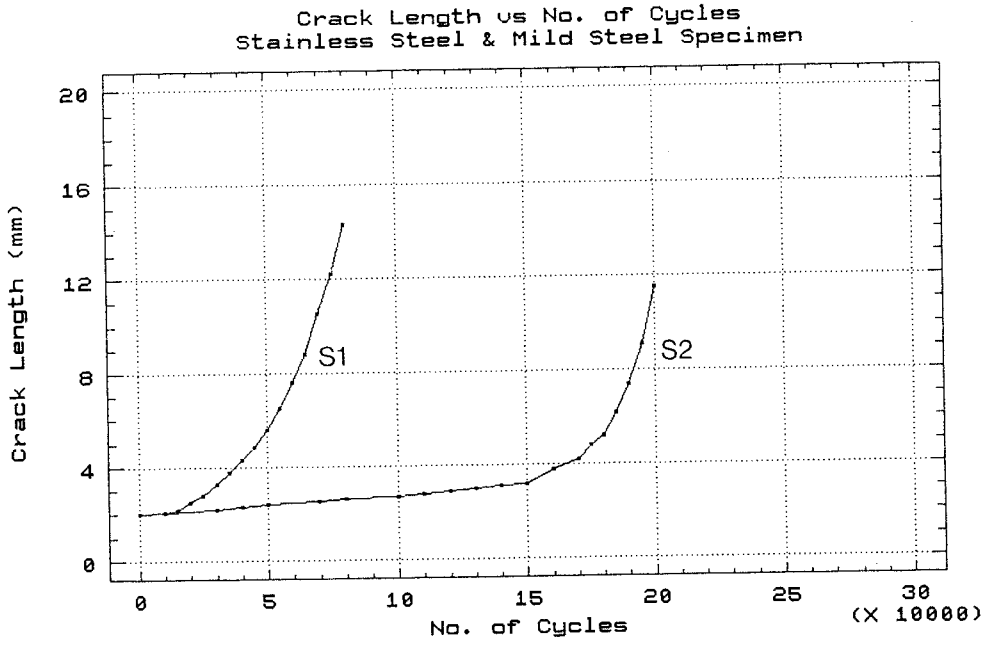

Graph 8.8

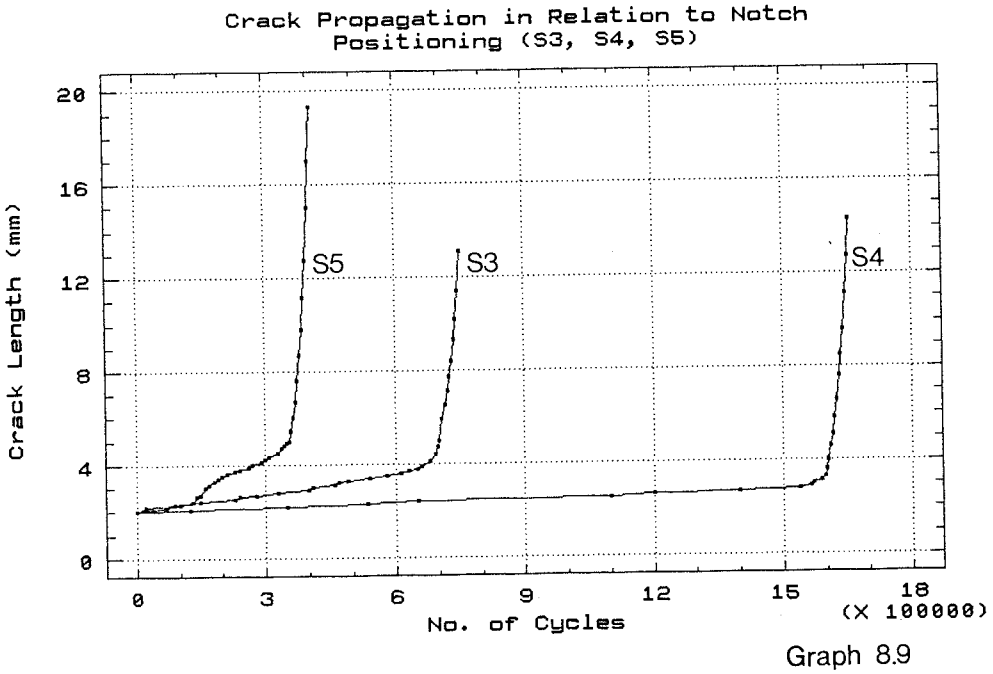

Graph 8.9

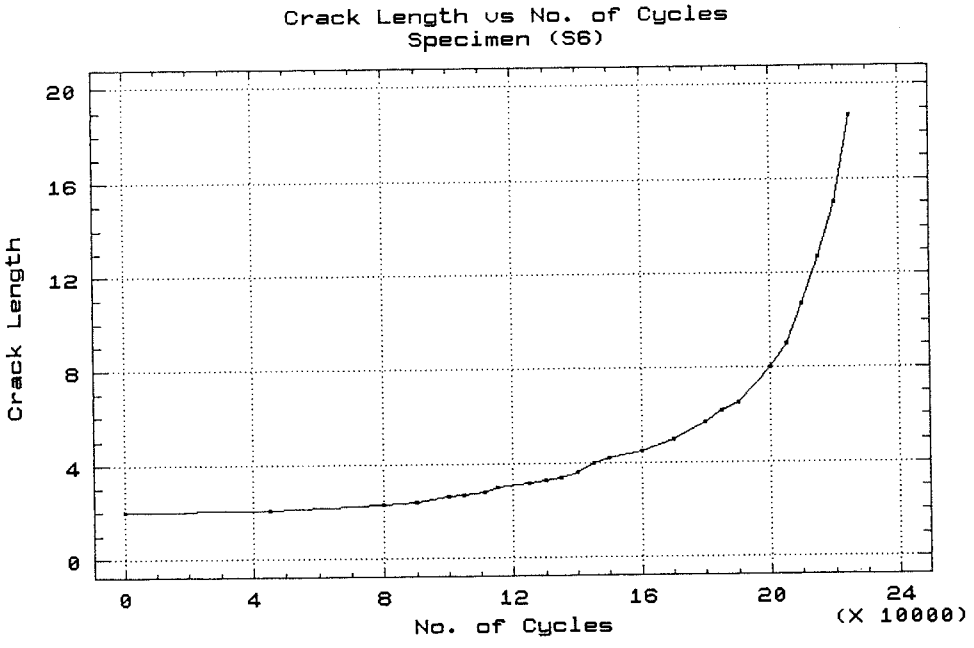

Graph 8.10

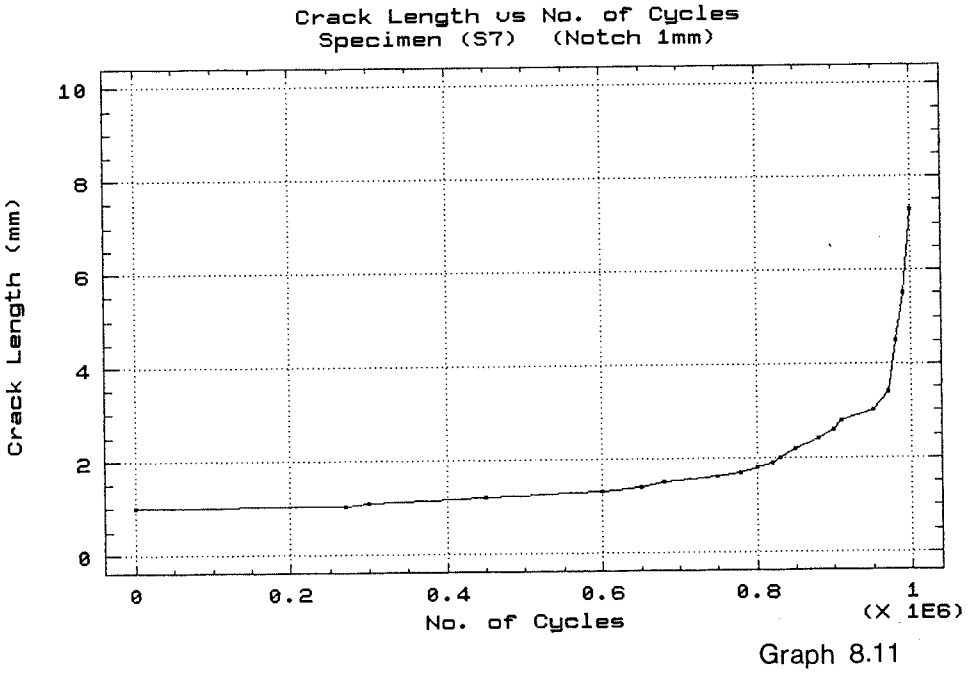

Graph 8.11

8.4.3.1 Analysis and Discussion of the Fatigue Crack Propagation Results.

The results from the fatigue crack propagation tests are very few to provide any firm quantitative analysis and conclusions. It is evident however, that as the overlayed specimens were tested in their "as cast" condition, residual stresses from solidification are present which will affect the fatigue crack growth rates.

The logarithimic plots of the rate of crack propagation against the stress intensity factor range of the non overlayed specimens are similar in shape to those suggested by the literature (Parker 1981) (Dieter 1988). In addition, based on Paris' law:

$$da/dN=C\cdot DK^{m}$$

and from graphs 8.1 and 8.2, m has been found to be approximately 3, which is a typical value for steels.

The existence of residual stresses within the weldment under cyclic loading will not affect the stress intensity factor range but will however, affect the R-value which quantifies the amount by which the mean stress value is removed from zero during cyclic loading.

$$R=\sigma_{min}/\sigma_{max} \text{ or } R=K_{min}/K_{max}$$

The effect of the R-value on the rate of fatigue crack propagation can be inluded in the Paris' law equation to give:

$$da/dN=C\cdot DK^{m}/(1-R)\cdot K_{C}-DK$$

From the form of the equation it can be seen that if, for example the fatigue crack encountered a region of residual tensile stresses, its rate of propagation would increase and the gradient of the logarithmic plot of

da/dN versus DK would also increase. If the crack ran into a region of compressive stresses, the opposite would occur.

In an overlayer residual stresses are expected to occur after solidification due to contraction. These tend to be tensile at the surface and compressive at the substrate (Landerman & Grotke 1978).

Since no specific experiments to determine the residual stresses within the deposit have been carried out, the only possible assessment of their presence in the weldment can be based on the existing fatigue crack propagation results and the various experimental observations.

The logarithmic plots of fatigue crack propagation against stress intensity factor range for the double spiral overlayers (graphs 8.6 and 8.7) seem to agree with the theory as the initial steepness of the gradient indicates residual tensile stresses.

Graph 8.4 suggests compressive residual stresses in the surface of the weldment and tension in the deposit near the interface. As can be seen from Plate XVIII the notch has been machined above the interfacial intersection of two beads. Graph 8.6 indicates that tensile residual stresses exist near the surface and compressive near the interface. Plate XX shows the specimen where the notch has been machined in the middle of the bead.

The crack propagation behaviour as encountered in the single spiral overlayer may be attributed to a combination of factors interacting with one another. It

appears that the geometry of the interface and in particular the deep penetration combined with the lower coefficient of expansion of the base metal causes local stress raisers which alters the residual stress distribution. These effects may also be enhanced by localised melting and heat treatment caused the arc after subsequent revolutions.

The erratic behaviour of crack propagation in the initial stages, (graph 8.3) may be attributed to experimental errors in the measurement of the crack length.

Multiple crack initiation observed in specimens S3, S4 and S7 may have contributed to the slow crack propagation rates encountered in the initial stages of the experiments.

8.4.4 Experimental Reliability.

The "exploratory" nature of the series of fatigue crack propagation experiments underlined the problem of having too many variables for a small number of specimens. However, they have clearly indicated the existence of complex residual stress fields within the weldment as a result of the continuous partial remelting and heat treatment of the spiral.

Direct comparison with the stainless steel specimen however may only be indicative because dilution has altered the composition of the overlayer.

8.4.5 In Service Performance.

The series of fatigue crack growth experiments have shown that the fatigue resistance of the overlayed specimens had improved in all cases with respect to the stainless steel specimen. The improvement exhibited enormous scatter; for example in order to develop a crack of 3mm (1mm+notch), whereas the stainless steel specimen needed to complete 26000 cycles, for the overlayed specimens the number of cycles varied from 120000 minimum to 1550000 maximum, ie. 4.6 to 59 times longer.

A common cause of failure in overlayed components is the existence of defects in the interface between the base metal and the overlayer. The presence of tensile residual stresses in this area will thus only aid crack initiation and propagation.

Therefore, in order to minimise the tensile residual stresses and their effect on the fatigue crack initiation and propagation stress relief heat treatment should be carried out. Although heat treatment would decrease the beneficial effects of compressive residual stresses on the crack initiation in the surface, this would be outweighted by the elimination of the tensile stresses as well as having a deposit with mechanical properties of a higher degree of uniformity.

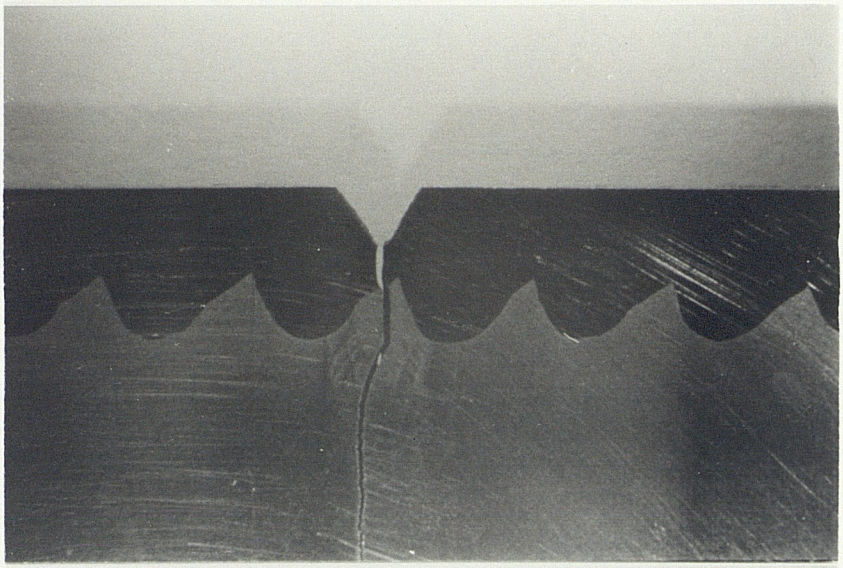

PLATE XVII. 2mm

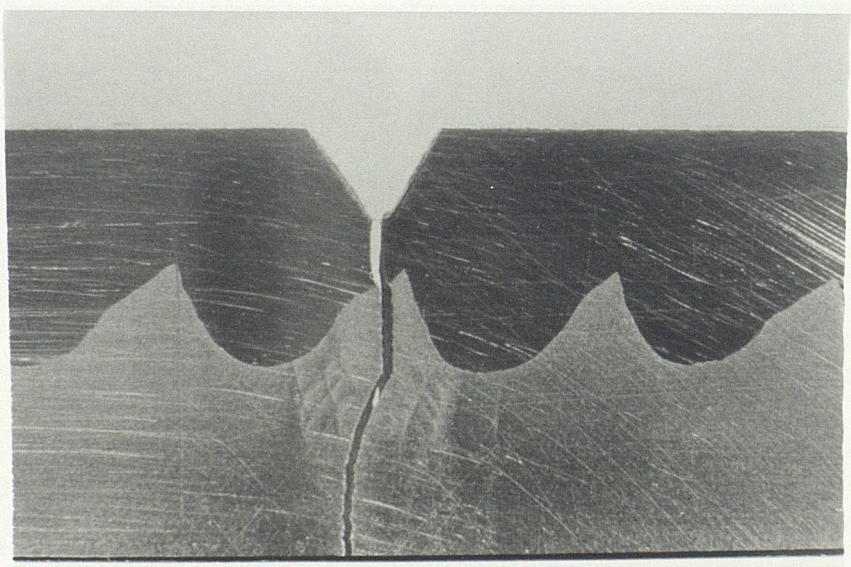

PLATE XVIII. 2mm

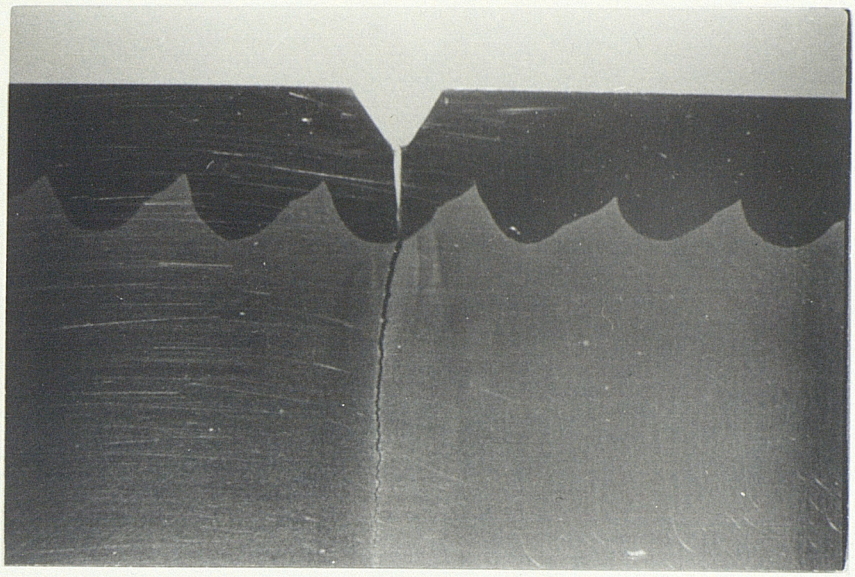

PLATE XIX. 2mm

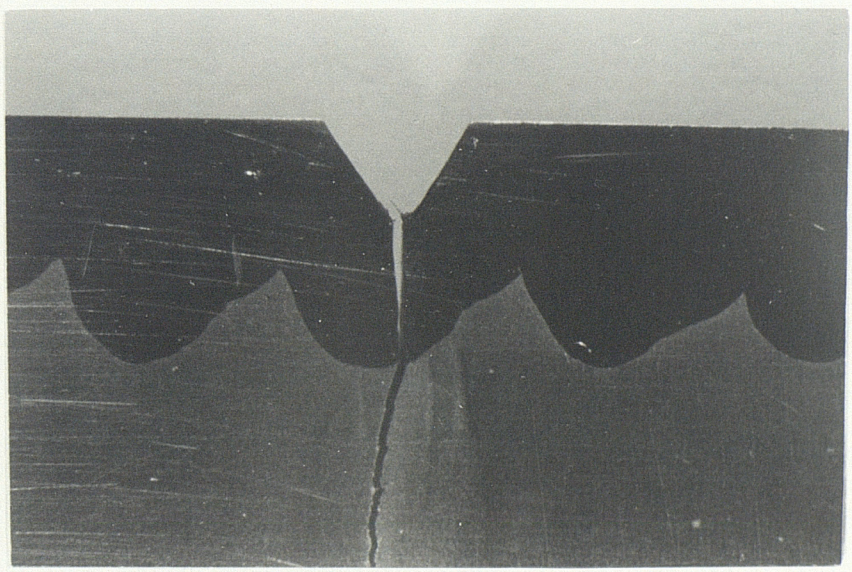

PLATE XX. 2mm

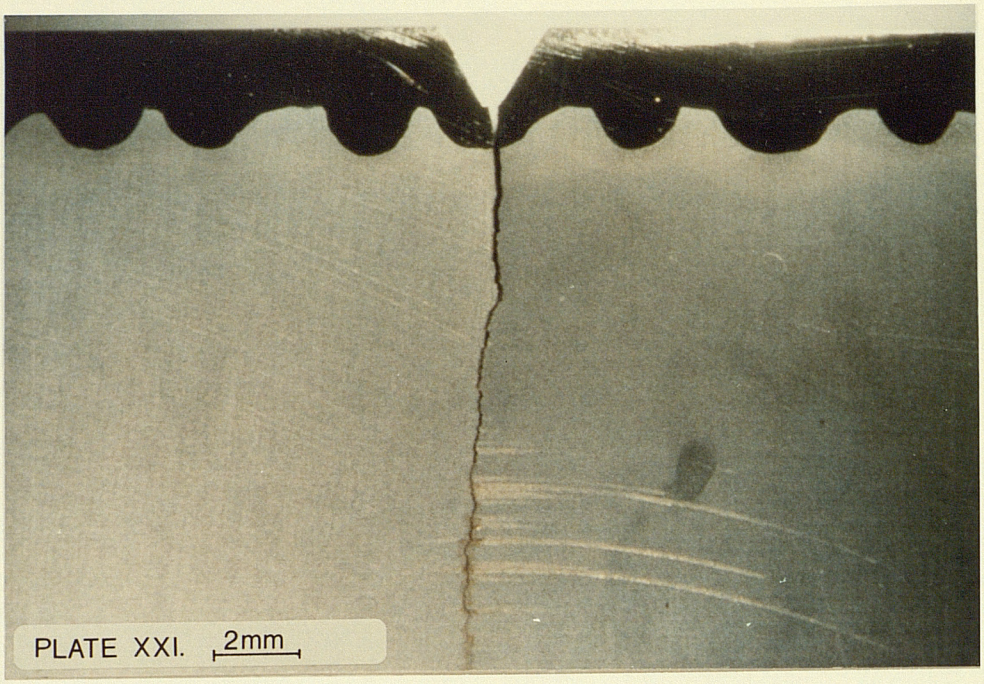

PLATE XXI. 2mm

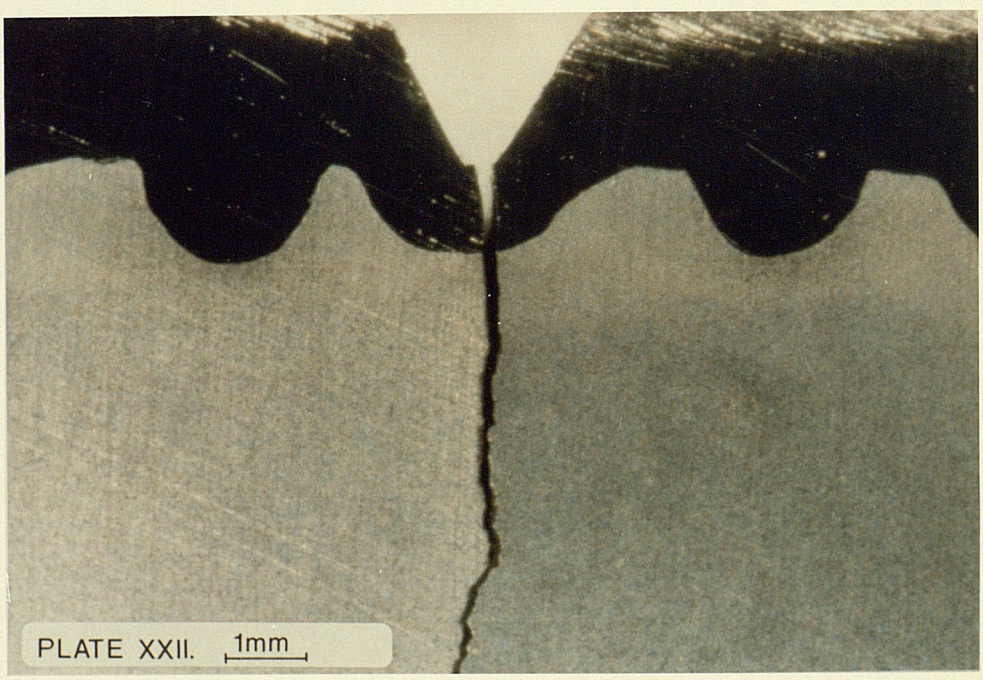

PLATE XXII. 1mm

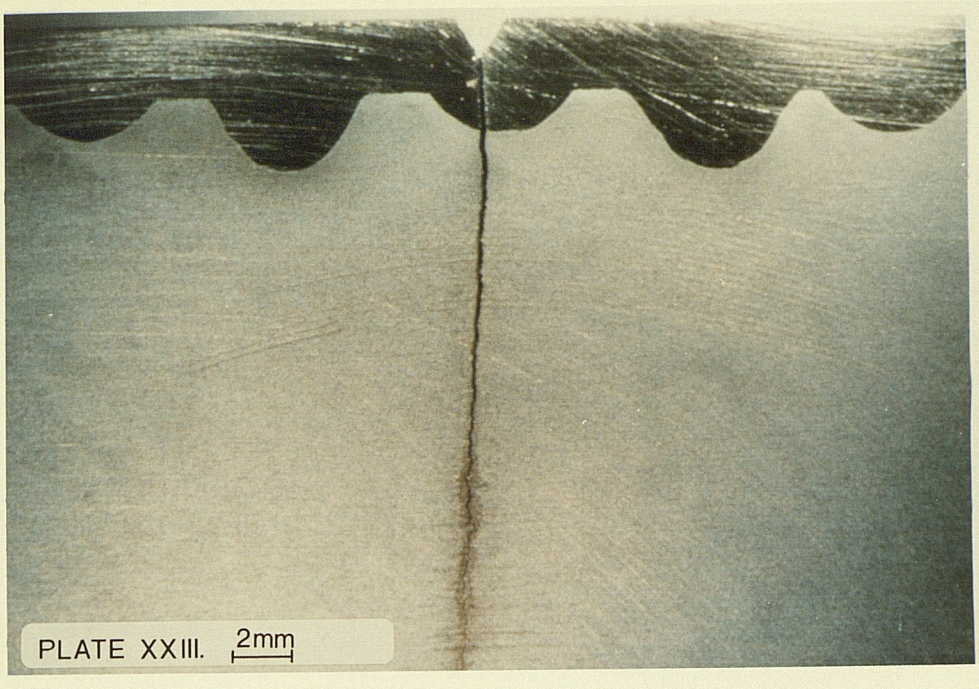

PLATE XXIII. 2mm

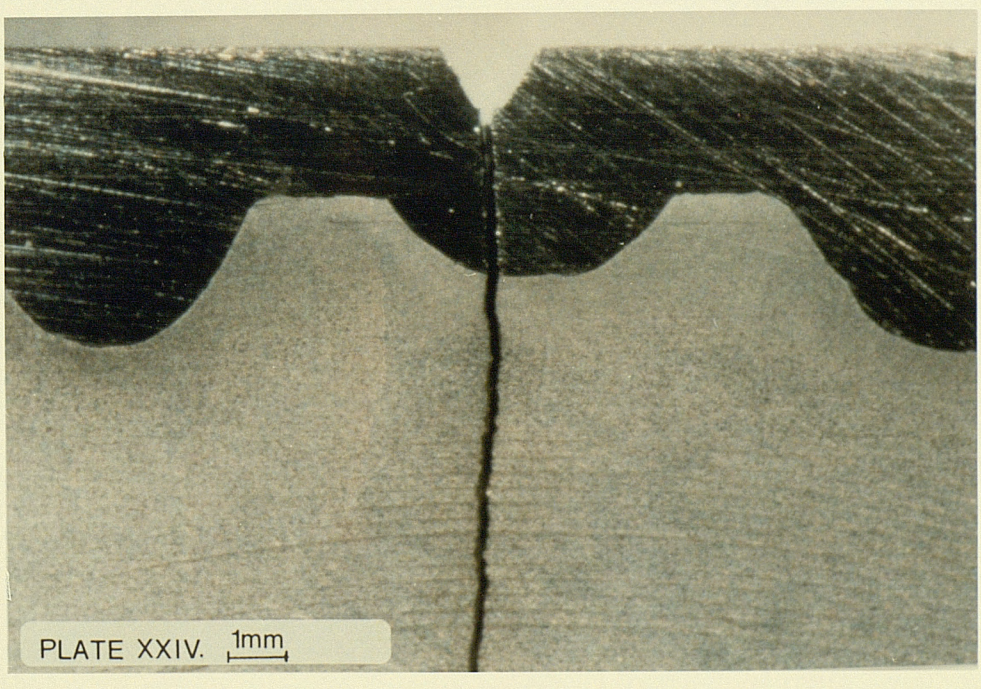

PLATE XXIV. 1mm

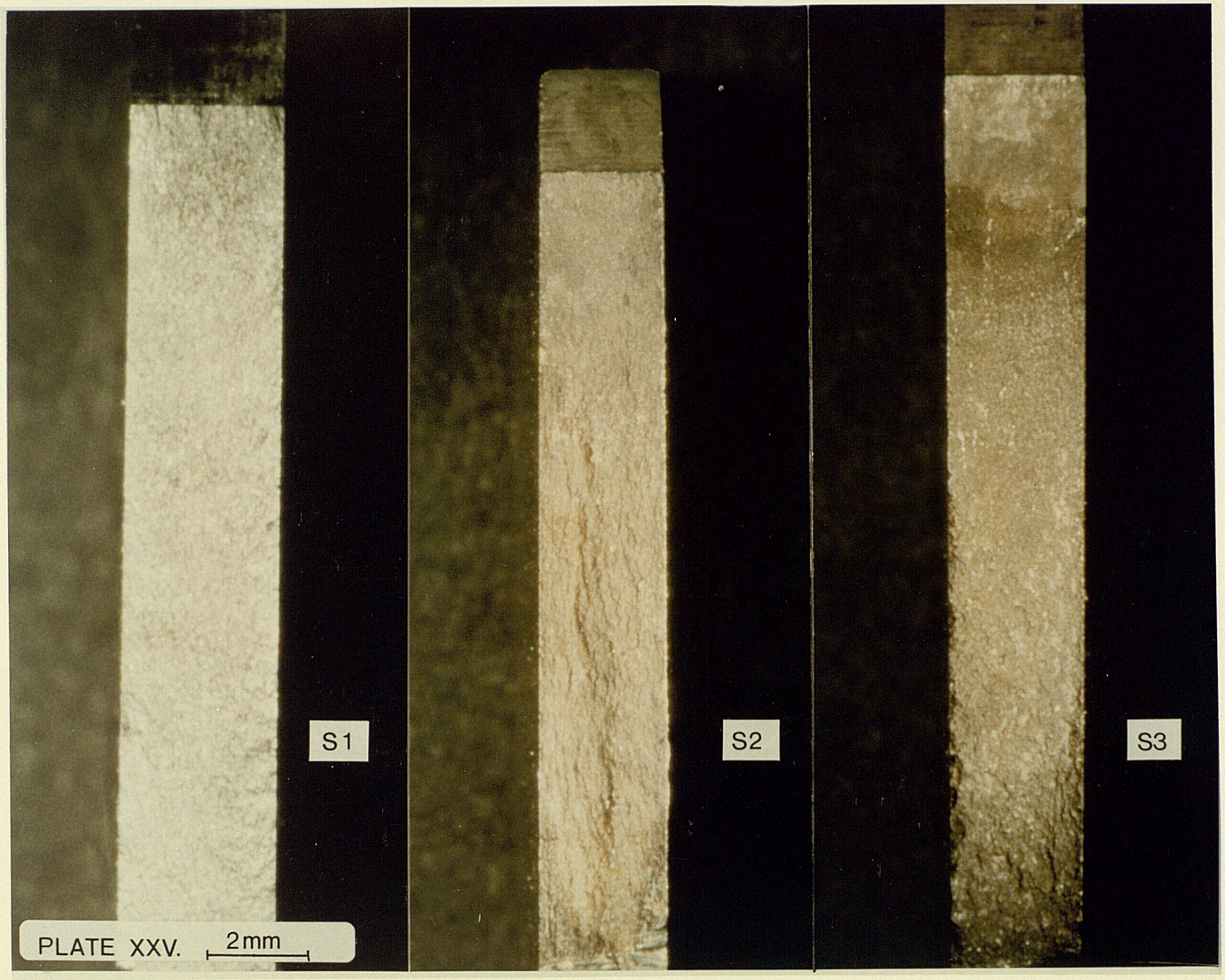

PLATE XXV.

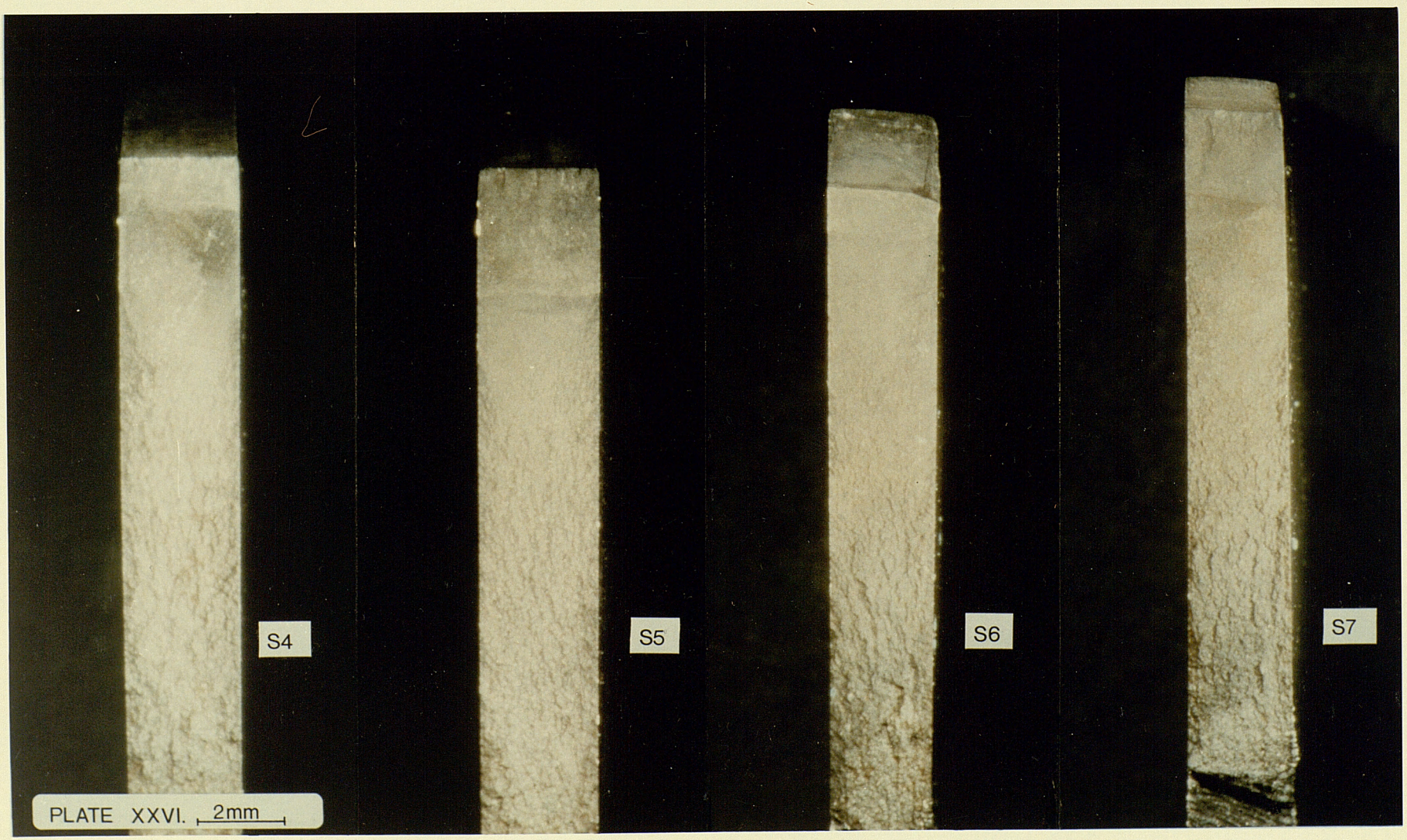
S4
S5
S6
S7
PLATE XXVI. 2mm

table 8.13 Fatigue Crack Growth Data
316S92 Stainless Steel Specimen (S1)

No.	N	a	DM Nm	DK $MNm^{-3/2}$	lnDK	da/dN nm	lnda/dN
1	0	2.0	23043	17.8	16.69	0	-17.78
2	10000	2.1	22709	17.5	16.70	19	-17.77
3	15000	2.2	22524	18.2	16.71	37.0	-17.11
4	20000	2.5	22227	19.1	16.76	55.5	-16.70
5	25000	2.8	21819	19.7	16.79	73.5	-16.42
6	30000	3.3	21336	20.9	16.85	91.7	-16.20
7	35000	3.8	20520	21.6	16.89	103	-16.09
8	40000	4.3	19704	22.1	16.91	119	-15.94
9	45000	4.9	18627	22.5	16.92	145	-15.74
10	50000	5.6	17366	22.7	16.93	165	-15.61
11	55000	6.5	15733	22.6	16.94	200	-15.42
12	60000	7.6	13915	22.3	16.94	231	-15.28
13	65000	8.8	11651				
14	70000	10.5	8683				
15	75000	12.2	5937				
16	80000	14.3	3408				

table 8.14 Fatigue Crack Growth Data
070M20 Mild Steel Specimen (S2)

No.	N	a	DM Nm	DK $MNm^{-3/2}$	lnDK	da/dN nm	lnda/dN
1	0	2.0	23155	17.8	16.69	0.00	-20.50
2	10000	2.1	23043	17.9	16.70	1.46	-20.34
3	30000	2.2	22783	18.4	16.73	3.37	-19.50
4	40000	2.3	22783	18.8	16.75	4.04	-19.32
5	50000	2.4	22746	19.1	16.76	5.22	-19.07
6	70000	2.5	22709	19.4	16.78	7.06	-18.76
7	80000	2.6	22672	19.8	16.80	7.50	-18.71
8	100000	2.7	22746	20.2	16.82	10.2	-18.40
9	110000	2.8	22709	20.5	16.84	10.8	-18.34
10	120000	2.9	22665	20.8	16.85	11.7	-18.26
11	130000	3.0	22598	21.1	16.87	12.6	-18.18
12	140000	3.1	22561	21.4	16.88	13.3	-18.13
13	150000	3.2	22524	21.7	16.89	27.1	-17.42
14	160000	3.8	22375	23.6	16.97	39.2	-17.05
15	170000	4.2	22153	24.6	17.02	81.0	-16.33
16	175000	4.8	22041	26.3	17.08	105.0	-16.07
17	180000	5.2	21633	27.0	17.11	145.0	-15.75
18	185000	6.2	20780	28.9	17.18	192.0	-15.46
19	190000	7.4	19629	30.9	17.24	254.0	-15.18
20	195000	9.1	17588	32.8	17.30	408.0	-14.71
21	200000	11.5	13358				

table 8.15 Fatigue Crack Growth Data
Overlayed Specimen (S3)

No.	N	a	DM Nm	DK $MNm^{-3/2}$	lnDK	da/dN nm	lnda/dN
1	0	2.0	24490	18.9	16.75	0.00	-19.00
2	15000	2.1	24416	19.3	16.77	9.53	-18.46
3	21000	2.2	24268	19.6	16.79	2.67	-19.74
4	90000	2.3	24491	20.2	16.82	1.55	-20.28
5	150000	2.4	24194	20.3	16.83	1.43	-20.37
6	230000	2.5	24119	20.6	16.84	2.22	-19.92
7	240000	2.6	24119	21.0	16.86	4.00	-19.34
8	280000	2.7	24194	21.5	16.88	2.20	-19.92
9	330000	2.8	23971	21.7	16.89	1.67	-20.21
10	400000	2.9	23897	22.0	16.90	2.50	-19.81
11	410000	3.0	24342	22.7	16.94	3.34	-19.52
12	460000	3.1	24082	22.9	16.95	3.34	-19.52
13	470000	3.2	24156	23.3	16.96	6.67	-18.83
14	490000	3.3	24082	23.6	16.97	2.86	-19.67
15	540000	3.4	23934	23.8	16.98	2.22	-19.93
16	580000	3.5	24119	24.3	17.00	2.86	-19.67
17	610000	3.6	23971	24.5	17.01	4.00	-19.34
18	630000	3.7	23897	24.8	17.02	5.00	-19.11
19	650000	3.8	24156	25.4	17.05	6.65	-18.83
20	660000	3.9	24082	25.7	17.06	10.5	-18.42
21	680000	4.1	23822	26.1	17.07	16.6	-17.91
22	690000	4.4	23563	26.8	17.10	37.5	-17.10
23	696000	4.7	23266	27.4	17.12	60.0	-16.63
24	700000	5.0	23006	28.1	17.15	133	-15.83
25	705000	5.9	22783	30.7	17.24	99.9	-16.12
26	715000	6.5	21983	31.4	17.26	79	-16.34
27	720000	7.1	20891	31.9	17.27	120	-15.94
28	725000	7.7	20186	32.7	17.30	130	-15.86
29	730000	8.4	18590				
30	735000	9.3	17588				
31	740000	10.2	15548				
32	745000	11.4	12839				
33	750000	13.1	9462				

table 8.16 Fatigue Crack Growth Data
Overlayed Specimen (S4)

No.	N	a	DM Nm	DK $MNm^{-3/2}$	lnDK	da/dN nm	lnda/dN
1	0	2.0	23043	17.8	16.69	0.00	-21.30
2	125000	2.1	22932	18.1	16.71	0.57	-21.28
3	350000	2.2	22858	18.4	16.73	0.49	-21.44
4	535000	2.3	22821	18.8	16.75	0.67	-21.13
5	650000	2.4	22821	19.2	16.77	0.35	-21.76
6	1100000	2.5	22783	19.5	16.78	0.36	-21.73
7	1200000	2.6	22746	19.8	16.80	0.67	-21.13
8	1400000	2.7	22746	20.2	16.82	0.59	-21.25
9	1540000	2.8	22709	20.5	16.83	1.2	-20.54
10	1566000	2.9	22635	20.8	16.85	6.4	-18.86
11	1571000	3.0	22412	20.9	16.86	8.3	-18.60
12	1590000	3.1	22301	21.2	16.87	11.0	-18.32
13	1598000	3.3	22153	21.7	16.89	50.0	-16.81
14	1600000	3.6	22078	22.6	16.93	100.0	-16.12
15	1605000	4.0	21782	23.5	16.97	100.0	-16.12
16	1610000	4.6	21559	25.1	17.04	110.0	-16.02
17	1615000	5.1	21225	26.2	17.08	120.0	-15.93
18	1620000	5.8	20668	27.6	17.13	150.0	-15.71
19	1625000	6.6	19963	29.0	17.18	180.0	-15.53
20	1630000	7.6	18961	30.4	17.23	190.0	-15.48
21	1635000	8.5	17663	30.9	17.24	200.0	-15.43
22	1640000	9.6	15733	31.0	17.25	260.0	-15.16
23	1645000	11.1	12987				
24	1650000	12.7	9944				
25	1655000	14.3	6939				

table 8.17 Fatigue Crack Growth Data
Overlayed Specimen (S5)

No.	N	a	DM Nm	DK $MNm^{-3/2}$	lnDK	da/dN nm	lnda/dN
1	0	2.0	23006	17.7	16.69	0.0	-19.69
2	40000	2.1	22858	18.1	16.71	2.9	-19.67
3	70000	2.2	22709	18.3	16.72	3.3	-19.52
4	100000	2.3	22709	18.7	16.74	3.3	-19.52
5	130000	2.4	22487	18.9	16.75	7.5	-18.71
6	140000	2.6	22450	19.6	16.76	15	-18.02
7	150000	2.7	22375	19.9	16.80	20	-17.73
8	160000	3.0	22301	20.8	16.85	20	-17.73
9	170000	3.1	22153	21.0	16.86	15	-18.02
10	180000	3.3	22116	21.7	16.89	15	-18.02
11	190000	3.4	22078	21.9	16.90	10	-18.42
12	200000	3.5	22041	22.2	16.91	10	-18.42
13	210000	3.6	22078	22.6	16.93	6.7	-18.82
14	230000	3.7	22041	22.9	16.94	6.7	-18.82
15	240000	3.8	21976	23.1	16.95	6.7	-18.82
16	260000	3.9	22153	23.6	16.97	6.7	-18.82
17	270000	4.0	22041	23.8	16.98	6.7	-18.82
18	290000	4.1	21893	24.0	16.99	6.7	-18.82
19	300000	4.2	22004	24.4	17.01	10	-18.42
20	310000	4.3	22190	24.9	17.03	10	-18.42
21	330000	4.5	21633	25.0	17.04	13	-18.13
22	340000	4.7	21596	25.5	17.05	20	-17.73
23	345000	4.8	21522	25.5	17.06	20	-17.73
24	350000	4.9	21448	25.7	17.07	20	-17.73
25	355000	5.0	21373	26.1	17.08	50	-16.81
26	360000	5.4	21077	26.9	17.10	100	-16.12
27	365000	6.0	20483	27.9	17.14	130	-15.86
28	370000	6.7	19704	28.9	17.18	160	-15.65
29	375000	7.6	18702	30.0	17.21	200	-15.43
30	380000	8.7	17217	30.8	17.24	220	-15.33
31	385000	9.8	15028				
32	390000	11.2	12097				
33	395000	12.8	8720				
34	400000	15.0	5157				
35	405000	17.0	2115				
36	410000	19.3	371				

table 8.18 Fatigue Crack Growth Data
Overlayed Specimen (S6)

No.	N	a	DM Nm	DK $MNm^{-3/2}$	lnDK	da/dN nm	lnda/dN
1	0	2.0	23192	17.9	16.70	0.0	-19.50
2	45000	2.1	23192	18.1	16.71	3.7	-19.40
3	80000	2.3	23155	19.1	16.76	7.7	-18.67
4	90000	2.4	23080	19.4	16.78	15	-18.02
5	100000	2.6	23006	20.1	16.81	20	-17.73
6	105000	2.7	23006	20.4	16.83	20	-17.73
7	111000	2.8	22969	20.8	16.85	30	-17.32
8	115000	3.0	22895	21.4	16.88	27	-17.44
9	125000	3.2	22821	22.0	16.91	20	-17.73
10	130000	3.3	22709	22.2	16.92	20	-17.73
11	135000	3.4	22635	22.5	16.93	30	-17.32
12	140000	3.6	22524	23.0	16.95	60	-16.63
13	145000	4.0	22338	24.1	17.00	60	-16.63
14	150000	4.2	22264	24.7	17.02	33	-17.22
15	160000	4.5	22041	25.4	17.05	40	-17.03
16	170000	5.0	21707	26.5	17.09	60	-16.63
17	180000	5.7	21114	27.9	17.14	79	-16.34
18	185000	6.2	20668	28.8	17.17	80	-16.34
19	190000	6.5	20149	28.9	17.18	120	-15.94
20	200000	8.0	18293	30.6	17.23	160	-15.61
21	205000	9.0	16809	31.0	17.25	270	-15.13
22	210000	10.7	14397	31.7	17.27	370	-14.81
23	215000	12.7	10538				
24	220000	15.0	6493				
25	225000	18.7	2968				

table 8.19 Fatigue Crack Growth Data
Overlayed Specimen (S7)

No.	N	a	DM Nm	DK $MNm^{-3/2}$	lnDK	da/dN nm	lnda/dN
1		1.0	23080	12.9	16.37	0.0	-21.90
2	270000	1.05	23080	13.3	16.39	0.33	-21.82
3	300000	1.1	23080	13.5	16.41	0.83	-20.90
4	450000	1.2	23080	14.0	16.45	0.67	-21.13
5	600000	1.3	23080	14.6	16.49	1.0	-20.72
6	650000	1.4	23043	15.0	16.52	2.5	-19.81
7	680000	1.5	23043	15.5	16.56	2.0	-20.03
8	750000	1.6	23006	16.0	16.58	2.0	-20.03
9	780000	1.7	23006	16.4	16.61	4.0	-19.34
10	800000	1.8	22969	16.8	16.64	5.0	-19.11
11	820000	1.9	22932	17.3	16.66	6.7	-18.82
12	830000	2.0	22932	17.7	16.69	10.0	-18.42
13	880000	2.2	22895	18.4	16.73	8.0	-18.64
14	900000	2.4	22858	19.2	16.77	8.0	-18.64
15	910000	2.6	22783	19.9	16.80	13.0	-18.13
16	950000	2.8	22746	20.6	16.84	8.0	-18.64
17	970000	3.0	22672	21.2	16.87	10.0	-18.42
18	980000	3.4	22450	22.3	16.92	50.0	-16.81
19	990000	4.5	21967	25.3	17.04	110.0	-16.07
20	1000000	5.5	21188	27.4	17.12	140.0	-15.78
21	1010000	7.3	19926	31.0	17.25	220.0	-15.32

CHAPTER NINE

General Discussion and Conclusions.

Chapter Nine General Discussion and Conclusions.

9.1 Introduction.

Each chapter in the experimental work section contains discussion and conclusions. In this section a general discussion of the current work is presented.

9.2 Pulsed MIG Welding: Control of Metal Transfer.

Undoubtably pulsed MIG welding provides a high degree of independence between the welding current and the metal transfer. In theory innumerable combinations of pulse parameters exist. However, in practice there are intrinsic and external factors that limit the control of metal transfer. In this work the scatter in the natural detachment times has been identified as an intrinsic factor and seems to be characteristic of the type of metal transfer. However, external factors such as the electrical characteristics of the welding machine or the adhesion of the electrode wire to the contact tube which results in a fluctuation of the arc length cannot be ruled out. For the elimination of any possible arc fluctuation caused by adhesion of the wire to the contact tube, it is recommended that the distance between the torch and the wire feeder is kept as short as possible.

9.3 Pulsed MIG Welding as an Overlaying Process.

The maximum deposition rates used during this work were 3.880Kg/h at 200A, although the maximum attainable deposition rate for the combination of welding wire and equipment is 5.836Kg/h. The maximum deposition rate is limited by the maximum mean current the welding set can operate and that is 350A.

The set up used for overlaying as well as for stringer bead depositions, proved to be very satisfactory for the experimental work. Definitely, improvements can be made if a production line arrangement is required.

9.3.1 Dilution.

The use of a pulsed current resulted in projected spray transfer at welding currents where globular transfer would usually take place with DC-MIG. Although this eliminated the problems of fusion defects associated with globular transfer, it resulted in deeper penetration and consequently higher dilution levels. By employing the single spiral overlaying technique dilution varied from 10.7% up to 33.7%. However, when using very low welding currents to achieve low dilution defects were prone to occur in the deposit as a result of unsatisfactory fusion caused by arc deflection. Although a solution to this problem was found by using very short arcs which eliminated arc deflection, an alternative deposition method was developed. This method employed the deposition of two spirals. The first spiral could be deposited using very low welding currents and since no overlap was employed, low dilution spirals without

overlap defects were possible. The advantage of this proposed method is that by keeping the gap of the first spiral as small as possible high welding currents may be used thus eliminating the possibility of fusion defects but at the same time low dilution results as most of the weldpool will be formed from the melting of the first spiral. Another advantage of this technique is that the second spiral is deposited in a channel within which high deposition ratios of molten metal can be contained. In the single spiral overlapping technique excessive filler wire deposition causes irregularities in the spiral resulting in defective coatings.

Although the resulting dilution from the experiments was 14%, improvement down to levels below 10% is possible.

Thus short circuit transfer can be replaced by free flight transfer and similar dilution levels obtained but without spattery metal transfer and the possibility of fusion defects.

9.3.2 Limitations due to Compositional Variations.

The composition of the specific electrode wire used demanded dilution levels of 7.5% maximum, in order to give a duplex austenitic/ferritic structure of 3% ferrite minimum. These dilution levels may be attained with the double spiral technique and certainly with multilayered deposits. However, although dilution levels were not kept as low as aimed for, both metallurgical soundness and corrosion resistance properties were maintained in the deposit.

9.3.3 Pulsed MIG Welding Compared with Other Welding Processes.

Pulsed Metal Inert Gas Welding is a very good versatile deposition technique superior to DC MIG with the potential for excellent control of metal detachment.

Comparison with other methods of similar deposition rates is difficult to make because the selection of a welding process depends on the combination of financial criteria and the levels of quality demanded by the specific application.

9.4 Fatigue Crack Propagation Experiments.

As expected the "exploratory" series of fatigue crack propagation experiments showed that residual stresses in the weldment affect the manner in which a crack propagates. However, examination of the results give a strong indication that the distribution of residual stresses within the weldment may be influenced by the geometry of the interface of the deposit as well as the different coefficients of expansion between the overlayer and the base metal.

In order to assess the distribution of residual stresses within the weldment and what factors influence such a distribution, further experiments are required. However, based on the above postulate, it may be possible to partially control the stress distribution within the weldment by controlling the geometry of the overlayer interface. However, such considerations are most likely to be outweighed by considerations concerning the effects of dilution on surface properties and microstructure.

CHAPTER TEN

Further Work.

Chapter Ten Further Work.

10.1 Introduction.

The diverse nature of the subject studied, offers a plurality of aspects for further research. However, three topics are proposed for further study.

10.2 Control of Metal Transfer.

Elimination of scatter in the detachment times can improve the precise control of metal transfer using pulsed current. Therefore, research could be carried out towards improving the general stability of the system.

10.3 Overlay welding techniques.

Research on multilayered deposits as well as further development of the proposed double spiral welding technique could be carried out using lower current, lower dilution primary deposits.

Further welding techniques may be tested such as weaving where a motor attached to the torch holder may provide the pendulum movement required.

10.4 Testing of Overlayers.

Fatigue crack propagation experiments on heat treated overlayed shafts could be carried out to compare their behaviour to that of non-heat treated specimens. Similarly research could be conducted on the manner in which a crack will propagate if it is initiated in the

deposit or in the interface in heat treated and non-heat treated specimens. Similarly the effect of flaws on the deposit or the interface, in the initiation and propagation of cracks could also be covered.

Finally the residual stresses in the coating after welding and how they are affected by welding and material parameters as well as deposition techniques could be investigated.

REFERENCES

REFERENCES.

Abonnenc L., 1925 Sur les lois de l' écoulement des liquides, par gouttes, le tube d' écoulement étant cylindrique et vertical.
Annales de Physique 1925 10 (III):161-249.

Adams Jr. C.M. 1958 Cooling rates and peak temperatures in fusion welding.
Welding Journal 1958, 37, (05), 210s-215s.

Agusa K., Nishiyama N., Tsuboi J., 1981 MIG welding with pure Argon shielding-arc stabilisation by rare earth additions to electrode wires.
Metal Construction, 1981, 13, (09), 570-574.

Allen D.J.,Earl C. 1984 Effects of Overlap and Deposition Technique on Weld Bead Shape.
Metals Technology, 1984, 10, (06), 242-248.

Allum C.J. 1985a Metal Transfer in Arc Welding as a Varicose Instability:I Varicose Instabilities in a Current Carrying Liquid Cylinder with Surface Charge.
J.Phys.D Appl. Phys.18 (1985), 1431-1446.

Allum C.J. 1985b Metal Transfer in Arc Welding as a Varicose Instability:II Development of Model for Arc Welding.
J.Phys.D Appl. Phys.18 (1985), 1447-1468.

Allum C.J. 1985c Welding Technology Data:pulsed MIG welding.
Welding & Metal Fabrication 1985,53,(01-02), 24-30.

Allum C.J.,Trindade E. 1984 Characteristics in steady and pulsed current GMAW.
Welding & Metal Fabrication 1984,52,(10), 264-272.

Allum C.J.,Quintino L. 1984a Pulsed GMAW:Interactions between process parameters-Part 1.
Welding & Metal Fabrication 1984,52,(02),85-89.

Allum C.J.,Quintino L. 1984b Pulsed GMAW:Interactions between process parameters-Part 2.
Welding & Metal Fabrication 1984,52,(03), 126-129.

Allum C.J. Quintino L. 1985a Control in fusion characteristics in pulsed current MIG welding, Part 1 Dependence of fusion characteristics on process parameters.
Metal Construction 1985a 17, (04), 242R-245R.

Allum C.J. Quintino L. 1985b Control in fusion characteristics in pulsed current MIG welding, Part 2 Simple model of fusion characteristics.
Metal Construction 1985b 17, (05), 314R-317R.

Amin A. 1983 Pulse Current Parameters for Arc Stability and Controlled Metal Transfer in Arc Welding.
Metal Construction 1983,15,(5), 272-278.

Amson J.C 1965 Lorentz Force in the Molten Tip of an Arc Electrode.
British Journal of Applied Physics 1965, 16, 1169-1179.

Amson J.C. 1972 An analysis of the gas shielded consumable electrode metal arc welding system.
Journal of Physics 1972 89-99

Andrews J.G.,Crane R.E. 1978 Fluid Flow in a Hemisphere Induced by a Distributed Source of Current.
Journal of Fluid Mechanics 1978, 84, 281-290.

Arata Y.,Futamata M.,Toh T. 1979 Investigation on Welding Arc Sound (Report 1) Effect of Welding Method and Welding Condition on Welding Arc Sound.
Transactions of Japanese Welding Reseach Institute 1979, 8, (1), 25-31.

Autio J.,Kettunen P.,Strom K. 1980 Detrimental Effects of Air Currents and their Elimination in MIG Welding.
Weldpool Chemistry and Metallurgy Proc.Con.1980.

AWS 1976 American Welding Society Welding *Handbook 7th Ed 1976 p52.*

Baeslack W.A. III, Lippold J.C., Savage W.F., 1979 Unmixed Zone Formation in Austenitic Stainless Steel Weldments.
Welding Journal 1979, 58, 06, 168s-176s.

Block M.J., Finkelnberg W. 1953 Uber die Axiale Ausdehnung des Anodenfallsgebiets beim Kohlelichtbogen.
Zeitschrift für Naturforschung, 8a, p.785.

Blodget O.W. 1984 Calculating cooling rates by computer programming.
Welding Journal 1984, 63, (03), 19-34.

Boughton P. et al. 1967 Two Years of Pulsed Arc Welding.
Welding & Metal Fabrication 1967, 10, 410-420.

Bradstreet B.J. 1968 Effect of Surface Tension and Metal Flow on Weld Bead Formation.
Welding Journal 1968,47,(07),314s-322s.

BSC 1986 British Steel Corporation Iron and *Steel Specifications 6th Edition.*

Christensen N.,Davies V. de L.,Gjermundsen K. 1965 Distribution of Temperatures in Arc Welding.
British Welding Journal 1965, (02), 54-75.

Colombier L.,Hochmann J. 1977 Stainless and Heat Resisting Steels 2nd Ed.,E.Arnold 1977.

Cooksey C.J.,Milner D.R. 1962 Metal Transfer In Gas-Shielded Arc Welding.
Physics of the Arc 1962 Proc.Con.1966.

Craig E. 1987 A Unique Mode of GMAW Transfer.
Welding Journal, 1987, 66, 12, (09), 51-55

Defize L.F.,van der Willigen P.C. 1960 Droplet Transfer During Arc Welding in Various Shielding Gases.
British Welding Journal 1960, (05), 561-305.

DeLong W.T.,Bradbury J.H.,Reid H.F. 1960 Preheated Welding Wires and their Effect on Welding Characteristics.
Welding Journal 1960, 39, (04), 328-333.

Dieter G.E. 1988 Mechanical Metallurgy. McGraw-Hill

Dunn G.J., Allemand C.D., Eagar T.W., 1986 Metal vapours in gas tungsten arc: Part I. Spectroscopy and Monochromatic Photography.
Metallurgical Transactions A, 1986, 17A, (10), 1851-1863.

Dunn G.J., Eagar T.W., 1986 Metal vapours in gas tungsten arc: Part II. Theoretical Calculations of transport properties.
Metallurgical Transactions A, 1986, 17A, (10), 1865-1871.

Eagar T.W., Tsai N.S. 1983 Temperature Fields Produced by Travelling Distributed Heat Sources.
Welding Journal 1983, 62, (12), 346s-355s.

Ecer et al. 1981 Heat flow simulation of pulsed current GTA welding.
Modelling of Casting and Welding Processes 1981 p.139-160

Essers W.G.,Walter R. 1979 Some aspects of the penetration mechanisms in metal inert gas (MIG) welding.
Arc Physics and Weldpool Behaviour. The Welding Institute 1979.

Felmley C.R. 1955 The Inert gas Metal arc Overlay Process.
Welding Journal 1955, 34, (06), 542-550.

Fenn R. 1987 The Welding Metallurgy of Stainless Steel.
Welding & Metal Fabrication 1987, 55, (10), 380-386.

Ghent et al. 1979 Arc efficiency in TIG welding.
Arc Physics and Weldpool Behaviour. The Welding Institute 1979.

Glickstein S.S. et al 1975 Investigation of Alloy 600 Welding Parameters.
Welding Journal 1975, 54, (4), 113s-122s

Glickstein S.S.,Yeniscavich W. 1977 A Review of Minor Element Effects of the Welding Arc and Weld Penetration.
Welding Research Council Bulletin 1977, No.226, (05).

Glickstein S.S. 1979 Arc modelling for welding analysis. *Arc Physics and Weldpool Behaviour. The Welding Institute 1979.*

Greene W.J. 1960 An Analysis of Transfer in Gas Shielded Welding Arcs.
Transactions of the AIEE 1960, (07), 194-203.

Gregory E.N. 1982 Surfacing by Welding.
Metal Construction 1980,12,(12),685-690

Guile A.E. 1979 Process at arc cathode roots on non-refractory arc cathodes with relatively thick oxide films.
Arc Physics and Weldpool behaviour. The Welding Institute 1979.

Guile A.E.,Hilton M.A.,McLelland I.A.,Reevees-Saunders R. 1975 Arc current distribution in "continuous high speed" anode tracks.
Journal of Physics D 1975, 8, p964.

Guile A.E.,Hitchcock A.H. 1978 Arc cathode craters on thin and thick oxide films on steel and copper.
Archiv. für Electrotechnik. 1978, Vol.60, p17.

Halmoy E. 1979 Wire Melting Rate, Droplet Temperature and Effective Anode Melting Potential.
Arc Physics and Weldpool behaviour. The Welding Institute 1979.

Halmoy E. 1982 Remanent Magnetism-A Cause of Arc Blow.
Welding Journal 1982, 61, (09), 43-47.

Halmoy E. 1986 Electrode Wire Heating in Terms of Welding Parameters.
The Physics of Welding,2nd Ed.,1986, Appendix A.

Harris P. Smith B.L. 1983 Factorial techniques for weld quality prediction.
Metal Construction 1983, 15, (11), 661-667.

Hazlett T.H., Parker E.R., 1956 Effect of individual coating ingredients on surface tension of iron electrodes.
Welding Journal, 1956, 35, (03), 113s-114s.

Hazlett T.H. 1957 Coating ingredients' influence on surface tension, arc stabilty and bead shape.
Welding Journal, 1957, 36, (01), 18s-22s.

Heiple C.R., Roper J.R. 1982 Effects of Minor Elements on GTAW Fusion Zone Shape.
Trends in Welding Research in the United States 1982, A.S.M, 490-520.

Heiple C.R, Roper R.J,Stagner R.T,Aden R.J. 1983 Surface Active Elements on the Shape of GTA,Laser,and Electron Beam Welds.
Welding Journal 1983,62,(03),72s-77s.

Houldcroft P.T. 1977 Welding Process Technology, 1977, Cambridge University Press, Chapter 4,p.83.

Ishizaki K. 1966 Interfacial Tension Theory of the Phenomena of Arc Welding-Mechanism of Penetration.
Proc.Con Physics of the Welding Arc 1962. Published 1966. p195-209

Jackson C.E. 1960 The Science of Welding.
Welding Journal 1960, 39, (04), (05), (06), 129s-140s, 177s-190s, 225s-230s.

Jilong Ma, Apps R.L. 1982 MIG Transfer: Discovery of importance to industry.
Welding & Metal Fabrication 1982,50,(09),307-316

Jilong Ma, Apps R.L. 1983a Analysing Metal Transfer during MIG Welding.
Welding & Metal Fabrication 1983,51,(03),119-128

Jilong Ma, Apps R.L. 1983b New MIG Process Results from Metal Transfer Mode Control.
Welding & Metal Fabrication 1983,51,(04),168-175

Keene B. J., et al 1985 Surface Properties of Liquid Metals and their Effect on Weldability.
Materials Science and Technology 1985,1,568-571.

Kou S. 1981 3-dimensional heat flow during fusion welding.
Modelling of Casting and Welding Processes 1981 p.129-138

Kou S., Wang Y.H. 1986 Weldpool Convection and its Effect.
Welding Journal 1986,65,(03),63s-70s

Lancaster J.F. 1954 Energy Distribution in Argon Shielded Arcs.
British Welding Journal 1954, 1, (09), 412-426.

Lancaster J.F. 1979 Metal Transfer in Fusion Welding.
Arc Physics and Weldpool Behaviour. The Welding Institute 1979.

Lancaster J.F. 1986 The Physics of Welding,2nd Ed.,1986.

Lancaster J.F. 1987 *Metallurgy of Welding, 4rd Ed. Allen & Unwin 1987.*

Landerman E., Grotke G. 1979 Residual Stress Considerations in Weldments for the nuclear Industry.
Weldments: Physical Metallurgy and Failure Phenomena. Proc. Conf. Bolton U.S.A. 1978. ASM/AIME/AWS. General Electric.

Lesnewich A. 1955 Electrode activation for inert gas shielded metal arc welding.
Welding Journal, 1955, 34, (12), 1167-1178.

Lesnewich A. 1958 Control of Melting Rate and Metal Transfer in Gas Shielded Metal Arc Welding.
Welding Journal 1958, 37, (08), 343s-353s.

Lin M.L., Eagar T.W. 1985 Influence of arc pressure on weldpool geometry.
Welding Journal 1985, 64, (06), 163s-169s.

Lin M.L, Eagar T.W. 1986 Effects of surface depression and convection and GTAW.
Advances in Welding Science and Technology ASM Proc. Conf. 1986 p47-51.

Ludwig H.C. 1967 *IIW Document 212-114-67.*

Maecker H. 1955 Plasmastomungen in Lichtbogen in Folge Eigenmagnetisher Kompression.
Zeitschrift Für Physik 141: 198-216.

Mahla E.M., et al 1941 Heat Flow in Arc Welding.
Welding Journal 1941, 20, (10), 559s-568s

Malmuth N.D., et al. 1974 Transient Thermal Phenomena and Weld Geometry in GTAW.
Welding Journal 1974, 53,(09), 388s-400s.

Mantel W. 1962 Physics of the Welding Arc.
Proc.Con Physics of the Welding Arc 1962. Published 1966.

Matsuda F.,Masao U.,Tanaka Y. 1983 Metal Transfer Characteristics in Pulsed GMA Welding.
Transactions of JWRI 1983, 12, 9-17.

McGlone J.C. 1980 A solution to the problem of weldbead geometry.
Ph.D Thesis 1980.

McGlone J.C. 1982 Weldbead geometry prediction - a review.
Metal Construction 1982, 14, (07), 378-384.

Meyers P.S., et al. 1967 Fundamentals of Heat Flow in Welding.
Welding Research Council Bulletin.1967,123,1-46.

Milner et al. 1960 Arc Characteristics and their Significance in Welding.
British Welding Journal, 1960, 7, 73-88.

Moreton J. 1984 Occupational Exposure Limits,1984-New Guidance on Airborne Pollutants.
Metal Construction 1984, 16, (09), 560-561

Mills G.S. 1979 Fundamental mechanisms in Penetration in GTA welding.
Welding Journal 1979, 58, (01), 21-24.

Moore D.C., Taylor E.A. 1955 Welding of Copper and Copper Alloys by the inert gas shielded self adjusting metal arc process.
British Welding Journal 1955, (10), 427-442.

Murty G.S. 1960 Instability of a conducting fluid cylinder due to axial current.
Ark. für Phys. 1960 Vol. 18 pp 241-250.

Murty G.S. 1961 Instability of a conducting fluid cylinder in the presence of an axial current, a longitudinal magnetic field and a coaxial conducting cylinder.
Ark. für Phys. 1961, Vol. 19 pp483.

Needham J.C. 1965 Pulse Controlled Consumable Electrode Welding Arcs.
British Welding Journal 1965, 12, (04), 191-197.

Needham J.C., Carter A.W., 1965 Material Transfer Characteristics with pulsed current.
British Welding Journal 1965, (05), 229-241.

Niles & Jackson 1975 Weld thermal efficiency of GTAW process.
Welding Journal 1975, 54, (1), 26s-32s

Nishiguchi et al. 1977 Study of bead surface profile.
IIW DOC. 212-371-77.

Norman E.W.L. 1984a Magnetic Arc Blow.Part 1 The origin of magnetic fields.
Metal Construction 1984, 16, (07), 441-445.

Norman E.W.L. 1984b Magnetic Arc Blow.Part 2 Effects and solutions.
Metal Construction 1984, 16, (08), 496-500.

Northup E.F. 1907 Some newly observed manifestations of forces in the interior of an electric conductor.
Proc.Amer.Phys.Soc. Vol.24, 1907 pp.474-497.

Oreper G.M., Eagar T.W., Szekely J. 1983 Convection in Arc Weldpools.
Welding Journal 1983, 62, (11), 307s-312s.

Paley Z., Hibbert P.D. 1975 Computation of temperatures in actual weld designs.
Welding Journal 1975, 54, (11), 385s-392s.

Parker A. P. 1981 The Mechanics of Fracture and Fatigue.
E& E.F Spon Ltd.

Patchett B.M. 1978 MIG Welding of Aluminium with an Argon-Chlorine Mixture.
Metal Construction 1978, 10, (10), 484-485

Pearson J.R.A. 1958 On Convection Cells Induced by Surface Tension.
Journal of Fluid Mechanics 4: 489-500.

Pintard J. 1966 Formation et Croissance des Gouttes. Forces auxquelles elles sont surmises avant et pendant le transfert.
IIW Doc 212-89-66.

Quigley M.B.C., et al 1973 Heat flow to the workpiece from a TIG welding arc.
Journal of Physics D: Applied Physics 6, 1973.

Lord Rayleigh 1879 On the Instabilities of Jets.
Proc. Lond. Math. Soc. Vol. 10 pp. 4-13

Raveendra J. Parmar R.S. 1987 Mathematical models to predict weldbead geometry for flux cored arc welding.
Metal Construction 1987, 19, (01), 31R-35R.

Riddihough M. 1949 Hardfacing by Welding,Published for "Welding" by The Louis Cassier Co.,Ltd.

Rollason E.C. 1984 Metallurgy for Engineers. *4th Ed. Arnold. 1984*

Rosenthal D. 1946 The Theory of Moving Source of Heat and its Application to Metal Treatment.
Transactions ASME 43 (11): 849-866.

Salter G.R.,Dye S.A. 1971 Selecting Gas Mixtures for MIG Welding.
Metal Construction and British Welding Journal 1971, 3, 06, 230-233.

Sambamurti S.V. 1983 Gas Shielding of the Welding Arc: Some Aspects.
Indian Welding Journal 1983, (01), 1-8.

Savage W.F. Strunk S.S. Ishikawa Y. 1965 The effect of electrode geometry on GTAW.
Welding Journal 1965, 44, (11), 489s-496s.

Smati Z. 1986 Automatic Pulsed MIG Welding.
Metal Construction 1986, 18, (01), 38R-44R.

Smith D. 1989 Welding Practices and Skills.
McGraw Hill 1989.

Smithells C.J. 1978 Metals Reference Book,5th Ed., *Butterworths 1978.*

Sozou C., Pickering W.M., 1976 Magnetohydrodynamic flow due to the discharge of an electric current in a hemispherical container.
Journal of Fluid Mech. 1976, 73, 641-660

Sozou C.,Pickering W.M. 1978 Magnetohydrodynamic flow in a Container due to the discharge of an electric current from a finite size electrode.
Proc.R.Soc. London A.362, 1978, 509-523.

Stol I. 1989 Development of an Advanced Gas Metal Arc welding process.
Welding Journal 1989, 68, (08), 313s-326s.

Street J.A. 1987 Practical Measurement of Voltage and Current in Arc Welding.
Metal Construction 1987, (11), 646-648.

Suits C.G., Poritsky H. 1939 *Physical Review 1939, 55, 1184-1191.*

Szekely J. 1986 The mathematical modelling of arc welding operations.
Advances in Welding Science and Technology 1986 p.3-14. ASM.

Szekely J.,Oreper G.M.,McKelliget J. 1987 Heat and Fluid Flow Phenomena in Arc Welding Operation.
Modelling and Control of Casting and Welding Processes [Proc.Con] 1987 p247-276.

Tsai N. *Ph.D Thesis M.I.T. 1982.*

Tsao K.C.,Wu C.S. 1988 Fluid Flow and Heat Transfer in GMA Weldpools.
Welding Journal 1988, 67, (03), 70s-75s.

Tuthill R.W. 1954 Arc Characteristics for Consumable Electrode Gas Shielded Welding.
Welding Journal 1954, 33, (02), 128-132.

Ueguri S.,Hara K.,Komura H. 1985 Study of Metal Transfer in Pulsed GMA Welding.
Welding Journal 1985, 64, (08), 242s-250s.

Velarde M.G.,Normand C. 1980 Convection.
Scientific American 1980, 243(1), (07), 79-93.

Villeminot P. 1967 Soudage MIG sous Argon d' acier doux, étude technique de la partie terminale, température de transfert.
Soudage et Technique Connexes 21(9/10):367-380.

Walsh D.W.,Savage W.F. 1985 Technical Note: Autogenous GTA Weldments Bead Geometry Variations Due to Minor Elements.
Welding Journal 1985, 64, (02), 59s-62s.

Waszink J.H.,Graat L.H.J. 1979 Der Einfluss der Gasstromung und der Electromagnetischen Kraft auf die Ablosung von Schweisstropfen.

Waszink J.H.,Graat L.H.J. 1983 Experimental Investigation of the Forces Acting on a Drop of Weld Metal.
Welding Journal 1983, 62, (04), 108s-116s.

Waszink J.H.,Piena M.J. 1986 Experimental Investigation of drop detachment and drop velosity in GMAW.
Welding Journal 1986, 65, (11), 289s-298s.

Waszink J.H.,Van der Heuvel G.J.P.M. 1982 Heat Generation and Heat Flow in the Filler Metal in GMA Welding.
Welding Journal 1982, 61, 269s-282s.

Wells A.A. 1952 Heat flow in welding.
Welding Journal 1952, 31, (05), 263s-267s.

Wienecke R. 1955 Uber das Geschwindigkeitsfeld der Hochstromkohlebogensaule.
Zeitschrift für Physik 1955, 143, 128-140.

Willingham D.C., Hilton D.E. 1986 Some Aspects of Fume Emissions from MIG Welding Stainless Steel.
Welding & Metal Fabrication 1986,54,(07),226-229

Wilson E. 1981 Metal inert gas (MIG) arc welding-Part 2.
Welding & Metal Fabrication 1981,49,(11),518-520

Wilson J.L.,Claussen G.E.,Jackson C.E. 1956 The Effect of I^2R Heating on Electrode Melting Rate.
Welding Journal 1956, 35, (01), 1s-8s.

Wilson L.B. 1925 Electric Welding, Pitman.

Woods R.A.,Milner D.R. 1971 Motion in the weldpool in arc welding.
Welding Journal 1971, 50, (4), 163s-173s.

Yamada T. Tanaka O. 1987 Fluctuation of the wire feed rate in GMAW.
Welding Journal, 66, (09), 35-42.

APPENDIX I

Bead Profiles.

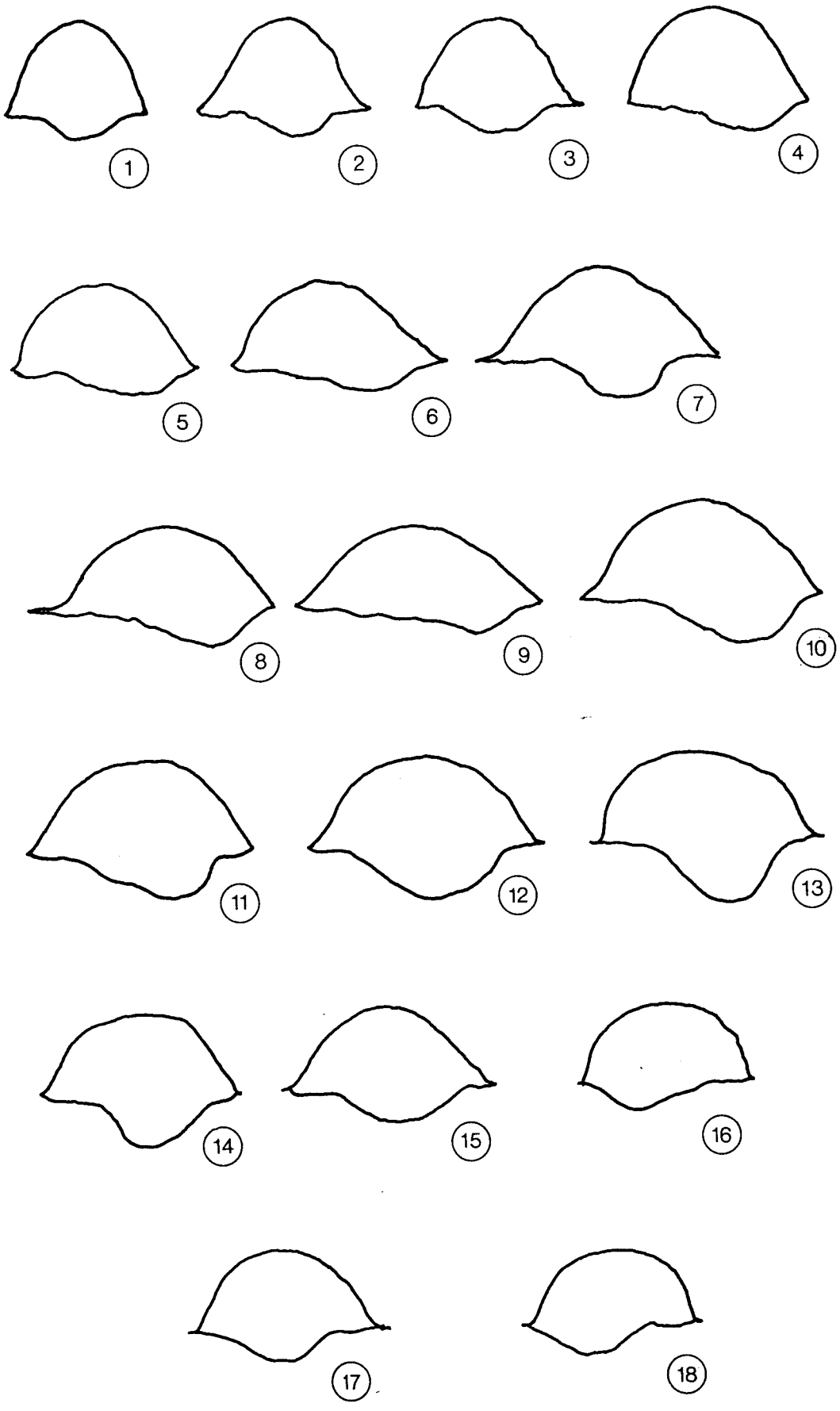

FIG. A.1 Bead Profiles from Table 7.1

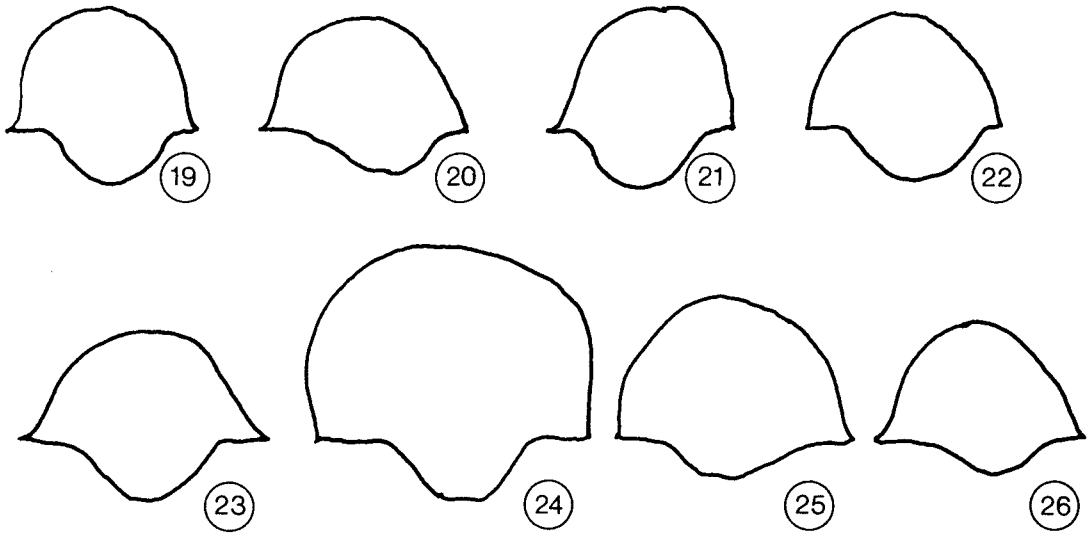

FIG.A.2 Bead Profiles from Table 7.2

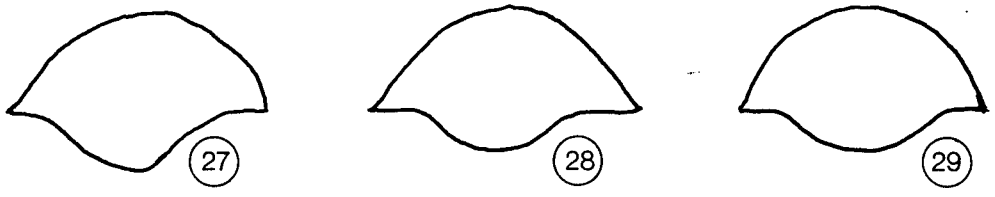

FIG.A.3 Bead Profiles from Table 7.3

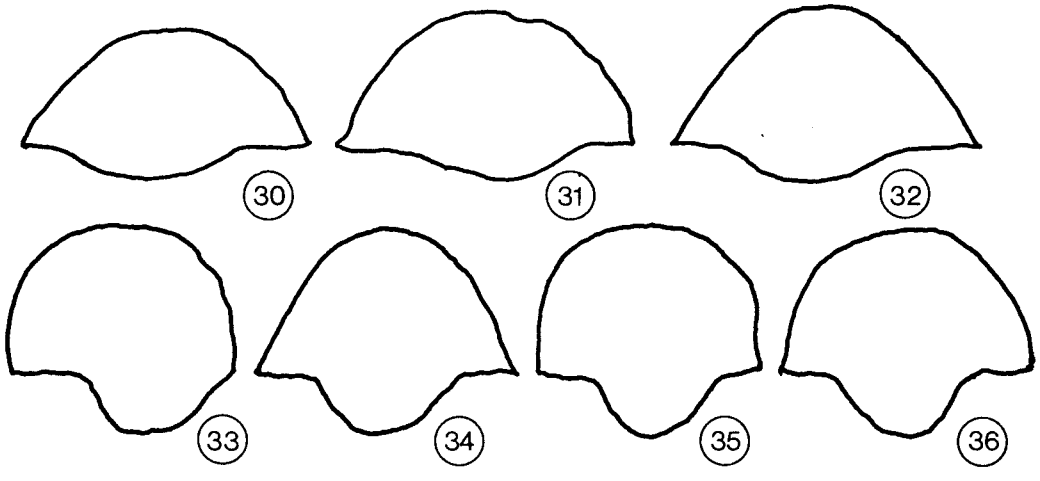

FIG.A.4 Bead Profiles from Table 7.4 5mm

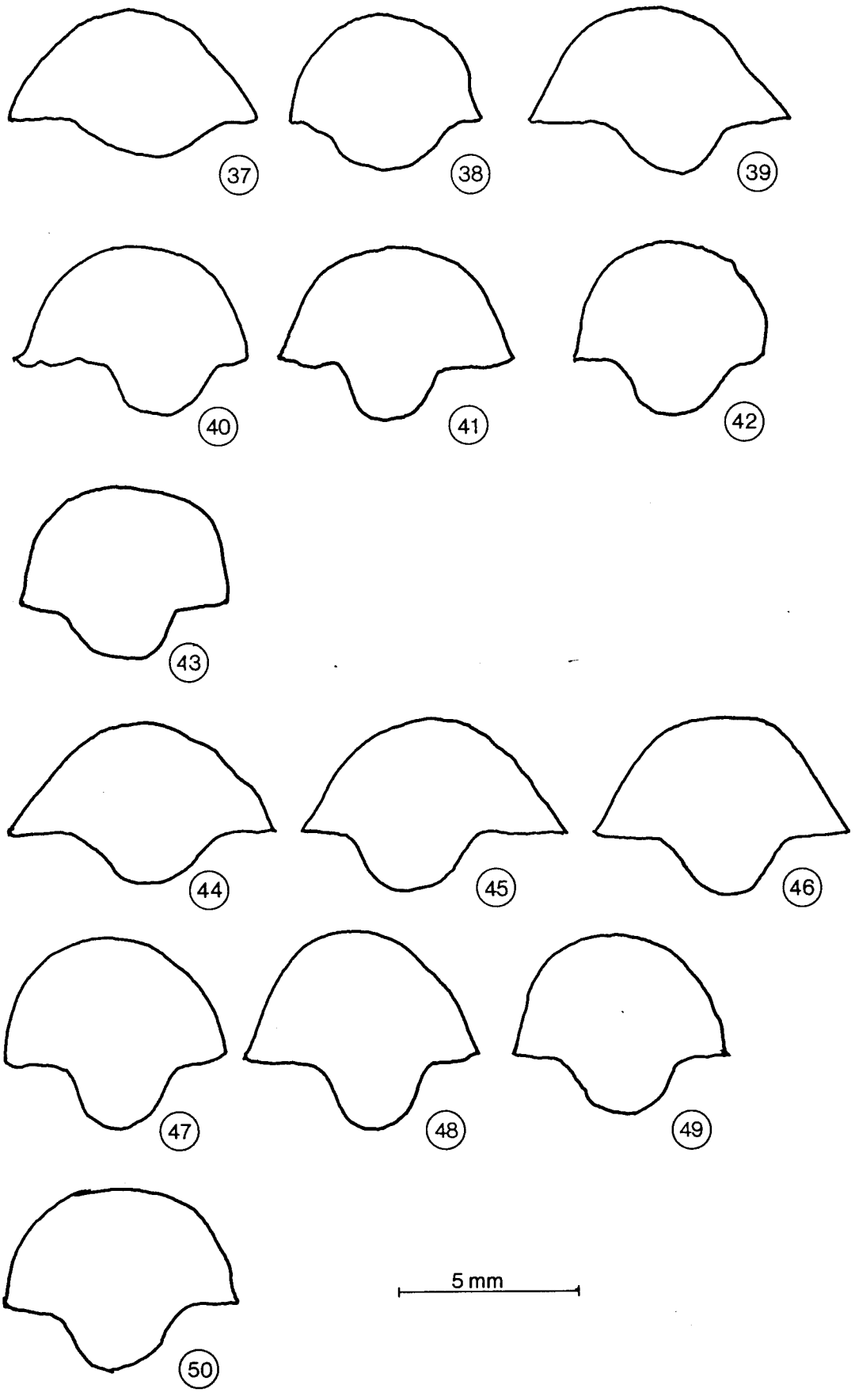
37
38
39
40
41
42
43
44
45
46
47
48
49
50
5 mm

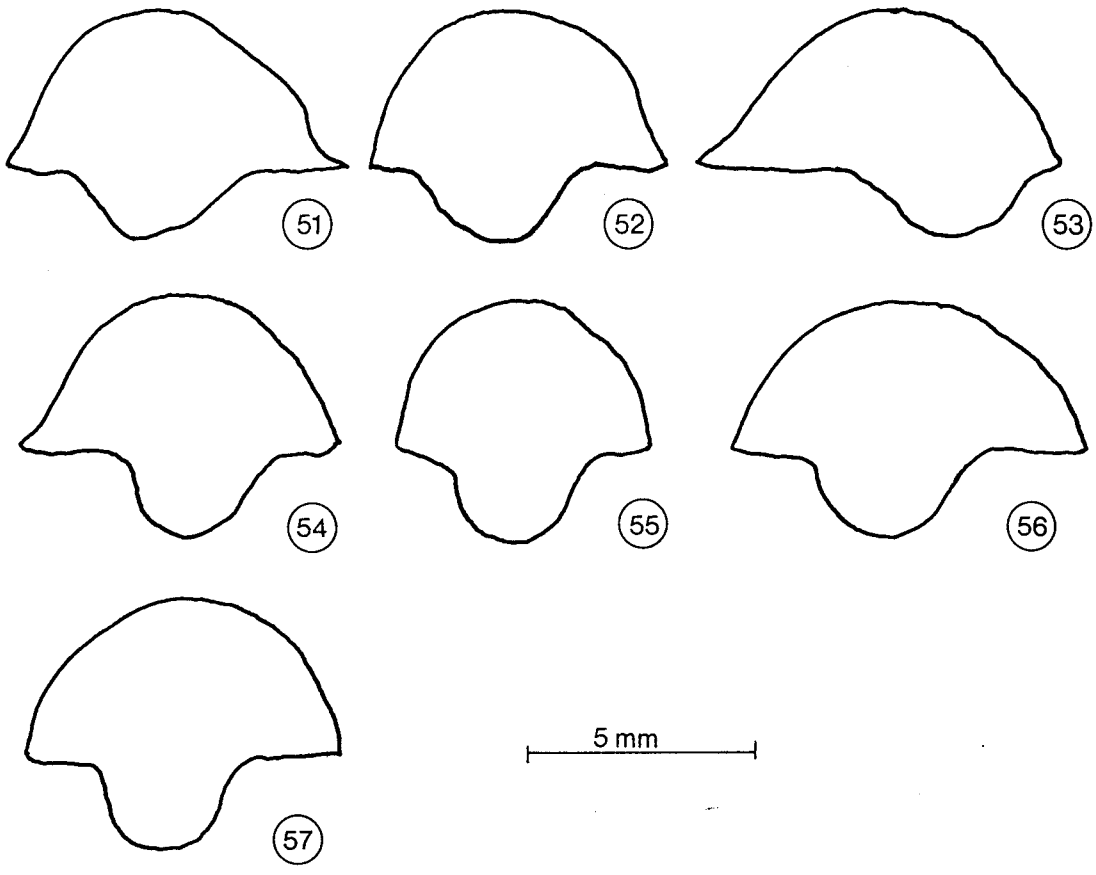

FIG.A.4 Bead Profiles from Table 7.4 (cont. ...)

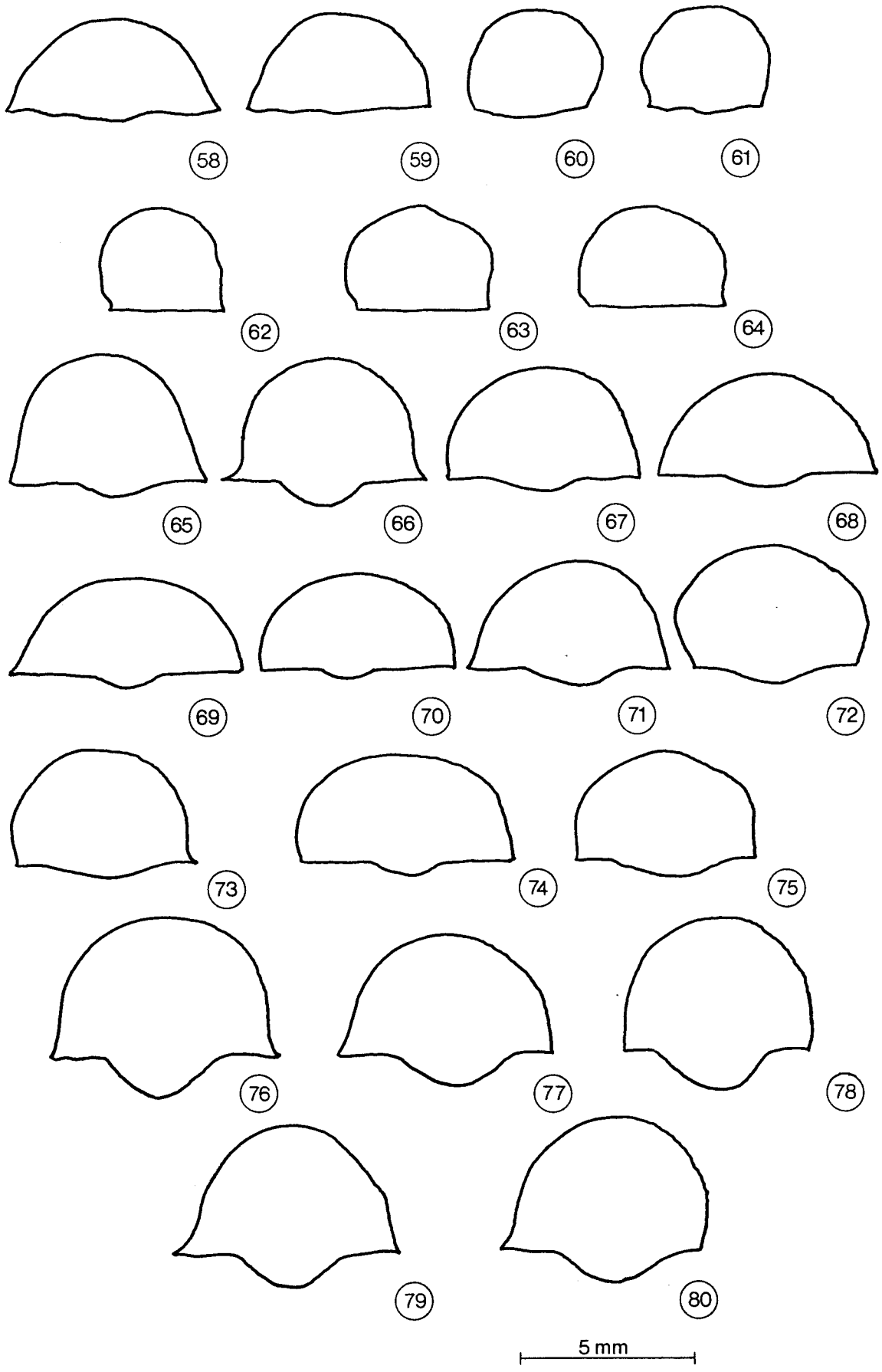

FIG. A.5 Bead Profiles from Table 7.5

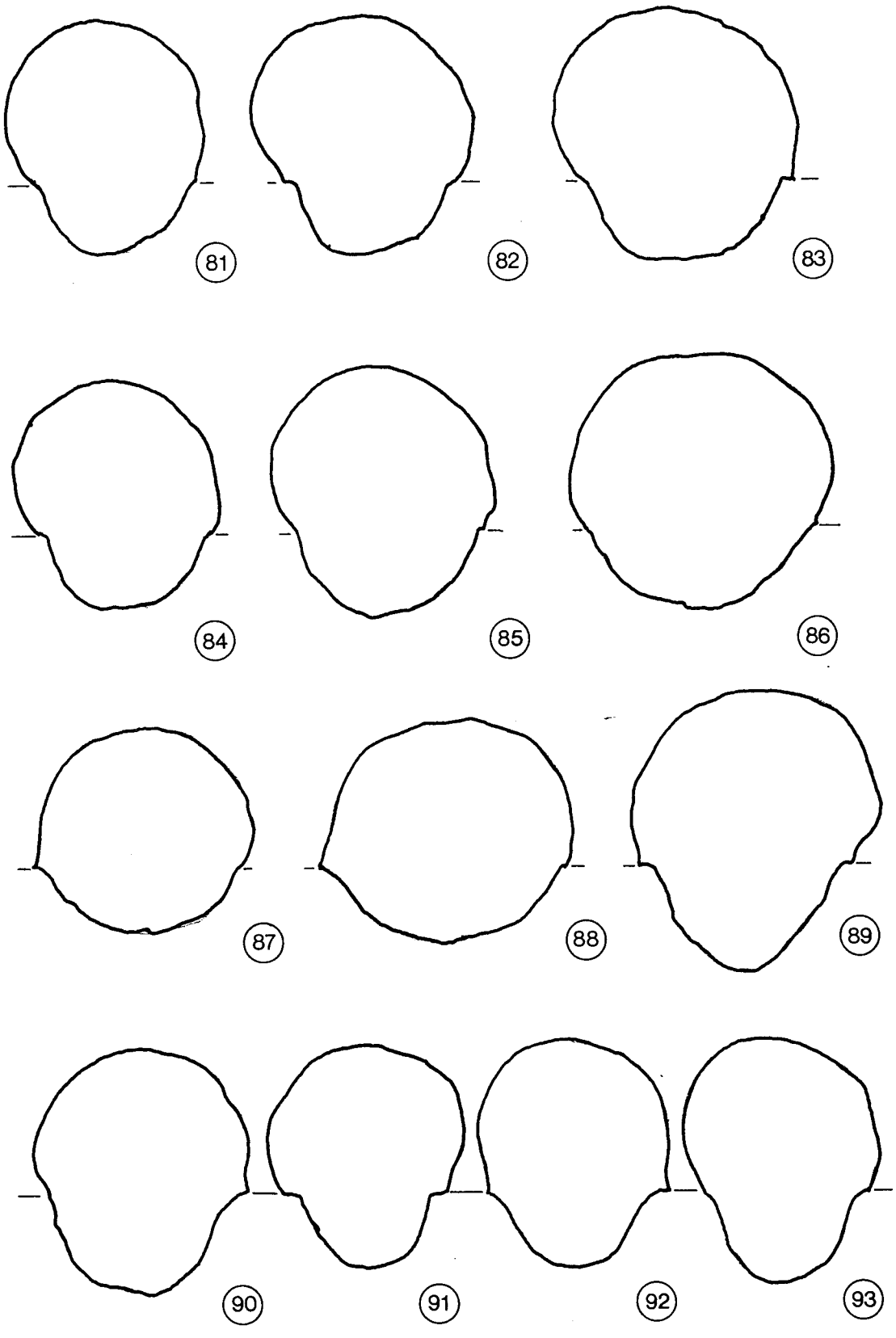
81
82
83
84
85
86
87
88
89
90
91
92
93
5 mm

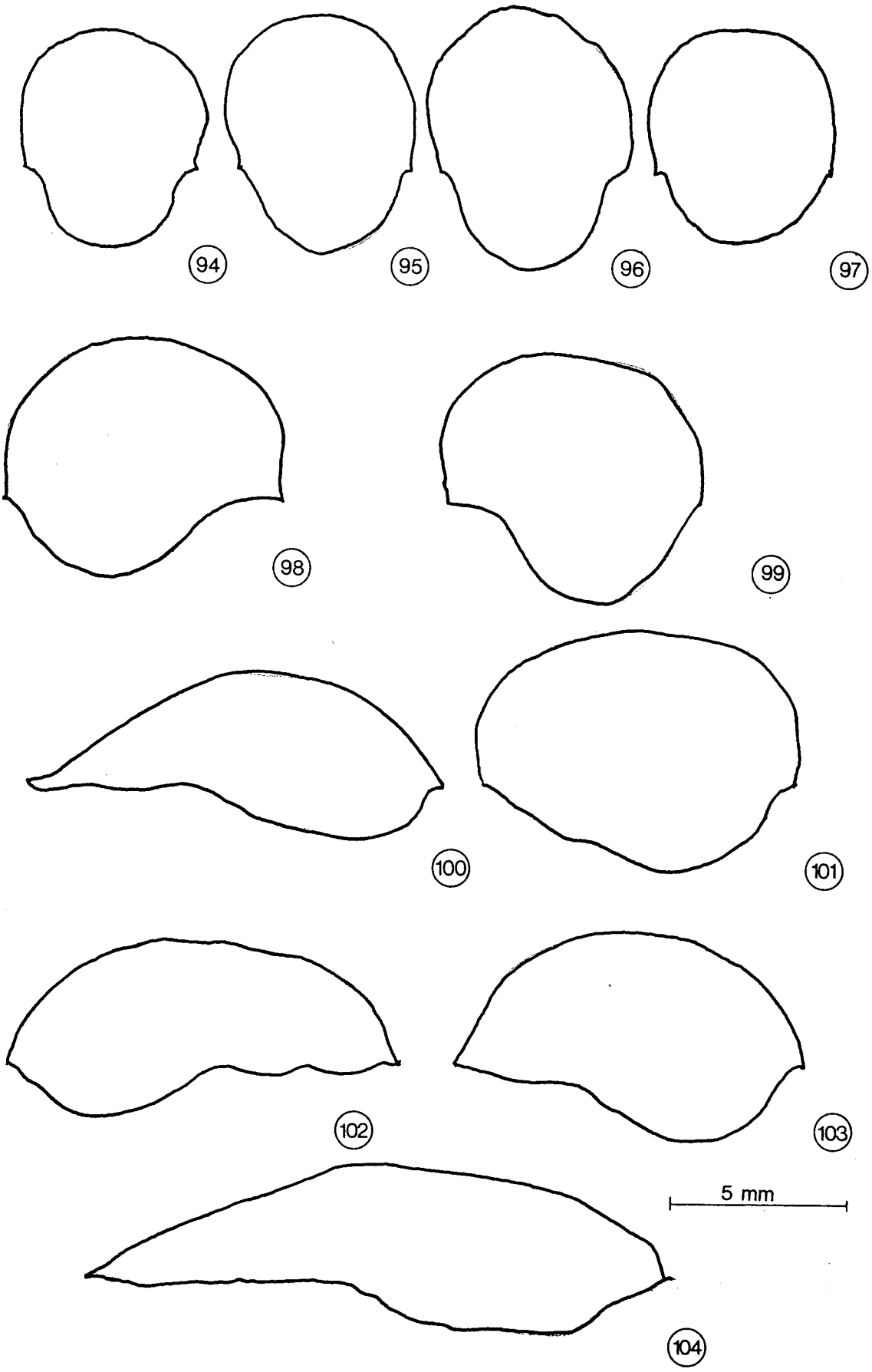
94
95
96
97
98
99
100
101
102
103
5 mm
104

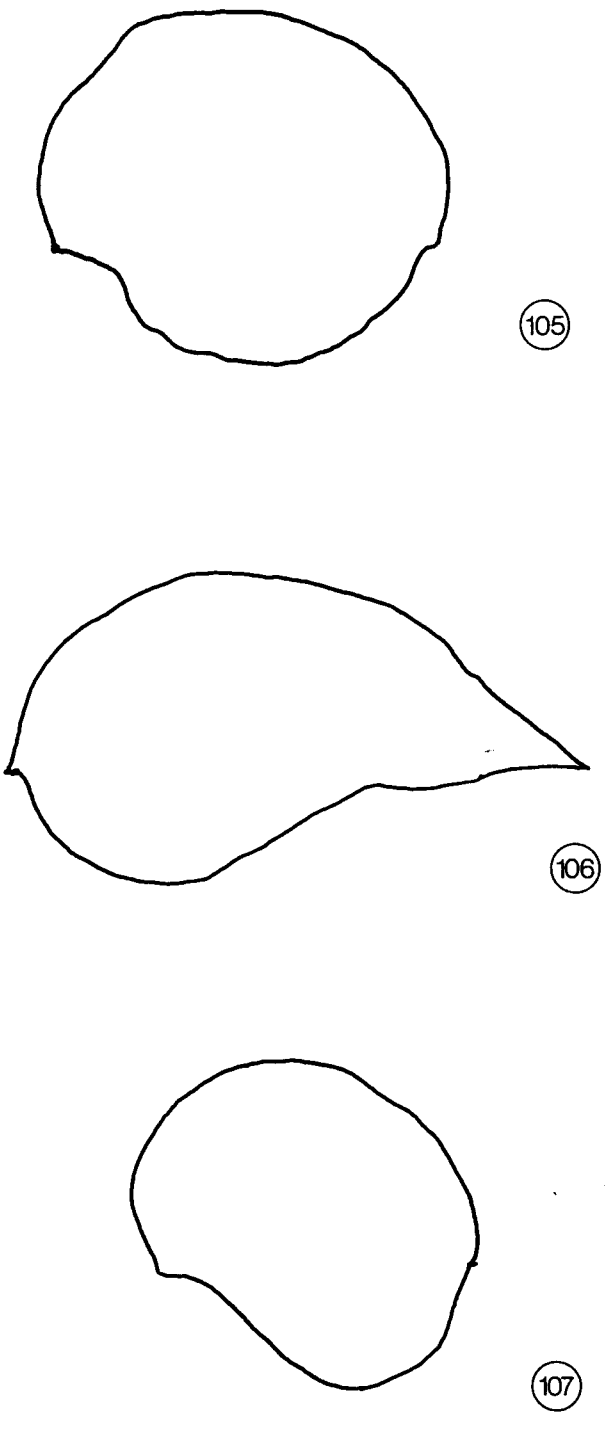

FIG. A.5 Bead Profiles from Table 7.6 5 mm